TECHNO-ECONOMIC FEASIBILITY OF SOLAR ASSISTED HEAT PUMP (SAHP) SYSTEMS FOR EUROPEAN SINGLE-FAMILY HOUSES

CELAL TILTAY

A thesis submitted in partial fulfilment of the requirements for the degree of Doctor of Philosophy

The University of Sheffield
Faculty of Engineering
Department of Mechanical Engineering

November 2023

The candidate confirms that the work submitted is his own and that appropriate credit has been given where reference has been made to the works of others.

ABSTRACT

Buildings account for about one-third of the global energy consumption and one-quarter of the total greenhouse gas emissions that cause global warming. These percentages are even higher in the single-family residential houses of the developed regions, such as Europe, due to the high living standards. As a solution, the building structures need to be more energy efficient in terms of construction and sustainable in terms of the energy supply side. However, research has shown that there are yet no building construction guidelines in around 110 countries worldwide. In addition, solar-assisted heat pump (SAHP) technology is one of the most promising solutions that can be applied to the single-family houses to reduce energy consumption, to electrify & meet all energy demands, and to increase the renewable energy share of the building sector. Despite the advantages, however, there is still a significant lack of awareness and a limited number of applications for the SAHP system in the building sector today. This thesis therefore investigates the techno-economic feasibility of different SAHP systems in residential single-family houses in order to unlock the full potential of the technology while ensuring that the energy demand side management is in line with the regional building standards. In order to actualize these objectives, a model-based formalised methodology has been implemented to design, validate, and analyse a representative typical single-family house and two different SAHP systems by employing the commercial software packages of TRNSYS and EES.

The results on the house model have demonstrated that the largest energy demand vector of a single-family residential house in European region is usually the space heating & cooling (SH & SC), followed by electrical energy (EE) for the household equipment, and domestic hot water (DHW). Moreover, it has been shown that the dynamic behaviour on the demand side is crucially important as it permits a better assessment of the performance of the energy delivery systems in real conditions. Regarding the technology implementation, the first proposed SAHP system is designed for a case study under the climatic boundary conditions of an EU candidate country. The results of this system showed that a basic SAHP configuration (PV+ air-HP) can satisfy the energy demand of 10077 kWh, which is the sum of all energy demand vectors of the representative house, with 20.15 m^2 PV installation when HP is connected and 38.3 m^2 PV installation when HP is disconnected. Moreover, the economic indicators have revealed that the system's payback time is 6.8 years and the LCOE is 0.121 €/kWh, proving that the system has already reached the grid-parity in the location of interest (compared to the grid energy price, 0.130 €/kWh). The second proposed SAHP system is designed under the climatic boundary conditions of three different European countries, representing cold, moderate, and hot climates. The results of this system have shown that an innovative configuration (PV/T+ water-HP) can perform better and substantially reduce the SH and DHW needs of the representative house in all climates. However, the techno-economic analyses have revealed that such systems may not be feasible for cold climates, while excellent results have been obtained for moderate and hot climates. In these locations, the proposed system can cover 9843.6 kWh and 7365.6 kWh of energies (which are the sum of SH, DHW, and EE demand vectors of the representative house) with 14.7 m^2 and 10.8 m^2 of PV/T installations, respectively. Also, the payback time and LCOE of the system are calculated as 7.4 years-0.122 €/kWh for the moderate climate (compared to the grid price of 0.123 €/kWh) and 7.5 years-0.177 €/kWh for the hot climate (compared to the grid price of 0.241 €/kWh), respectively. Furthermore, the implications of all results are critically discussed.

ACKNOWLEDGEMENTS

I profoundly thank my main supervisors; Professor Mohamed Pourkashanian, Professor Lin Ma, and Dr Kevin J Hughes for their guidance throughout my Ph.D. Their technical feedback during our weekly meeting helped me to identify my research topic and to better understand the field.

I would like to particularly thank and express my sincere gratitude to my co-supervisors; Professor Derek B. Ingham and Dr Stavros Michailos for their guidance, feedback, and constructive encouragement throughout my Ph.D. journey. I would not be able to make it without their endless support!

I would also like to acknowledge my sponsor, the Republic of Türkiye (Turkey) Ministry of National Education, for funding my PhD study at the University of Sheffield in the United Kingdom.

Many thanks to my esteem colleagues at the Energy 2050 research institute of the University of Sheffield for their support and friendship; Mustafa Erçelik, Dr Godfrey Udeh, Wenjun Peng, Dr Oscar Rafael Pupo Roncallo, and Dr Nidiana Rosado Hau. Also, to my other friends; Dr Kemal Balandiz, Mr Naim Deniz, Dr Cemal Karaaslan, Mr Nihat Aras, Mr Embiya Yusufoğlu, and others whose names deserve to be mentioned but are missing.

I owe special thanks to my friends; Ibrahim Halil Özdemir and Mehmet Nuri Şayran. I went through devastating moments in especially last one and half years... moments that almost made me quit my study. However, they were always there and offered the most meaningful moral support and encouragement that I needed to finish what I started. For sure, I could not have achieved all this without you!!

Foremost, I cannot thank my parents, Mr. Sıdkı Tiltay and Mrs. Cemile Tiltay, my brother and sisters, and my extended family enough. I feel blessed that I have such an extraordinary

family. Finally, my son Ali Sıtkı Tiltay, I am wordless to express how much I miss and love you. I dedicate my thesis to you!

-To my beloved Son…

LIST OF PUBLICATIONS

Journal Papers

1. C. Tiltay, S. Michailos, D. B. Ingham, L. Ma, K. J. Hughes, M. Pourkashanian "Techno-economic assessment of solar PV + heat pump systems for net-zero energy European single-family houses: A case study in Turkey". Manuscript was sent to supervisors for revisions, it will be submitted to Energy and Conversion Management. (**Chapter 5**).
2. C. Tiltay, S. Michailos, D. B. Ingham, L. Ma, K. J. Hughes, M. Pourkashanian "Feasibility analysis of a novel PV-thermal (PV/T) + heat pump system for combined heat & power provision in European single-family houses". Under preparation, it will be submitted to Sustainable Energy Technologies and Assessments. (**Chapter 6**).

Poster Presentations

1. C. Tiltay, D. B. Ingham, L. Ma, M. Pourkashanian "Hybrid solar-assisted heat pump systems: Dynamic residential heat and power" Mechanical Engineering Conference and Poster Event. 27 June 2019, University of Sheffield. (**Chapter 4**).

CONTENTS

LIST OF FIGURES

LIST OF TABLES

NOMENCLATURE

Abbreviations

ASHP	Air Source Heat Pump
a-Si	Amorphous Silicon
ATE	Annual Total Energy
CAPEX	Capital Expenditures
COP	Coefficient Of Performance
DHW	Domestic Hot Water
DS-SAHP	Direct Serial SAHP
EE	Electrical Energy
EED	Electrical Energy Demand
EES	Engineering Equation Solver
EPBD	Energy Performance of Building Directive
ETC	Evacuated Tube Collectors
EU	European Union
FIT	Feed-In Tariff
FPC	Flat Plate Collectors
GHGs	Greenhouse Gases
GHI	Global Horizontal Irradiance
GSHP	Ground Source Heat Pump

GWP	Global Warming Potential
HP	Heat Pump
IAM	Incidence Angle Modifier
IDS-SAHP	Indirect Serial SAHP
IEA	International Energy Agency
IPCC	Intergovernmental Panel on Climate Change
IWEC	International Weather for Energy Calculations
LCC	Life Cycle Cost
LCM	Lumped Capacitance Method
LCOE	Levelized Cost of Energy
LMTD	Log-mean Temperature Difference
MPP	Maximum Power Point
NG	National Grid
NOCT	Nominal Operating Cell Temperature
NPV	Net Present Value
NTU	Number of Transferred Units
NZEB	Net Zero Energy Building
O&M	Operating & Maintenance
ODP	Ozone Depletion Potential
OPEX	Operational Expenditures

PPTD	Pinch Point Temperature Difference
PT	Payback Time
PV	Photovoltaic
PV/T	Photovoltaic / Thermal
RES	Renewable Energy Sources
SAHP	Solar-Assisted Heat Pump
SC	Space Cooling
SH	Space Heating
STES	Sensible Thermal Energy Storage
TES	Thermal Energy Storage
TFES	Total Final Energy Supply
TMY	Typical Meteorological Year
TRNSYS	Transient System Simulation Tool
VCC	Vapour Compression Cycle
WSHP	Water Source Heat Pump

Symbols and Units

A	Specific surface area, m^2
C_p	Specific heat capacity, kJ/kg.K
d	Thickness, m

eff	Effectiveness, (-)
G	Solar irradiance, W/m^2
h	Specific enthalpy, kj/kg
I	Current, A (ampere)
k_B	Boltzmann constant
$\dot{m}$	mass flow rate, kg/s
η	Efficiency, (-)
P	Power, W
P	Pressure, Pa
Q	Heat, Joule
R	Thermal resistance, m^2K/W
Ref	Reference, (-)
s	Entropy, J/K
T	Temperature, °C or K
U	Thermal transmittance, $W/m^2.K$
V	Volume, m^3
Vol	Voltage, V
λ	Thermal conductivity, W/m.K

Chemical Symbols

CH4	Methane

CO	Carbon monoxide
CO2	Carbon dioxide
H_2O	Water
O_2	Oxygen

CHAPTER 1

Introduction

1.1 RESEARCH BACKGROUND

1.1.1 Energy Demand and Fossil Fuels Dominance

Energy has always been among the most crucial elements in life. Throughout the history of humanity, energy has been converted into different usable forms and utilized for various purposes. As humans have evolved, the use of energy has been a main pillar in the major advances in civilisation.

Before the 18th century, energy demand for societies was almost entirely supplied by human and animal power or traditional biomass sources such as wood and dung. The demand for energy primarily increased due to population growth during this time. However, the technological innovations that have occurred between the 18th and 19th centuries have paved the way to the Industrial Revolution which refers to the transition of manufacturing processes from hand production or basic tools to factory systems, machinery, mass production, and chemical manufacturing [1]. Hence the increasing level of industrialization, and incessant technical innovations, combined with the rapid population growth, increase energy demand unprecedentedly [2], [3].

This dramatic growth of energy consumption has been fuelled mainly by coal [4]. As a result, fossil fuels (coal, oil, natural gas, etc.) began to be the primary source of energy in the world in the 19th century [5]. At the beginning of the 20th century, 96% of the total energy production was supplied by coal, however, this trend has declined over the years as the crude oil and natural gas began to be consumed in the 21st century.

Today, energy demand appears to be pertinent to the population level, economic growth, and industrialization of the countries [6]. However, still more than 80% of the world primary energy demand is supplied by fossil fuels. In this percentage, based on the latest statistics of the International Energy Agency (IEA) [7], the crude oil has the largest share with 30.9%,

followed by coal and natural gas with 26.8% and 23.2%, respectively. Moreover, the energy demand has increased by an annual average rate of 1.8% since 2011, and several studies anticipated that fossil fuels will remain as the main source to meet this growth in the future [8].

1.1.2 Climate Change and Mitigation Options

An inevitable side-effect of the fossil fuels' dominance explained in the previous section is the environmental concerns. This is due to the greenhouse gases (GHGs)[1], chiefly carbon dioxide (CO_2), emitted into atmosphere during the combustion of carbon-rich fossil fuels.

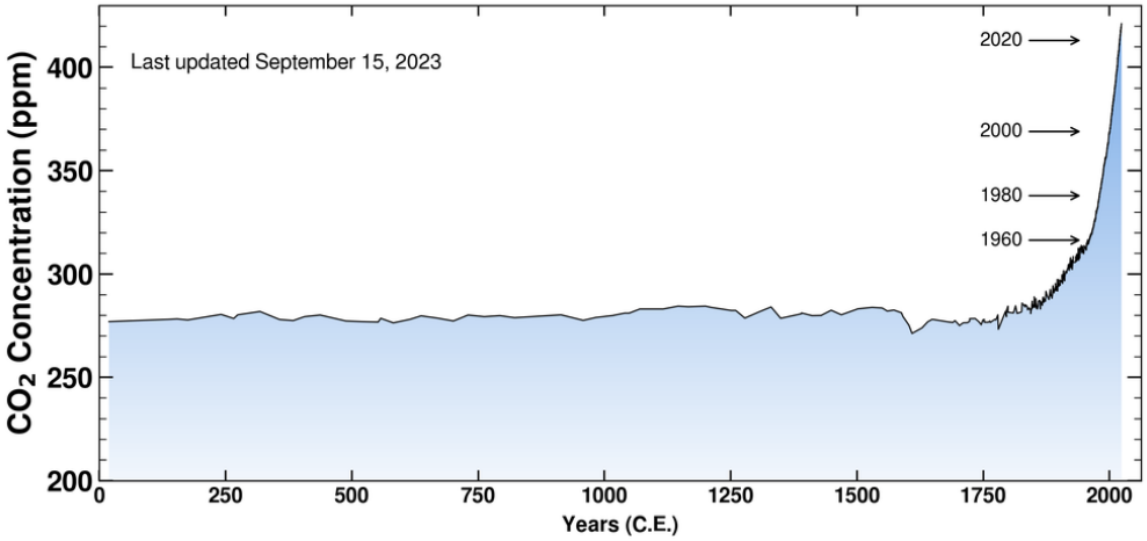

Figure 1.1: Current CO_2 concentration in the atmosphere at the Mauna Loa Observatory (latest CO2 reading of 15th September 2023 was 418.50 ppm) [9].

[1]Kyoto Protocol counts six main gases as GHGs; Carbon dioxide (CO2), Methane (CH4), Nitrous oxide (N2O), Hydrofluorocarbons (HFCs), Perfluorocarbons (PFCs), and Sulphur hexafluoride (SF6) [312]. However, CO2 is the largest and the most significant contributor for the global warming due to its long life and high radiative forcing [313].

Measurements at the Mauna Loa Observatory [10] show that there has been an unprecedented increase in the amount of CO_2 concentration in the atmosphere since the last century . Figure 1.1 illustrates the level of CO_2 concentration on 15 of September 2023 and compares it with the historical emissions of the last 2000 years [11].

Linking to this, the rapid increase in CO_2 concentration leads to a cumulative heat build-up in the Earth's atmosphere, which in turn increases average global temperature, causing global warming [12]. Moreover, the Fifth Assessment Report (AR5) of the Intergovernmental Panel on Climate Change (IPCC) states that human activities (with 95 % probability) has been the primary cause of the observed global warming since the mid-20th century [13]. IPCC in its Fourth Assessment Report (AR4) concluded that CO_2 emissions that occurred before the industrial time (see Figure 1.1) was principally because of deforestation and other land-use-change activities, but the emissions released after this time were mainly due to the human activities (including combustion of the fossil fuels), which is the prime cause of the global warming and eventually climate change [14].

The IEA has shown that the increasing emissions of greenhouse gases in the atmosphere in the 21st century will continue to warm the Earth further, leading to long-term changes in all parts of the climate system and the possibility of severe, irreversible and widespread impacts on humans and ecosystems [13], [15].

In order to put limitations on this continuation, the first universal and legally binding negotiation of the United Nations Framework Convention on Climate Change (UNFCCC) took place in Paris in 2015 (COP21). The final commitment, approved at the COP21, is to hold the global temperature rise to "well below" 2°C above pre-industrial levels with an equivalent CO_2 concentration of 450 ppm in the atmosphere by 2050, and that to follow efforts to limit the increase to 1.5°C above pre-industrial levels [16], [17]. However,

restricting the temperature rise to 2°C [12] and CO_2 concentration to 450 ppm is becoming stringent because 80% of the carbon dioxide emissions set as a threshold for 2035 are already about to be reached [6], [12], [18]. Thus, there is an urgent need to shift the energy production from carbon-intensive fuels to less-carbon-intensive or completely environmentally friendly sources in order to combat the worsening effects of climate change [12]. For this purpose, the latest roadmap for the global energy sector provided by the IEA is the report of 'Net Zero by 2050' [19] which aims to reduce the global GHG emissions as close to zero as possible. Based on the Net-Zero report, research, policies, and capital management should be directed towards sustainable technologies to achieve a low-carbon energy environment [15]. Proposed strategies and technological options for reducing carbon dioxide emission, and equivalently combating the climate change are summarised as follows [19], [8], [12], [14], [20]:

- Reducing energy consumption in all sectors.
- Increasing the use of renewable energy sources in all sectors.
- Creating modern energy generation techniques and altering current methods.
- Utilizing innovative and cost-effective energy storage options.
- Using smart grids, micro-grids and distributed generation technologies.
- Capturing and utilizing/storing CO_2.

1.2 BUILDINGS SECTOR AND NET-ZERO-ENERGY-BUILDING CONCEPT

The building sector have the highest final energy consumption, followed by industry and transport [21]. Based on the latest statistics [22], the buildings (residential, commercial and public) consume around 30% of the total final global energy consumption and contribute approximately 25% of the total CO_2 emission. Moreover, the energy consumption of the sector has been increasing by 1.2% per year since 2000 [23]. As a result, analysing the energy consumption in the building sector is crucial.

In addition, regional disparities show that people living in developed countries are three to five times more energy consumers and GHG emitters per capita compared to the ones living in developing and non-developed countries [24]. As a result, the buildings sector energy consumption percentages are even higher in the most developed regions/countries, mainly due to population growth, high living standards and comfort levels, and developments in building services. For example, in European countries, energy use in the building sector reaches up to 41% of total final energy consumption [25].

The demand for energy services is influenced by various building typologies that vary in terms of their physical (size, geometry, construction, etc.) and operational (activities, internal loads, ventilation rates, schedules, etc.) characteristics. Therefore, understanding how energy is utilised depends on the classification of building types. With this regard, the buildings are categorized as residential/domestic (including single-family, multi-family, and mobile homes) and non- residential (including offices, hosting, educational, leisure, etc.). Among these types, around 75% of the energy used in building sector worldwide is for residential purposes, with single-family houses accounting for a large share [24].

In order to reduce the energy consumption of the buildings, one of the most effective approaches is to construct high-performing envelopes (different parts of a structure, such as external walls, roof, etc., that divide the indoors from the outdoors) [26]. Thus, selecting energy-efficient materials when designing a new construction or retrofitting an existent building is of crucial importance to reduce the energy consumption of the buildings while ensuring the thermal comfort of the residents. However, as of 2022, still about 110 countries do not have a mandatory building construction guidance or standard (even in the European region, see Chapter 4), which means that more than 2.4 billion m^2 of floor space were constructed without complying with any energy-related performance standards [27].

The disaggregation of building consumption by energy services, so-called end-uses, is also important for users to identify cost-effective energy-saving methods. With this regard, end-uses for the energy consumption in buildings can be divided into thermal energy end-uses including space heating and cooling, water heating, and cooking; and electrical energy end-uses including lighting and electrical appliances [23]. However, the thermal (space heating (SH), space cooling (SC), and domestic hot water (DHW)) demands represent the largest share of the energy requirement of the whole residential sector in many countries [28], and approximately 80% in the European countries [29]. This high weight of the energy consumption of the thermal end-uses of the building sector in Europe is even comparable with some other main end-uses of other sectors, such as passenger cars in the transportation sector [24]. Nevertheless, still approximately two thirds of thermal energy use in buildings is supplied by fossil fuels today [30]. In order to decrease the energy consumption and the corresponding GHG emissions into the atmosphere, hence the building sector must be more energy efficient and sustainable, particularly in the developed regions. This is achievable only by means of enhancing and retrofitting the buildings' envelopes and/or proposing central and efficient technological solutions for the energy supply, such as renewable energy and heat pump technologies [30].

As stated above, the building sector is responsible for around a third of energy consumption and a quarter of CO_2 emissions globally. In order to face the environmental crisis, hence reducing energy consumption and utilizing energy-efficient supply technologies & clean energy sources in buildings are of crucial significance. With this regard, the net-zero-energy building (NZEB) concept gains importance [19]. In a NZEB, first, the building envelope is retrofitted (if it was already constructed) or enhanced (if it is newly constructed) to reduce energy consumption. Second, over a certain period of time, typically one year, the amount of energy production and consumption reaches a net zero energy equilibrium. Third, during

this time, the amount of energy required to keep the comfort of the building occupants within acceptable limits is produced on or near the building by renewable energy sources [31]. As a result of these significant aspects, the NZEB concept is at the forefront of climate policies.

1.3 RENEWABLE ENERGY AND HEAT PUMP UTILIZATION IN BUILDINGS

Renewable energy is a main pillar of the transition to decarbonized and sustainable energy systems, and it is obtained from such sources that are naturally replenished, such as solar, wind, marine, hydro, geothermal, and bioenergy [32]. On a global scale, there has been a tremendous growth in the utilization, implementation, and penetration of the renewable energy sources (RES) into all sector in recent years. This trend is accompanied by the rapid cost reductions for several renewable energy technologies (particularly for solar and wind power), desires to combat the climate change, and governmental supports to diversify and secure energy supply [32], [33].

The world total final energy is supplied across three main energy carriers: heat, fuel, and electricity. The percentile distribution of these carriers reveals significant insights about the renewable energy statue. Today, still only a small fraction of the world total final energy supply (TFES) is produced from RES. Based on the latest available data, this proportion was 12.68% in 2021 [35], where the largest shares were renewable electricity (6.81%), renewable heat (4.82%), and renewable fuel (1.05%). Figure 1.2 shows the proportion of these renewable energy carriers in the TFES in 2021.

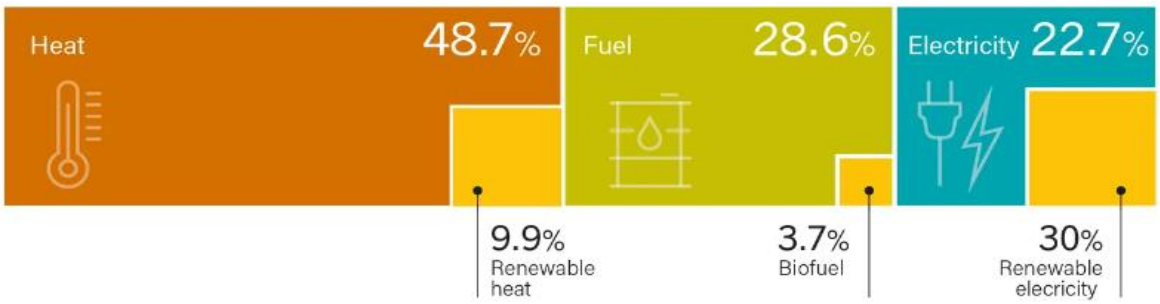

Figure 1.2: The share of different renewable energy forms in the TFES, 2021 [34].

The majority of TFE is supplied in the form of direct heat (48.7%, see Figure 1.2), where renewables contribute around one in ten of this proportion with the geothermal, solar, and biomass sources. The second largest energy carrier in the TFES is the fuel (28.6%), where the renewable energy contributes only 3.7% of this percentage which is mainly used as liquid and gaseous fuels for transport. The third TFES carrier is the electricity (22.7%) and the renewable energy contributes around one-third of this proportion with various sources, such as solar, wind, hydro, biomass, and geothermal [34].

As stated in the previous section, building sector is the largest energy consumer that requires energy in the form of both heat and electricity. Accordingly, integrating renewables into the buildings, to produce both heat and electricity, becomes a necessity for a decarbonized building sector. However, RES currently meets less than 14% of the total energy demand in buildings [23]. This is often due to the cost, compatibility, design, and operational challenges of integrating renewable resources into buildings. In this perspective, solar is the most appropriate RES that can be used in buildings to generate renewable heat and electricity due to the on-site energy production avoiding the inherent challenges of energy, such as transportation and distribution [35].

For electrical energy (EE) generation, silicon-based PV panels dominate today's market with efficiencies ranging between 10-20% [36]. Although their conversion efficiency is low, PV cells actually absorb as high as 90% of the incoming solar radiation but only 15% of this proportion is converted into electricity [37]. The gap, which is almost 75% of the incoming solar radiation, is converted into recoverable and reusable heat. However, in PV panels this heat is not utilised, instead, it accumulates on the PV cells and is released into the atmosphere over time, which increases the temperature of the cells and reduces their efficiency [38]. An alternative approach to the waste heat accumulated on the PV cells is to use a novel collector type called photovoltaic/thermal (PV/T). PV/T stands for photovoltaic and thermal solar

components combined on the same panel structure to produce power and usable heat at the same time. This design allows the combined electrical and thermal efficiency of the panels around 70% [39], which makes PV/T panels particularly suitable for residential buildings as it maximizes the energy generation per m^2 of the limited roof spaces. However, a robust and mature PV/T market has not yet been established globally.

For the solar-heat in buildings, evacuated tube collectors (ETC) and flat plate collectors (FPC) are the market-mature collector types whose operational temperature range is between 60-220 Cº, with efficiencies exceeding 50% [40]. In most domestic applications (where the required temperature is usually in between 30- 60 Cº [41]), the thermal output of these panels is stored and utilized for different purposes, such as SH and DHW. Based on the latest data [41], [42], however, 86% of the building-installed solar thermal collectors worldwide are used for DHW-only provision. Applications aiming to also provide SH constitute only 6% of the installed capacity. This low proportion is primarily due to the mismatch between the high space heating demands and the low solar availability in the winter seasons. As a result the most common utilization of the building-installed solar thermal panel systems is limited to DHW-only generation worldwide [43].

Another essential solution for a decarbonized building sector is to use heat pump (HP) technology. The HPs are electrically driven vapour compression cycles (VCC) which can be reversed to provide both heating and cooling. A HP extracts heat from a low temperature reservoir (air, water, or ground), amplifies this heat and transfers to a higher temperature sink with the aid of a compression process in the cycle. Due to the compression process, the HPs are more energy efficient than conventional gas boilers or electrical heaters [44]. This high efficiency leads the thermal demands of the buildings can be substantially lowered with the HP utilization. Moreover, due to the electrically driven compression process, HPs electrify the thermal demands, unlocking the potential to increase the share of RES in

buildings, especially for solar energy [45]. However, despite the advantages, still only 10 % of the building's thermal demand is satisfied by heat pumps globally. Thus, more policy support and technical innovations are required to enhance the market adaptation and remove the barriers to the widespread utilization of the technology [44].

1.4 AIMS AND OBJECTIVES

This thesis focuses on the combination of solar energy and heat pump technology, called solar-assisted heat pump (SAHP) systems to overcome the issues stated in the previous sections, such as high energy consumption of the residential building sector, lack of building construction guidance or standards, and the insufficient utilization of the solar energy and HP technologies in the buildings. Globally, the development of SAHP technology is constrained by uncertainties brought on by a lack of information about such systems as a result of high capital investment costs and the limited number of applications. In order to close this research gap, this thesis therefore aims to investigate the techno-economic feasibility of the SAHP systems for residential single-family houses at the distributed level in the European region while ensuring that the energy demand side management is in line with the regional building standards. The thesis therefore has two novelty aspects. First, a detailed guideline is given on how to dynamically obtain (different from building standards) not only SH and SC, but also other demand vectors (e.g. DHW and EE) needed by a single-family house. Second, moreover, possible innovative configurations for maximising the energy output of SAHP systems are explored. The contribution of the thesis is given in Section 2.10 and the novelty aspects of the study are detailed in each corresponding main research chapters (4, 5, and 6).

The objectives determined to achieve the aim of the thesis are as follows:

1. To examine all components of building applied SAHP systems individually and identify

the research gaps by reviewing recent pioneering studies in the literature.

2. To determine the suitable modelling approaches and software.

3. To model an exemplary residential single-family house for the purpose of evaluating the dynamic energy consumption of the thermal and electrical end-users of the European buildings, which can serve a guide for the locations where the authorities do not set the building regulations.

4. To illustrate how to design, model, and size a fundamental SAHP system holistically, as well as to demonstrate the techno-economic competitiveness of such systems in a case location where the SAHP systems have high potential but lack awareness.

5. To evaluate the techno-economic feasibility of an innovative SAHP system in different climatic boundary conditions of the European region, representing cold, moderate, and hot climates.

1.5 THESIS STRUCTURE

This thesis contains 7 chapters. **Chapter 1** introduces the essential research background information and identifies the key aims and objectives of the thesis. **Chapter 2** presents a comprehensive literature review on the SAHP systems. The chapter begins with the designs, working principles, and market overviews of the individual components that constitute the building applied SAHP systems, including different solar panel types, storage units, and heat pumps. Then, different configurations of the solar + HP systems are reviewed. Moreover, a critical review of the state-of-the-art pioneering studies in the literature is presented to clearly identify the research gaps. The final section of the chapter is dedicated to the summary of these gaps and the contribution of the thesis to the existing literature. **Chapter 3** presents an overview of the methodology of the thesis by explaining the methods and software used to actualize the research. **Chapter 4** provides a study on how to calculate the

dynamic energy demand profiles of an exemplary residential building using the lumped capacitance building component of the commercial TRNSYS software. The study aims to be used for accurately sizing and designing energy-generating systems and be a guide for the locations where the building energy regulations do not exist. In **Chapter 5** a basic PV+HP system is modelled holistically to analyse the techno-economic competitiveness of such SAHP systems with the grid energy price for the locations that do not have enough attention to the technology. An air-sourced HP is used in the system which has the technical possibility of reversing the thermodynamic cycle to provide SH during the winter and SC during the summer seasons. As a result, the system aims to electrify and supply all energy demand vectors of a typical European residential single-family house with the HP and PV units to reach the NZEB concept. **Chapter 6** analyses an innovative SAHP system that contains the PV/T panels, stratified storage tanks, and a water-sourced HP unit. The system aims to investigate the techno-economic feasibility of such SAHP systems in different climatic boundary conditions by means of meeting all SH, DHW, and EE demand vectors of an exemplary single-family house in three different European cities.

Chapter 7 draws an overall conclusion for the thesis and underlines possible future works with recommendations.

CHAPTER 2

Literature Review

2.1 INTRODUCTION

This chapter provides details on the subjects stated in Chapter 1 and consists of ten main sections. First, solar thermal and electricity generation methods are discussed separately through different panel types including the FPC, ETC and PV in different sections. Then, hybrid PV/T panels are reviewed considering their design and performance. In addition, the thermal energy storage options are discussed including sensible and latent storage units. Further, the heat pump technology and the concept of the solar + HP combination are reviewed separately. Moreover, the solar-assisted heat pump applications are critically reviewed and comprehensively discussed. Finally, the last two sections present a summary of the key findings of the literature review and research gaps that are fulfilled with the thesis.

2.2 SOLAR THERMAL ENERGY

Solar energy has a high capability of delivering efficient and low-cost thermal energy both for domestic and industrial uses. Classification of the solar thermal collectors can be various. Based on their size, solar thermal systems can generically be divided into two categories: large-scale and small-scale systems [46]. The large-scale systems are usually in charge of delivering the heating demand of the industrial applications or generating electricity in mega-Watts, which are usually based on Rankine cycles. Small-scale systems, on the other hand, are mainly used in residential buildings such as single-family houses through the solar thermal collectors. A general overview of the marked-ready solar thermal collectors and comparison of their specifications is presented in Table 2.1.

Solar thermal collectors convert the incident solar radiation into thermal energy and transmit it to a working fluid flowing through the collectors [47]. The obtained thermal energy can be used for domestic hot water or space heating or be stored in a thermal storage tank for later uses. Regarding their temperature outputs, solar thermal collectors may be categorised

as stationery and sun tracking & concentrating collectors. The sun tracking & concentrating solar collectors consist of parabolic trough collectors, linear Fresnel collectors, parabolic dish reflectors, and heliostat field collectors. The range of temperature outputs of these collectors is in between 60 ℃ and 2000 ℃ [47]. Whereas the stationary collectors consist of flat-panel collectors (FPC), evacuated tube collectors (ETC), and compound parabolic collector and that their temperature output is usually in between 30 ℃ and 240 ℃ [46]. Considering these temperature outputs, as a single-family house requires a heat source less than 100 ℃ for domestic hot water and space heating, it is obvious to conclude that the FPCs and ETCs are the most suitable collector types that can be employed in single-family house applications [47], [48]. Thus, in the following sections, only these collector types are investigated in detail.

Table 2.1: Solar thermal collectors and their specifications by Kalogirou [47].

	Collector Type	**Absorber Type**	**Concentration ratio**	**Operation Temperature (℃)**
Stationary	Flat plate	Flat	1	30-80
	Evacuated tube	Flat or Tubular	1	50-200
	Compound parabolic	Tubular	1-5	60-240
Single-axis tracking	Linear Fresnel	Tubular	10-40	60-250
	Parabolic through	Tubular	15-45	60-300
	Cylindrical through	Tubular	10-50	60-300
Two-axes tracking	Parabolic dish reflector	Point	100-1000	100-500
	Heliostat field	Point	100-1500	150-2000

2.2.1 Flat Plate Collectors (FPC)

Flat plate collectors have a low maintenance cost and the simplest design compared to other solar collector types. The output temperature of a flat plate collector is generally between 30 °C and 80 °C, hence they are utilized commonly in building applications for domestic hot water production [47].

Flat plate collectors can be glazed or unglazed. They usually have a fixed permanent position and do not track the sun. The solar irradiation first passes through a transparent coverage and heats up an absorber plate attached to the heat carrier tubes. The absorbed energy is then transferred to the working fluid in these tubes and conveyed for subsequent use or storage. The components of a typical FPC consist of the following components as shown in Figure 2.1 [47], [46]:

• Glazing (single or double): the glazing is transparent and used to reduce the convection and radiation losses.

• Tubes or passages: used to transfer or direct the flowing fluid from the inlet to the outlet.

• Absorber plate: used to absorb the incident solar irradiation and to hold the tubes or passages.

• Headers: used to charge and discharge the working fluid.

• Insulation: used to reduce the collector heat losses (back and sides).

• Casing: used as a box to hold the above components in place and protect them from dust or moisture.

For an optimum orientation, Kalogirou [49] states that the FPCs should be directed towards the equator, which means that the collectors should face north in the southern hemisphere

and south in the northern hemisphere. For the optimum tilt angle of the collector, in addition, the latitude of the location can be used with $\pm$10-15^{o} angle variations.

Despite the advantages, however, it has to be noted that the FPCs perform better in sunny or warm climates and their performance may significantly be affected in cold, cloudy and windy days. Furthermore, this unfavourable weather conditions might cause system failures as moisture and /or condensation lead to early deterioration of internal materials [47].

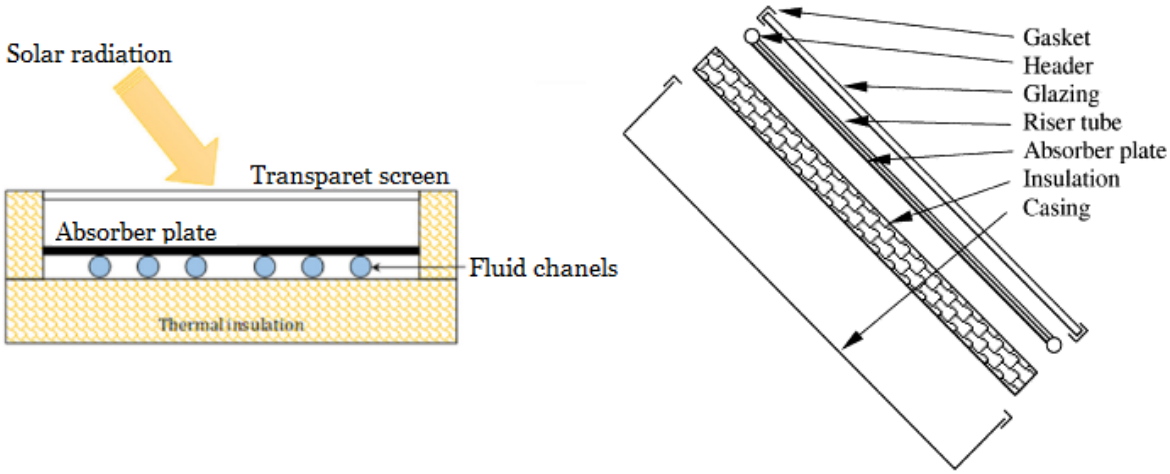

Figure 2.1: A schematic of a typical flat plate collector [47].

Another drawback for the FPC is the low efficiency resulting (i) from convectional heat losses through the glass cover for glazed or through the ambient air for unglazed, and (ii) from the absence of the sun tracking. Finally, compared to other collector types, flat plate collectors have the lowest efficiency profile.

2.2.2 Evacuated Tube Collectors (ETC)

In today's market, evacuated tube collectors (ETC) are a key component of solar thermal utilization and widely used for applications where higher temperatures are required. They are commonly employed in residential buildings for the domestic hot water and space heating supply. The operating temperature range of a typical ETC is between 50 °C and 200

°C [50]. Unlike the FPC, these collectors perform better in unfavourable climates and are suitable even for cold weather conditions due to their tubular design. Thus, their thermal performance is significantly higher than those of flat panels [51], [52].

The design and operation principles of the ETCs are different from other solar thermal collectors. As shown in Figure 2.2, an evacuated tube collector is made of identical glass pipes that are placed in parallel. Each evacuated pipe has two tubes. While the first one is called the absorber / inner tube and coated with a selective material, the second one is called the outer tube and is transparent. The reflection properties of both tubes are minimum and they are fused together on top to form a vacuumed area. When the solar radiation passes the transparent outer tube, it goes through the vacuumed area in between two tubes. This vacuum allows the solar radiation to pass through but prevents the heat to be transferred. Hence, the solar heat is kept inside the inner tube [50].

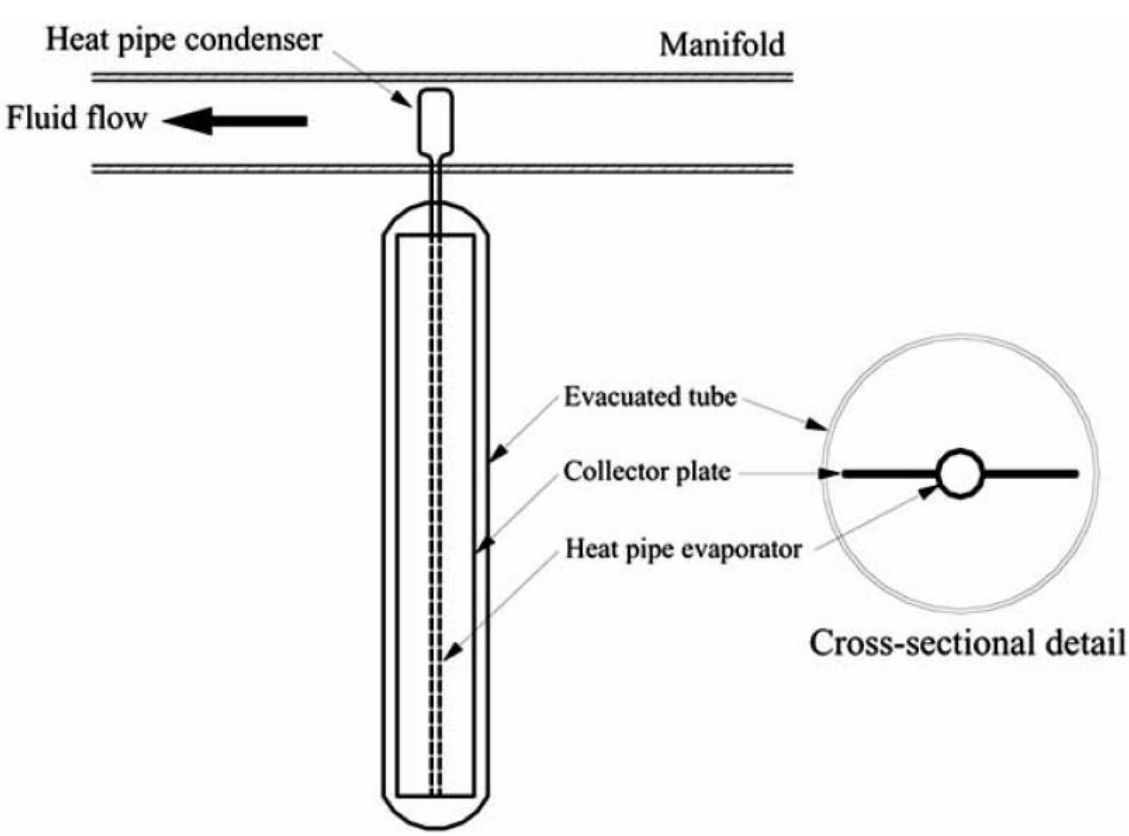

Figure 2.2: A schematic view of an evacuated tube collector with the cross section [53].

Unlike the FPCs, the operation principle of an ETC is based on liquid–vapour phase change materials. A highly efficient thermal conductor called heat pipe, which is a sealed copper pipe, is placed inside the vacuum-sealed glass tubes. This pipe contains a small amount of working fluid (e.g. methanol) that undergoes a phase-change cycle and that it is attached to the absorber (inner) tube for heat transfer. At the top of the pipe, a metal tip is attached to work as a condenser. In the cycle, the working fluid (inside the heat pipe) is evaporated by the solar heat that is kept in the inner tube. The vapour then goes to the condensation at the heat sink and releases its latent heat. After the condensation, the fluid goes back to the collector and the cycle is repeated [53].

With this vacuum design between two concentric glass tubes, convection and conduction heat losses become almost negligible, providing significantly higher performance than other types of solar thermal collectors.

2.3 SOLAR PHOTOVOLTAIC (PV)

The most common solar electricity generation in today's market is through photovoltaic (PV) panels. For the terminology, the "photo" refers to light and the "voltaic" means electricity. A PV panel is made of photovoltaic cells, also known as solar cells. A PV cell is a device converting sunlight into direct electricity without any heat engines interfering. It consists of thin layers of semiconductor materials, which generate electricity when exposed to sunlight. Photovoltaic cells have at least two layers of the semiconductor materials charged positively or negatively which are called the p and n layers. When the cell is exposed to the light, an electrical field occurs between these two layers causing a potential difference. This voltage existence is called photovoltaic effect and can be connected to a circuit to generate electricity [54], [55].

On a PV panel, single photovoltaic cells are connected in serial-parallel configurations to

form modules, and the modules are connected in groups to form an array as shown in Figure 2.3.

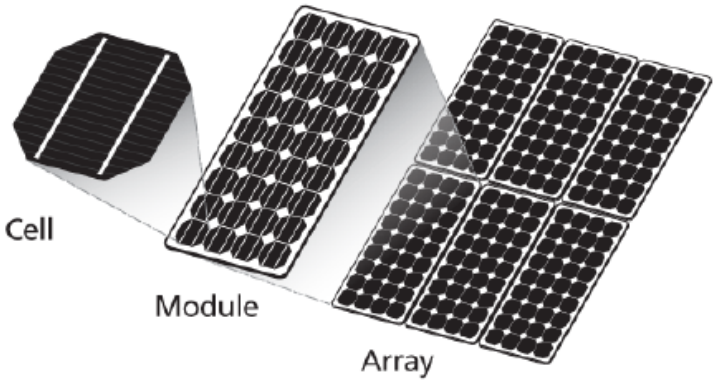

Figure 2.3: Configuration of a photovoltaic cell, module and array.

2.3.1 PV Panel Types and Performance

Several different semiconductor materials can be used to form the layers of a solar cell where each material has its own advantages and disadvantages. Based on these materials, solar photovoltaics can be divided into five main categories as shown in Figure 2.4.

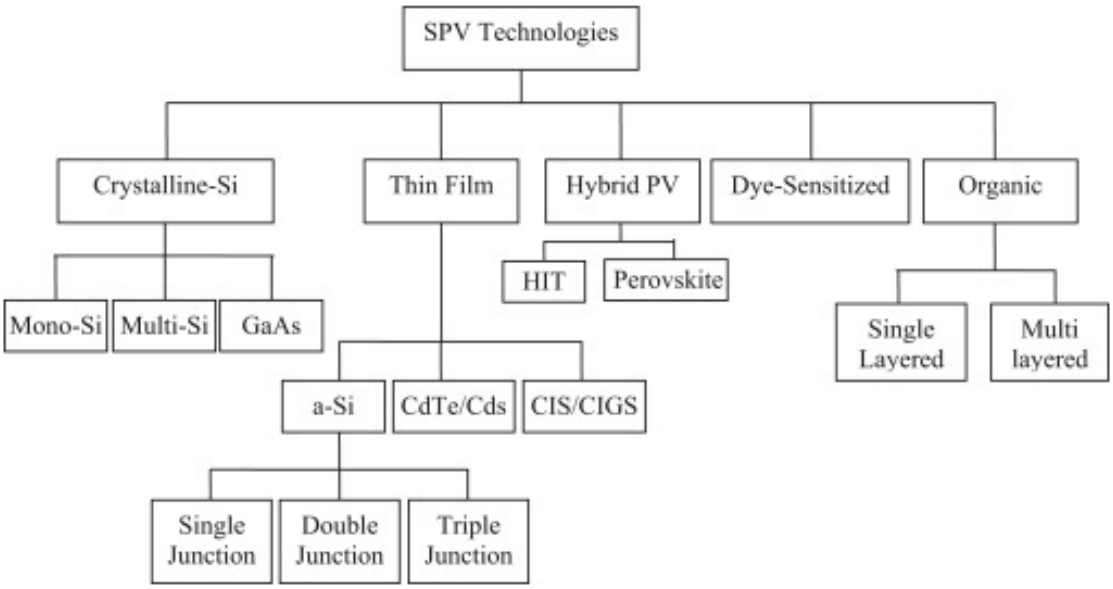

Figure 2.4: Different cell materials for solar PV [56].

As silicon is a safe and abundant semiconductor material and has a high conversion efficiency resulting in good performances, it is the most preferred cell material worldwide [57]. Today, the crystalline based silicon cells (consisting of the mono-crystalline and multi/polycrystalline silicon cells) dominate PV market, accounting for about 90% of the total residential solar panel market [56]. However, non-crystalline based amorphous silicon cells (falling under the thin-film solar cell category, see Figure 2.4) are on a fast track and have the potential to become widespread. Due to this high market adaptability, the proposed systems in this thesis use the silicon-based photovoltaic cells, hence the hybrid, dye-sensitized, and organic materials are not investigated in the following sections.

2.3.1.1 Mono-crystalline PV panels

Mono-crystalline PVs are the oldest, and the most used and efficient panel type. For these panels, the cells are manufactured with the Czochralski method where a cylindrical shape ingot is formed with a molten vat of pure silicon at a high temperature [53]. It is then sliced into thin silicon wafers to be used in the solar modules. Mono-crystalline panels have the highest efficiency and power capacity rates. This is because a mono-crystalline cell contains a single layer of crystal silicon allowing electrons to easily move throughout the cell [54]. Currently, the highest reported conversion efficiency of a mono-crystalline cell under the standard test conditions is 26.7% [58]. However, a typical commercial mono-crystalline cell today has an efficiency range from 15% to 22% in the PV market [57]. Similarly, most mono-crystalline PV panels have a power output usually in between 320-375W [59]. This high performance makes the mono-crystalline panels suitable for residential uses, as fewer panels would be required to generate a certain amount of power in the limited roof area. Another advantage of these panels is that they have a relatively longer lifespan [60]. On the other hand, a mono-crystalline panel are the less cost-effective option among the other three types because purification & fabrication of silicon wafers is an expensive process. Therefore,

the cost reduction through different manufacturing methods or other materials, such as polycrystalline silicon, has taken the attention of many researchers and manufacturers [56].

2.3.1.2 Poly-crystalline PV panels

Poly-crystalline silicon is a material that contains small silicon crystals. The cells are manufactured by pouring molten raw silicon into a square mould which it is then cooled and sliced into blocks and wafers [54]. The polycrystalline panels are less efficient than mono-crystalline panels as they consist of multiple silicon cells where the movement of the electrons is restricted, resulting in efficiency penalties. The efficiency rate of a commercial polycrystalline panel in today's market is in between 13% - 17% and the power output is usually between 240W-300W [56], [58], [59]. Although they are less efficient than mono-crystalline cells, poly-crystalline cells have been commonly utilized in the past decades for module manufacturing, as they are more cost-effective. The low cost allows poly-crystalline panels to gain a significant market share, especially in the last two decades as shown in Figure 2.5.

2.3.1.3 Amorphous silicon (a-Si) PV panels

Amorphous silicon (a-Si) panels are made of non-crystalline silicon and the structure of the silicon in the cells is disordered. They are the first commercially produced and the most developed thin-film PV technology that has an impact on today's PV market (shown in Figure 2.5). The cells are manufactured by deposition of the silicon on large and low-cost substrates such as glass, steel, polymer, or plastic [61]. The manufacturing process does not require high temperatures; hence, less energy is utilized for the production. Furthermore, the sunlight absorptivity rate of the amorphous silicon solar cells is about 40 times higher than those of crystalline-based silicon cells [61]. Therefore, the thickness required to produce an a-Si cell is almost 200 times less than the thickness required by an equivalent crystalline silicon cell [53]. These two factors (less energy requirement and material use) reduce the

cost substantially hence makes the amorphous silicon solar panels the cheapest option among the other types.

However, the lower conversion efficiency of the amorphous silicon solar cells is still a major cause of concerns as the commercially available cells have a typical efficiency rate of 4-8% [58]. This places a significant drawback for residential utilization as lower efficiency leads to more space coverage compare to crystalline silicon cells for a same power output. Moreover, the degradation of the power output of the a-Si panels in outdoor conditions is much faster than crystalline silicon cells. Therefore, amorphous silicon solar panels require to be replaced more often, which means more long-term recurring costs [59], [62].

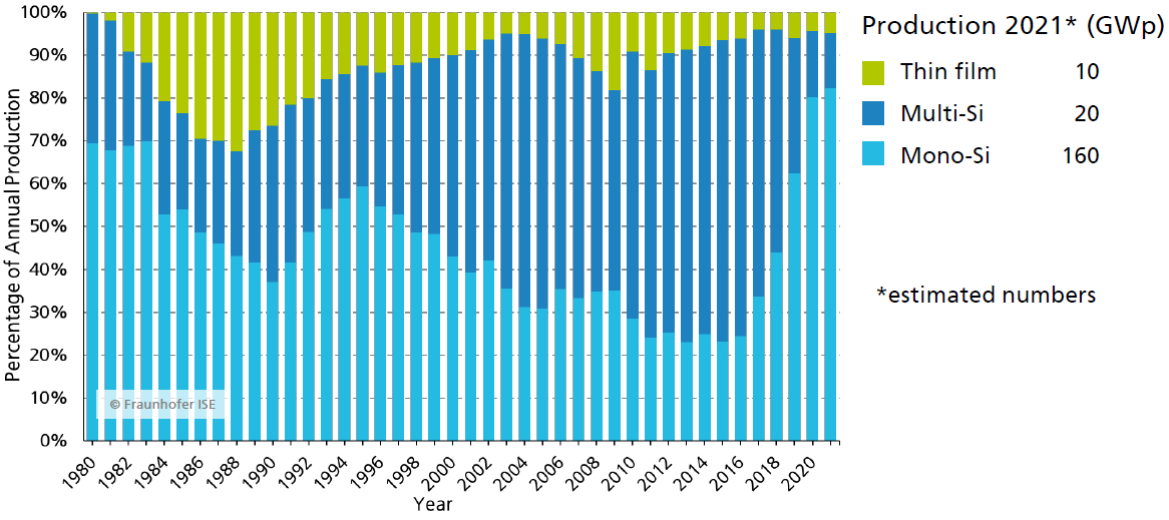

Figure 2.5: Percentage of PV production by technology, worldwide [58].

2.3.2 Factors Affecting the PV Performance

As stated in the previous section, photovoltaic is the most suitable technology for solar electricity generation in residential houses. However, the majority of the commercial photovoltaic panels dominating the PV market (discussed in the previous section) has a conversion efficiency less than 20%. There are many parameters affecting this low efficiency rate including thermal absorptivity and degradation of the utilized material, the maximum power point of the produced module, and atmospheric condition (such as solar

irradiation, wind speed and ambient temperature) [63]. Among these, solar irradiance and the cell's operation temperature have a direct impact on the overall electrical efficiency of a PV module. Detailed temperature and efficiency correlations based on weather conditions and the cell's working principles can be found in works conducted by Skoplaki and Palyvos [64], [65]. For solar irradiance, an increase in the amount of sunlight results in an obvious increase in the produced current and consequently increases the power output of the module [66].

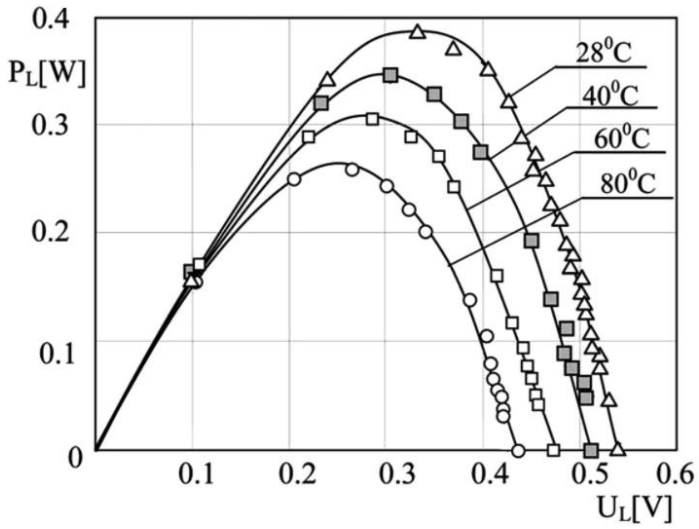

Figure 2.6: The temperature effect on the power output of a mono-crystalline silicon PV [67].

For the temperature, however, an increase in the cell temperature decreases the open-circuit voltage of a PV module, hence reducing the power output of the module as shown in Figure 2.6. This occurs because silicon is a semiconductor material sensitive to heat. When the temperature of the cell increases, the band gap of the semiconductor material decreases, and lower energy is required for the electrons to break the bond [68], [67]. As a result, the PV cell becomes less efficient, and generates less electricity. Zhang et al. [38] experimentally showed this where an increase of 1 C^0 in the PV cells causes an efficiency reduction between 0.25% - 0.5% for most silicon panels.

One of the main reasons for the temperature increase in the cells is the internal dissipation of solar energy during the power production in the PV cell [68]. When the sunlight hits a PV surface, the cells normally absorb around 90% of the incident solar radiation, nevertheless, only a small proportion (15%) of the absorbed energy is converted into electricity. The rest of the absorbed incident energy is not used. Instead, it is released into the atmosphere in the form of heat, which passes through the cell structure leading the extreme working conditions as high as 50 °C above the ambient. Another undesirable consequence is that the structure of the module can be damaged permanently if the thermal stress remains for long periods [69]. For an optimum PV performance, therefore, a low temperature distribution across the PV cells is essential, which is achievable through a novel panel type called photovoltaic/thermal explained in the next section.

2.4 SOLAR PHOTOVOLTAIC/THERMAL (PV/T) PANELS

2.4.1 Fundamental Concepts

Photovoltaic/thermal (PV/T) is a panel type that can generate solar electricity and solar thermal energy at the same time from one integrated component. Although a significant amount of R&D work has been progressed in recent decades, a robust and mature PV/T market has not been established. A PV/T has the same panel structure as the conventional solar thermal collectors (e.g. see FPC, in Section 2.2) but its absorber is covered by a PV layer [70]. In other words, the PV is utilized as a thermal absorber for the thermal collectors. The main components of a typical flat-plate PV/T panel is shown in Figure 2.7.

In a PV/T panel, the PV layer generates electricity while the absorbed thermal energy is transferred to a working fluid instead of dissipating it to the environment [63], [69]. This thermal energy can be used for the DHW and space heating needs or be stored in a storage unit for a later utilization. An example can be found in the works conducted by Herrando et al. [71] where it is shown that a PVT system can cover 51% of electrical and 36% of the

DHW demands for a residential house located in London - UK. Similarly, Hazami et al. [72] found that a PVT system can meet the majority of the DHW and power needs of a single Tunisian house with the maximum thermal and electrical exergy efficiencies of 50% and 14.8%, respectively.

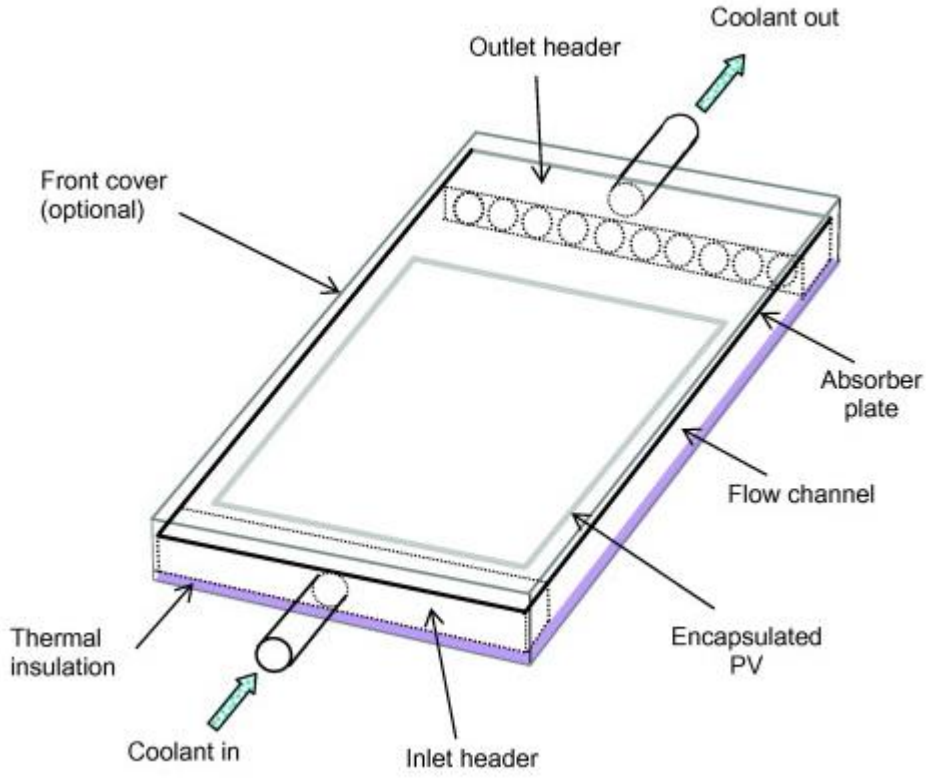

Figure 2.7: Typical layout of a flat-plate PV/T panel, Chow [69].

Due to the negative effect of the temperature on the PV performance explained in the previous section, removing heat from the PV assists to improve the cell efficiency. As a result, the electrical efficiency of the PV/Ts increase. Moreover, waste heat recovery allows the combined efficiency (thermal + electrical) of a single panel reaches to as high as 70-80% [73]. Other advantages of the PV/T panels can be listed as follows [70], [74], [75], [76] :

• **Less space utilization**; it is acknowledged that the thermal efficiency of the PV/T panels is lower than the individual conventional solar thermal collectors. However, PV/T panels have a higher combined -electrical and thermal- efficiency than the conventional panels per unit area. Therefore, a space covered with PV/T panels usually gives more energy per unit

area than when the same space is covered with conventional individual solar thermal and/or PV panels. This is particularly important for the residential buildings as the available rooftop area for solar panels is usually limited to 50% of the total roof area [77]. Thus, PV/T panels can bring a practical solution for maximizing the energy generation per $m^2$of the limited roof areas.

• **Architectural uniformity**; PV/T panels are perceived aesthetically better than side-by-side separate placement of the conventional solar thermal and PV panels, hence can keep the architectural uniformity on the roof.

• **Cost;** linking to the combined efficiency, PV/T panels reduce the energy cost generated per unit area. In addition, the cost required to install one combined panel is less than installing two separated arrays of solar thermal collectors and PVs side-by-side.

2.4.2 PV/T Panel Types and Design

A PV/T design can be categorized based on many different approaches such as the working fluid that cools the PV cells and remove the excess heat, the material used for the PV cells, the sun tracking system, and being glazed or unglazed. Despite the distinctive approaches in the literature, however, a generic classification can be based on the structure of the design. In a recently published review paper, Jia et.al [78] classified common types of the PV/T panels as flat-plate, concentrated, and other various types.

Starting with the flat-plate PV/T panels, they harvest solar beam and/or diffuse radiation without tracking the sun. They also have the simplest design, require little maintenance, and are the most developed PV/T panels compared to the other types [79]. Flat-plate PV/T panels are generally utilized in applications where the moderate temperatures are required, due to the FPC characteristics (see Section 2.2). Therefore, they can be used in building applications for space heating and domestic hot water provision. As they do not track the

sun, their position is optimised for specific locations, and usually fixed to an integral part of the building such as wall bodies or rooftops [78]. A fundamental flat-plate PV/T is made of the solar cells, a flat absorber, fluid tubes, sealed and insulation materials which are limiting the conduction losses. Flat-plate PV/Ts can be glazed or unglazed but a glass cover has the advantages of protecting the absorber, and reducing both radiation and convection losses [80].

Based on the working fluid, there are three types of the flat-plate PV/Ts namely, air-PV/Ts, liquid-PV/Ts, and air-liquid-PV/Ts. An air flat PV/T is essentially the same as the liquid ones but the only difference is that the ducts are used for heat removal instead of the tubes. Although there is plenty of work conducted for air and air-liquid PV/Ts, the most accepted and adopted working fluid for the flat-plate PV/Ts is liquid, more specifically water [78], [80]. This is because water, as a working fluid, has a higher thermal stability then the air, hence leading to a better overall efficiency [81]. Therefore, in this thesis, only water-based PV/T (w-PV/T) panels are used and explained in detail.

Figure 2.8 shows the different types of the w-PV/Ts based on the components and the fluid flow methods. In the literature, the most accepted classification comes from Zondag et al. [70], where four different w-PV/T types are presented based on flow pattern of the water and the method of the heat exchange. These are 1) sheet-and-tube, 2) channel, 3) free-flow, and 4) two-absorber, as shown in Figure 2.8.

Among these designs, sheet-and-tube PV/T (Figure 2.8-1) is the most preferred design in the key literature. This is because integrating a conventional PV panel into a traditional flat-plate thermal collector is the easiest and most cost-effective way to manufacture a PV/T panel without any significant modifications. Although utilizing more than one glass cover (Figure 2.8-2) can enhance the thermal insulation of the panel, it reduces the electrical

efficiency of the panel due to the additional reflections of each cover. Similarly, in channel-PV/T panels (Figure-2.8-3), evaporation of the free-flow causes the thermal efficiency penalties. Finally, in the two-absorber PV/T panels (Figure 2.8-4), the design of the channels is of critical importance. This is because, if the channels are too wide, a thick glass would be required to withstand the high water pressure, which is not desirable in terms of cost and efficiency. For these reasons, sheet-and-tube PV/T panels are used in this thesis.

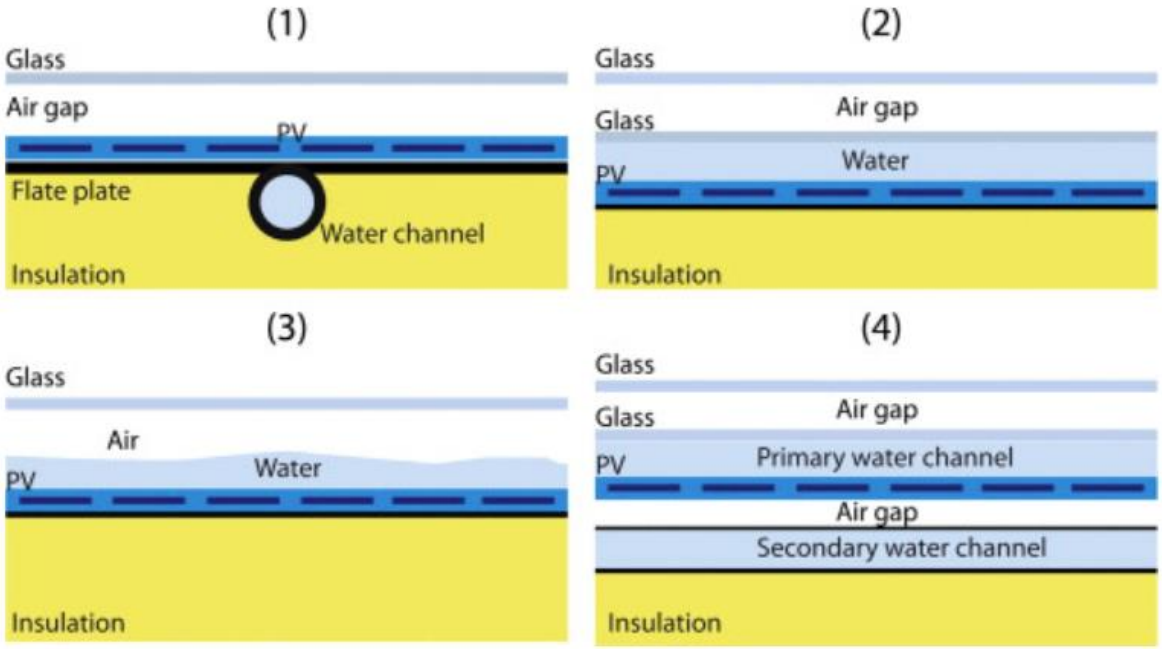

Figure 2.8. Cross section of different w-PV/T types [81].

Furthermore, sheet-and-tube w-PV/T panels can be covered or uncovered. As mentioned above, covered PV/T panels have a higher performance than uncovered panels. This is because the absorber of the panel is not in direct contact with the ambient, hence the thermal heat losses are reduced. Therefore, it is generally convenient to utilize a coverage to minimize the losses, although it is acknowledged that the electrical efficiency may be proportionally affected due to the reflection caused by coverage material, which is generally glass. However, Aste et al. [81] stated that the air gap between the glass and the absorber should be thin enough to increase the thermal insulation ability, which is usually between

15 mm and 40 mm thick. In addition, the glass thickness should not be high for efficiency reasons, hence the commonly accepted thickness in the literature is 3mm - 4mm [82], [83]. Further, the area of a glazed panel is commonly not considered larger than 3 m^2 to increase the stability, as wind and structural loads may occur on the cover's surface; although some manufacturers use more durable materials to overcome this issue, such as polyvinyl fluoride and polycarbonate [80].

Regarding the photovoltaic part of the PV/Ts, the most commonly utilized PV technology is the silicon based photovoltaics, in particular crystalline silicon cells (see Section 2.3) [82], [84]. Moreover, for the reasons explained in detail in Section 2.3.1.1, mono-crystalline photovoltaic cells are used in this thesis.

Regarding the construction of the sheet-and-tube w-PV/T panels, the photovoltaic part is attached to a flat-plate absorber as aforementioned. The flat design of the absorber leads an easy attachment as it has a suitable flat surface for the cells of the PV laminates to be connected. The most common method for this connection is called gluing technique, where a thermos-conducting glue (resistant to high temperatures) is used to connect the cells and absorber as detailed in [81]. For the absorber, two properties are of critical importance, which are thermal conductivity and specific heat capacity. For the former, a high value is always favourable because a greater thermal conductivity allows a faster passage of the heat flux from the PV cells to the fluid. For the latter, however, a low value is desirable as a lower specific heat capacity permits fast reaction times to the fluctuating ambient temperatures [81]. Due to these two characteristics, the absorber of a PV/T panel is generally made of metallic materials. Table 2.2 shows the suitable metallic materials with their important parameters, where it is acknowledged that steel and polymers are in rare utilization.

Table 2.2: Important parameters of the suitable absorber materials [81].

Absorber materials	Thickness (mm)	Density (kg/m^3)	Thermal conductivity (W/mK)	Heat capacity (J/kgK)
Copper	~0.3	8920	380	350
Aluminium	~1	2700	160	900
Steel	~2	7860	50	450
Polymer	~2-3	900-1500	0.2-0.8	1200-1800

The second type of Jia et al. [78]'s PV/T classification is the concentrated PV/Ts, as mentioned earlier. Concentrated type PV/Ts use a reflector to focus the incoming solar radiation on a PV surface. The reflectors can be dish, parabolic and Fresnel types [69]. For the applications requiring high temperatures, a larger reflector can be used with an optical device between solar radiation and the absorber surface to increase the radiation intensity, hence reducing the PV area. The direct current generated by a concentrated type PV/T is much higher than the flat-plate types, thus yielding a higher electrical efficiency [85]. However, they are much more expensive than the flat-type PV/Ts due to their design complexity and sun tracking systems. In addition, reducing the temperature of the PV cells in a concentrated PV/T is critically important as the cells can be irreversibly damaged due to the high working temperatures resulting from high concentration ratios [86]. Maintenance costs, as a result, are also higher than those of flat-plate PV/Ts [87].

Finally, the third type of the PV/T classification is the ones named as 'other-types' including phase change material integrated, thermoelectric generator integrated, solar still integrated, and nano-fluid integrated PV/T types [78]. However, due to the system complexity,

excessive installation costs, and sun-tracking requirements, concentrated and novel-type PV/T panels are not suitable types for single-family applications. Therefore, the second and third types are out of the scope of this thesis.

2.4.3 Performance Factors of the PV/Ts

The design has a critical impact on the overall performance of the PV/T panels. Thus, the material used, thermal conductivity of the absorber, number of the covers and collector dimensions were some parameters investigated in the previous section. However, there are also environmental and operational parameters that affect the efficiency of a water based PV/T panel. Three main factors are of crucial importance affecting the electrical and thermal performance of the PV/Ts. These are the climatic conditions, mass flow rate of the working fluid, and the size of the storage tank in a PV/T system.

Climatic condition is a generic term here describing the application's ambient air temperature, wind speed, solar irradiation, and location (latitude and longitude). A combination of these parameters can define the overall performance of a solar PV/T energy system in a specific location. This performance can be assessed by a dimensionless value called solar fraction (S*f)* which refers to the proportion of the total energy demand (thermal and/or electricity) covered by solar energy. The typical value of the solar fraction of a PV/T system is found to be ranging between 40% - 90% depending on the climatic conditions and the total energy demand of the application [88], [72], [89], [90].

The second critical factor is the mass flow rate of the working fluid, which is water in this case, circulating in the PV/T tubes. The circulation can be natural or forced as stated by Chow et al. [91], where the forced flow is achieved commonly by using circulation pumps. There are numerous investigations in the literature attempting to assess the effect of the mass flow rate of the working fluid on the performance of the PV/Ts, and to standardize a common

flow rate for similar applications. Some examples can be found in [92], [93] and [89]. Regarding the performance assessment, the generally accepted conclusion is that PV/T efficiency is a function of the flow rate (mass flux). This is because an increase in the water velocity in tubes enhance the heat transfer coefficient of the tube which results a better heat transfer, hence efficiency [94]. However, it has to be noted that, a higher flow rate for the forced circulations may cause turbulence in the flow which can cause an irregular mixing in the storage tank instead of a stratified mixing [81]. Without a stratified mixing in the storage unit, however, the temperature of the fluid entering the PV/T will be higher and this can reduce the panel efficiency greatly. This phenomenon is explained in detail in the next section.

As for the standardization of the mass flow rate, on the other hand, there is no clear agreement on an optimum value in the literature. However, many reported values fall in the range of 0.0008 - 0.015 kg/s per m^2 of the PV/T panel area [93], [95]. An example can be seen in Figure 2.9 taken from a TRNSYS model conducted by Kalogirou [92] for the monocrystalline PV cells based water type flat-plate PV/T panels. The reported optimum flow rate is 25 l/h (0.007 kg/s) for a total panel area of 5.1 m^2, which is equivalent of 0.0014 kg/s.m^2. Even higher values, such as 0.04 kg/s.m^2, has been reported in some other building integrated applications where the PV cell temperature reaches very high values due to the poor heat dissipation [81]. This disagreement among the researchers regarding the high spectrum of the flow-rate values is bearable to some extend as each system has a different structure and configuration. In addition, each author investigates the optimum value for different purposes. While some aim to maximize the thermal and electrical efficiency of the panels, others target energy savings. Therefore, it is important to optimize or carefully select the mass flow rate of the water when designing a PV/T system as the system configuration would vary based on this selection.

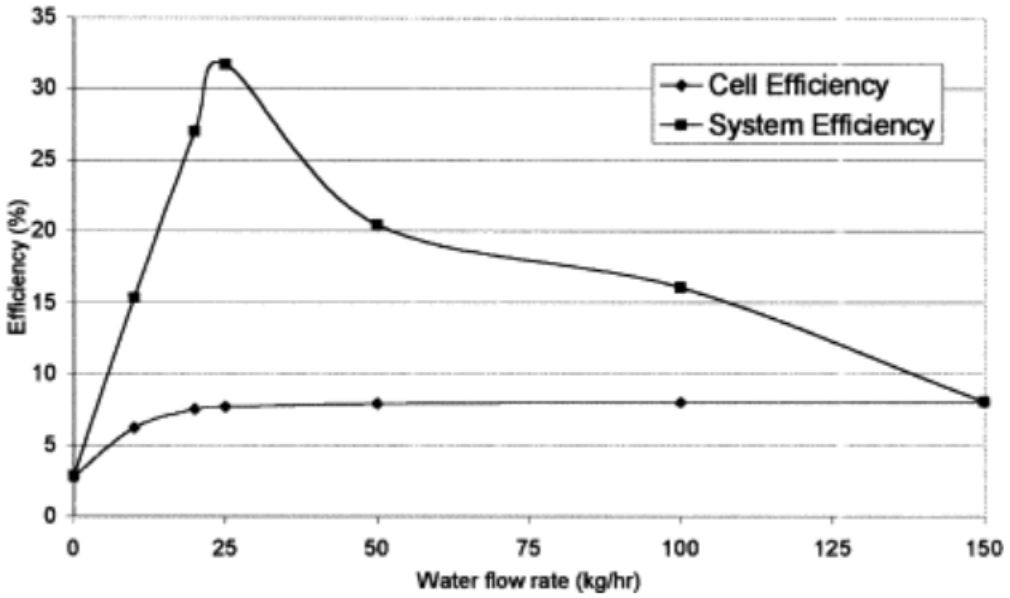

Figure 2.9: The effect of water flow rate on a PV/T panel efficiencies, Kalogirou [92].

The final critical parameter affecting the overall performance of a water-PV/T is the size of the storage unit. Based on a specific installation panel area, a larger tank size leads to better thermal and electrical efficiencies due to the density and heat capacity of the working fluid. This is because (when a tank storage unit is used) the fluid exiting the bottom of the tank can reach a lower temperature before entering the inlet manifold of the PV/T panel [96]. However, tank size must to be carefully optimized or selected. This is because if an excessive temperature drop at the bottom of the tank occurs, the energy consumption of an auxiliary heating device would become greater to supply the specific temperature requirement of the application [81]. More details of the storage unit selection are given in the next section.

2.5 THERMAL ENERGY STORAGE (TES)

Thermal energy storage means storing of “heat” or “cold” in a storage medium and is one of the most fundamental components of a SAHP application. In such systems, solar radiation is absorbed in the form of heat by thermal collectors or PV/T panels and is transferred to the working fluid of the panels. The heat storage unit then receives this working fluid and is

charged by the solar thermal energy so that it can be accessed and discharged when the heat source does not provide energy at a continuous rate. These charging, storing and discharging processes are shown schematically in Figure 2.10.

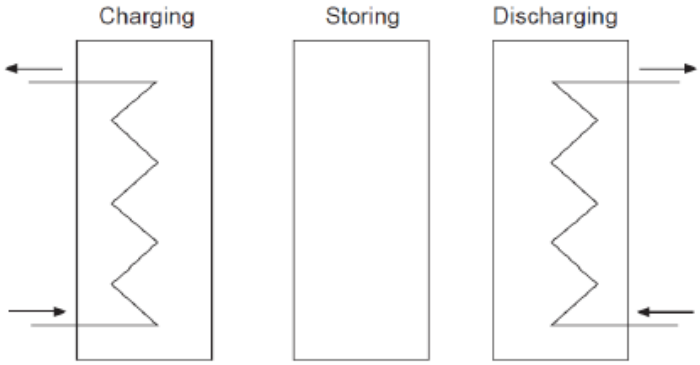

Figure 2.10: Schematic of a thermal energy storage cycle [97].

Kalogirou [49] stated that the storage unit has a direct impact on the performance, cost and reliability of the solar applications. This is because enhancing the thermal storage leads to extending the operational hours of an energy-generating system and reducing the auxiliary power consumption. Thermal storage can also be applied seasonally for locations where solar irradiation level is low for prolonged periods [98]. However, storing the working fluid at a favourable temperature for one or two days is a common practice in literature for domestic small-scale applications [75]. This is also vitally important for the SAHP systems because the fluid entering the heat pump become warmer resulting in a greater coefficient of performance.

Storing of the thermal energy may be achieved in various ways including thermo-chemical reactions. Due to the complexity and less cost-effectiveness of the thermo-chemical storage [99], [100], however, only thermal energy storage (TES) applications are investigated here, which are generally classified as sensible-TES (STES) and latent-TES (LTES, associate with phase change materials) [98]. Figure 2.11 shows a broad classification of all TES options including chemical storage.

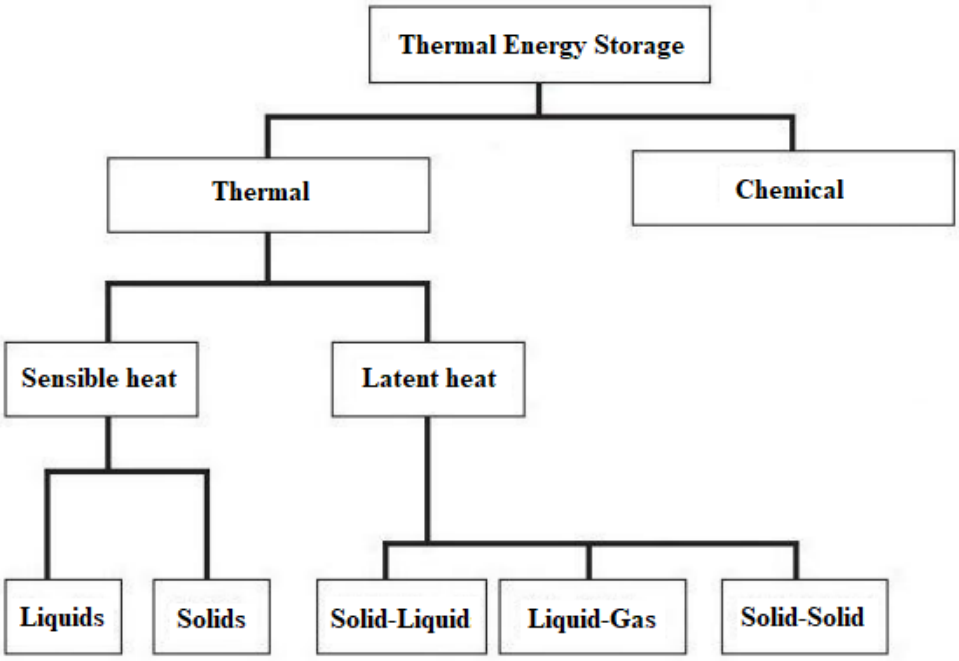

Figure 2.11: Classification of the TES [101].

A TES system can be assessed based on different characteristics such as capacity, power, efficiency, storage period (charging and discharging), and cost [101]. Table 2.3 presents these characteristics based on sensible and latent thermal energy storage methods. Technically, the most significant requirements for these characteristics are: a high capacity and power rate to achieve a greater energy density, a high efficiency rate to achieve lower energy losses during the storage period, an adequate heat transfer rate to achieve a faster charging / discharging period, and a lower cost to achieve an economically viable storage system [102].

In the literature, it is found that the STES is a well-developed technology with various building applications. Moreover, low installation costs -together with high capacity, power, and heat transfer rates (see Table 2.3)- makes the sensible-TES particularly applicable for DHW and space heating provision of small-scale residential buildings [99], [100], [101]. Therefore, the sensible thermal energy storage is used in this thesis and analysed further in coming paragraphs. On the other hand, the latent-TES is a developing technology that has

attracted a significant interest recently. It comprises changing the phase of a storage medium, usually between the solid and liquid phases, but solid-gas, liquid-gas and solid-solid phase changes are also available [100]. More details can be found for the LTES in leading studies conducted by Kenisarin and Mahkamov [103], Agyenim et al. [104], and Nazir et al. [105].

Table 2.3 Typical characteristics for the thermal energy storage methods [101].

TES Method	**Capacity (kWh/t)**	**Power (MW)**	**Efficiency (%)**	**Storage Period**	**Cost (€/kWh)**
Sensible TES (STES)	10-50	0.001-10	50-90	Days/months	0.1-10
Latent TES (LTES)	50-150	0.001-1	75-90	Hours-/months	10-50

STES is the simplest, cheapest and most mature way of storing heat in solar applications. A STES system is made of a storage medium (material used for the storage, solid or liquid), a container (usually a tank), inlet/outlet devices, and/or insulation materials [102]. In most basic terms, thermal energy is stored by increasing the temperature of a storage medium. During the charging/discharging periods, heat capacity and the temperature change of the storage medium is used, and the storage medium does not undergo a phase change [101]. Different materials can be used as the storage medium, and that they can be in liquid or solid forms. A high specific heat capacity, less space utilization (related to the density) and low cost are the most significant properties when selecting a storage medium. However, there are other properties that are unneglectable such as, thermal conductivity, diffusivity and long-term stability [106]. Table 2.4 outlines the suitable liquid and solid materials used for

sensible thermal energy storage. From the table, it is seen that water is the most favourable material to be used as it has the highest specific heat capacity and is the cheapest and most abundant material in comparison to the others. Additionally, it is non-toxic and has an operating temperature of 0-100℃, making the water particularly suitable for residential SAHP applications as this temperature range is close to the temperature of the fluid leaving the typical solar collectors. In this thesis, therefore, water is selected as the storage medium.

Table 2.4: Specifications of some suitable liquid/solid mediums for STES [101].

Available Storage Medium	**Liquid - Solid**	**Temperature range (℃)**	**Density (kg/m^3)**	**Specific Heat (J/(kg.K))**
Rock	Solid	20≤	2560	879
Brick	Solid	20≤	1600	840
Concreate	Solid	20≤	2240	880
Aluminium	Solid	20≤	2707	896
Cast iron	Solid	20≤	7900	837
Water	Liquid	0-100	1000	4190
Engine oil	Liquid	≤160	888	1880
Ethanol	Liquid	≤78	790	2400
Propane	Liquid	≤97	800	2500
Isopentanol	Liquid	≤148	831	2200

The container of a STES unit, which uses water as the medium, is usually tanks. A wide variety of materials can be used to manufacture a tank, such as stainless steel, aluminium,

copper, concreate, fiberglass and plastic [106]. Koçak et al. [107] stated that different equipment can be placed inside the tanks such as auxiliary electric heaters, heat exchanger coils and stratification structures. Han et al. [108] illustrated some of these technics which are widely used is solar residential applications for DHW and/or space heating, shown in Figure 2.12.

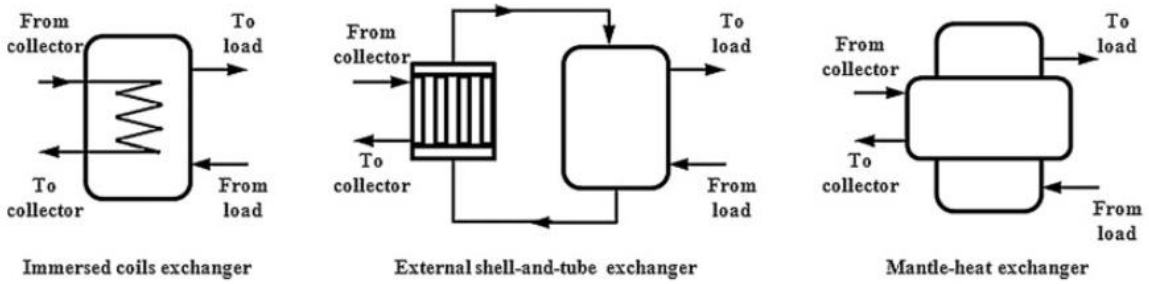

Figure 2.12: Feasible methods of the heat exchangers placed inside or outside of the hot water storage tanks [108].

In order to reduce the thermal losses, hot water tanks can be externally insulated with materials having low heat transfer properties such as glass or mineral wool and polyurethane [109]. Ideally, heat losses should be adequately minimised to increase the system efficiency.

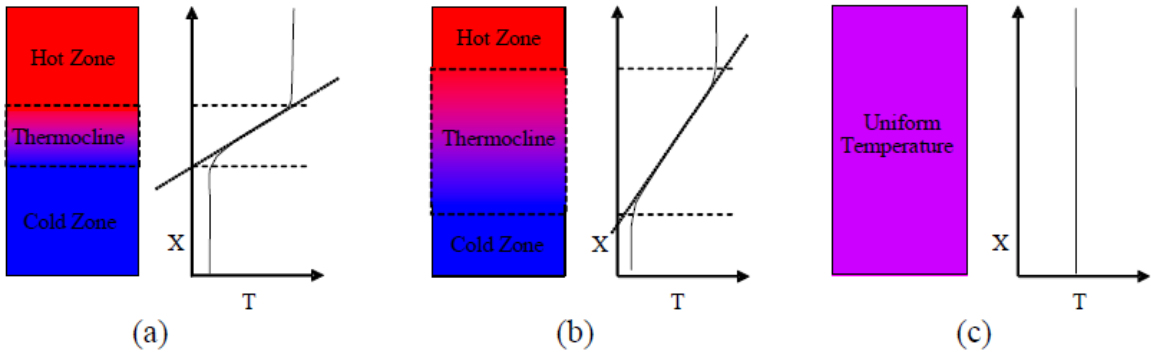

Figure 2.13: Different level of stratification in a storage tank [110].

Another parameter to increase the efficiency is the stratification of the water in the tank. For a water-based storage tank, the stratification (also called the thermocline) is the movement of the hot water at the top and cold water at the bottom of the tank due to the buoyancy effect

and gravity [106]. More specifically, the water density decreases with higher temperatures. This leads warmer water to rise an upwards position towards the top of the tank and colder water to sink a downwards position towards the bottom of the tank [107]. Therefore, stratification acts as a thermal barrier separating cold and hot water, and maintaining the density and temperature gradients. Figure 2.13 illustrates three different stratification levels; (a) high stratification, (b) moderate stratification, (c) fully mixed (no stratification).

Stratification of the thermal storage leads to better thermal performance both for the end-users and solar units. This is because, first, the useful heat potential of the top layer of the tank (where the end-user is connected) increases. Secondly, cold water at the bottom of the tank (where the solar panels are connected) returns to the solar collector hence increasing the collector efficiency and reducing the auxiliary heating consumption. Hollands et al. [111] proved this and reported that performance of an adequately stratified water tank can be 38% higher than a fully mixed tank.

In literature, three methods have been found to achieve a stable thermal stratification. The first two are heating the vertical walls of the tank, and utilizing a heat exchanger inside or outside of the tank. However, the third method is the simplest and most cost effective solution where it allows the water to enter a suitable temperature layer in the stratified tank. Shah and Furbo [112] detailed this methods for solar thermal storage applications.

Furthermore, there are some other geometrical and operational parameters affecting the stratification of the tank. While the geometrical factors include shape, size, aspect ratio, and inlet/outlet geometry of the tank; the operational factors consist of inlet flow rate, initial water temperature in the tank and charging/discharging periods. Zurigat et al. [113], and Lavan and Thompson [114] analysed the effects of inlet and outlet geometries and reported that inlet geometry has a significant impact but the outlet shape of the tank does not have a

strong influence on the stratification. In their pioneering book, Dincer and Rosen [115] suggested that the storage depth can be increased for a better stratification. Similarly, authors in [81] stated that the flow rate of the tank's inlet should be carefully selected as a higher inlet flow rate can lead to a uniform storage.

In conclusion, design of the TES for a solar-based system is of critical importance and cannot be neglected. Methods, manufacturing materials, storage mediums & containers, insulation materials, geometrical aspects and operational conditions are analysed in this section to carefully select suitable storage units in the SAHP systems proposed in this thesis.

2.6 HEAT PUMP (HP) TECHNOLOGY

Heat pumps are essentially electrically driven vapour compression devices that can provide heating, cooling or both for various applications. The working principle of the HPs is based on transferring heat from a source to another by running a refrigeration cycle [88], [116]. Thermodynamically, heat flows from a warmer atmosphere to a cooler one, however, in a HP cycle heat is accepted from a low-temperature source and is rejected to a higher-temperature medium [45]. The difference from a refrigeration cycle is, therefore, the heat flow direction, accordingly the end-users.

A typical HP consists of four main components: an evaporator, a compressor, a condenser and an expansion valve. Figure 2.14 shows a schematic diagram of these four components and the pressure-enthalpy (p-h) diagram of the cycle operation. In an ideal HP cycle, the refrigerant (also called working fluid) is in a two-phase (liquid + vapour) state when the system starts operating, the low-grade heat is absorbed by the evaporator of the HP and transferred to the refrigerant (4-1). Then the refrigerant in the saturated vapour state leaves the evaporator and enters the compressor where its temperature and pressure increase (1-2). It is then sent to the condenser for the extraction of the available high-grade heat by the

condenser fluid (2-3). After the condenser, the refrigerant is in the saturated liquid form and passes through the expansion valve to be cooled further (3-4), turning into a mixture of liquid and vapour (4-1). After the expansion, the working fluid enters the evaporator again and the cycle repeats [117].

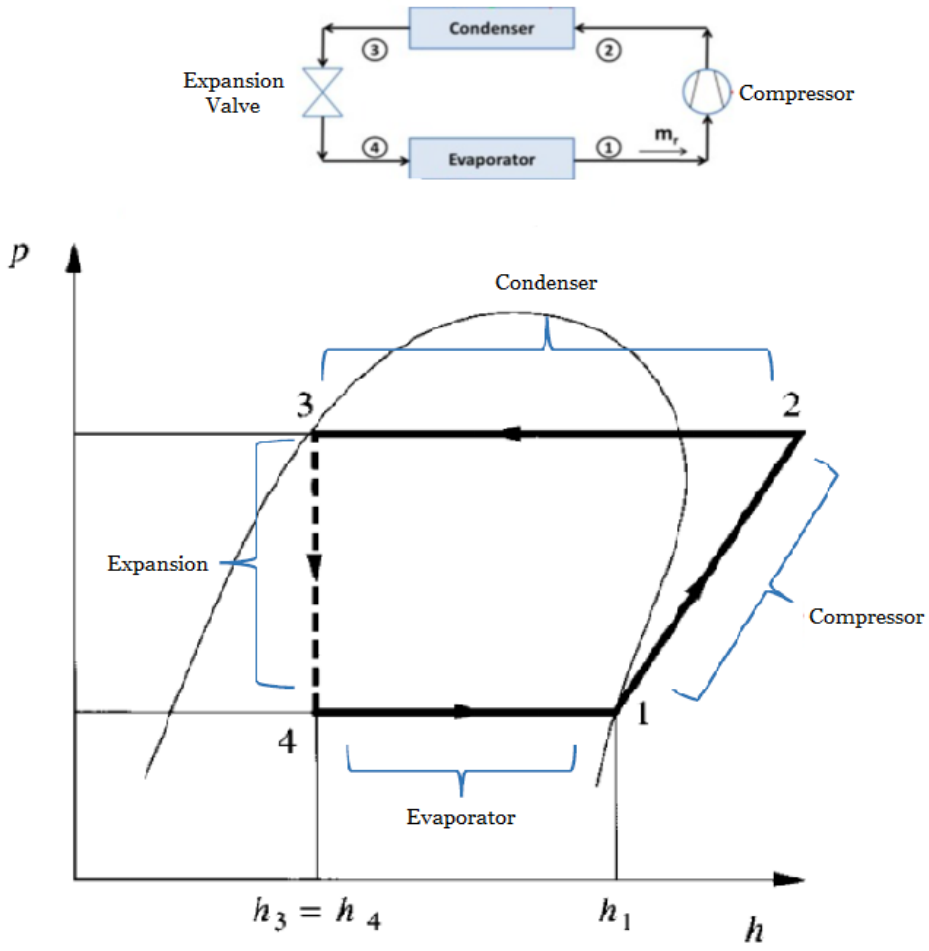

Figure 2.14: Schematic diagram of a typical heat pump and p-h diagram of an ideal HP cycle, modified from [118], [89].

With the above operation principle, a HP can be used to provide space heating or domestic hot water by using a suitable low-grade heat source. However, HP's expansion valve is reversible; this means that the working principle of the cycle can be reversed. When the position of the valve is changed, the working fluid of the HP flows in opposite direction, as a result, the condenser and evaporator of the same HP can act as the new evaporator and

condenser, respectively. The reversible operation is particularly important as it allows the same HP to be used for space cooling when it is needed [119].

The main performance evaluation parameter of a heat pump is the coefficient of performance (COP) value, which is the ratio of the heat gain in the condenser to the compressor power consumption [117]. Hepbasli and Kalinci [119] states that there are many parameters affecting the COP value of a HP including the temperature of the low-grade heat source, the temperature of the condenser's useful heat, the refrigerant type and the evaporation temperature. Among these, however, the evaporation temperature is of critical importance as it allows the low-grade heat source to be used in the system.

For a successful HP application, the availability of a cost-effective heat source, preferably with a higher temperature for the HP's evaporator, is desirable. With this regard, the heat source can be air, water or ground [120]. The air sourced HPs (ASHP) are economically viable and have the simplest design. They are also the most mature HP technology so that called traditional HPs in the literature [43], [121]. However, the coefficient of performance (COP) of the ASHPs decreases significantly due to the reduction of the available heat for the HP's evaporator in cold ambient air temperatures during the winter periods [122]. This creates efficiency penalties and the system usually requires an auxiliary backup system. Thus, the ASHPs are best suitable for moderate climatic conditions. For the ground sourced HPs (GSHP), the soil (ground) has the advantage of providing a stable temperature to the HP's evaporator but the installation of the pipes to the ground is not cost-effective, hence the total system is not an economically viable option for small scale applications such as single-family houses [123], [124]. Finally, the water-sourced HPs (WSHP) are also feasible options for buildings when it is fuelled by solar water-based thermal energy [123], [125]. In their study, Tzivanidis et al. [126] found that the solar fuelled WSHPs outperforms the ASHPs while their COP is about 5.2 and 3, respectively. Furthermore, this option has the

advantage of being applied to the existing thermal systems, especially when most of the DHW supply relies on water-based solar collectors as aforementioned. However, for the solar-assisted WSHPs, the major challenge is the heat injection into the storage medium, hence space cooling is usually not technically feasible with such combinations.

2.7 DESIGN OF THE SOLAR ASSISTED HEAT PUMP (SAHP) SYSTEMS

Regardless of the system outputs, the combination of solar energy and HPs is often named as the solar-assisted heat pump (SAHP) systems in the literature [43], [88], [127], [128]. Many studies focused on the layout of these systems, which is generally classified as parallel or serial [129]. In parallel systems, solar thermal collectors and the HP unit independently supply useful heat to the users. One of the most common practices for parallel systems is the connection of both collectors and the HP units to the same storage tank. With this connection, when the thermal energy supplied by the solar collectors is not sufficient, the HP unit operates separately to meet the demand. However, it is important to note that the heat pump utilized in such systems is usually an air source HP [130]. Therefore, disadvantages associated with the ASHP type may be observed and the system may not be able to provide enough energy without an auxiliary heating device, especially in winter periods. In a parallel connection, moreover, solar heating is usually prioritized to achieve a lower power consumption in the HP's compressor and to provide direct solar heating whenever it is possible; hence the HP unit is only used when solar direct thermal heating is unfavourable. This leaves the HPs to operate usually in unfavourable weather conditions and leads to efficiency penalties. Figure 2.15 illustrates the generic schematic of a parallel SAHP system for DHW provision where the HP utilizes the air as the heat source. The arrangement of the system's components is based on the end-users. Therefore, applications targeting the space heating can be arranged differently. An example of a parallel indirect SAHP system configured for the space heating is shown in Figure 2.16.

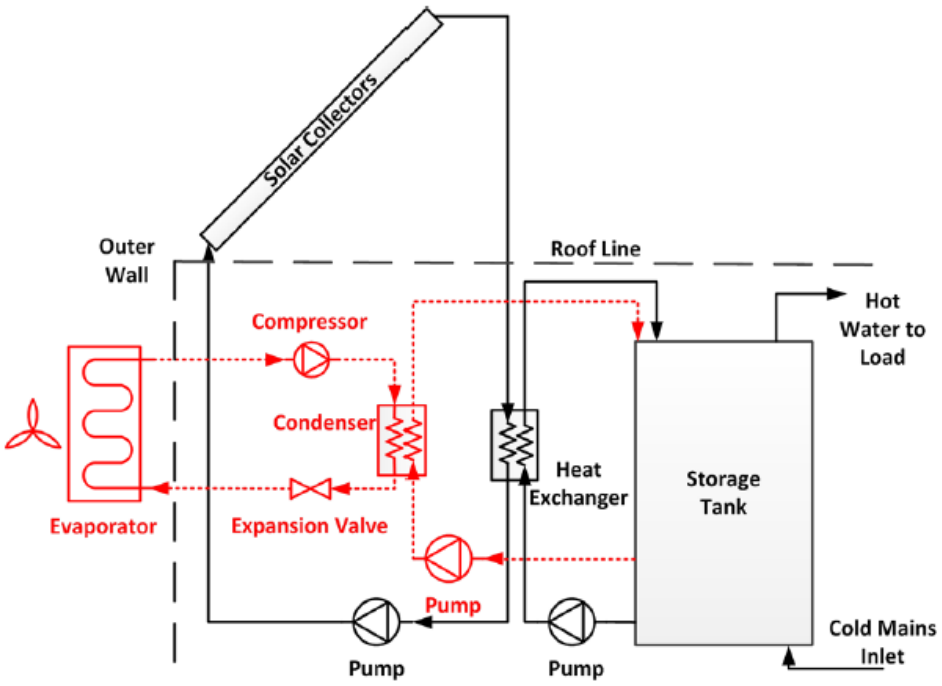

Figure 2.15: Schematic representation of a parallel SAHP system for DHW provision [130].

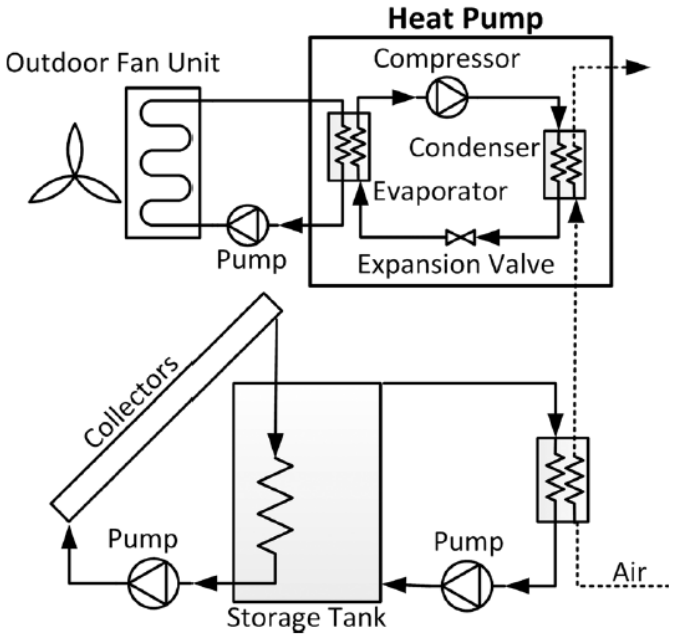

Figure 2.16: Schematic representation of a parallel SAHP system for space heating provision [130].

In the serial systems, on the other hand, solar thermal energy can be used as a heat source for the evaporator of the HP [129], [131]. In other words, solar collectors are connected to the heat pump unit, hence HP's heat source becomes solar thermal energy which is a more favourable source than the ambient air. When the SAHP is in serial connection, the thermal energy can be transferred directly or indirectly to the HP's evaporator. Therefore, a serial connection can be built with two different designs; direct serial SAHP (DS-SAHP) and indirect serial SAHP (IDS-SAHP) [132]. Examples of direct serial systems can be found in Chow et al. [133] where the absorber of the solar collectors acts as an evaporator to the HP unit, a schematic example is shown in Figure 2.17. Therefore, the working fluid of the solar collector is also the refrigerant of the HP unit. This design allows the highest possible evaporation temperature that can be used as there are no additional heat transfer losses in between the solar thermal absorber and the HP's evaporator. Despite these advantages, Harrison [134] underlined the potential risks of the refrigerant leakages occurring when the refrigerant flows from the HP unit to the solar absorber. This can create health and safety hazards [89], and make the direct systems impractical for domestic applications.

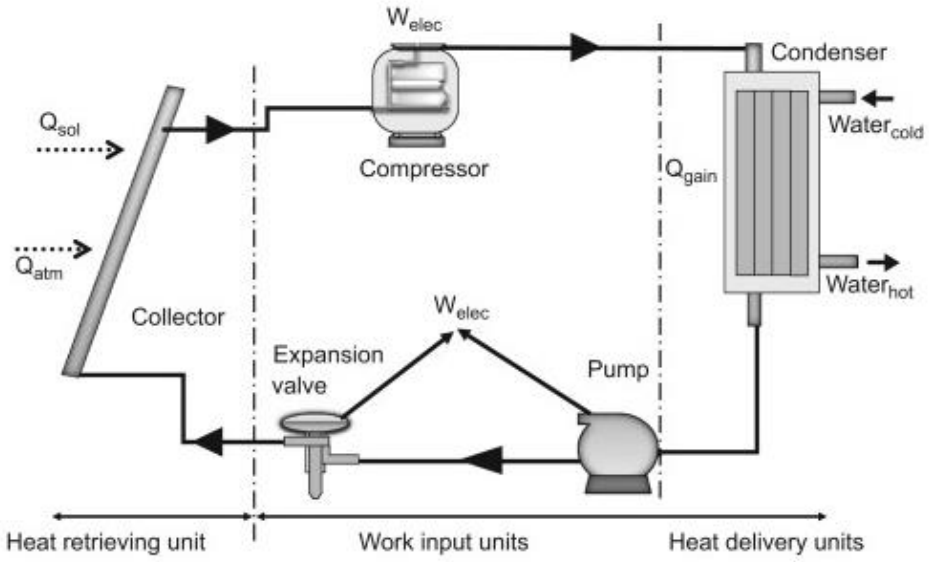

Figure 2.17: A schematic representation of the direct serial SAHP systems [135].

In indirect serial systems, by contrast, the solar energy is transferred to a heat exchanger or a TES tank, which are used as the heat source for the HP's evaporator. As the heat source is the solar thermal energy conveyed by the working fluid of the solar collectors, technically, a liquid-sourced heat pump can be implemented as a closed unit into the system [130]. This concept is illustrated in Figure 2.18 for a DHW application, and in Figure 2.19 for a space heating application.

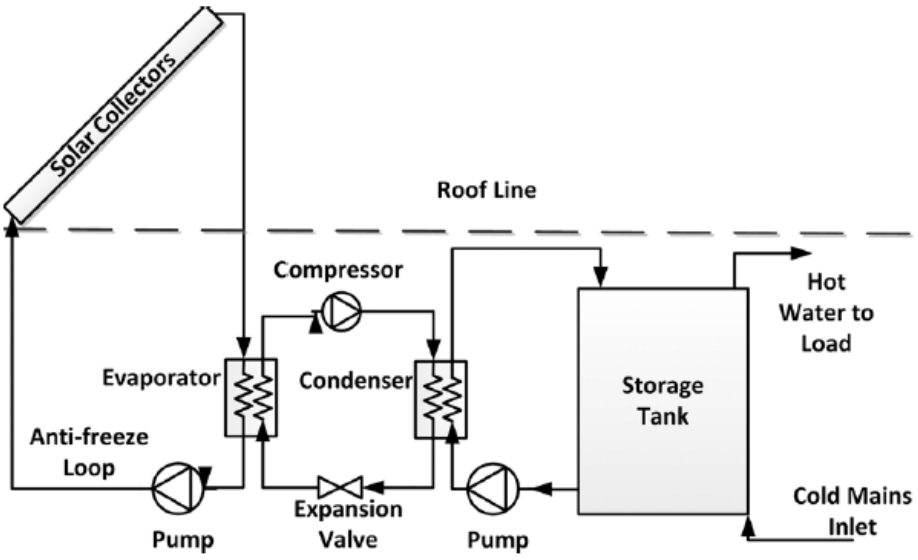

Figure 2.18: A schematic representation of the indirect serial SAHP systems for DHW provision [130].

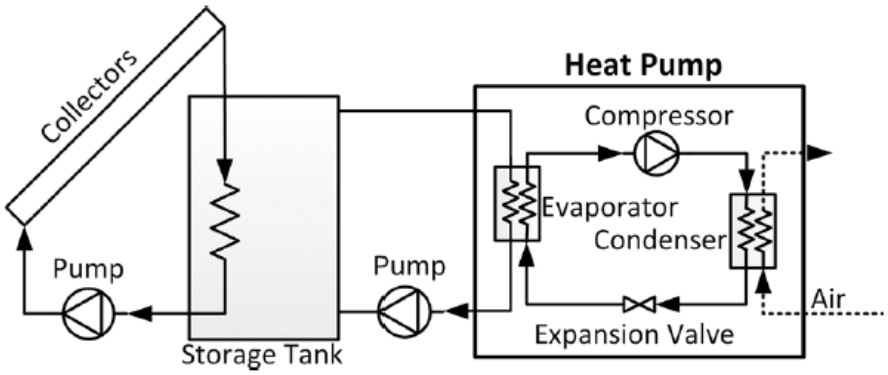

Figure 2.19: A schematic representation of the indirect serial SAHP systems for space heating provision [130].

It is important to note that in the indirect serial systems that supply space heating (see Figure 2.19), the circulation pump should operate only when the temperature rise across the collectors is higher than a pre-set minimum temperature. The pre-set temperature is usually just above the average temperature of the storage medium to not cool the tank [43].

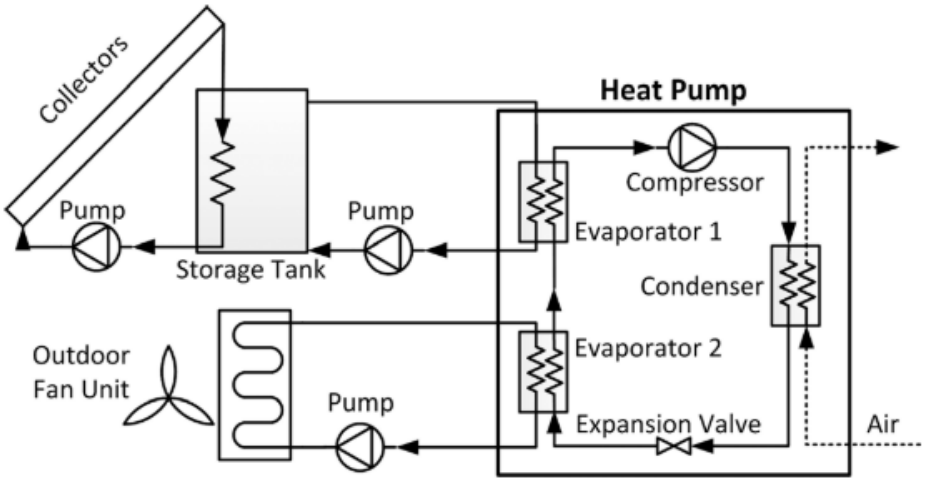

Figure 2.20: A schematic representation of the dual-source SAHP systems [130].

Another possible configuration for the SAHP is to connect the solar heat with a dual-source HP. A schematic view is given in Figure 2.20. In these systems, the HP consists of two evaporators allowing to utilize two different heat sources. Although the heat source can be solar, air or the ground; the majority of the studies in the literature is built based on solar thermal + ambient air configuration. Examples can be found in the work conducted by Lazzarin [136] and Kaygusuz [137]. The operation principle of this configuration is similar to the parallel systems as the weakness of the solar source is intended to be compensated by the air source. Therefore, the early studies of this type are classified as parallel systems [136]. But in fact, the connection design of the heat sources and the HP is similar to the serial SAHP. This is because the HP unit receives the heat indirectly from both sources to operate. However, the dual-source HPs may not be favourable in cold climates as both sources perform poorly during the winter, hence they are more effective in mild and hot

climates especially when the ambient air temperature is not extreme [43]. Moreover, in addition to the space heating and/or DHW provision, dual-source SAHP systems can be utilized also when space cooling is requested [138]. This is particularly practical for domestic applications as the same system can provide space cooling with the aid of the reversible working principle of the HP. In this regard, HP can receive the building's hot air and reject it to the ambient without sending it to the solar collectors which reduce their efficiency.

Overall, the configuration of the SAHP systems is a massive area of research. The literature provided in this section shows that there is no a standardized system configuration. Each design has its own advantages and that the best possible system configuration for a specific application is based on different parameters such as the heat source, environmental conditions, HP selection and the end-users.

2.8 A CRITICAL REVIEW ON THE SAHP APPLICATIONS

In the previous sections, the components of a SAHP system, such as solar thermal collectors, PV panels, PV/T collectors, thermal energy storage units, and the heat pump units, and the design of solar-assisted heat pump systems have been investigated separately with the pioneering key literature in order to reveal the crucial aspects of the system design. In this section, however, a critical review of the combination of these separate components, which forms the SAHP systems, is presented in light of the state-of-art key literature. In this review, the ground source HPs are excluded as they are not suitable for the small-scale systems (see Section 2.6). Thus, the scope of the review is on the SAHP systems suitable for single-family houses, mostly located in Europe.

SAHP systems have been analysed in various aspects in the literature. Some studies have focused on the performance of the SAHP systems in cold climates. One of the most

comprehensive and pioneering studies on this aspect was conducted by Good et al. [31], where the authors examined various solar panel types to achieve net-zero energy building applications. In their study, solar thermal, solar PV and solar PV/T panel types were compared for an exemplary single-family house. The total energy demand of the house was presented in electricity units. For the HP unit, in addition, an air-to-water type was connected in parallel to support the heating demand. A schematic diagram of this study is shown in Figure 2.21.

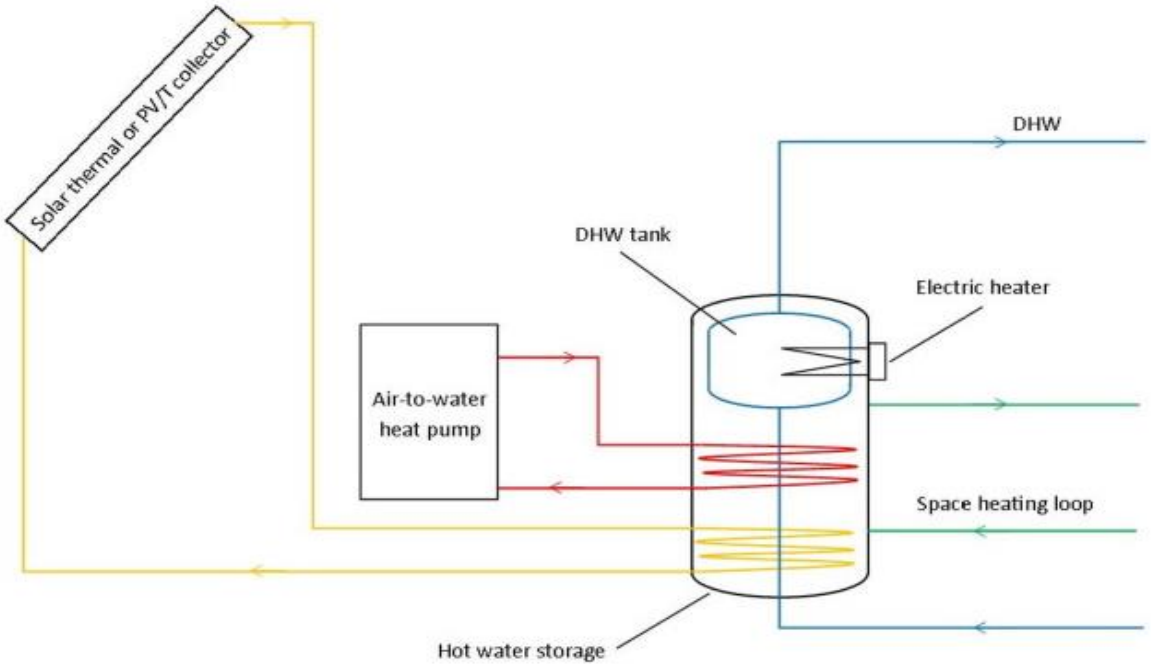

Figure 2.21: A schematic diagram of the study conducted by Good et al. [31].

The results of the study showed that the system could achieves a net-zero energy balance only with the PV+ASHP combination. In addition, the authors underlined that this configuration was the easiest combination to implement and was the most suitable in places where heat pump applications are not widespread. Also, they stated that the results substantially depend on the climatic boundary conditions. However, the main weakness of the study is the failure to address the cost of the proposed systems. For example, it is not clear whether the system proposed with the PV/Ts outperforms the one with the PVs in terms

of economy or not. Hence, the study would have been more conclusive if the authors considered a fundamental economic analysis.

In another study, Bridgeman and Harrison [139] modelled an indirect SAHP system for DHW-only provision in Canadian climatic conditions, shown in Figure 2.22. The model was built in the Engineering Equation Solver (EES) software and was experimentally validated with a test rig prepared by the authors. In the study, a water-sourced HP (with the working fluid of R134a) was used to feed a hot water storage tank. The most remarkable conclusion of the study was the COP value of the HP, which could reach as high as 3.31 in such extreme climates. In the study, however, the components of the system are not optimized, hence the results might have been enhanced if further analyses were conducted.

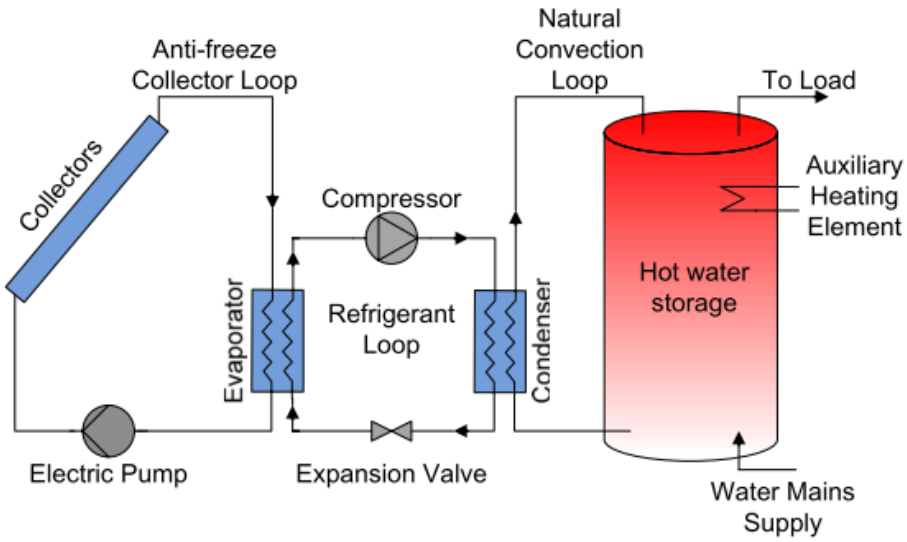

Figure 2.22: Schematic diagram of the indirect SAHP system for DHW provision, conducted by Bridgeman and Harrison [139].

Some studies investigate the effect of the working fluids of the solar panels and HPs on the total system performance. In a recent study, Bellos et al. [140] analysed a SAHP system driven by nanofluid-based PV/T panels for a space heating application in Greece, illustrated in Figure 2.23. The system was modelled in the EES software, and validated against the experimental literature studies. A water-sourced HP was placed between the storage tank

and the load side. The electricity generated from the PV/T panels was used to power the compressor of the HP and any excess electricity was sent to the grid. It is worth mentioning that the system was analysed and optimised in steady-state conditions. The authors examined various nanofluids alongside the pure water for the PV/T panel and tested different working fluids for the HP unit. Their results showed that the most favourable nanofluids for the PV/T panels were water/Cu and water/Al_2O_3, and for the HP it was R152a. Moreover, water/Cu nanofluid in the PV/T panel led to a 4.8 % improvement in the total energy efficiency and a 5.75% increase in heating production. In this study, the authors provided a substantial amount of modelling details and obtained the demand load profiles of the representative house. This study is a good example for such combinations with only one drawback; the absence of the cost analysis.

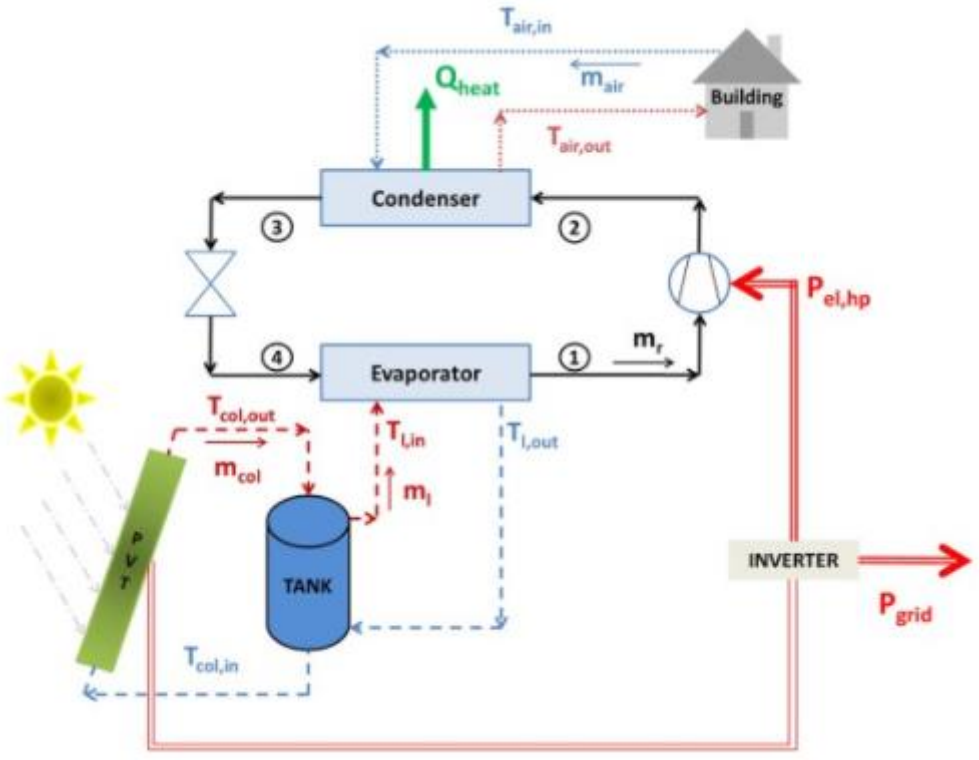

Figure 2.23: PV/T based SAHP system for space heating, conducted by Bellos et al. [140].

In moderate and warmer climates, performance of a SAHP system can achieve extremely high values with solar thermal collectors. In accordance, the combination of different panel

types (ETC or FPC) with the water-sourced HPs for provision of the DHW or the space heating has been investigated extensively. In a detailed publication, Çağlar and Yamali [141] proved this experimentally. In their system, ETCs and a WSHP unit were connected in serial for SH-only of a representative single-zone building located in Turkey. The collector efficiency of their system was above 80% and that the maximum COP value of the system was reported as 6.38. Similarly, Sterling and Collins [142] used the TRNSYS software to model an indirect SAHP system (FPCs-based) for DHW-only provision and proved that the system outperformed the conventional solar water heating systems (electric heaters, boilers etc.) both energetically and economically.

Comparison of the serial and parallel SAHP systems have drawn many researchers' attention to reveal the best possible configuration for the specific applications. Kim et al. [143], for example, carried out one of the most comprehensive comparative investigations of the serial-type and parallel-type SAHP systems. The study was conducted to provide DHW-only. They analysed the conventional FPC and PV/T panels with water and air sourced HPs through direct and indirect configurations. In the study, six different combinations were created to reveal the best possible connection based on the annual performance. Their results showed that the IDS-SAHP connected with the PV/T panels had the superior operation time. For the annual average heat capacity and the COP value, however, the same configuration had inferior values of 3.76 kW and 3.17, respectively. These results are quite logical as the parallel connection was designed with the air source HP; which means that the system can provide much more energy during the summer period when the outside temperature is favourable.

In another interesting recent study, Vega and Cuevas [144] used TRNSYS to compare the overall performance of a SAHP system providing DHW and SH for a typical mid-rise building in the climatic boundary condition of three different Chilean cities. Performance

evaluation of the serial and parallel connections were given individually, however, the authors' main objective was to model a system switching between serial and parallel mode depending on the solar irradiation level. For this purpose, they used a dual-source HP with solar thermal collectors. A control strategy was proposed to execute the switching when the optimum irradiation value is reached. A schematic representation of this study for space heating is provided in Figure 2.24. The most notable conclusion of this study was that such a design was feasible with a proper control strategy, and the performance of the individual components increased with the serial connection. However, the details of the control strategy could have been clearer in the study, especially when the control is one of the main aspects of the study.

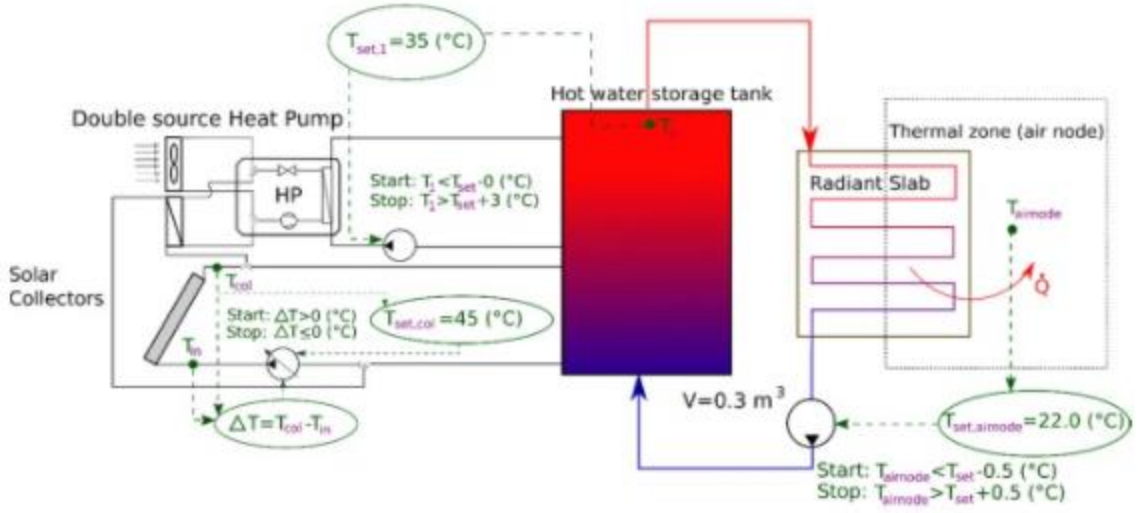

Figure 2.24: A serial/parallel based SAHP system for space heating, designed by Vega and Cuevas [144].

For a successful SAHP design, the demand side load profiles, such a DHW, space heating/cooling, and electricity, need to be known to properly size the energy supply technologies. With this regard, the TRNSYS [145] software has been used intensively in the literature as it provides impressive flexibilities, such as graphical interface, writing of equations, built-in validated components, etc. An example can be found in work conducted

by Chargui and Sammouda [146] where an exemplary residential house, coupled with a HP unit, was modelled. Some other authors provided more detailed examples which can be found in works conducted by Calise [147] and Emmi et al. [148]. They both utilized ASHRAE and/or European building standards to construct a representative house model in the TRNSYS and provided sufficient details for the modelling, but did not generalized their results for other locations. Finally, the literature in this field is extremely limited.

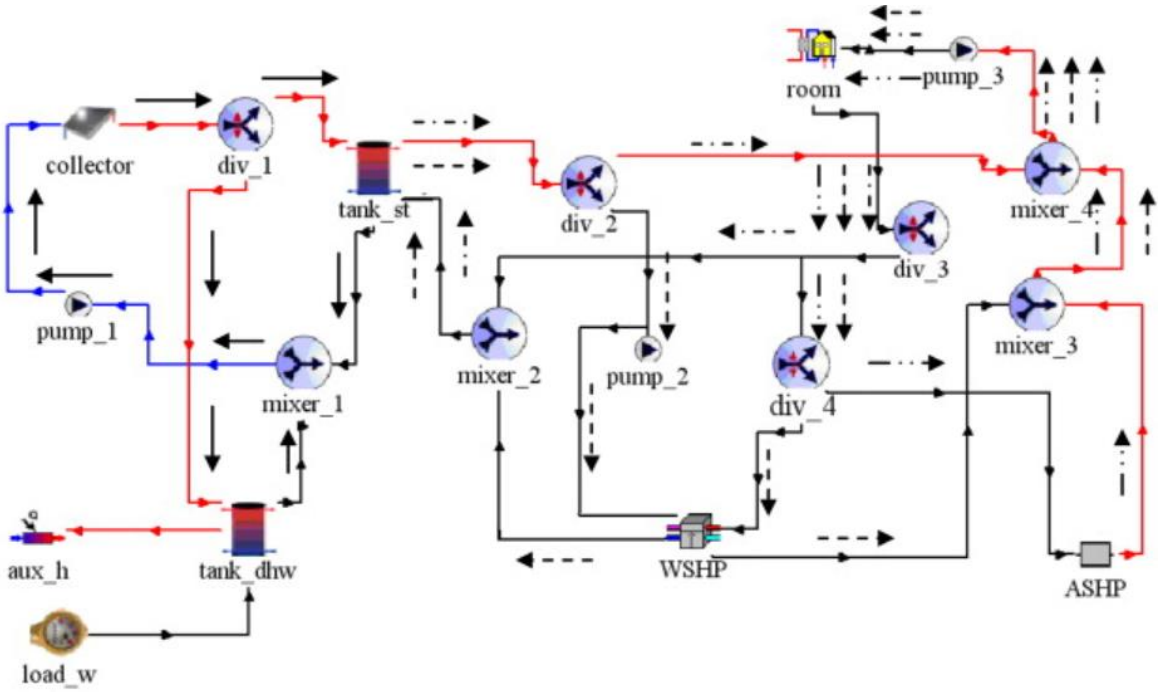

Figure 2.25: The SAHP system designed by Li et al. [149].

Different authors have conducted sensitivity analyses of the individual components and their impacts on the overall efficiency of the SAHP systems. Li et al. [149], for example, used TRNSYS to investigate the performance of a complex SAHP system to provide DHW and SH for a six-story dorm building in Beijing, China (shown in Figure 2.25). In the study, the authors assumed a 40 L/ (person-day) with a temperature of 55 ℃ for the DHW provision and proposed seasonal energy storage for the space heating. The influence of optimizing the main components (solar collector area and storage tank size) was analysed and that the performance of the proposed system was compared with a traditional heating system. A

WSHP is utilized between the solar collectors and the storage tank. Their results showed that the optimum tank size should be between 0.5/m^3- 0.8/m^3 per m^2 of the collector area (0.5-0.8 m^3/m^2) to achieve an acceptable storage efficiency. For the collector area, however, they suggested an area of 130-160 m^2 to meet the building's total heating demand. With these optimized values, the COP value of the system was found to be between 3.3 and 4.2. They finally concluded that their system reached a 52% of monthly energy-saving ratio. Despite the good procedure for the system optimization, however, the lack of information on the building's demand load is the main weakness of the study.

The utilization of the PV/T panels in SAHP systems has drawn the attention of many researchers as it is relatively a new concept compared to the conventional solar thermal collectors. In a recent study, Obalanlege et al. [89] analysed the performance of a PV/T based SAHP system for SH and EE demand in Belfast, UK. The main objective of the study was to investigate the effect of the variations in the system's most important parameters –in particular: solar irradiation, water flow rate, and storage tank size on the overall performance of the SAHP system. R407c was selected as the working fluid of the HP, while all other circuits were run with the water. A WSHP was used and placed between the glazed PV/T panel and a representative single-zone building (5m×3m×3m), as shown in Figure 2.26. The authors provided substantial details of their model which was validated against experimental literature. They focused on the total (thermal + electrical) efficiency of the PV/T panels and the COP of the HP. Throughout the simulations, the minimum COP value of HP was reported as 4.2. They also reported that PV/T efficiency can increase by 6.5% when the storage tank size increased from 1L to 100 L. Similarly, rising the flow rate of the panel's circuit from 3L/min to 17L/min, increased the PV/T's total efficiency by 3.5%. This study is a good example of the PV/T + WSHP combination in recent pioneering literature that provides two different energy vectors; SH and electricity.

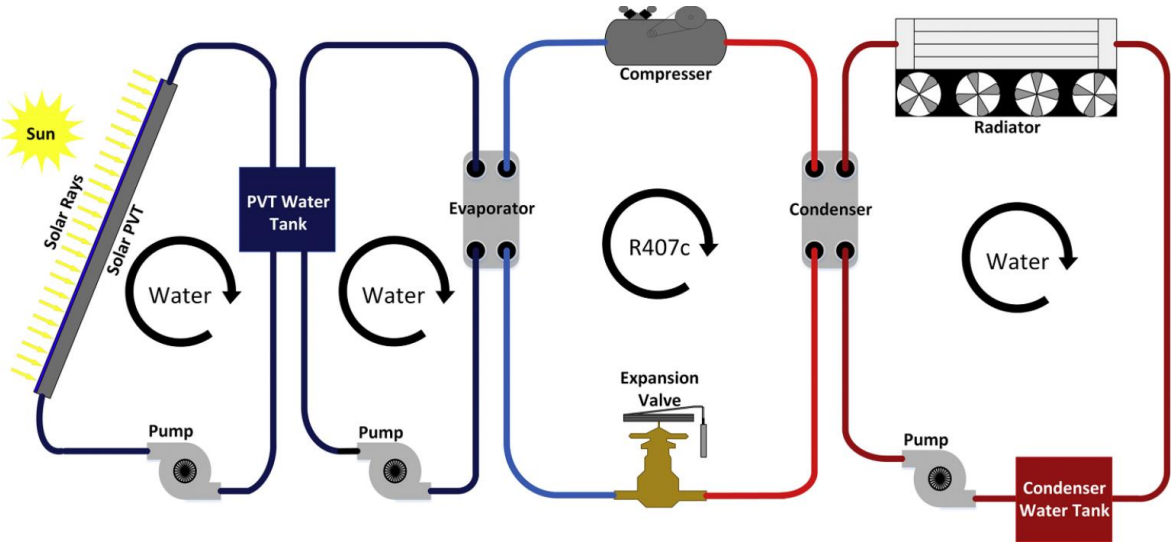

Figure 2.26: The PV/T based SAHP system, designed by Obalanlege et al. [89].

Studies aim to provide more than two energy vectors, such as space heating or cooling, domestic hot water, and electrical energy, from the SAHP systems are quite rare in the literature. In a highly cited publication conducted by Ramos et al. [150], a PV/T based SAHP system was modelled in TRNSYS for combined heating, cooling and power provision in different European cities. A simplified schematic of their TRNSYS model is shown in Figure 2.27. In the paper, four different configurations were considered but only the PV/T based water-to-water HP was modelled in the TRNSYS. The authors aimed to generate SH, SC, DHW, and electricity for an exemplary residential building in different European Union countries. In addition, an economic evaluation of the system was conducted to reveal the feasibility of the tri-generation system. Their results showed that the system can reach at least 60% of the SH and DHW, and 100% of the cooling needs (electrified) of the exemplary house in many locations. They finally reported that the LCOE of their system was varying between 0.06-0.12 €/kWh, which were close to the grid energy prices in the selected locations. These results seem exceptionally impressive. However, the authors did not clearly show the details of their model in the paper. In particular, it is not clear that how the heat dissipation of the system in cooling mode during the summer time was achieved. In addition,

the calculations for the other configurations before the TRNSYS model were extremely oversimplified. Therefore it is not known whether the authors rely on the assumption or the technical feasibilities. The issues in this paper also have been reported and criticised by Lazzarin [43].

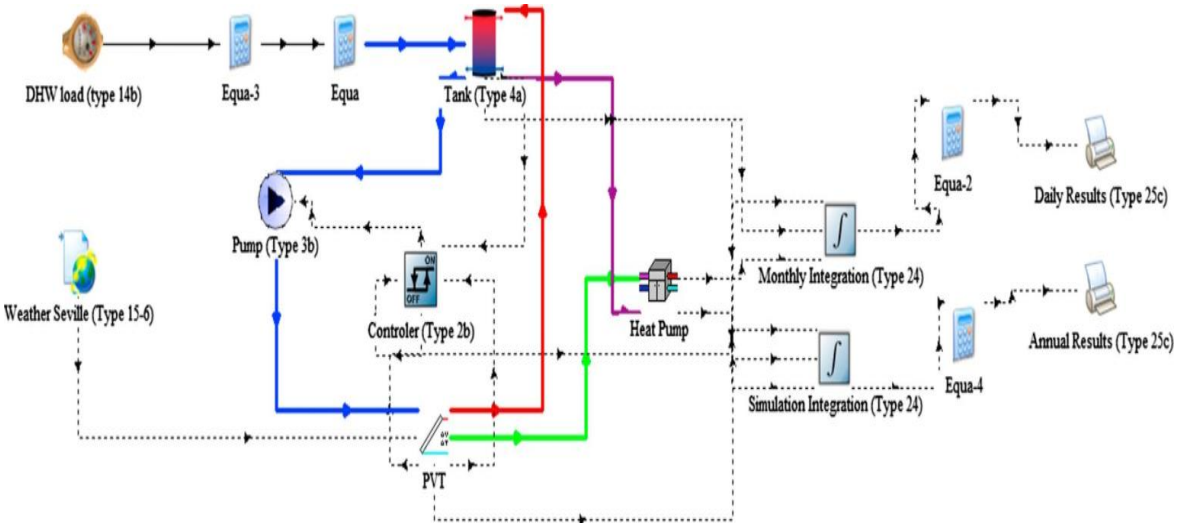

Figure 2.27: The TRNSYS modelling of the tri-generation SAHP system, conducted by Ramos et al. [150].

Another example can be found in work performed by Braun et al. [151], shown in Figure 2.28. The authors used TRNSYS to show the feasibility of a novel PV/T based SAHP tri-generation (heating, cooling and power) system. The system was designed for a two-zone office building with a total usable area of 630 m^2, and the load profiles were created for three different climates in Germany by using TRNSYS. The authors considered a novel system configuration where the PV/T panels were operated during the night to dissipate the heat in the cooling seasons, and during the day to provide the heat in the heating season. They also performed a parametric study to optimize their system based on the panel and the tank sizes. The results of the system proved that the annual cost of such a system was comparable with the conventional solar heating and cooling systems. In terms of the novelty, modelling details, exemplary house design, system optimization, and the cost analysis, the study

presents excellent inspirations. However, the only missing point in the system is the provision of the DHW, although the system design was suitable for such demand due to the serial system configuration.

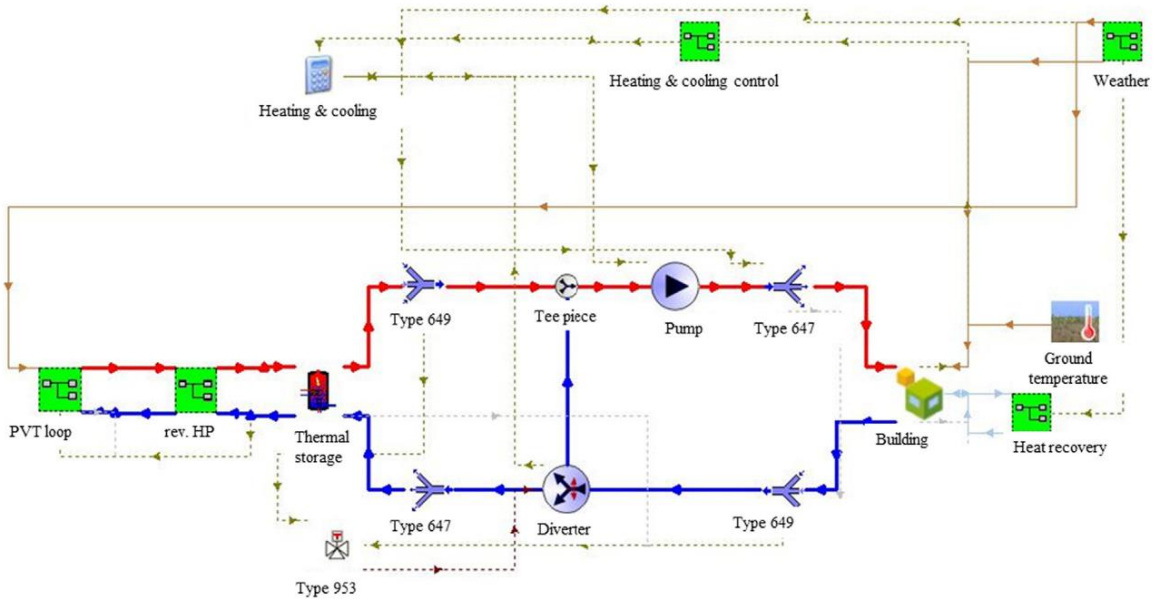

Figure 2.28: The TRNSYS modelling of the tri-generation SAHP system, conducted by Braun et al. [151].

In addition to these applications, some authors provided recent comprehensive review papers where more studies can be found based on SAHP systems. Poppi et al. [152], for instance, provided a techno-economic review of SAHP systems for residential buildings. Vaishak and Bhale [117] provided the current status and future prospects of the PV/T-based SAHP systems. Lazzarin [43] reviewed HPs and solar energy, and provided future insights on these systems.

2.9 SUMMARY AND KEY FINDINGS OF THE LITERATURE REVIEW

Summary and key findings of this chapter are presented section by section as follows:

Section 1: The introduction of the chapter was presented.

Section 2: This section highlighted the available solar thermal collectors and their operational principles for domestic thermal energy generation utilized for space heating and domestic hot water provision in small-scale applications, such as single-family houses.

Key findings:

- The users in a residential building typically requires temperatures of 45-50℃ for DHW and 30-35℃ for SH needs for the thermal comfort. Among various collector types, including sun-tracking and concentrated collectors (e.g. parabolic trough collectors, linear Fresnel collectors parabolic dish reflectors, compound parabolic collectors, etc.), flat panel collectors (FPC) and evacuated tube collectors (ETC) have been found to be the most suitable collector types to be applied to single-family houses due to the cost-effectiveness of the collectors, technology maturity, and temperature output of the collectors.

- While ETCs do not require an additional solar tracker due to their tubular design, FPCs can be attached to such devices, but this choice is not cost-effective. Instead, FPCs are oriented towards the equator with a tilt angle of ±10-15º location's latitude.

Section 3: This section investigated the solar electricity generation through photovoltaic panels and the factors affecting the PV panel efficiency.

Key findings:

- Almost 90 % of the PV market worldwide today is based on silicon-based mono-crystalline and polycrystalline cells.

- Mono-crystalline based PV panels are the most mature technology and have the highest conversion efficiency and longest lifespan time among other types. Although they were less cost-effective in comparison to the polycrystalline and amorphous silicon cells, recent technological developments have reduced the production cost substantially. Therefore, it has been highlighted as the optimum cell type to be used in this thesis.

- Performance of a PV cell substantially reduces with the temperature increase during the operation where extreme working conditions as high as 50 °C above the ambient occurs, which can permanently damage the cell structure. For optimum performance, therefore, the PV cells have to be adequately cooled.

Section 4: This section analysed the novel type solar photovoltaic/thermal (PV/T) panels. Basic concepts, design principles and performance factors were presented.

Key findings:

- PV/T is the concept of generating solar electricity and solar thermal energy simultaneously from one integrated component. Although a considerable amount of work has been devoted to R&D, a robust and mature PV/T market has not yet been established.

- PV/T has been highlighted as the most suitable panel type to be used in building environments as it increases the electrical efficiency of the PV cells, maximizes the energy generation in limited spaces, and provides low-cost energy per unit area of the installation.

- The most critical factors that affect the performance of a PV/T panel are climatic conditions (including ambient temperature, wind speed etc.), the mass flow rate of the panel's working fluid, and the storage tank size. However, there are no standardised values for these factors in the literature as each application is built with different specifications. For an optimal design, therefore, these parameters have to be carefully selected or parametrically analysed.

Section 5: This section revealed the available thermal energy storage units that can be used for SAHP systems. Storage methods, mediums, and containers were investigated, together with manufacturing and insulation materials.

Key findings:

- Sensible thermal energy storage is chosen for this thesis as it has a lower instalment cost

and high storage capacity for domestic applications.

- Water is selected as the storage medium of the study because it is abundant and has the highest specific heat capacity among other suitable mediums.

- A vertical storage tank is considered for the system as it allows a higher stratification level.

Section 6: This section provided details about the HP technology. The fundamental working principle of a HP cycle was given and different types of the HPs were analysed.

Key findings:

- Ground-sourced HPs (GSHP) may not be economically viable for small-scale applications in moderate and hot climates. On the contrary, air-sourced HPs (ASHP) and water-sourced HPs (WSHP) are found to be better options for such applications due to the simple design and installation, and fewer component utilization when constructing a HP-based energy system.

Section 7: This section analysed the design principles of the SAHP systems to reveal the best possible solar+ HP configuration.

Key findings:

- Serial-indirect SAHP systems outperform other designs (including parallel and serial-direct connections) in terms of performance and cost. Therefore, the serial-indirect connectivity is selected for the proposed SAHP systems in this thesis.

- It is found that there is no a standardized system configuration for the SAHP systems as each system has distinctive parameters such as the heat source, environmental conditions, HP selection, and the end-users.

Section 8: This section provided a critical literature review of the existing SAHP systems for small-scale residential applications.

Key findings:

- It is found that many feasible ways exist to build a SAHP system. Therefore, the SAHP systems cannot be standardised as each system has its own advantages for each specific application. However, the combination of solar PV with an ASHP unit is found to be the most practical solution for locations where the SAHP systems are not adequately adapted. Moreover, the combination of the solar thermal collectors (including the PV/T) with a WSHP unit is highly profitable as it maximises the system's energy outputs such as SH, DHW, and EE, especially when it is connected with the PV/T panels. Nevertheless, the PV/T-based SAHP systems are still in their early stage. Thus, the PV/T-based tri-generation systems are rarely found in the literature.

- In order to correctly size a SAHP system, the demand side load profiles should be known. However, the energy demand side of the reviewed studies is generally based on fixed or pre-set load profiles. This leads to imbalances between energy supply and demand, even in some well-designed multi-citation studies.

- The existing applications usually focus on the performance of the SAHP system, hence the economic analyses are largely ignored.

- In the literature, the SAHP systems built for DHW-only have been investigated intensively. Systems providing SH + DHW have also gained much attention. However, systems supplying more than two energy vectors, such as SH+DHW+EE or SH+DHW+SC+EE are rarely found in the literature.

- TRNSYS software has been employed extensively in the modelling studies.

2.10 RESEARCH GAPS AND CONTRIBUTION OF THE THESIS

The most critical research gaps identified in the literature which this thesis aims to fill are as follows:

- From the literature search, it was concluded that there is not enough evidence on how to calculate the dynamic energy consumption assessment of the thermal and electrical end-users of the residential buildings, and that many studies base their energy demands on pre-assumed repetitive profiles which creates mismatches between energy demand and supply sides. This thesis therefore aims to fill this research gap by providing a comprehensive study on how to calculate and acquire all energy consumption profiles of the residential buildings while staying within the boundary conditions of the European countries.

- A grid-connected distributed PV system generating low-carbon electricity on the rooftop of the residential buildings combined with an electrically driven ASHP can significantly supply the primary thermal and electrical energy demands of the buildings and reduce the grid dependency. As a result, the PV+ASHP combination is considered one of the most fundamental and cost-effective technological solutions to decarbonize the building sector and to achieve the net-zero-energy residential building concept in the European countries. Despite the advantages, however, it is observed in the literature that the number of installed PV+ASHP systems has not been sufficient in some European countries (such as Turkey), although the optimal operating conditions (e.g. solar radiation and moderate climatic conditions) exists. Therefore, this thesis attempts to fill this research gap by conducting a case study, for the first time, to reveal the techno-economic competitiveness of the PV+ASHP technology with the national grid electricity in the location of interest.

- The combination of solar energy and HPs is often referred to as a solar-assisted heat pump (SAHP) system, regardless of the system outputs and components. However, in the literature, there is a significant amount of interest in SAHP systems that provide only hot water. Many systems include the appropriate combination of different types of solar panels (ETC, FPC, PV, PV/T, etc.) and a WSHP but usually produce no more than two energy demand vectors such as DHW + electricity, SH only or SH + electricity. As detailed in the

critical literature review, all these systems have their own strengths and weaknesses, but what they have in common is that they improve the overall system efficiency compared to conventional systems such as HP alone, solar alone, boilers, etc. Despite their advantages, only a few studies use PV/T + WSHP systems to produce more than two energy demand vectors such as SH, DHW and EE, hence there is a significant research gaps in the literature in this field. This is often due to poor system designs that lead to the system being oversized and resulting in high economies for the system. In addition, there is currently no standardized modelling and testing approach, as a result, a poor design in these systems can significantly degrade performance, especially when solar penetration is not maximized. In order to assess these issues and fill the research gap, this thesis presents a novel PV/T+WASHP configuration to generate SH, DHW, and EE simultaneously and investigates the techno-economic feasibility of the combination in different climates of the European region.

CHAPTER 3

Methodology

3.1. INTRODUCTION

This chapter provides information about methods, software selection, mathematical models, and materials that are used in the thesis. The chapter contains three main subsections. In the first part, the thesis methodology and the software selection of the thesis are explained. The second part provides details of the main software of the thesis, TRNSYS, and the modelling details of the most common components (called 'Type') of the software that are necessary to build a SAHP system. The third part is devoted to the second modelling software of the thesis, EES. Finally, a general conclusion is drawn for the chapter.

3.2 THESIS METHODOLOGY AND SOFTWARE SELECTION

In this thesis a model-based system engineering (MBSE) approach is used. This approach is a formalized methodology utilized to design, validate, and analyse complex systems before the actual system development [153]. The models in this methodology serve as a representation of the real systems and are at the centre of the design process. Therefore, the models should not be confused with real systems as they will always be an imperfect copy of reality [49]. In the system models, the physical and functional architecture of the real systems are represented by a set of connected block diagrams which contain a detailed list of characteristics that the system must have in order to function. In order to represent the system architecture, models are developed utilising specialised purpose-built languages. However, models alone cannot describe if the requirements of the system are met, hence they should be coupled with the simulation tools/software to observe the effect of the changes in the characteristics of the design [154].

The first step in modelling a SAHP system is the selection of the software used to represent and simulate the system. Simplified well-known energy simulation programs for this purpose, such as HOMER [155], iHOGA [156], Polysun [157] etc., have important features

of computational speed, low cost, little technical expertise, and fast turnaround [158]. However, they have constrains of flexibility, limited control over assumptions, and restrictions of different components [159]. Other well-adapted energy simulation tools are Energy Plus [160] and RETScreen [161] which have the strength of accurate and detailed simulation capabilities. However, they cannot perform advanced calculations for non-standard combinations, such as SAHP, as such systems require advanced optimizations and analysis on the individual components [162]. Therefore, for the SHAP systems, where the applications or load characteristics are significantly non-standard, detailed simulation tools are required to achieve accurate results. In this regard, TRNSYS [145] software provides these detailed modelling and simulation characteristics. Moreover, it has an extensive and validated built-in HVAC and renewable energy components library that no other simulation tools have [159], hence it is used as the main platform to simulate all SAHP systems proposed in this thesis. However, modelling a SAHP system is a complex task due to the unpredictable nature of the inputs such as the performance characteristics of the HP unit. Thus, the possibility of using a combination of alternative programs together should be left open when designing such systems. When modelling a HP unit in a SAHP system, the thermodynamic properties of the working fluid in the HP cycle should be known to model the component without manually entering these parameters. Since the TRNSYS does not provide such information, the HP unit of the proposed SAHP systems in this thesis is modelled with the EES [163] software. The EES eases the solution for non-linear equations and has integrated functions for thermodynamic and heat transfer problems, hence it is utilized as a co-simulator when designing the SAHP system. Further details of these tools are given in the following sections.

3.3 THE TRNSYS SOFTWARE

TRNSYS is an acronym for ‘Transient System Simulation’ and is a quasi-steady simulation

software having a modular structure used to investigate the HVAC systems, renewable and electrical energy systems, building thermal analysis, and performance and control of the transient systems [145]. The program has two main parts. The first part is an engine (known as KARNEL) that reads and processes the input files (in *.dck format) to solve differential or algebraic equations, establish convergence, and plot the system variables [162]. The second part of the software is a library which contains pre-developed components prefixed as 'Type'. The Types are independent mathematical models that are experimentally validated and can function individually as well as in a group of different components to form a complex system. The TRNSYS library has more than 150 Types including the HVAC and renewable energy components, building samples, weather data, controllers, etc. [164].

The built-in components (Types) in the TRNSYS library can be altered or even a new one can be produced. Although TRNSYS is a FORTRAN-based software, different coding languages (e.g. C++, EES, PASCAL, and EXCEL) that are capable of creating dynamic link libraries (DLL), can be used to make these modifications or generate custom components. This is a significant feature that creates more reliability and flexibility for the simulation and distinguishes the software from the others [165].

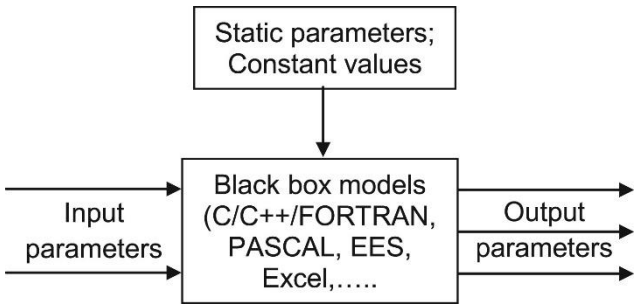

Figure 3.1: Modelling concept of the TRNSYS [166].

The core principle of TRNSYS is to model each component of an energy system as a standalone "black box" and then connect these boxes in a user-friendly graphical interface. When the TRNSYS is executed, first, the main workspace (called simulation studio) is

opened and a project file, known as a deck file (in *.tpf format), is generated for the simulation engine operating behind the simulation studio. In order to operate a component, two main characters should be known; constant PARAMETERs (e.g. number of components, coefficient values, etc.) and time dependent INPUTs (e.g. weather data). After this setup, the users can connect the selected boxes (components) graphically by simply dragging and dropping them. During the operation, the OUTPUTs (e.g. electrical or thermal performances, energy generation, etc.) of a component is calculated time-dependently as a function of the constant PARAMETERs and time dependent INPUTs. This modelling concept of the TRNSYS is visualized in Figure 3.1. In order to connect different components, the KARNEL engine uses a method called 'Successive Substitution Method' that links the output of a box to the input of another. This method permits calling the relevant components whenever they are needed to converge the solution. Overall, due to these flexibilities over the components and the design, the architecture of the simulation studio, and the modelling and simulation strengths, the TRNSYS environment is analogous to the physical experiments [154], [162], [164], [166].

In this thesis, the TRNSYS is used as the main platform to model the proposed SAHP systems. All TRNSYS components used for this purpose are summarized in Table 3.1. The fundamental components to construct a SAHP system, such as the reference building model, different solar panel types, etc., are detailed in the main research chapters of the thesis (Chapters 4, 5 and 6). In this chapter, nevertheless, details of the other remaining components which are used to connect and/or provide information for the main components, are explained. These components are usually seen as auxiliary but are necessary when modelling a complex system as they assist to construct the complete system. In the following sections, details of these components are provided. However, it should be noted that only the components whose parameters are changed (e.g. efficiency values, control signals,

assumptions, etc.) are described below. In addition, other components are used directly with the default parameters in the TRNSYS, hence they are not explained here and can be found in [145], [167].

Table 3.1: TRNSYS components used to model the SAHP systems in this thesis.

Component	**Type**	**Component**	**Type**
Building	88	Inverter	48a
Solar PV	103a	Hydronic Pumps	110
Solar PV/T	50a	Fluid Diverters (Controlled)	11b
Weather data	15-6	Fluid Diverters	11f
Differential Controllers	165	Tee-piece Mixers	11h
Thermostat controller	166	Forcing Functions	14h
Fluid Heater	138	Water Draw	14b
Water storage tanks	4a	Printers	25b and 25h
Printegrators	46a	Periodic integrator	55
TRNSYS-EES connection	66a	Plotting	65d

3.3.1 Selection of Pump Component in the TRNSYS

Type 110 is a variable speed pump in the TRNSYS library and is used in the proposed systems to circulate the working fluid between solar panels and the thermal energy storage units. Type 110 allows the sustaining of any output mass flow rate from zero to a nominal

rate. The control signal value changes the pump's mass flow rate linearly, hence the pump speed is variable. In addition, Type 110 does not consider the effects of pressure drop. Also, similar to the majority of TRNSYS pumps and fans, Type 110 accepts the mass flow rate as input but ignores it except when performing mass balance checks [167]. This means that the actual flow rate in the pump is an output, hence it is a function of the control signals and the maximum nominal rate set in the parameters of the display menu. In all variable speed hydronic pumps used in this thesis, the efficiency is taken as 70 % (as it is the efficiency value of the typical pumps in the market [168]). [169]). Also, it is assumed that the power consumption of the pumps is neglected as this consumption constitutes a small fraction of the annual total energy demand (lower than 0.5%) of other end-users (e.g. SH, SC, DHW, and EE) [168].

3.3.2 Selection of Hydronic Components in the TRNSYS

Type 11 of the TRNSYS library represents the hydronic components of the software including; tee-pieces, flow diverters (including the temperature-controlled diverters), and flow mixers through different unit numbers. In the proposed models of this thesis, however, tee pieces (Type 11h), flow diverters (Type 11f), and temperature controlled (TC) flow diverters (Type 11b) are used.

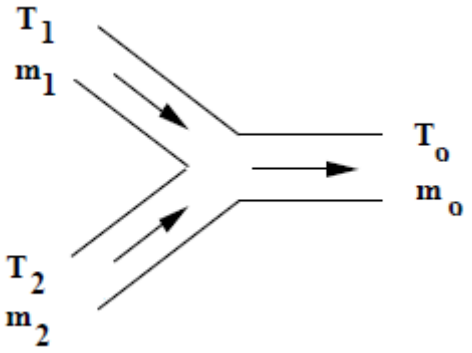

Figure 3.2: A schematic representation of the tee-piece in the TRNSYS library [167].

For the tee-pieces, the component is named Type 11h in the TRNSYS library and it is used in the thesis when supplying DHW to the users and mixing the fluids for the solar loop (see

Appendix 6-A, named as solar and DHW mixers). Type 11h mixes two inlet flows of the same fluid with different temperatures or humidity rates [169]. However, for the proposed models of this thesis, the effects of the humidity are neglected in the calculations (see Figure 3.2). Thus, the temperature and mass-energy balance of the mixed fluid is calculated as follows [167]:

$$T_0 = \frac{T_1 \times m_1 + T_2 \times m_2}{m_1 + m_2} \quad \text{(3.1)}$$

$$m_0 = m_1 + m_2 \quad \text{(3.2)}$$

where T_0 and m_0 are the temperature and mass flow rate of the mixed fluid to the users, respectively, while T_1, T_2, m_1, and m_2 are the temperatures and mass flow rates of the two inlet fluids, respectively.

Another component of the Type 11 is the tempering valves named as Type 11b. Tempering valves are actually flow diverters that are controlled by a temperature signal. In heating applications, it is a common practice to cool a heat source outlet by mixing it with a cold flow in order to meet the user's temperature requirements. For these scenarios in this thesis (e.g. when the temperature of the heat source is higher than the pre-set DHW temperature (50 °C) for the users), the tempering valves are used with the tee pieces to cool the heat source outlet. A schematic diagram of this combination is given in Figure 3.3 where the tee piece is positioned in 'A' and the tempering valve is in 'B'.

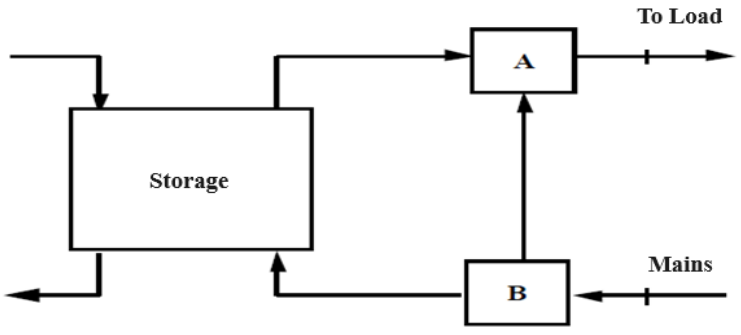

Figure 3.3: A schematic diagram of the tempering valve and tee-piece utilization [170].

The other flow diverter component of the TRNSYS library is the Type 11f and is employed in the Chapter 6 of the thesis to divert the hot stream of the solar unit to one of the two loops. Similar to the tempering valves, Type 11f uses a control signal to direct the incoming fluid to the one of the outputs proportionally or completely. A schematic diagram of the Type 11f is shown in Figure 3.4, where the incoming fluid is diverter one of the two exits with the aid of a damper controlled by a control signal (γ).

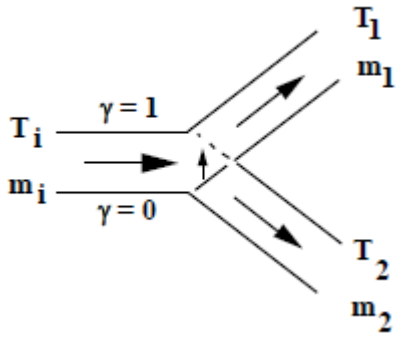

Figure 3.4: A schematic of the flow diverter, Type 11f [167].

As the main goal of the Type 11f is to direct the fluid, hence the outputs temperatures are the same with the incoming fluid temperature, but the mass flow rates of the outputs are determined by the γ control signal, which can be any value between 0 and 1. The correlation of the control signal and the mass flow rate of the outputs are formulated as follows:

$$T_1 = T_i \ \& \ T_2 = T_i, \ m_1 = m_i \times (1-\gamma) \ and \ m_2 = m_i \times \gamma \quad (3.3)$$

where the T_i, T_1, and T_2 are the temperatures of the inlet, first outlet, and the second outlets, respectively. Similarly, m_i, m_1, and m_2 are the mass flow rates at the inlet, first outlet, and the second outlets, respectively.

3.3.3 Selection of Forcing Function Components in the TRNSYS

Type 14 of the TRNSYS library represents the forcing functions that generate a time-dependent forcing function using a sequence of discrete data points that represent the function's value at different points throughout a cycle. The component can be used for

various purposes as long as the data points are known, such as lighting and occupying a building, implementing temperature values to a specific component, etc. For these purposes, the TRNSYS library has built-in forcing function components that can be used without modification [171]. However, the components used in this thesis are named Type 14h and Type 14b, which are the general forcing functions and water-draw forcing functions, respectively. These components are altered in the proposed models in Chapters 4, 5, and 6 of the thesis by adding instant values of the data points that are used, such as water draw values at each hour of a day.

3.3.4 Selection of Controller Components in the TRNSYS

The TRNSYS library has a wide selection of controllers, from simple thermostats to advanced PID or differential controllers. In this thesis, a room thermostat (Type 166) and numerous differential controllers (Type 165) are used to control the proposed models.

The Type 166 represents a thermostat that is used in residential houses. The component aims to monitor a single temperature and provides a signal for heating or cooling control, which are determined by pre-set and monitoring temperatures [169]. The component is employed in all building models in Chapters 4, 5, and 6 to monitor the zone temperature of the representative building in the models. The set-point temperatures for the heating and cooling in the models are selected as 20 ℃ and 26 ℃, respectively.

Type 165, however, is the main control component that is employed in all the proposed models in the thesis. It is used to control solar components, pumps, fluid diverters and mixers, and electrical heaters. Although the component is not restricted to the temperature inputs, in the thesis it is used for the temperature control. The Type 165 component generates an output control signal (γ) that is either ‘1’ (ON) or ‘0’ (OFF). The value for the control signal is selected based on comparing a temperature difference between two pre-selected

temperature values (upper (T_H) and lower (T_L)) with two dead-band temperatures [146]. For a solar collector, for example, the upper temperature (T_H) is the panel's outlet temperature, and the lower temperature (T_L) is the panel's inlet temperature. The values of these upper and lower temperatures and dead bands are different for each proposed model in the thesis and are given in the corresponding chapters (4, 5, and 6). Further, a new value for the control signal at a time step depends on the value in the previous time step. This dependency can be formulated as follows [167]:

<u>If the control signal was previously 'ON' (γ=1)</u>

$if\ \Delta T_{LDB} \leq (T_H - T_L),\ \ then\ the\ controller\ stayed\ 'ON'\ (\gamma = 1)$…….…… (3.4)

$if\ \Delta T_{LDB} > (T_H - T_L),\ \ then\ the\ controller\ is\ swithced\ \ 'OFF'\ (\gamma = 0)$…..…..… (3.5)

<u>If the control signal was previously 'OFF' (γ=0)</u>

$if\ \Delta T_{HDB} \leq (T_H - T_L),\ \ then\ the\ controller\ is\ swithced\ \ 'ON'\ (\gamma = 1)$…..…… (3.6)

$if\ \Delta T_{HDB} > (T_H - T_L),\ \ then\ the\ controller\ stayed\ \ 'OFF'\ (\gamma = 0)$…..……..… (3.7)

where ΔT_{HDB} and ΔT_{LDB} are the pre-set higher and lower dead-band temperatures, respectively. A schematic diagram of this correlation is shown in Figure 3.5.

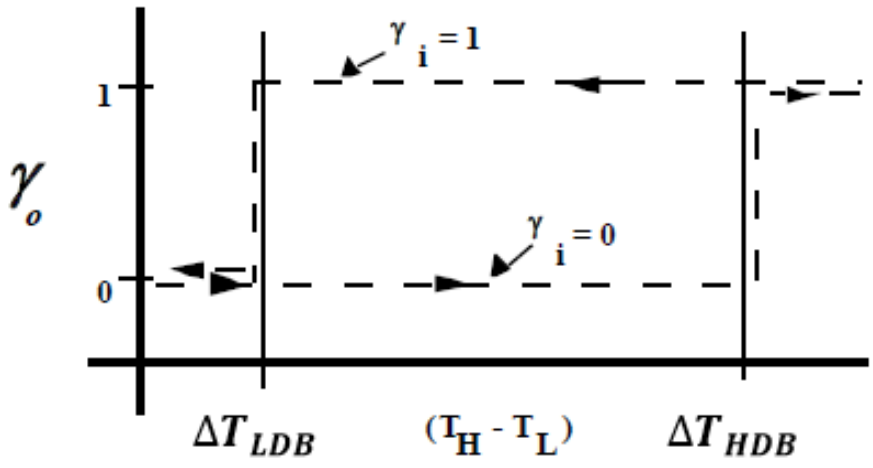

Figure 3.5: Working principle of the Type 165 [170].

Finally, the Type 165 controller has a high limit cut-out function activated when the high limit condition is surpassed, hence setting the control signal to zero (0) regardless of the dead-band temperatures.

Furthermore, other components, such as plotters, printers, periodic integrators, and printegrators, are used in the proposed models of the thesis without any modifications, hence their mathematical references can be found in [145], [167].

3.4 EES SOFTWARE

EES is an acronym for Engineering Equation Solver [163] that provides numerical solutions for linear or non-linear algebraic and differential equations [172]. Therefore, it has to be noted that the software is an equation solver, different from other software packages (e.g. TRNSYS, Energy Plus, etc.), it does not solve assignments that are formed by using a previous programming language. Due to this nature, the user needs to comprehend the problem first and write the equations by applying the physical principles and relations. After this setup, the EES solves these equations in a short computational time compared to the users developing their own iterative methods [140]. In addition, the software has other capabilities, such as conducting optimizations, checking units, making parametric and uncertainty analyses, and plotting high quality graphs and tables. Apart from these technical specifications, moreover, the EES has an extensive database of built-in thermodynamic and heat transfer properties of various substances. This point is of crucial importance as it leads the software to not only be an equation solver but also a powerful tool for creating custom-made mathematical models. Thus, the EES is capable of integrating the equation-solving capability with the property data flexibility to form engineering systems, such as thermodynamic cycles [173].

Due to these reasons, the heat pump (HP) unit of the proposed SAHP systems in this thesis

is modelled with the EES software. All components of the HP are modelled based on the thermodynamic functions (involving conservation of energy and mass) and property database of the EES. Detailed descriptions of this model and the governing equations behind each component are provided in Section 5.3.2 of this thesis. Since the EES is an equation-based software, the developed model is validated against experimental literature studies by applying the same boundary conditions as those in the experiment. The model is then optimized to find the optimum design points of the HP's parameters (see Chapter 5).

Finally, the EES can be called from the TRNSYS software. As stated earlier in this chapter, modelling a SAHP system is a complex task, hence calling the EES from the TRNSYS permits the creation of a model that can use the capabilities of both programs [171]. The combination of the TRNSYS and EES is straightforward due to the built-in Type 66a component of the TRNSYS that enables the combination without any modification [164]. Such a link is created in the proposed SAHP systems by using the output variables of the EES model as the input variables of the TRNSYS model.

3.5 CONCLUSION

This thesis uses a model-based methodology to investigate the feasibility of the proposed SAHP systems. The TRNSYS software is used as the main platform to model and simulate the entire solar-assisted heat pump systems. The reasons to choose the TRNSYS for this purpose is due to its extensive library containing most of the validated components of the SAHP systems. This is particularly important for the users as it saves both programming and computational time. However, as the TRNSYS environment does not contain the thermodynamic functions and the property databases of the utilized substances (e.g. water, air, refrigerants), the EES software is used in conjunction with the TRNSYS in the thesis to model the HP unit of the models. The EES software is an equation solver that contains thermodynamic properties of the hundreds of fluids which can be used to model the HP unit

of the proposed SAHP systems in the thesis. All developed models are validated against experimental literature studies to show the creditability of both software packages. The results of the validated system models are then investigated annually to reveal the feasibility of the proposed SAHP systems. The details of these models, validations, and results are presented in the main research chapters of the thesis, Chapters 4, 5, and 6.

In summary, the modelling and simulation of all the proposed SAHP systems were conducted by coupling the TRNSYS and EES software packages. The TRNSYS is the central platform to control and simulate the whole systems while the EES is used to model and optimize the heat pump units in the SAHP systems.

CHAPTER 4

Dynamic Energy Consumption Evaluation of a Typical European Single-Family House

4.1. INTRODUCTION

The building sector consumes almost one-third of the world's energy and is responsible for a quarter of GHG emissions. Depending on the region, the energy consumed in buildings vary significantly around the world, such as 41% in the US, 39% in the UK, 39% in Turkey, 37% in Japan, 42% in Brazil, 41% in the EU, and 50% in Botswana [174], [175], [176], [177]. Moreover, the residential sector, where the single-family houses have one of the largest shares, accounts almost 70% of these consumptions [178].

The end-users of the energy consumption of the buildings can be divided into two groups: thermal energy end-users including space heating (SH) and cooling (SC), domestic hot water (DHW), and cooking; and electrical energy (EE) end-users including lighting and electrical appliances. On a global scale, thermal energy occupies 77% of the buildings' total energy demand, while the remaining 23% is required in the electricity form [23], [179]. Moreover, the thermal energy demands represent more than 50% of the energy requirement of the residential single-family houses in many countries [178], and approximately 80% in the European countries [24]. In order to reduce this high consumptions, hence developing the necessary energy efficiency strategies on the building side, utilizing electrical appliances that are low-energy class, and using construction materials that has low heat transfer characteristics are essential [177], [179].

The building envelopes are distinctive elements of a structure that separate the indoors from the outdoors, such as external walls, roof, windows, etc., and they are responsible for most of the energy consumption loads, such as heating and cooling [26]. In order to reduce the energy consumption in buildings, these elements therefore must be energy efficient and sustainable. For the construction, in particular, assembling high-performing building envelopes is of critical importance when designing a new construction or retrofitting an existing building [26]. However, this can only be achieved if the buildings are constructed

based on a set of standards that are composed of performance requirements, thermal transmittance characteristics of the utilized materials for the building envelopes, and energy efficiency strategies. For the buildings constructed or retrofitted based on an energy efficiency standard/guidance, a substantial amount of energy savings can be obtained, as shown by many studies [178], [24], [180].

The building standards/regulations are usually obligated by the regional organizations, governments or local authorities. In the European Union regions, for example, the Energy Performance of Building Directive (EPBD) of the European Union has been implemented through a series of legislations. The latest of these is Directive 2018/844/EU [179], which was amended from the Directive 2010/31/EU [181] on the buildings' energy performance and Directive 2012/27/EU [182] on buildings' energy efficiency. The Directive 2018/844/EU [179] aims to reduce the final energy consumption in the buildings and to achieve a 40% reduction of the GHGs by 2030 through energy-efficient buildings that require minimum thermal and/or electrical energy. Also, meeting the reduced energy consumption by renewable sources and related technologies (heat pumps, CHP units, etc.) is equally important. In the directive, these energy-efficient buildings are named net-zero-energy-building (NZEBs). Based on the policy framework of the directive, new and existing (through renovations) buildings should be NZEBs. In a NZEB, the amount of energy required to keep the inhabitants' thermal comfort within acceptable limits is generated near the building ideally by the renewables [31]. For a specified period of time, typically one year, the amount of energy generation and consumption on the building reach a balance, hence becoming net-zero-energy.

For the other European countries that are not in the EU, however, each country uses its own building/construction standards that are either implemented from the ASHRAE standards [183] of the USA or from the neighbouring countries. Turkey, for example, uses its own

standards named TS-825 [184], shaped mainly based on the USA, EU, and German regulations. However, as of today, there are still countries in the European region that have no building standards, such as Albania, Montenegro, North Macedonia, and Bosnia and Herzegovina [185].

Moreover, based on the latest statistics [186], on a global scale, approximately 110 countries do not have a compulsory guidance/standard when constructing a building, which is the equivalent of more than 2.4 billion m^2 of floor area that is built without relying on any energy-related standards [27]. In these countries, the implemented local policies are either not compulsory or are just for non-residential buildings [180]. Considering the long lifetime of the buildings and the number of countries that have no building standards, the energy loss is considerably high globally.

On the other hand, one of the crucial steps in correctly assessing the energy load profiles of an energy-efficient living space is assessing the dynamic parameters of the construction. Some of these parameters are the dry bulb temperature (ambient temperature), solar radiation, wind speed, and humidity, which are changing form hour to hour. However, in almost all existing building standards, the evaluation of the energy loads is only for the SH and SC and is based on fixed or pre-determined parameters [179], [183], [184]. Among these parameters, solar radiation and ambient temperature are the most critical ones and have the greatest influence on the energy consumption of a building. However, when they are assumed constant (as in building standards), the energy demand profiles are either over- or underestimated, which often leads to uncertainties when designing, selecting, or sizing equipment on the energy supply side [187], [188], [189].

Furthermore, from the studies reviewed in Chapter 2 (Section 2.8), it was shown that almost all studies based energy demands on pre-assumed recurrent load profiles, which creates

mismatches between the energy demand and supply sides. From these studies it was evidenced that there is still a significant lack of guidance on dynamic calculation methods of the required energy consumption for SH, SC, DHW and EE end-users of buildings and almost no special attention has been paid to dynamically obtain these end-users for residential buildings. This study therefore attempts to fulfil this research gap by providing a complete guide on how to calculate and obtain all the energy consumption profiles of a typical single-family residential house within the boundary conditions of an EU candidate country (Turkey) and the EU directives for building standards. The novelty and importance of this chapter are to provide a comprehensive guide to dynamically (unlike the building standards) obtain SH and SC, and other demands vectors (e.g. DHW and EE) that a residential single-family house requires. Hence, the study contributes to the existing literature by calculating not only dynamic SH and SC demands but also DHW and EE consumption profiles in residential buildings using the validated building energy simulation components of the TRNSYS software. The dynamic behaviour on the demand side assists in better estimating the performance of the energy generation systems in real conditions. Furthermore, the proposed calculation methods are applied to find the energy consumption profiles of a typical single-family house but the methods can be reused and applied to any building type in any location worldwide. Finally, the scope of this study is obtaining the energy consumption load profiles, hence the technology implementation (which is the upcoming Chapters 5 and 6) is not within the scope of this chapter.

This chapter is organized as follows; the first stage of the chapter (**Section 4.2**) gives an overview of the selected location and provides a fundamental validation of the utilized data before the actual model development of the representative single-family house. The second step (**Section 4.3**) evaluates the dynamic space heating and cooling demand profiles by employing the Type 88 building model component of the TRNSYS. As the DHW and the

electrical energy demands are heavily dependent on consumer habits, the third (**Section 4.4**) and fourth (**Section 4.5**) subsections of the chapter are to present the calculation methods for obtaining the energy demand profiles of the DHW and EE, respectively. Finally, a conclusion (**Section 4.6**) is drawn for the chapter.

4.2 LOCATION SELECTION, MODEL VALIDATION, AND CLIMATIC DATA

This section provides details of the selected location to model the exemplary typical single-family house and a fundamental validation on the TRNSYS weather data component (Type 15-6) before developing the single-family house model.

4.2.1 Selected Country and its Building Standards

The representative single-family house in this study is created and tested in Izmir, Turkey. The reason for selecting this location is, first, Turkey is a transcontinental country that has land in both Europe and Asia, representing the exemplary house in different continents. The second reason is that Turkey is located in between the temperate Mediterranean and subtropical zones, hence it has four different climate zones [190], representing the exemplary single-family house in different climatic zones (according to the Köppen Classification [191], there are five main climatic zones in the world). The third reason is that Turkey is a European Union (EU) candidate country [192] that has its own building standards, assisting to represent the exemplary house in light of more than one building regulation. The specific reason to select the city of Izmir, however, is that it is one of the most populated cities in Turkey that has a building typology similar to the single-family housing (villas, detached houses, etc.) [193], [194]. Figure 4.1 shows this location on a world map.

Moreover, in terms of the building standards, Turkey started to pay more attention to the energy efficiency in buildings in 2000 with the standard named TS-825 [184] (Thermal

Insulation Requirements for Buildings). TS-825 contains material characteristics of the building envelopes, calculation methods to obtain the heating and cooling loads, and fixed monthly average ambient temperatures and solar radiation values for different regions in the country. In addition, it has been obligating the maximum overall heat transfer coefficients of the buildings constructed after 2000. However, when taking into account that the residential buildings constructed before 2000 accommodate almost 67% of the country's population [195], [196], it is clear to conclude that residential buildings in Turkey have a considerable energy-saving potential.

Figure 4.1: Location of the selected city [197].

4.2.2 Validation of the TRNSYS Weather Data

Weather data information is a vital part of this study as it shapes the design of the exemplary building's envelopes. For this purpose, the built-in weather data component of TRNSYS, Type 15-6) is employed, which has data implemented from 8 different external sources. These external sources are the Typical Meteorological Year (TMY), the TMY's version 1

(TMY1), and version 2 (TMY2) (all three are based on NREL's National Solar Radiation Database [198]), International Weather for Energy Calculations (IWEC) [199], Canadian Weather for Energy Calculations (CWEC) [199], EnergyPlus weather format [200], Meteonom files [201], and German 2004 and 2010 weather formats. All these files provide a typical year-round distributed weather data information for different locations and have already been implemented into the TRNSYS software where the users can select a location of interest.

In this thesis, the Meteonom weather data file (built-in the TRNSYS) is used as it contains comprehensive data sheets for different locations in Turkey, including Izmir. The Meteonom files provide the weather information for a typical meteorological year, moreover, it contains a total number of 59 outputs for each location including the parameters, such as ambient temperature, wind speed, solar radiation, etc.

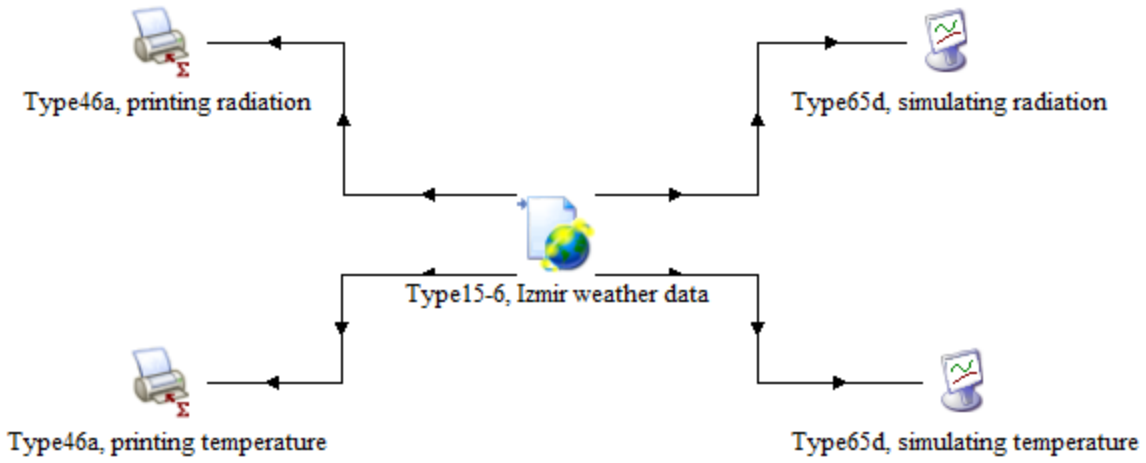

Figure 4.2: Screenshot of the TRNSYS simulation studio for the data validation.

However, to demonstrate the accuracy of the TRNSYS built-in data and to build confidence for the modelling of the exemplary single-family house in the following sections, the monthly average ambient temperature of Izmir from Type 15-6 is compared with the monthly average ambient temperature values of TS-825 (Thermal insulation requirements

of the selected country, see Section 4.2.1). For this purpose, first, a simulation studio is created in the TRNSYS to read the weather data values in Izmir. A screenshot of this studio is shown in Figure 4.2. Then, these monthly values are compared with the TS-825's values in Figure 4.3. It should be noted that the TS-825 values are a combination of temperature values for 16 different cities, including Izmir. This is because TS-825 divides the country into four different regions and assumes a constant monthly average temperature value for each region; the first region has 16 different cities, including Izmir. A complete list of these regions and the associated constant temperature values are presented in Appendix 4-A.

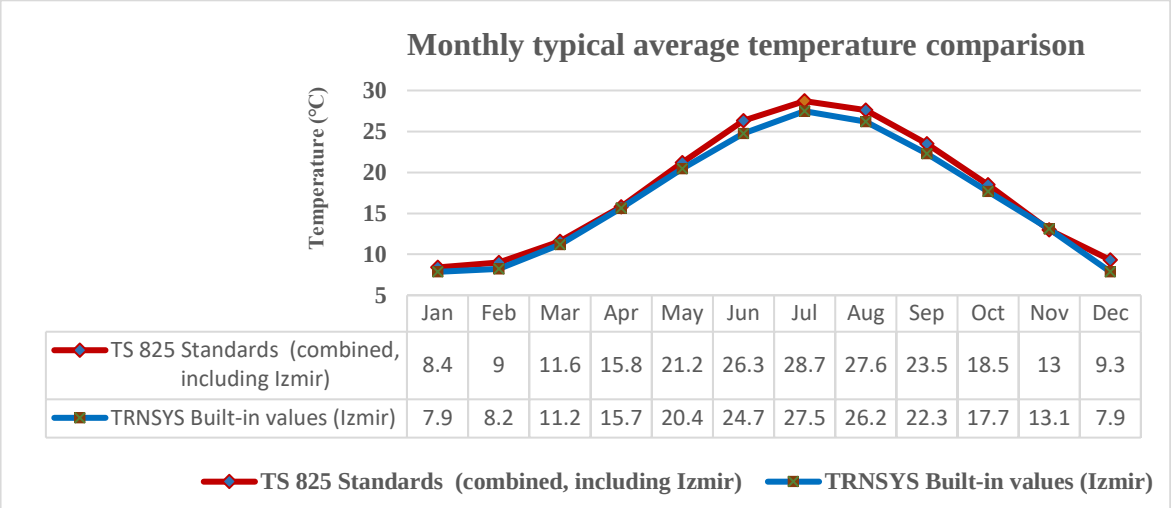

	Jan	Feb	Mar	Apr	May	Jun	Jul	Aug	Sep	Oct	Nov	Dec
TS 825 Standards (combined, including Izmir)	8.4	9	11.6	15.8	21.2	26.3	28.7	27.6	23.5	18.5	13	9.3
TRNSYS Built-in values (Izmir)	7.9	8.2	11.2	15.7	20.4	24.7	27.5	26.2	22.3	17.7	13.1	7.9

Figure 4.3: Comparison of TS-825 data and TRNSYS built-in data for Izmir.

Figure 4.3 compares the monthly typical average temperature values of the TS-825 data with the TRNSYS data for Izmir. From the figure, it is clearly seen that the Type-16 Meteonom data is in good agreement with the TS-825 data. Slight differences, especially in the summer months, are because TS-825 data is the combination of more than one location, where some cities are much hotter and/or colder than Izmir during the year in this region (see Appendix 4-A).

4.2.3 Climatic Data of the Model

It should be remembered, as stated in the previous section, the total horizontal radiation, which is also called the global horizontal irradiance (GHI), and the ambient temperatures are the decisive parameters when designing a building envelope. Subsequent to the model validation, in order to model the representative house and obtain its dynamic load profiles in the upcoming sections, therefore, the hourly distribution of these parameters has to be known. For this purpose, the validation studio is used and the relevant data is read and printed hourly (8760 h) and is presented in Figure 4.4. It has to be stated that the GHI here is the amount of total solar radiation incident on a horizontal surface (sum of direct, diffuse, and ground-reflected radiations) and is accumulated per square metre over a year for the selected location.

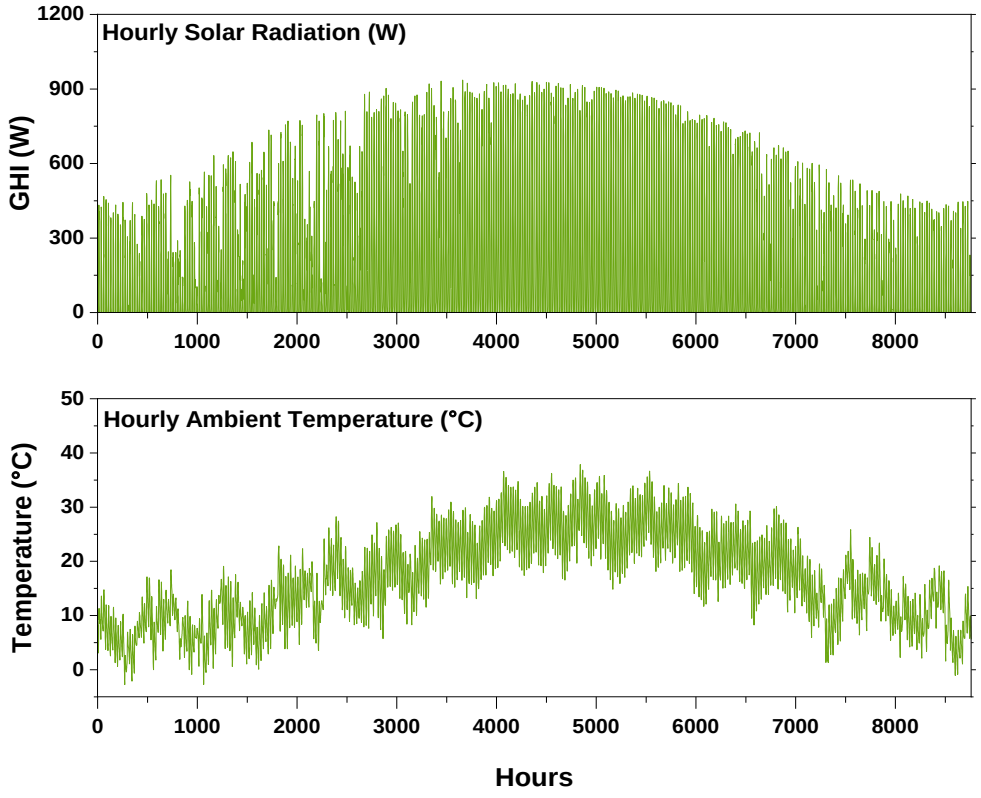

Figure 4.4: Hourly year-round solar radiation and ambient temperature of the selected location.

4.3 EVALUATION OF THE SPACE HEATING AND COOLING DEMANDS

This section evaluates the dynamic space heating and cooling demand profiles of the representative house on a fundamental typical building modelled in TRNSYS. The demand profiles are evaluated by using the weather data of the Type 15-6 component of the TRNSYS addressed in the previous section. The study is conducted with the following steps: first, the input data of the model, such as building characteristics, wall's envelope, specification of the utilized materials, etc., are determined by using both TS-825 standards [184] and the EU directives (2018/844/EU [179]). Then, the representative building is modelled in the TRNSYS environment by employing the Type-88 component, which is a single zone (lumped capacitance) building model. The final step provides results of the exemplary building's dynamically modelled space heating and cooling demand profiles.

4.3.1 Proposed Envelopes and Their Thermal Transmittance Values

The building model developed in this section is designed to present the energy consumption of a typical single-family residential house. Although it may not be a choice in reality, the building is assumed to be a single zone without internal walls to simplify the energy demand calculations. The total floor area of the building is 100 m^2, and four external walls are oriented in four directions with a square shape (10m x 10m). The height of the external walls is 3 m where two identical double-glazed windows with a total area of 4 m^2 are placed on the east and west walls. The total area and the pitch angle of the building's roof are 106 m^2 and 20^{o}, respectively. The external door has a total area of 2 m^2 which is placed on the north-face wall. 4 people are assumed to be the residents of the building as the average household size of a single-family houses is close to this value based on [202]. Finally, the occupancy rate is assumed to be 100%. However, it should be recognised that the energy demand will be high given that this assumption may be lower during working hours, especially on weekdays when residents are at work or school. However, in cases where the number of

users is higher, this assumption is made to compensate for the higher energy demand. Figure 4.5 demonstrates a simple sketch of the building while Table 4.1 provide a summary of the building's specifications.

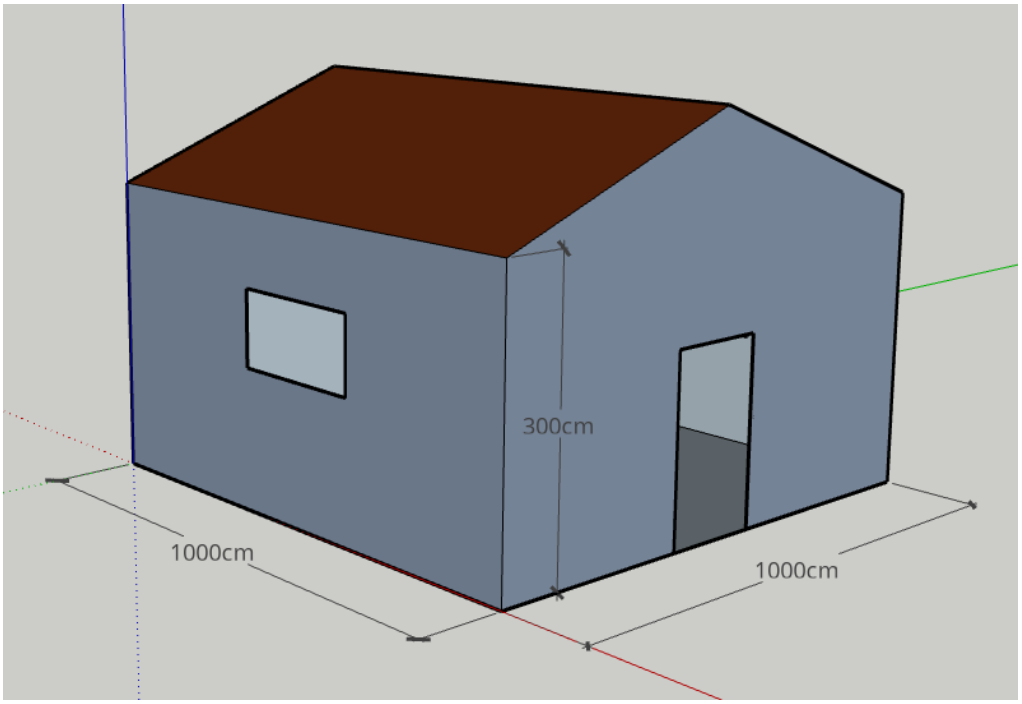

Figure 4.5: Sketch of the designed building.

Table 4.1: Summary of the building specifications.

Parameter	Value	Parameter	Value
Total floor area	100 m^2	**Number of persons**	4
Height	3 m	**Total window area**	4 m^2
Total external wall area	130.5 m^2	**Total door area**	2 m^2
Total roof area	106 m^2	**Roof pitch angle**	20º
Building Volume	466 m^3	**Occupancy schedule**	100%

An envelope, which means the structure of a building elements (e.g. external walls, floor, ceiling, etc.), has a great impact on the energy consumption of the buildings. In order to

reduce the energy consumption, it is vital to design the envelope of the building based on the local energy standards consisting of the material (used in the envelopes) specifications, maximum and minimum thermal transmittance values, energy-saving strategies, and calculation methods. These standards are provided by the regulations of each region and/or country. Many countries in the world have regulated their standards based on neighbouring countries and/or the ASHRAE standards of the USA [203]. Turkey, however, has adopted EU directives and standards [204], international ISO standards [205], and German DIN standards [206] to its own conditions and summarized them in TS-825 [184]. In TS-825, material characteristics, energy-saving strategies, the performance of different building types, and calculation methods of the dwelling's annual energy demand have been summarized. In addition, it provides the recommended maximum thermal transmittance values (called U value) of the building envelopes. A "U" value defines the ability of a material's heat transfer rate. Table 4.2 shows these recommended maximum U values from the TS-825 for different envelopes of a building for the selected city, Izmir.

Table 4.2: Recommended 'U' values for the selected city based on TS-825 standards [184].

Location	**U_{wall} (W/m^2K)**	**U_{floor} (W/m^2K)**	**$U_{ceiling}$ (W/m^2K)**	**U^*_{window} (W/m^2K)**
Izmir	0.70	0.45	0.70	2.40

(U^*_{window}: TS-825 recommends that thermal transmittance of the windows should be reduced to 1.8 W/m^2K).

The U value of a material is the inverse of its thermal resistance. Theoretically, the total thermal resistance of a building element consisted of uniform layers that are perpendicular to the direction of the heat flux and can be calculated as follows [207], [206]:

$$R_T\left(\frac{m^2.K}{W}\right) = \frac{1}{U} = R_i + R_1 + R_2 + \cdots + R_N + R_e \quad \text{.....} \quad (4.1)$$

where $R_1 + R_2 + \cdots + R_N$ are the thermal resistances of the single layers, and R_i and R_e are the surface thermal transmission resistance of the interior and exterior, respectively. Based on TS-825 [184] and EU standards [204], the design values of surface resistances (R_i and R_e) are 0.13 and 0.04.

The thermal resistance of a uniform single layer, however, is calculated according to the following expression [207]:

$$R_T\left(\frac{m^2.K}{W}\right) = \frac{d}{\lambda} \quad \text{.....} \quad (4.2)$$

where d and λ are the thickness and thermal conductivity of the layer, respectively.

When calculating the SH and SC load profiles, the utilized materials in the structure of the walls, ceiling, and flooring are of critical importance as their thickness and thermal conductivity decide the amount of heat transfer from the building to the ambient (Equation 4.2). With this regard, the materials having a lower value of thermal conductivity, such as insulation materials, is desirable. In particular, thermal insulation materials with a thicker layer of implementation are favourable as a properly insulated structure can reduce the heating demand by as high as three times [208]. However, it is not always feasible to design a building envelope with excessive insulation layers and/or very low thermal conductivity materials from an economical point of view. Therefore, it is critically important to implement such materials that are in line with the recommended standards. In this chapter, 9 different materials have been implemented in the envelopes of the representative house. For the external walls, a plaster-brick-insulation-brick-plaster (from the interior to the exterior) combination is selected. This is an applicable method in the EU and TS 825-EN standards for the single dwellings. Similarly, flooring and ceiling combinations are arranged

based on the TS 825-EN standards. For the flooring, a PVC-screed-insulation-light concrete combination is applied. The reason for the PVC flooring is because it is a common practice in almost every house in the selected location. For the ceiling, a combination of gravel concrete-waterproof layer-insulation-reinforced concrete-plaster is selected. Table 4.3 provides the thermo-physical specifications of these utilized materials. Moreover, Table 4.4 shows the summary of the building envelope, together with other properties of the utilized materials including thickness, and thermal conductivity and it summarizes the calculated thermal transmittance value of the building based on equations (4.1) and (4.2).

Table 4.3: Thermo-physical properties of the utilized materials and the calculated total thermal capacitance of the building (data source [184],[204], [126], [209]).

Specification / Material	Plaster	Brick	Insulation	PVC	Screed	Gravel Concrete	Water proof Layer	Reinforced Concrete
Specific Heat Capacity (kJ/kg. K)	1	1	0.8	0.9	1	0.96	0.75	0.87
Density (Kg/m^2)	2000	1800	40	1500	1800	2300	32	2300
Total Thermal Capacitance (kJ/K)					59044.9			

As it is seen from Table 4.3, the calculated U values are below the TS-825's maximum recommended U values (see Table 4.2). Moreover, the values are also in good agreement with the studies in the literature ([180], [210], [175]) conducted for residential single-family houses around the world. Hence they can be used, with confidence, in the next section when calculating the dynamic SH and SC demand profiles of the TRNSYS Type-88 representative house.

Table 4.4: Summary of the proposed envelopes for the exemplary single-family house and the calculated thermal transmittance values for these envelopes (data source [184],[204], [126], [209]).

Surface	Composition	Thickness (d Value) (m)	Thermal Conductivity (λ Value) (W/m. K)	Thermal Resistance (R Value) (m^2K/W)	Calculated Thermal Transmittance (U-Value) (W/m^2K))	Overall Thermal Transmittance (U-Value) (W/m^2K)
Exterior Walls	Ri	-	-	0.130	0.401	0.437
	Finishing Layer (Plaster)	0.015	1.000	0.015		
	Brick	0.120	0.810	0.148		
	Insulation	0.100	0.050	2.000		
	Brick	0.120	0.810	0.148		
	Finishing Layer (Plaster)	0.015	1.000	0.015		
	Re	-	-	0.040		
Total		0.37		2.496		
Flooring	Ri	-	-	0.170	0.387	
	PVC Flooring	0.020	0.230	0.087		
	Screed	0.030	1.000	0.030		
	Insulation	0.060	0.035	1.714		
	Light Concrete	0.200	1.100	0.182		
	Re	-	-	0.400		
Total		0.310				
Ceiling	Ri	-	-	0.100	0.468	
	Gravel Concrete	0.07	2.200	0.032		
	Waterproof Layer	0.01	0.038	0.263		
	Insulation	0.08	0.050	1.600		
	Reinforced Concrete	0.18	2.200	0.082		
	Finishing Layer (Plaster)	0.02	1.000	0.020		
	Re	-	-	0.040		
Total		0.36				
External Door	-	-	-	-	1.800	
Windows	-	-	-	-	1.800	

4.3.2 Modelling the Exemplary Single-Family House

Subsequent to the location selection and obtaining the building's thermal transmittance values, in this section, the details of the TRNSYS Type-88 representative building model are provided. The modelling of the Type-88 is conducted based on the Lumped Capacitance Method (LCM) [167] where it is assumed that there are no temperature gradients on the building structure, such as external sunlight heating, which changes the building zone's temperature. Therefore, the model neglects solar gains and assumes an overall thermal transmittance value (U value, Table 4.4) for the building. However, the building is subjected to internal gains such as from lighting, equipment, and people. As a consequence of the LCM, the structure of the building is taken as a single temperature with an overall thermal capacitance as calculated in the previous section (see Table 4.3). Figure 4.6 shows the screenshot of the TRNSYS Type-88 building model with the summary of the calculation boxes from internal gains, heating load, and infiltration rates, explained below.

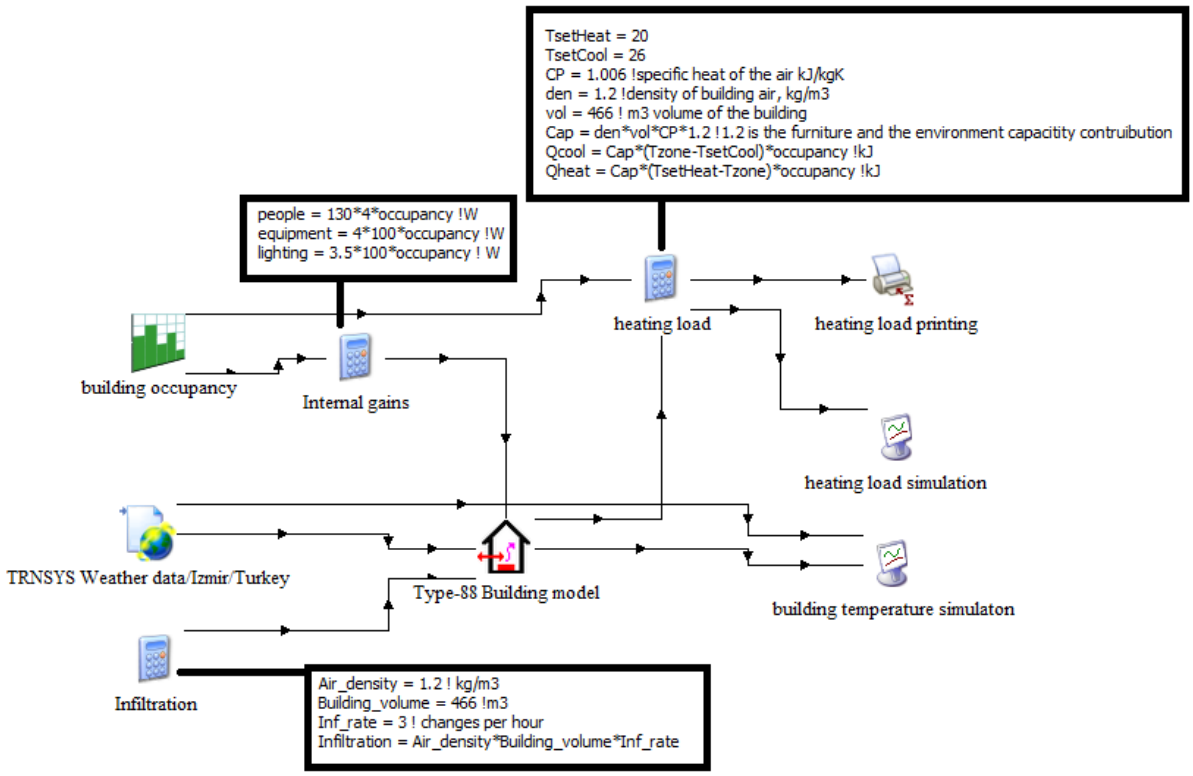

Figure 4.6: Screenshot of the Type-88 building model.

In the model presented in Figure 4.7, five different TRNSYS components/types are used. These are summarised as follows [167]:

• **Type 88:** The central component of the representative building that receives input values from the different components and processing the central energy balance equations in the KARNEL engine of the TRNSYS.

• **Type 15-6:** The weather data component built-in TRNSYS (see Section 4.2.3). The location is set for Izmir and it provides the Meteonorm weather input values to the Type-88.

• **Type 14h:** The time-dependent forcing function component built-in TRNSYS that provides the repeated-pattern forcing functions (indicating discrete data points at various times through one cycle) to the Type 88 (see Chapter 3). In the present model, Type 14h is used to specify the occupancy rate of the residents.

• **Type 46a:** The "Printegrator" in the TRNSY library (see Chapter 3), where the results from Type 88 are integrated. In the present model, the hourly space heating demand values are integrated and printed on daily and monthly bases.

• **Type 65d:** This is an online graphics component and is named as "Online Plotter" in the TRNSYS library, which is used to plot the selected variables from Type 88 at specified intervals of time (0.125 h, in the present model). The selected results are displayed on a separated plot on the screen while the simulation of the model is in progress. The component is used to simulate the building's zone temperature and the heating load profile in the model.

In terms of the mathematical modelling, however, the zone temperature for hourly resolution of the representative building is calculated by the following central energy balance equation [167]:

$$\frac{T_{zone}}{dt} = \frac{UA}{Bcap}(T_{amb} - T_{initial}) + \frac{\dot{m}_{vent} Cp_{air}}{Bcap}(T_{vent} - T_{initial}) + \frac{\dot{m}_{inf} Cp_{air}}{Bcap}\left(T_{inf} - T_{initial}\right) + \sum Q_{gains} \quad \text{(4.3)}$$

where U, A and $Bcap$ are the building's loss coefficient, total surface area, and total capacitance, respectively; $T_{amb}, T_{zone}, T_{vent}, T_{inf}, T_{initial}$ are the ambient, zone, ventilation, infiltration and initial zone temperatures, respectively; $\dot{m}_{vent}$ and $\dot{m}_{inf}$ are the mass flow rates of ventilation and infiltration, respectively, and Q_{gains} is the internal heat gains from the lighting, equipment and people.

The mass flow rate of the ambient air that infiltrates through the building's envelope is calculated using the following expression [167]:

$$\dot{m}_{inf} = Air_{den} \times B_{vol} \times Inf_{rate} \quad \text{(4.4)}$$

Similarly, the capacity of the building is calculated as follows [209] :

$$B_{cap} = Air_{den} \times B_{vol} \times CP_{air} \times CAP_{cont} \quad \text{(4.5)}$$

where Air_{den} and B_{vol} are the density of the air and volume of the building, respectively; Inf_{rate} is the infiltration rate of the ambient air per hour; CP_{air} is the specific heat of the ambient air, and CAP_{cont} is a constant representing the capacity contribution of the living space in the building (e.g. furniture) and is taken as 1.2 based on [211].

The internal heat gains (Q_{gains}) from the lighting, people and equipment are formulated as follows [206], [209]:

$$Q_{gains} = \left[N_P \times Q_P + (Q_L + Q_E)A_f\right] \times Occupancy\ Rate \quad \text{(4.6)}$$

where N_P is the number of residents; Q_P, Q_L, Q_E are the heat gains from people, lighting, and equipment, respectively; A_f is the total floor area of the house, and $Occupancy\ Rate$ is the level of the occupancy from the residents of the building.

Finally, the hourly dynamic heating and cooling demands of the building are calculated as follows [167]:

$$\frac{dQ_{HEAT}}{dt} = B_{cap} \times (T_{setHeat} - T_{zone}) \times Occupancy\ Rate \quad (4.7)$$

$$\frac{dQ_{COOL}}{dt} = B_{cap} \times (T_{zone} - T_{setCool}) \times Occupancy\ Rate \quad (4.8)$$

where $T_{setHeat}$ and $T_{setCool}$ are the set point temperatures for heating and cooling, respectively.

In addition, the following assumptions have been applied to the building model:

• The effect of the heat bridges has been neglected when calculating the U-values to not overestimate the heat losses of a building that is modelled based on the LCM and having no solar gain [167].

• Natural ventilation is considered, hence ventilation values are not used in equation 4.3.

• Infiltration rate is assumed as 3 changes per hour [120], which takes into account not only air changes from the building's cracks but also air changes caused by window and door operations.

• LCM is used, hence the solar gain's effect is neglected on the T_{zone}.

• Heat gain per person is taken as 130 W [203], [212].

• Heat gain from lighting per m^2 of the floor area is taken as 3.5 W [184].

• Heat gain from equipment per m^2 of the floor area is taken as 4 W [184].

• The heating set temperatures is assumed as 20 ℃ to achieve the usual comfort levels for the residents. This means that the space heating is required only when the temperature of the

zone falls below the set temperature value. Hence the Equation 4.7 runs only when $T_{setHeat} > T_{zone}$.

• The cooling set temperature is assumed as 26 ℃, which is a common practice for the cooling set points. This means that cooling of the house is required only when the temperature of the zone exceeds the set temperature value. Hence the Equation 4.8 runs only when $T_{setCool} < T_{zone}$.

• Finally, the occupancy rate of the building is assumed as 100% as detailed in Section 4.3.1.

4.3.3 Results of Dynamic Space Heating and Cooling Load Profiles

The simulation results of the heating and cooling load profiles of the TRNSYS Type-88 building model are presented in this section. The annual simulations are conducted for 8760 h with a time step of 0.125 h. Figure 4.7 shows the dynamic hourly demand profiles of the heating and cooling load demands of the representative house for the typical year. As seen from the figure, the space heating demand is much higher than the cooling demand of the house for the selected location. More importantly, in May, September, and October, the building does not require heating or cooling as it is in the thermal comfort zone temperatures of 20 ℃ and 26 ℃ levelled by the set point temperatures of heating and cooling, respectively (see Figure 4.9). For a clear inspection, the hourly demand profiles are integrated and printed on a monthly basis with the Type 46a “printegrator” component of the model and are shown in Figure 4.8. The calculations are carried out for the meter square of the total usable floor area of the building. Based on these calculations, the total annual heating and cooling demands are calculated as 5721 kWh and 594 kWh, respectively.

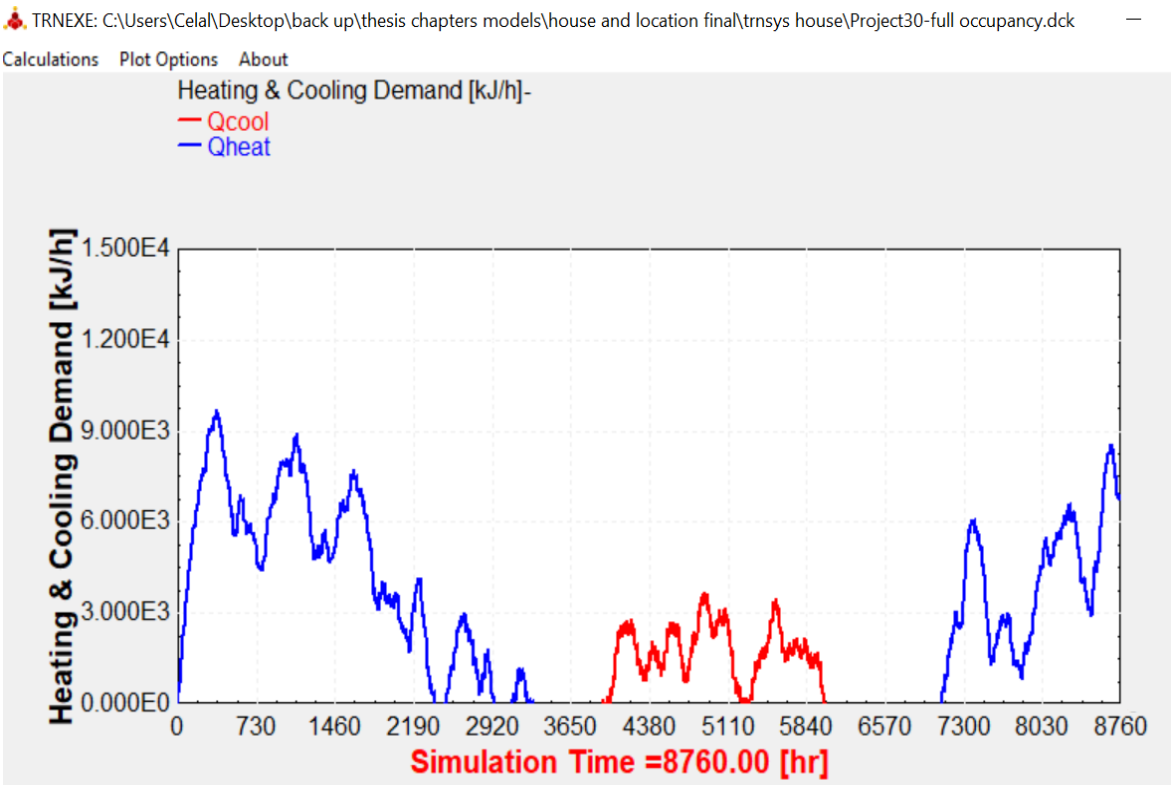

Figure 4.7: Dynamic hourly heating and cooling demand profiles of the exemplary building.

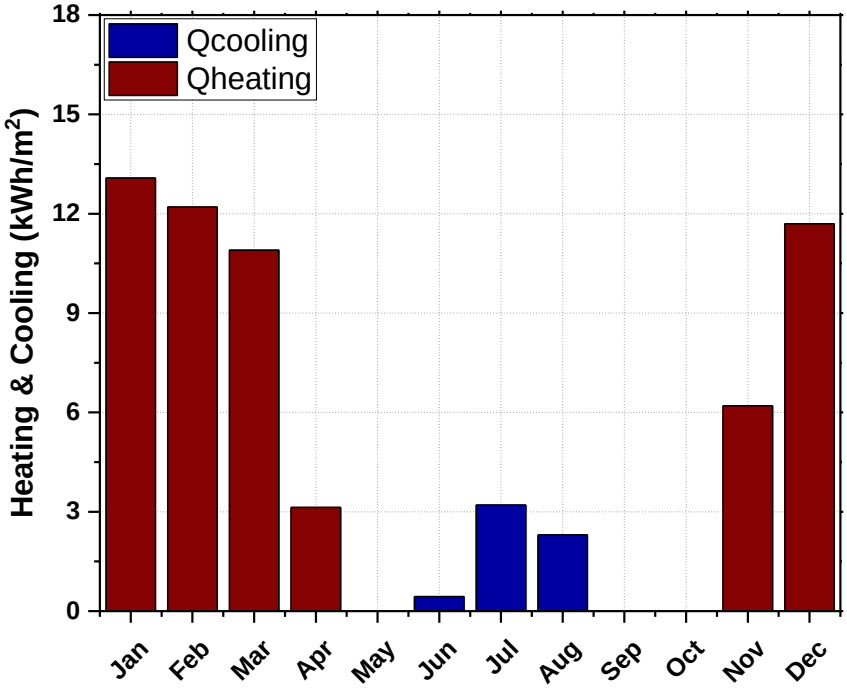

Figure 4.8: Monthly heating and cooling demands per m^2 of the building's total floor area.

For the typical single-family house, it is seen from Figure 4.8 that the maximum total monthly heating load occurs in January, with a demand profile of 13.08 kWh/m^2. This is reasonable because the ambient air temperature is at its minimum value during this month (see Figure 4.9). Moreover, the maximum hourly heating load of the building is found to be 2.651 ≈2.7 kW on 15th January between 11-12 a.m. (the coldest ambient temperature is observed in the same day as -2.7 ℃ at 8 a.m., see Figure 4.9). This value is the peak point of the heating load profile and is used as a reference to design the proposed heating systems in this thesis. Similarly, the maximum total monthly cooling load is observed in the hottest month of the year, July, with a demand value of 3.2 kWh/m^2. In addition, the maximum hourly cooling load is printed as 0.99 kW ≈ 1 kW on 24th of July between 3-4 p.m.

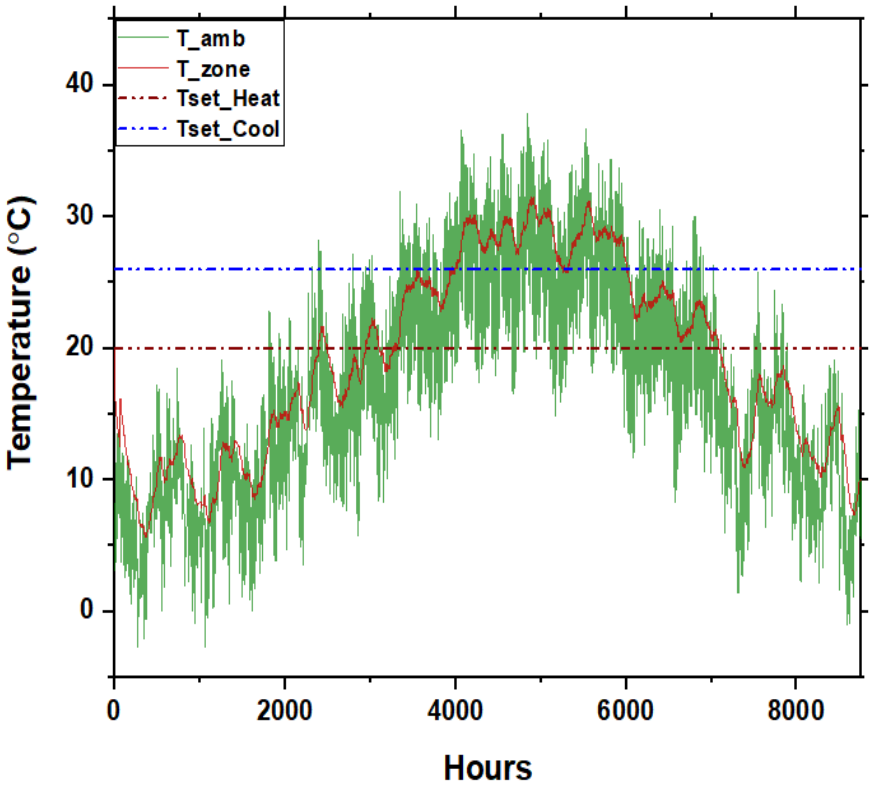

Figure 4.9: Hourly distribution of the ambient, zone, and set points (heating and cooling) temperatures throughout the typical year.

Finally, in Figure 4.9, the hourly distribution of the ambient, the building's internal zone, and the comfort level temperatures (heating and cooling) of the building over the typical year of the Meteonorm data in TRNSYS are presented. It is clearly seen that the zone temperature profile follows a similar trend with the dynamic energy demand profile that is shown in Figure 4.7. This is best explained by the effect of the dynamic input parameters of the model (e.g. ambient temperature, solar radiation, wind, etc.) on the energy consumption of the building, detailed in Section 4.2, and shows the successful implementation of the building model. During the non-heating season, finally, as the zone temperature of the building is in between the set point temperatures (20 ℃ and 26 ℃ for heating and cooling, respectively), there is no energy consumption for the representative house.

4.4 EVALUATION OF THE DOMESTIC HOT WATER (DHW) DEMAND

The domestic hot water consumption profile is subject to a high degree of variation from day to day, location to location, and person to person. The dominant effects of this variation are the user's habits, the weather, and the socio-economic conditions of the people. Therefore, a widely accepted consumption profile that can be associated with a specific location or country is not available. In order to size their DHW system, some authors measured their own hot water consumption profiles as in [213], [214]. This method, however, is not always practical, hence a robust calculation method has to be established.

In the absence of monitored data for Izmir, the DHW load profile is constructed based on commonly accepted assumptions in the literature. According to data from Energy Saving Trust (EST, an independent UK-based organization) [215], the variation of the DHW consumption is in the range of 25-300 litres per day per person although an average figure appears to be nearer the lower limit. Another key finding of the EST [215] is that the mean delivery temperature of the hot water (with 95% of confidence) is close to 50 ℃, which is significantly different from the traditionally assumed value of 60 ℃. In another study

conducted in a cold environment, the authors [216] concluded that the sharp peak in the DHW consumption profiles are observed during the morning hours between 7-9 a.m. and during the evening hours between 8-10 p.m. with an average consumption of 4.1 L/person/h. When adding the non-peak average value of 1.1 L/person/h in the study, the daily consumption of DHW was found close to 38 L/person/day.

It is acknowledged that during the summer period the consumption pattern is higher than in the winter period due to frequent bathing. On the contrary, during the cold months, the temperature required for hot water is much higher than in the summer season. Therefore, Kalogirou [92] stated that the thermal energy needed for DHW throughout one year is reasonably constant. For his study conducted for a Greek city [92], 30 L/person/day of DHW was used, moreover, he concluded that using anything than a repetitive load profile is impractical to simulate the DHW demand profile over one year. Yilmaz [217] used 40 L/person/day of DHW for a typical Turkish house when he investigated residential solar water heating systems in Turkey. In another study, Uctug and Azapagic [218] used 100 L/day of DHW for a typical Turkish house, which is around 30 L/person/day when considering a family of 3.

Therefore, in this thesis, the daily DHW load profile is assumed to be repetitive throughout the typical year and that a daily consumption value of 160 L (40 L per person) at 50 °C is considered to achieve the usual thermal comfort levels. In order to calculate the energy demand profile for the DHW, however, the daily consumption profile has to be known. For this purpose, the profile from Kalogirou [92] is used which is shown in Figure 4.10. As seen from this figure, the sharpest peak loads are observed during the morning and evening hours, which is in line with the literature suggestions [216].

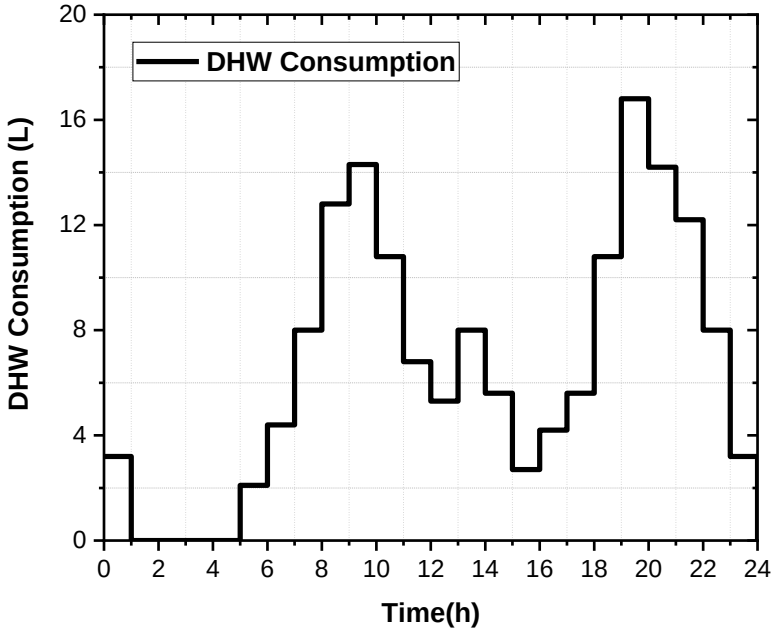

Figure 4.10: Daily DHW consumption profile.

In terms of the modelling, however, the daily thermal energy demands for DHW can be formulated as follows [218]:

$$Q_{DHW} = V_{DHW} \times Cp_w \times \rho_w \times (T_{SET} - T_{city}) \quad \text{(4.9)}$$

where V_{DHW} ($\frac{L}{day}$) is the daily volumetric DHW consumption, Cp_w ($4.18\frac{kJ}{kg.C}$) is the specific heat of the water, ρ_w ($1\,\frac{kg}{L}$) is the density of water, T_{SET} (℃) is the set temperature of the DHW (50 ℃), and T_{city} (℃) is the temperature of the inlet water coming from the mains. In order to calculate the energy demand for DHW, the only unknown parameter in Equation 4.9 is the temperature of the inlet water (T_{city}).

In the literature, the temperature of the inlet water is usually assumed to be constant ([216], [72]), which makes the DHW demand profile constant throughout the year. However, the actual main water temperature differs from month to month. This is critical as the temperature differences between seasons can significantly affect the total thermal energy required for the DHW. For this purpose, the monthly average mains water temperature of

the selected location is illustrated in Figure 4.11, together with the pre-set DHW temperature which is aimed to be delivered to the residents of the representative house (data is obtained from [218]). In Figure 4.11, hence the region between the city's main water temperature and the DHW's pre-set delivery water temperatures represents the DHW energy consumption profile.

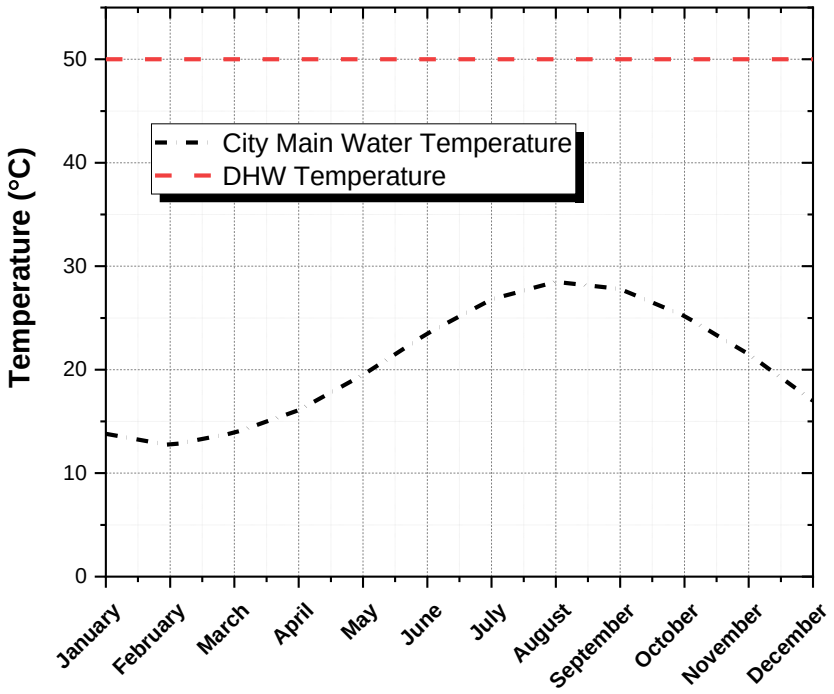

Figure 4.11 : The monthly average inlet water temperature and DHW pre-set temperature (data source [218]).

Based on Equation (4.9) and Figure 4.11, the monthly energy demand for the DHW consumption of the representative single-family house is calculated and presented per m^2 of the total floor area of the building in Figure 4.12.

In Figure 4.12, the monthly results are shown based on the meter square of the total usable floor area (100 m^2) of the representative house. As it can be observed from this figure, when the monthly results are aggregated, the ratio of total annual DHW energy demand to the building's usable floor area is found as $14.97 \approx 15$ kWh/m^2.a. This is precisely the equivalent

of a 1497 kWh of energy annually for a 100 m^2 of the total useful floor area. In addition, the maximum monthly loads occur in January and March with an energy requirement of approximately 156 kWh/month.

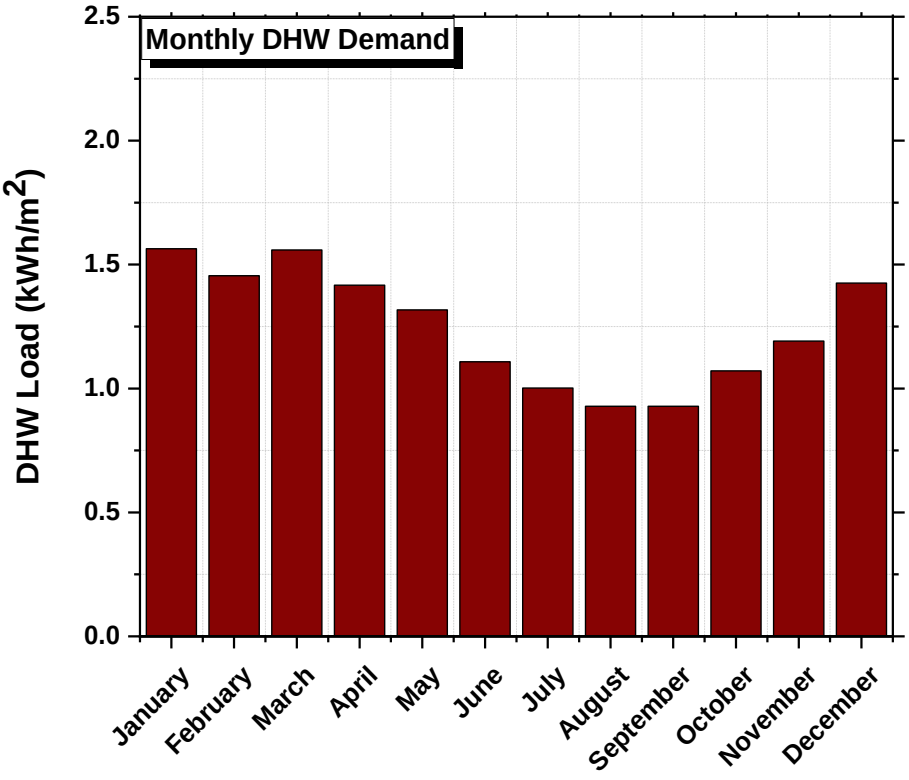

Figure 4.12: Monthly DHW demand profile.

On the other hand, the maximum daily and hourly DHW energy needs are observed during the month of February with the values of 5.20 kW and 0.73 kW, respectively. This is because the inlet temperature of the mains water temperature is the lowest in this month with a value of 12.7 ℃ (see Figure 4.11). It should be noted that although its city's inlet water temperature is the lowest, the maximum monthly energy demand does not occur in February as this month has fewer days (28) compare to January (31) and March (31).

4.5 EVALUATION OF THE ELECTRICAL ENERGY (EE) DEMAND

Similar to the DHW requirement, the amount of electricity used by a single-family house can vary significantly. This is because of the structural differences between the countries

(e.g. lack of electricity), householders' habits, and climates. Also, the EE demand of a typical house depends on whether or not heating and cooling loads are added. Since these loads are calculated dynamically, in this section, the EE demand only includes the electricity consumption of the household equipment. Hence, when calculating the EE demand, the power consumption of the household equipment that is commonly used in a typical single-family house is considered. Table 4.5 summarises these typical equipment and their monthly energy consumption, together with their name, power consumption, and usage frequency.

Table 4.5: Monthly electrical energy demand of the representative house (data source: [219], [220], [221]).

Equipment	Power Consumption (W)	Number of Equipment	ON-Time (h)	Number of Weekly Usage	Weekly Energy Consumption (kWh)	Monthly Average Energy Consumption (kWh)
Refrigerator	46	1	24	7	7.73	188.8
Dish Washer	510	1	2.17	5	5.53	
Washing Machine	980	1	2.3	1	2.25	
TV	70	1	4	7	1.96	
Iron	1000	1	0.1	4	0.40	
Vacuum Cleaner	700	1	0.5	2	0.70	
Oven	1500	1	1	2	3.00	
LED Light Bulb	7	3	5	7	0.74	
Kettle	2500	1	0.2	7	3.50	
Toaster	800	1	0.1	7	0.56	
Electric Hob	1000	1	0.75	7	5.25	
Microwave	700	1	0.1	7	0.49	
Laptop/PC	50	2	2	7	1.40	
Phone Charging	4	2	1	7	0.06	
Others	-	-	-	-	10.00	

For the table, it should be noted that the selection, number of the equipment, usage habit, and power consumption of the equipment may change significantly from person to person

and manufacturer to manufacturer. Hence, the utilized method can be modified and reused to calculate the monthly EE demands. Based on the data in Table 4.5, the monthly and daily energy consumptions of the representative single-family house are calculated as 188.8 kWh and 6.3 kWh, respectively. Also, the representative house's annual EE demand per meter square of the useful floor area is calculated as 22.65 kWh/m^2.a. Furthermore, the obtained results are in good agreement with the electricity consumption of the other typical single family houses in the literature [222], [223].

Finally, the hourly distribution of the representative house's total daily EE demand is adjusted from the study of Aberilla et al. [224], which is also used in [225] & [127] with a similar trend and is suggested for the selected location by [226] & [227]. Figure 4.13 shows this daily distribution of this 6.3 kWh total EE demand for the selected location, where the hourly maximum load is observed as 608 W.

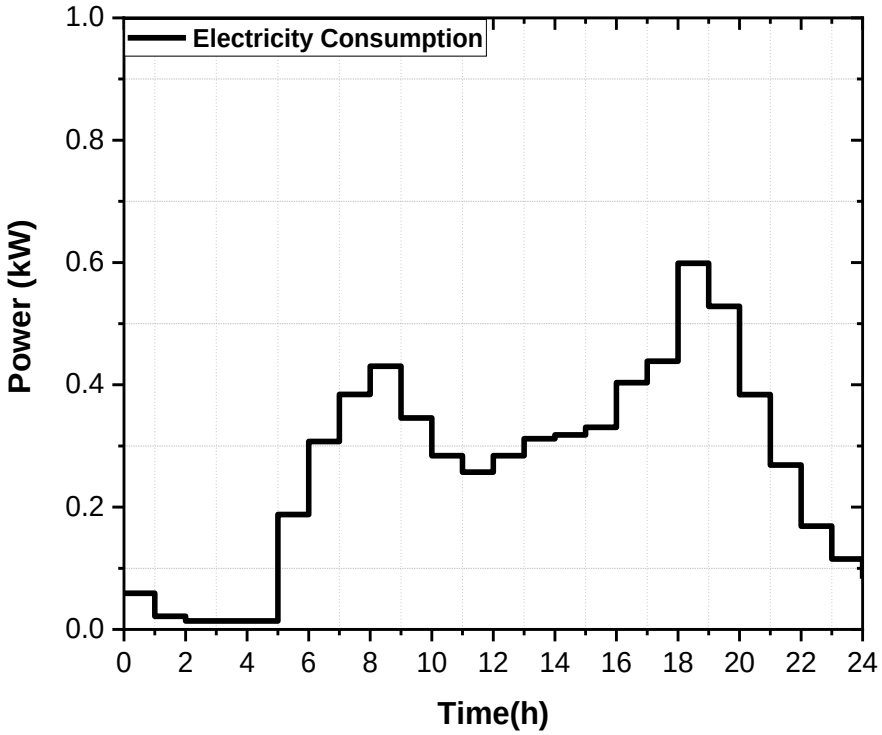

Figure 4.13: Hourly EED demand profile of a typical heating season day.

4.6 CONCLUSION

Residential single-family houses account for one of the largest consumptions and are inevitably responsible for significant emissions in the building sector. Space heating (SH) and cooling (SC), domestic hot water (DHW), and electrical energy (EE) end-users are the primary vectors causing this high consumption. Among these demands, while the SH and SC demands are mainly affected by the building envelopes and are the largest energy-consuming vectors, the DHW and EE demands are usually influenced by the choices of the residents and often have lower energy consumption compared to the first two. In order to reduce these consumptions, particularly SH and SC demands, hence building envelopes must be constructed based on performance standards that are obligated by governments or local authorities. Today, however, there are still approximately 110 countries worldwide that have no building standards including the one located in the European region. Moreover, almost all building standards that are in force based their energy consumption calculations on fixed or pre-determined constant weather data values, such as solar radiation, ambient temperatures, etc. When designing an energy delivery system, however, this assumption leads to imbalances between the energy demand and supply sides. As a result, the energy delivery systems are usually under or oversized.

In order to address these issues, this chapter therefore investigated the dynamic energy consumption evaluation of a typical European single-family house and provided a complete guidance on how to obtain not only SH and SC but also DHW and EE demand vectors of an exemplary building in light of the building standards of the EU and an EU candidate country, Turkey. For this purpose, the exemplary building that had a single zone and a 100 m^2 useful floor area was modelled using the Type 88 lumped capacitance building model component of the commercial software, TRNSYS. The results of the model were simulated hourly and

were aggregated and analysed daily, monthly, and annually with the built-in component of the TRNSYS.

The dynamic results revealed that space heating was the biggest contributor to the energy consumption of the representative house, with an annual total energy demand of 5721 kWh. Also, the daily peak load of the heating demand was observed as 2.7 kW on the coldest day of the year, on 15th January. In addition, the total annual cooling demand was found to be 594 kWh, with a daily peak load value of 1 kW occurring during the hottest day of the typical year, 24th of July.

For the DHW consumption, it was concluded that a 40 L of hot water consumption per person at 50 ℃ was an acceptable value for the selected location. By considering the location's variable monthly mains water temperature, the annual total DHW demand of the representative house was found as 1497 kWh. The daily DHW consumption profile, however, depends on the consumer's highly variable habits. In this study, however, a generalized daily consumption profile was adapted from the well-accepted literature studies for the selected location. Based on this, the maximum daily and hourly consumptions were found to be 5.20 kWh and 730 W, respectively.

As the EE consumption varies significantly from user to user, and from manufacturer to manufacturer (for the equipment), it was concluded that the most appropriate method to evaluate the EE consumption was to consider the essential electrical equipment used in a typical single-family house. After this consideration, the electrical energy consumption of this equipment was calculated based on the user's utilization frequency of the equipment. With this method, the monthly and annual EE demands were found to be 188.8 kWh and 2265 kWh, respectively. Further, the daily consumption and hourly peak load were found by using a similar methodology as in the DHW calculations, hence they were found as 6.3

kWh and 608 W, respectively. These results, consequently, showed that the exemplary single-family house had a total of 10077 kWh of combined thermal and electrical energy (SH+ SC+DHW+ EE) demand annually.

Overall, the dynamic energy consumption profiles of the typical single-family house presented in this study can be used to accurately size and design any energy generation systems, and the SAHP systems in this thesis. The dynamic behaviour on the demand side will help to better assess the performance of the energy delivery systems in real conditions. Moreover, the energy demand calculation methods presented in this study can be modified and reused as a guideline for any location where the calculation methods are not regulated by the local authorities.

CHAPTER 5

Techno-Economic Performance Assessment of the Combined Heat Pump and Solar PV Systems for the Net-Zero-Energy European Single-Family Houses: A Case Study in Turkey

5.1. INTRODUCTION

The EU aims to reduce its GHG emissions by 80-95% by 2050 compared to the 1990 level [228], [19]. In order to achieve this goal, decarbonisation of the energy sector becomes a necessity. In today's energy mix, buildings account for approximately 40% of the total energy consumption of many European countries, but renewable energy supplies only 11% of this rate [29]. Moreover, the energy required for the space heating & cooling (SH and SC) and domestic hot water (DHW) end-users of a typical single-family house can reach up to 80% of the total energy consumed in the house, where the rest is required in the form of electrical energy (EE). These demands are mainly supplied by fossil fuels [179], hence resulting in high emissions. As a solution, the EU has implemented a number of legislations (e.g. 2018/844/EU [179], etc.) to achieve the "Net-Zero-Energy-Building (NZEB)" concept in buildings, which promotes to reduce the energy consumption of these end-users (SH+SC+DHW+EE) and meet them ideally by the renewable energy sources.

Electrification of the thermal end-users (e.g. SH and SC) of the residential building sector is recognized as an essential pathway to decarbonize the building sector, as it permits the renewable electricity utilization in buildings [228], [229], [230]. With this regard, heat pumps (HPs) and solar photovoltaics are seen as the main pillars of the electrification scenarios in buildings [19], [231]. A grid-connected distributed PV system generating low-carbon electricity on the rooftop of a residential building combined with an electrically driven HP can significantly reduce the primary thermal demands of the building and the grid dependency. As a result, the PV+HP combination is considered one of the most fundamental and cost-effective technological solutions to decarbonize the building sector and to achieve the NZEB concept in the European region [232], [36], [231], [233].

For the electrically driven HPs, the COP is a performance assessment function and is the ratio between the useful heating/cooling supplied to the users and the power used to operate

the HP's compressor. With this regard, a higher COP for a HP system means the lower power consumption while ensuring the same heating or cooling outputs. When used for the thermal demands (SH and SC) in buildings, HPs reduce the amount of energy needed to satisfy these demand due to their high COP values compared to boilers or electrical heaters [43]. The HPs also electrify the thermal energy demand of the buildings as they require only electricity to operate their compressor, thereby allowing renewable electricity, such as solar PV, to be implemented into buildings [234].

Among all HP types detailed in Chapter 2 (including the air-sourced HPs (ASHP), see Sections 2.6, 2.7 and 2.8), the air-to-air HPs have the lowest capital investment and simplest installation [235]. They utilize a lower sink temperature (typically 30 ℃) compared to other HP types (e.g. ground source HPs (GSHPs), typically 40 ℃) [236]. Thus, the lower sink temperature enhances the COP of the heat pump further and consequently reduces the operating cost by approximately 20% [230]. Further, although efficiency penalties may occur, the ASHPs can operate in extreme weather conditions (up to – 25 ℃). For locations having mild climatic conditions, in particular, the ASHPs yield excellent COP results due to the moderate ambient conditions providing a high-quality heat source to the evaporator side of the HPs [237]. Due to these reasons, a PV+ASHP system is usually seen as the most fundamental solar-HP combination that can reduce the energy consumption, electrify the thermal energy demands, and be easily retrofitted new and existing buildings of many European buildings intended to be designed for the NZEB concept [235].

Currently, according to the statistics of the European Heat Pump Association [238], almost 17 million HP units have already been installed in European buildings in 2021, covering approximately 14% of the heating/cooling market. In addition, heat pump sales grew by 34% in 2021 compared to the previous year. This high growth rate assures that the HPs will play a central role in the electrification of the European buildings' thermal demand over the

coming decades. Similarly, grid-connected rooftop PV systems have been integrated into European buildings at an ever-increasing rate in the last decade. Only between 2012 and 2022, the installed PV capacity increased more than twelvefold from 20.1 GW to over 242 GW, almost 50% of which was at the distributed level on building roofs [239].

Turkey is a candidate country for the European Union and is located between the temperate Mediterranean and subtropical zones of the Europe, hence it has a large number of cities that show the characteristics of the mild climates suitable for ASHP systems. It is among the top five countries in the European region regarding solar radiation potential. The cumulative installed PV capacity of the country exceeded 9.5 GW, which makes it among the top 10 countries in the world in terms of centralized solar power generation [57]. However, the distributed installed PV capacity at the rooftop of the residential buildings constitutes only 1 % of the total installed PV capacity of the country [57]. Moreover, Turkey is still far behind the widespread utilization of HP technology. In fact, there is no clear data on the installed HP applications from the officials or from the literature [238], [240], [124]. Therefore, there is a great potential for heat pumps fed by distributed PV electricity to replace fossil-fuel based thermal systems and decarbonize the building sector in the country.

As shown in Chapter 2 with [137], [138], [131], [132], [125], [241], [120], [124], [116], [127], [128] a quite limited number of studies have been conducted on solar and HP combination in Turkey, particularly on PV+ASHP systems. In addition, a majority of these studies are based on the GSHP + solar PV systems or individual implementation of the PV and HP systems. Considering the climatic suitability of the region, size and importance of the market, and the energy and GHGs saving potentials, it is remarkable that PV+ASHP systems have not yet been adapted and investigated adequately in such locations. Taking these aspects into account, it is not clear how PV + ASHP energy systems can perform holistically in terms of energy and economy when the net-zero-energy buildings are targeted.

This study therefore aims to provide a detailed technical and economic analysis of the combined air source heat pump and solar PV systems designed for the European building sector to achieve the NZEB concept, with the focus on the EU candidate country Turkey's boundary conditions. The main objectives are to demonstrate how to design, model, and size such systems holistically, and to show the possible energy savings and the life cycle cost assessment of solar PV electricity by means of the ASHPs in residential single-family houses. The application of a state-of-the-art holistic modelling procedure, together with dynamically derived energy demand and supply sides, contributes to the existing literature for a better understanding of the performance of such systems in real conditions. The results of this study assists in better understanding the dynamic performance of a fundamental PV+HP technology implemented into a single-family house built in the previous chapter for the NZEB concept.

The model and the techno-economic approach in this study can be replicated and applied to the boundary conditions of many other locations to answer the same research question. An in-depth research on different climates is not in the scope of this research, only fundamental technical parameters affecting the system performance and economic analyses are applied. This makes it possible to easily assess the profitability of the combined heat pump and solar PV systems.

To achieve the main aim of the study, the chapter is designed as follows;

In Section 5.2, a description of the proposed system is provided.

In Section 5.3, the modelling details of the proposed PV+ASHP system are provided. Modelling of the silicon-based PV panel is conducted in TRNSYS by employing Type 103. Further, the HP cycle is modelled in the EES software. In the last stage of this section, the proposed models are validated against both experimental and theoretical literature studies.

Validation results show only minor deviations from these studies, hence the developed models are used, with confidence, to measure the energetic and economic performance of the proposed system.

In Section 5.4, results and discussions on the optimization of the system are presented. The parameters used for the Type 103 PV model are taken from the manufacturer data, hence no further optimization analysis is completed. For the HP, however, parameters affecting the performance of the HP are varied to obtain the optimum design conditions. These parameters, more specifically, are the pinch point temperature difference (PPTD) in the HP's evaporator, the mass flow rate of the heat source, and the refrigerant type circulated in the HP cycle.

In Section 5.5, results and discussions on system's daily, monthly, and annual performances are presented. The annual performance results are evaluated based on two different cases; 50 % of space heating and cooling demand coverage (based on "Solar Heating and Cooling Roadmap" of the International Energy Agency), and 100 % of the annual total energy demand coverage (based on the NZEB concept of the EU legislation on buildings). In both cases, the monthly energetic performances results of the PV+ASHP model are shown. Based on this evaluation, the optimum case is selected and the system is further analysed for its daily performance. The daily performance results are evaluated based on the coldest day of the year (15^{th} January) when the total solar radiation is the lowest.

In Section 5.6, a detailed economic analysis is provided to investigate the economic viability of the proposed system. The economic analyses are conducted based on two different indicators: payback time (PT) and levelized cost of energy (LCOE). While the former indicator is used to estimate the return time of the investment, the latter shows the economic competitiveness of the proposed system compared to the grid electricity.

In Section 5.7, an overall conclusion is drawn for the chapter.

5.2 SYSTEM DESCRIPTION

When the PV+HP technologies are applied to the buildings designed for a NZEB concept, there are numerous technical parameters that must be considered to assess the annual energetic and economic profitability of the system. These can be summarised as; types of the HP and PV, energy demand profiles of the building, utilization of the thermal or electrical storage systems, connectivity and the purpose of the HP unit to the building, etc. This section provides details of such parameters, where a schematic view of the proposed system is given in Figure 5.1.

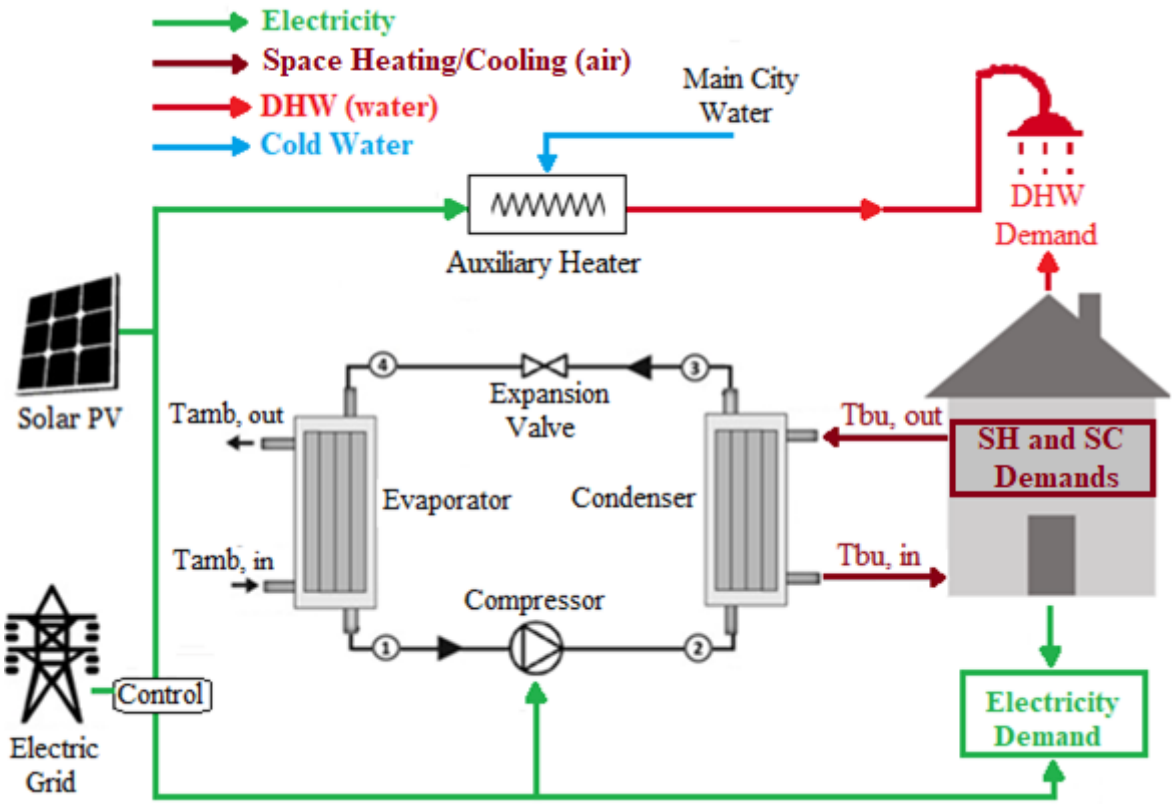

Figure 5.1: Schematic representation of the proposed PV-ASHP system.

The proposed model in this study, shown in Figure 5.1, is a PV+ASHP system that aims to dynamically generate all energy demand vectors (SH, SC, DHW, and EE) of a single-family house. The model consists of three main units; a solar PV unit, a HP unit, and a

representative building unit and two auxiliary components; an auxiliary water heater and an utility grid. The building represents the exemplary residential single-family house which was modelled with the Type 88 component of the TRNSYS for Izmir/Turkey in Chapter 4. Thus, the location and the demand profiles of the house are known parameters.

Modelling of the solar PV is carried out in the TRNSYS software by employing the Type 103 component. Due to the reasons stated in Chapter 2 (Section 2.3), a mono-crystalline PV is selected. In addition, the HP unit is modelled in the EES software. An air-to-air heat pump (a2aHP) is selected to meet space heating and cooling demands of the representative house.

Since the air-to-air heat pumps cannot provide DHW (due to the end-product of the HP, hot air) [235], a 1 kW capacity (based on the hourly peak load of the DHW demand) auxiliary heater is visualized on the schematic diagram to represent the DHW demand coverage by the PV and/or grid electricity. The proposed system aims to produce sufficient energy to meet the dynamic electrified total energy demand vectors of the representative house and to be net zero on an annual basis. The system is assumed to be connected to the grid with the Feed-in Tariff (FIT), hence the grid acts as a battery storage unit for the system with no limit on the capacity. With this regard, when the electricity generation from the PV exceeds the demand, the surplus electricity is exported to the grid or vice versa. The modelling details, working principles, and the control strategy of the system are presented in the following sections.

5.3 MATHEMATICAL MODELLING AND VALIDATION OF THE SYSTEM

5.3.1 Modelling of a Mono-Crystalline Silicon PV Panel in TRNSYS Environment

Modelling of the solar PV panel is carried out in the TRNSYS software. The Type 103 sub-model has two modelling modes available. The first mode is based on the single diode model, which solves a four-parameter equation iteratively based on the characteristics of the

current (I) and voltage (V) output of the cells [167], [242]. A simple solar cell (current source), a parallel connected diode, and a serial connected resistor constitute this model. The correlation between I and V is as follows [243]:

$$I = I_L - I_o \left[exp\left(\frac{q(V+IR_s)}{\gamma\kappa T_c}\right) - 1\right] \quad (5.1)$$

where I_L and I_o are the light current and saturation current, respectively, Rs and Tc are the cell series resistance and cell temperature, respectively, and γ, q ($1.6\text{x}10^{-19}$) & κ ($1.38\text{x}10^{-23}$ J/K) are the empirical PV parameter, charge of the electron, and Boltzmann constant, respectively.

The cell temperature (T_c) in Equation 5.1 is described as follows [243]:

$$T_c = 3.12 + 0.25\frac{G}{G_{ref}} + 0.899T_a - 1.3V_{wind} + 273 \quad (5.2)$$

Similarly, the light current (I_L) is based on the cell temperature and irradiance density which is formulated as follows:

$$I_L = \frac{G}{G_{ref}}[I_{sc,ref} + \mathcal{M}I_{sc}(T_c - T_{c,ref})] \quad (5.3)$$

where G is the irradiance density, V_{wind} is the wind speed, T_a is the ambient temperature, $\mathcal{M}I_{sc}, I_{sc,ref}, T_{c,ref}$ and G_{ref} are solar cell short-circuit temperature coefficient, solar cell short-circuit current, temperature and incident radiation at the reference conditions, respectively.

Finally, the saturation current (I_o) is a temperature-dependent value and described as follows:

$$I_o = I_{o,ref}\left(\frac{T_c}{T_{c,ref}}\right)^3 \quad (5.4)$$

where $I_{o,ref}$ is the reserve saturation current at the reference conditions.

The single diode model provides the maximum power output of the PV circuit (P_{PV}=I×V) over the entire voltage range for a given irradiance by solving Equations 5.1, 5.2, 5.3, and 5.4 numerically, and is used in this section to depict the I-V curve when validating the model.

The second method is based on the evaluation of the instantaneous power generation from the global horizontal irradiance (GHI, in W/m^2) for a given installed area (m^2) and is used to observe the panel efficiency and to size the panel area for the case study.

The performance of a PV module is a function of three main parameters. These are the physical properties of the utilized material for the PV cell, the temperature of the PV cell during the operation (T_c), and the total DNI on the tilted PV modules (G^{tot}). The power output for a given area A_{Pv} (m^2), therefore, is expressed as follows [244]:

$$P_{PV} = \eta_{PV} x A_{Pv} x G^{tot} x PF(t) \quad \text{..... (5.5)}$$

where PF is a dimensionless value representing the ratio of total PV cell area to the total PV module area, and η_{PV} represents the PV efficiency and is given by Habib et al. [245] as follows:

$$\eta_{PV} = \eta_r \eta_{pc} \left[1 - \beta (T_c - T_{c,ref})\right] \text{.....} \quad \text{(5.6)}$$

where η_r is the reference module efficiency, η_{pc} is the efficiency of the power conditioning (for a perfect maximum power tracker (MPPT), η_{pc} is equal to 1), β is the array efficiency temperature coefficient (for silicon cells, it is in the range of 0.004-0.006 per ºC [244]), $T_{c,ref}$ is the cell's reference temperature (ºC) and T_c (ºC) is the cell temperature which can be defined as follows [244], [246]:

$$T_c = T_a + \left[\frac{(NOTC-20)}{800}\right] G^{tot} \text{.....} \quad \text{(5.7)}$$

where T_a (ºC) is the ambient temperature, and the $NOTC$ (ºC) is the nominal cell operating temperature. It is important to note that η_{pc}, β, and $NOTC$ depend on the physical properties of the materials used to construct the PV module, which are typically obtained from the manufacturers' specification sheet.

5.3.2 Modelling of the Heat Pump Unit Using the EES Software

The EES is an acronym for 'Engineering Equation Solver' software [172]. In Chapter 3, the details of the EES software and its capability on solving nonlinear algebraic and differential equations have been provided. The EES also provides built-in thermodynamic functions of different fluids, which provides a practical solution to model any thermodynamic cycle, including the heat pump (HP) cycles. In this section, the steady-state modelling details of an air-to-air heat pump in the EES software are presented.

A heat pump cycle is a vapour compression cycle and has four main components, namely, evaporator, compressor, condenser and expansion valve, shown in Figure 5.2. As stated in Chapter 2, the expansion valve is reversible, hence HPs can provide both heating and cooling. During the heating mode, the evaporator uses the ambient air as its heat source (Tamb,in) and evaporates the refrigerant of the HP cycle at state 1 to the saturated vapour. The refrigerant then enters to the compressor where it is compressed to a high temperature and pressure at state 2. When the refrigerant passes through the condenser of the HP cycle, it cools down to state 3 to the saturated liquid by the cold air temperature exiting from the building (Tbu, out) where the useful heat is transferred to the air entering the building (Tbu, in). The working fluid of the HP then passes through the expansion valve at state 4 where its temperature and pressure is reduced. After the expansion, the refrigerant re-enters the evaporator and the cycle repeats. For the cooling mode, however, the cycle is reversed and

the same process is repeated. Modelling of this HP process is represented by the following zero-order equations, (5.8) to (5.36), which operate at finite capacity for the heating mode.

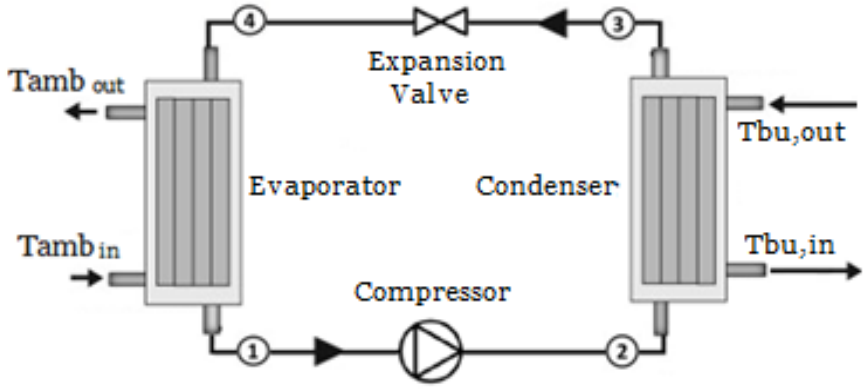

Figure 5.2: The heat pump cycle.

Modelling of the evaporator and condenser:

The evaporator and condenser of a HP cycle are essentially heat exchangers. For the reasons detailed in Chapter 2, both the evaporator and condenser employed in this study are selected as a double pipe counter-flow heat exchanger. When modelling a heat exchanger, three different methods can be employed; 1- Pinch Point Temperature Difference (PPTD) method, 2- Log-mean Temperature Difference (LMTD) method, and 3- Number of Transferred Units (NTU) effectiveness method [247].

The PPTD is the point when the hot and cold streams in the heat exchanger are at their closest approach. The pinch point in a counter-flow usually occurs at the inlet or outlet of the heat exchanger. Due to the complexity of the heat exchanger's models, it is often convenient to employ the simplifying assumptions. Therefore, the PPTD is essentially an assumption made between the inlet and / or outlet of the two fluids. Hence when one of the fluids' temperatures is known, the other fluid's temperature becomes known [248].

The LMTD method can be used to determine the size of a heat exchanger when the inlet and outlet temperatures and the mass flow rate of both fluids, and the type of the heat exchanger

are known. The NTU method, on the other hand, is a practical approach to determine heat transfer rate in the heat exchanger and the outlet temperatures of both fluids, when the inlet temperatures of both fluid and the type of the heat exchanger are known [173].

In this section, the HP unit is modelled based on the PPTD and NTU methods. This is because of the predefined heat exchanger's type and inlet temperatures of the fluids (for the heat source:$T_{amb,in}$, for the house side: $T_{bu,out}$).

Modelling of the evaporator side: The heat input rate from the ambient to the evaporator of the HP (see Figure 5.2) is calculated as follows [173]:

$$Q_e = m_{air} \times Cp_{air} \times (T_{amb,in} - T_{amb,out}) \quad (5.8)$$

where m_{air} and Cp_{air} are the mass flow rate (kg/s) and specific heat capacity (kJ/kg.K) of the ambient air, $T_{amb,in}$ and $T_{amb,out}$ are the temperatures (°C) of the ambient air entering and exiting from the evaporator. Similarly, the evaporator heat input can also be expressed based on the refrigerant cycle as follows [140]:

$$Q_e = m_{ref} \times (h_1 - h_4) \quad (5.9)$$

where m_{ref} is the mass flow rate of the HP's refrigerant, and h_1 and h_4 are the specific enthalpies (kJ/kg) of the refrigerant at state 1 and 4, respectively.

By using the PPTD method, it is assumed that pinch point temperature difference in the evaporator is initially ΔT_e. Therefore, the relation between the evaporation temperature (T_e) and the $T_{amb,in}$ can be expressed as follows [247], [249], [116]:

$$T_e = T_{amb,in} - \Delta Te \quad (5.10)$$

Since the evaporation temperature is equal to temperature of the refrigerant at state 1, by using the NTU method, the evaporator's heat capacity can be written as a function of the

evaporation temperature (T_e) and the temperature entering the evaporator side ($T_{amb,in}$) as follows [140]:

$$T_1 = T_e \quad \text{(5.11)}$$

$$Q_e = m_{air} \times Cp_{air} \times (T_{amb,in} - T_e) \times \left(1 - \exp\left[-\frac{U_e \times A_e}{m_{air} \times Cp_{air}}\right]\right) \quad \text{(5.12)}$$

where the U_e and A_e are the total heat transfer coefficient (kJ/s.m^2.K) and the total area (m^2) of the evaporator, respectively.

Modelling of the condenser side: Similar to the evaporator side, the heat rejection rate from the condenser of the HP to the building is calculated as follows [173]:

$$Q_c(Q_{heating}) = m_{bu} \times Cp_{air} \times (T_{bu,in} - T_{bu,out}) \quad \text{(5.13)}$$

where m_{bu} and Cp_{air} are the mass flow rate (kg/s) and specific heat capacity (kJ/kg.K) of the building air, respectively, $T_{bu,in}$ and $T_{bu,out}$ are the temperatures (°C) of the building air exiting and entering to the condenser, respectively. The condenser heat rejection can also be expressed based on the refrigerant cycle as follows [140]:

$$Q_c = m_{ref} \times (h_3 - h_2) \quad \text{(5.14)}$$

where h_3 and h_2 are the specific enthalpies (kJ/kg) of the refrigerant at state 3 and 2, respectively.

Since the condensation temperature is equal to temperature of the refrigerant at state 3, by using the NTU method, the condenser heat capacity can be written as a function of the condensation temperature (T_c) and the temperature exiting the building side ($T_{bu,out}$) [140]:

$$T_3 = T_c \quad \text{(5.15)}$$

$$Q_c = m_{bu} \times Cp_{air} \times (T_c - T_{bu,out}) \times \left(1 - \exp\left[-\frac{U_c \times A_c}{m_{bu} \times Cp_{air}}\right]\right) \quad \text{(5.16)}$$

where U_c and A_c are the total heat transfer coefficient (kJ/s.m^2.K) and total area (m^2) of the condenser, respectively.

The condensation temperature (T_c) is assumed as 35 ℃ based on the similar size studies in the literature [250], [140] to achieve an acceptable level of final temperature on the $T_{bu,in}$.

Furthermore, it is important to note that the fluid qualities for the evaporator at state 1 ($x1$) and for the condenser at state 3 ($x3$) are assumed to be saturated vapour and saturated liquid, respectively. In addition, since the temperature of the evaporation at state 1 is known by the PPTD method (Equations 5.10 and 5.11), and the condensation temperature at state 3 (T_c=35 ℃=T3) is given, the other properties of the refrigerant cycle at each state can be found with the thermodynamic properties of the refrigerant in the EES software as follows.

For the evaporator (state 1): the enthalpy, entropy, and pressure at the state 1 are the functions of the fluid quality ($x1$) and the temperature (Te) of the refrigerant at this stage. Therefore, the below functions can be written as follows [247], [172]:

$$s1 = Entropy(Refrigerant, T = T1, x = x1) \quad (5.17)$$

$$h1 = Enthalpy(Refrigerant, T = T1, x = x1) \quad (5.18)$$

$$P1 = Pressure(Refrigerant, T = T1, x = x1) \quad (5.19)$$

where $s1$, h, and $P1$ are the specific entropy, enthalpy and pressure of the refrigerant at state 1, respectively, when the temperature and the fluid quality of the refrigerant are equal to Te and $x1$, respectively.

For the condenser, the enthalpy, entropy and pressure at the state 3 are the functions of the fluid quality ($x3$) and the temperature (T_c) of the refrigerant at this stage. Therefore, the similar functions can be written as follows [247],[172]:

$$s3 = Entropy(Refrigerant, T = T3, x = x3) \quad (5.20)$$

$$h3 = Enthalpy(Refrigerant, T = T3, x = x3) \quad (5.21)$$

$$P3 = Pressure(Refrigerant, T = T, x = x3) \quad (5.22)$$

where *s3*, *h3*, *P3* are the specific entropy, enthalpy and pressure of the refrigerant at state 3, respectively, when the temperature and the fluid quality of the refrigerant are equal to *T3* and *x3*, respectively.

Modelling of the compressor:

The compressor modelling of the HP cycle here is based on the work of Brunin et.al [251], work where it is assumed that the compressor of the cycle is both reversible and adiabatic. Therefore, the specific entropy of the refrigerant at state 2 is equal to state 1:

$$s2 = s1 \quad (5.23)$$

Due to the steady state conditions, the pressure losses during the condensation is neglected as stated in [248]. Therefore, the condensation pressure at state 3 is equal to state 2:

$$P2 = P3 \quad (5.24)$$

Since two properties of the refrigerant in the HP cycle are known for the compressor at state 2, the other properties, namely, temperature and fluid quality are the functions of the refrigerant's pressure and entropy at state 2:

$$T2 = Temperature(Refrigerant, s = s2, P = P2) \quad (5.25)$$

$$x2 = Quality(Refrigerant, s = s2, P = P2) \quad (5.26)$$

Until now, the only unknown property is the enthalpy of the refrigerant at state 2 (h_2) to complete the compressor model. In theory, it can be assumed that h_2 is also a function of entropy and pressure properties at state 2. However, in real conditions, the actual

compressors are not 100 % efficient, which means that there are some enthalpy losses during the compression process. Therefore, the enthalpy at state 2 on the saturation curve of the refrigerant is the ideal enthalpy, which is a function of the refrigerant's pressure and entropy at state 2, and is expressed as follows:

$$h2, s = Enthaply(Refrigerant, s = s2, P = P2) \quad (5.27)$$

where $h_{2,s}$ is the ideal enthalpy of the refrigerant at the saturation curve of the refrigerant.

In order to find the actual enthalpy (h_2), therefore, the compressor's actual isentropic efficiency equation on the saturation curve of the refrigerant at state 2 can be implemented which is defined as follows [247]:

$$\eta_{comp,isentropic} = \frac{(h_{2,s} - h_1)}{(h_2 - h_1)} \quad (5.28)$$

The same efficiency can also be obtained from the pressure ratio in between the condenser (P_3) and the evaporator (P_1) as follows [251], [252]:

$$\eta_{comp,isentropic} = 0.874 - 0.035 \times (\frac{P3}{P1}) \quad (5.29)$$

By solving Equations 5.27-5.29, the actual enthalpy (h_2) becomes known for the compressor model in real conditions. Once the actual enthalpy at state 2 and 1 are known, the work input to the compressor (W_{comp}) can be formulated as follows [248]:

$$W_{comp=} m_{ref} \times (h_2 - h_1) \quad (5.30)$$

Modelling of the expansion valve:

The expansion in the refrigerant is assumed as isentropic, which means that the enthalpy losses are neglected. Hence, the refrigerant's enthalpy in the HP cycle at state 4 is equal to

state 3:

$$h4 = h3 \quad (5.31)$$

Similarly, due to the steady-state conditions, the pressure losses during the evaporation are neglected as stated in [248]. Therefore, evaporation pressure at state 1 is equal to state 4:

$$P4 = P1 \quad (5.32)$$

Since two properties of the refrigerant in the HP cycle are known for the expansion valve at state 4, other properties, namely, temperature, entropy, and fluid quality are the functions of the refrigerant's pressure and enthalpy at state 4:

$$T4 = Temperature(Refrigerant, h = h4, P = P4) \quad (5.33)$$

$$x4 = Quality(Refrigerant, h = h4, P = P4) \quad (5.34)$$

$$s4 = Entropy(Refrigerant, h = h4, P = P4) \quad (5.35)$$

After modelling all four HP components, finally, the coefficient of performance (COP) of the HP can be calculated based on the condenser heat output Q_c and compressor work input W_{comp} as follows [173]:

$$COP_{HP} = \frac{Q_c}{W_{comp}} \quad (5.36)$$

Overall assumptions of the HP model are summarised as follows:

• The condensation temperature (T_c) is taken as 35 ℃ based on [140], [116], [250].

• The temperature exiting from the building and entering the condenser ($T_{bu,out}$) is 20 ℃ and 26 ℃ for the heating and cooling modes, respectively, as these are the set point temperatures from the building zone during the heating and cooling seasons (see Chapter 4).

• A 4 kW capacity HP (Q_c) is selected based on the peak SH heating demand profile of the representative house (detailed in Chapter 4) to ensure a continuous heat supply (the peak SC load is lower).

• The compression process is adiabatic [248].

• The expansion process is isentropic [173].

• The pressure drops during the evaporation and condensation are neglected [248].

• The overall heat transfer effectiveness of both heat exchangers is taken as 65 % [247], [253].

• The PPTD between the heat source and the evaporator is variable (during both heating and cooling). The following section investigates the effect of this variable on the system performance (optimization section).

• The mass flow rate of the air entering the evaporator (m_{air}) is variable (during both heating and cooling). The next section investigates the effect of this variable on the HP performance (optimization section).

• The ambient air temperature and the zone temperature entering the evaporator (during the heating and cooling, respectively) are dynamic.

Finally, a screenshot of the HP model in the EES software is attached in Appendix 5-A.

5.3.3 Validation of the Type 103 PV Model

The built-in TRNSYS models contains default values that can be changed by the users. The screenshots of the TRNSYS Type 103 model's interface with these default values are attached in Appendix 5-B and 5-C. The interface has 4 main sections: 'Parameter', 'Input',

'Output', and 'Comment'. The 'Parameter' section requires the constant parameters to be added by the user (see Appendix 5-B). While the 'Input' section requires the inputs that are dynamically changing or the parameters that can be changed by the users (e.g. ambient conditions, see Appendix 5-C). The third section is 'Output' showing the results of the model by solving of the governing equations of the model: (5.1), (5.2), (5.3), (5.4), (5.5), (5.6), and (5.7) in section 5.3.1. Finally, the 'Comment' section allows users to make any notes or comments for the model.

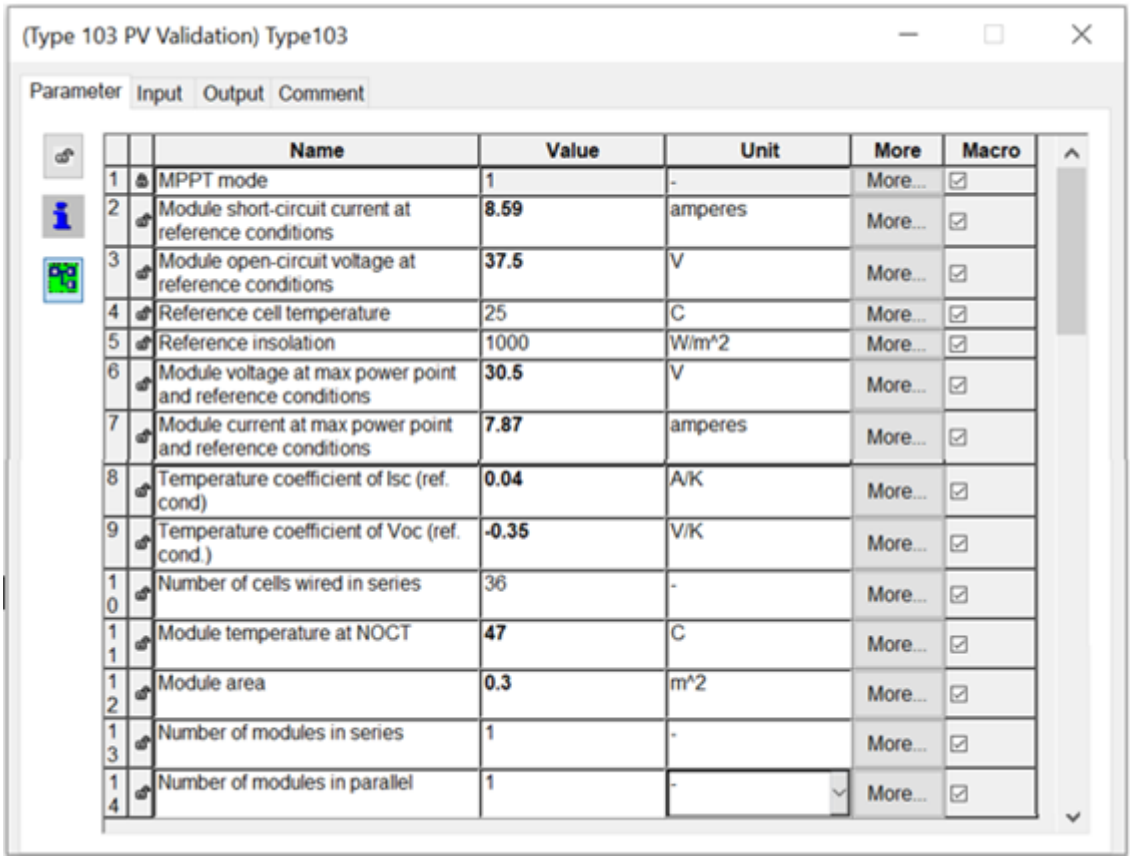

	Name	Value	Unit	More	Macro
1	MPPT mode	1	-	More...	☑
2	Module short-circuit current at reference conditions	**8.59**	amperes	More...	☑
3	Module open-circuit voltage at reference conditions	**37.5**	V	More...	☑
4	Reference cell temperature	25	C	More...	☑
5	Reference insolation	1000	W/m^2	More...	☑
6	Module voltage at max power point and reference conditions	**30.5**	V	More...	☑
7	Module current at max power point and reference conditions	**7.87**	amperes	More...	☑
8	Temperature coefficient of Isc (ref. cond)	**0.04**	A/K	More...	☑
9	Temperature coefficient of Voc (ref. cond.)	**-0.35**	V/K	More...	☑
10	Number of cells wired in series	36	-	More...	☑
11	Module temperature at NOCT	**47**	C	More...	☑
12	Module area	**0.3**	m^2	More...	☑
13	Number of modules in series	1	-	More...	☑
14	Number of modules in parallel	1	-	More...	☑

Figure 5.3: Type 103 model parameters based on the experimental work of Baccoli et al. [254].

In this study, the Type 103 TRNSYS PV model is validated against the experimental work conducted by Baccoli et al. [254]. For this purpose, first, the default parameters and the inputs of the Type 103 PV model are changed based on the experimental reference

conditions. Figure 5.3 shows this parameter box of the Type 103 PV model adjusted based on the experimental work of Baccoli et al. [254].

The experimental work presented in [254] was conducted based on the weather conditions of Cagliari-Italy on 9th August 2019 between 6.30 a.m. and 20.30 p.m. In order to obtain the same input conditions, in the TRNSYS Type 15-6, the same location is selected, and the simulation run date is adjusted based on the experiment's date and hours. In addition, a validation project is created consisting of Type 15-6 (weather data file), the Type 103 (PV model), a simulator tool, and a printer to read the data. A screenshot of this validation study is shown in Figure 5.4.

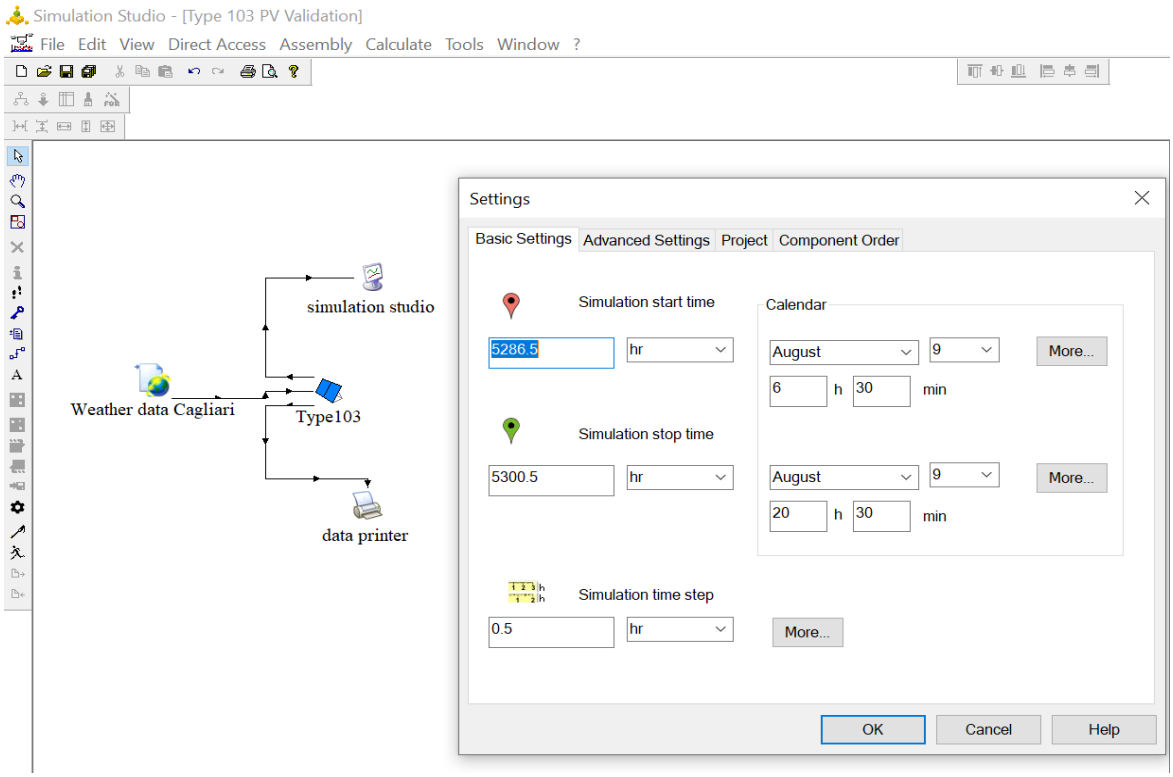

Figure 5.4: Screenshot of the Type 103 PV validation setup in the TRNSYS environment.

After setting the 'parameter' and 'input' boxes based on the experimental work, and creating the validation project in TRNSYS, the project is run for the specified time and location of the experiment. The electrical power production (W) of the present model (the

Type 103) with a 0.3 m^2 panel area is compared with the electricity generation of the same panel area as in the experimental work. The result of this comparison is shown in Figure 5.5, where very minor deviations are obtained (maximum 2.7 % at around 11.30 a.m.). The reason for these deviations can best be explained by the difference between the approximate solar radiation data in TRNSYS and the precisely measured climate data of the test location.

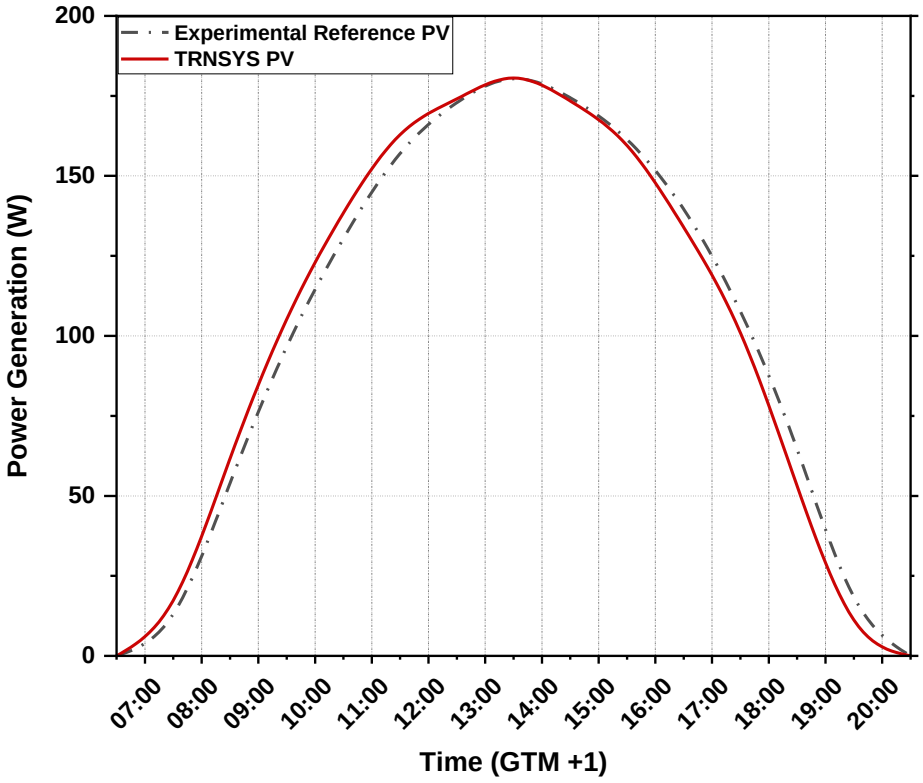

Figure 5.5: Comparison of the power production from Type 103 PV model and the experimental work conducted by Baccoli et al. [254].

5.3.4 Validation of the HP Model

The validation of the present HP model is conducted by comparing its results with the numerical study of Camdali et al. [253] for a ground source HP, and with the experimental study of Abu-Mulaweh [255] for an air source HP. For both validations, any parameters outside of the HP's refrigerant cycle are taken from the studies and provided to the EES. In

the present model, the COP of the HP cycle, the compressor work, and the temperatures at stages 1, 2, 3, and 4 are calculated and compared against those referenced in [253] and [255]. It is important to note that both studies utilized R134a as the refrigerant. Table 5.1 summarises the input parameters of Camdali et al. [253].

Table 5.1: Input parameters into the investigation by Camdali et al. [253].

Parameters	**Values**
Heating load (kW)	1.4
Isentropic efficiency of compressor	0.7
Total heat transfer coefficient of evaporator (kW/m^2 °C)	0.64
Total heat transfer area of evaporator (m^2)	0.35
Source temperature entering the evaporator (°C)	5
Source temperature exiting the evaporator (°C)	−5
Total heat transfer coefficient of condenser (kW/ m^2 °C)	0.02
Total heat transfer area of condenser (m^2)	10
Air temperature going into condenser (°C)	20
Air temperature going out condenser (°C)	30

For the input parameters of the experimental study of Abu-Mulaweh [255], the cycle operated with pressures between 212 kPa and 1117 kPa, and with temperatures between -8.5 ℃ and 78.7℃. Therefore, the pressures and temperatures at states 2 and 4 are given parameters in the HP cycle. In addition, the mass flow rate of the refrigerant is given as 1.06 g/s (0.00106 kg/s). These given parameters from both studies are then implemented into the present model and the results are obtained.

Table 5.2: HP model validation against the previous numerical and experimental studies.

Variable	**Camdali et.al** [253] **(numerical)**	**Developed Model**	**Abu-Mulaweh** [255] **(experimental)**	**Developed Model**
COP	3.31	3.22	3.5	3.8
Compressor Work (W)	426.16	428.13	51.6	53.1
T1 (℃)	-6.6	-6.9	10.5	11.42
T2 (℃)	49.6	49.2	78.7	81.1
T3 (℃)	33.2	32.9	17.9	18.7
T4 (℃)	-6.6	-6.9	-8.5	-8.2

Results of the present model, and those of Camdali et al. [253], and Abu-Mulaweh [255] are compared in Table 5.2, where it is shown that the developed model is in very good agreement with the experimental and numerical data reported in the literature.

5.4 RESULTS AND DISCUSSIONS ON THE SYSTEM OPTIMIZATION

In this section, the design parameters of the model's components are optimized and presented. For the Type 103 PV model, a mono-crystalline silicon panel with an 18 % of rated efficiency is selected from Solar Electric, a UK-based PV manufacturer [256]. The selected panel type is STKM-72-320 [257] to represent a typical panel efficiency in the market, hence no further optimization is conducted and the Type 103 PV model is operated based on the manufacturer parameters seen in Figure 5.6.

However, the optimization of the HP model is achieved through a fundamental analysis of the HP cycle's most important parameters affecting the system performance. These are namely; the mass flow rate of the heat source, PPTD between the heat source and the evaporation temperature, and the working fluid of the cycle. The optimization is performed under steady-state conditions by varying these parameters within the upper and lower limits. For each design point, the equations from (5.8) to (5.36) are employed iteratively. Furthermore, since the HP cycle is reversible, i.e. the evaporator and condenser of the cycle during the heating mode become the new condenser and evaporator during the cooling mode, the optimisation of the system was performed for only one mode (heating mode).

Prior to the optimization calculations for the HP model, the known parameters and the pre-set model values are summarized as follows; first, the condenser operating temperature was set to 35 ℃, detailed in Section 5.3. In addition, the condenser's cold side ($T_{bu,out}$) was also a known parameter (20 ℃, and 26℃ during the cooling season when the cycle is reversed) due to the thermal comfort of the building (Chapter 4). Similarly, the condenser capacity

was set to 4 kW, detailed in Section 5.3. Finally, the effectiveness of both heat exchangers (HX_eff) was set to 0.65 as it is an acceptable level for counter-flow heat exchangers [248], [250], detailed in Section 5.3.

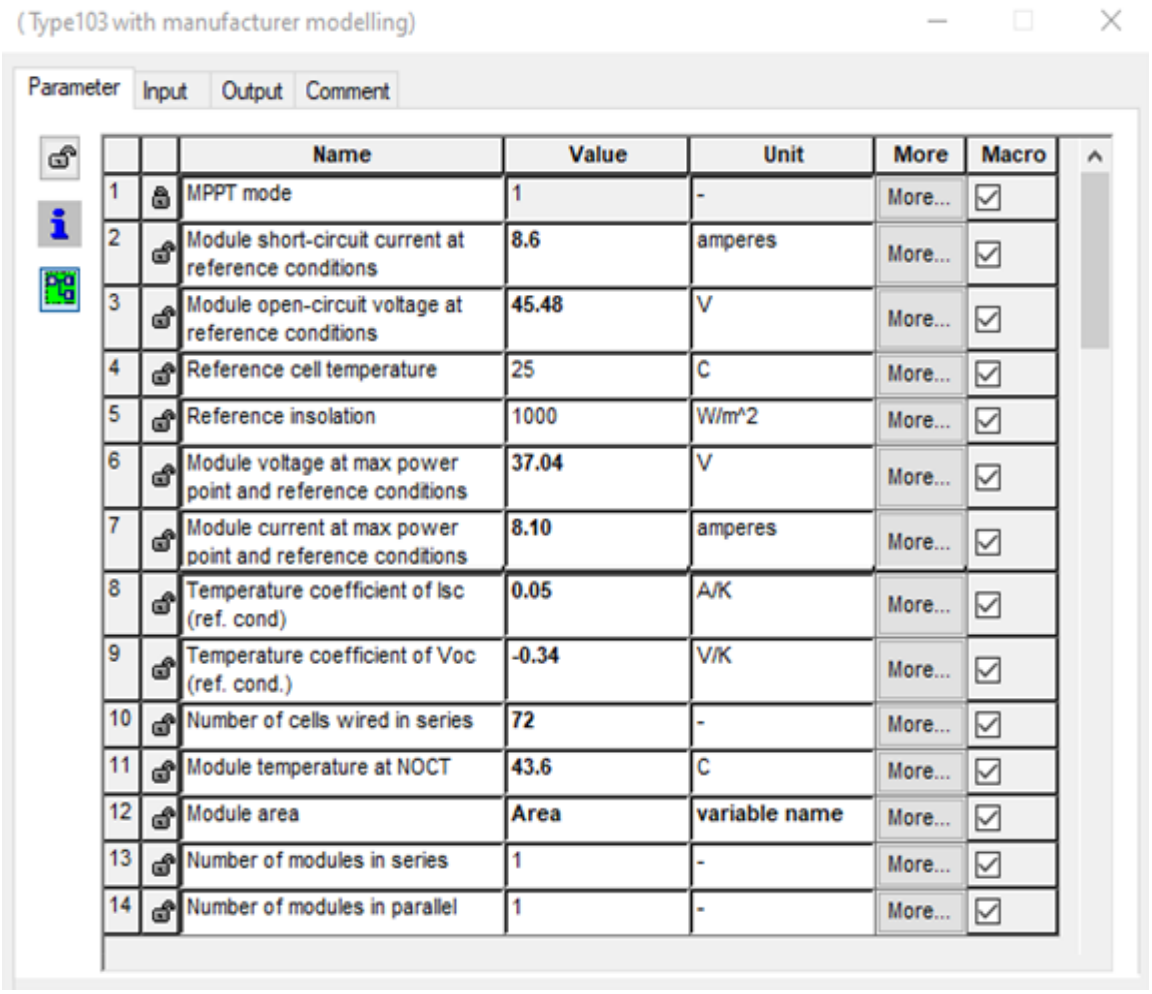

		Name	Value	Unit	More	Macro
1		MPPT mode	1	-	More...	☑
2		Module short-circuit current at reference conditions	8.6	amperes	More...	☑
3		Module open-circuit voltage at reference conditions	45.48	V	More...	☑
4		Reference cell temperature	25	C	More...	☑
5		Reference insolation	1000	W/m^2	More...	☑
6		Module voltage at max power point and reference conditions	37.04	V	More...	☑
7		Module current at max power point and reference conditions	8.10	amperes	More...	☑
8		Temperature coefficient of Isc (ref. cond)	0.05	A/K	More...	☑
9		Temperature coefficient of Voc (ref. cond.)	-0.34	V/K	More...	☑
10		Number of cells wired in series	72	-	More...	☑
11		Module temperature at NOCT	43.6	C	More...	☑
12		Module area	Area	variable name	More...	☑
13		Number of modules in series	1	-	More...	☑
14		Number of modules in parallel	1	-	More...	☑

Figure 5.6: The manufacturer input parameters [257], used in the Type 103 PV model.

As seen from the above two paragraphs, due to the interaction with the building side, the main parameters of the condenser (during the heating mode), such as condenser capacity (4 kW) and condenser's heating temperature, become clear to pre-set. However, the evaporator parameters mainly depend on the condition of the heat source which varies dynamically. Therefore, the optimization analyses of the HP model are carried out based on the interaction of the heat source and the evaporator parameters. The same process is applied to the cycle when the HP is in the cooling mode. The most critical parameters of an evaporator are the

temperature of the heat source and its flow rate to the evaporator. Thus, changing these parameters, while other input values (particularly the condenser heat output to cover the peak demand) are pre-set, leads to obtaining the optimum design points where the overall system performance is maximized. It has to be mentioned that the parametric optimization first starts with analysing different refrigerant types to obtain the effect of the refrigerant on the performance of the model. With these approaches, practically, 780 different combinations (6 refrigerants, 13 flow rates, and 10 PPTD values) have been analysed.

5.4.1 Finding the Optimum Refrigerant Type for the HP

This section tests the effects of six different refrigerant types on the HP's performance and shows this in Figure 5.7. For this comparison, the most commonly utilized working fluids in an HP cycle [140], [258], [43] are selected, which are namely; R134a, R410A, R407C, R32, R245fa, and R152a. The thermodynamic properties of these refrigerants are taken from the EES library. As the optimum values of the mass flow rate and the PPTD have not been found yet, these parameters are based on commonly used evaporator values in the literature. Thus, the mass flow rate is assumed as 0.4 $\frac{kg}{s}$ [248] and the PPTD value is taken as 8 K [116], where the other parameters are as summarized in the introduction part of Section 5.4

Figure 5.7 shows the HP performance based on these selected working fluids at different ambient temperatures that the location of the system may have during the winter season. From the figure, it can be seen that R407C, R245fa, and R410A perform the least, but the performance of R245fa increases significantly at higher ambient temperatures. In contrast, R152a, R32, and R134a outperform the previous three, but differ little among themselves, especially at lower temperatures. Nevertheless, R152a clearly shows the highest performance among all fluids. In addition to the high performance, it also has zero Ozone Depletion Potential (ODP), and a very low value of Global Warming Potential (GWP) of

140 [258]. Therefore, R154a is selected as the working fluid of the cycle and is further examined in the total system.

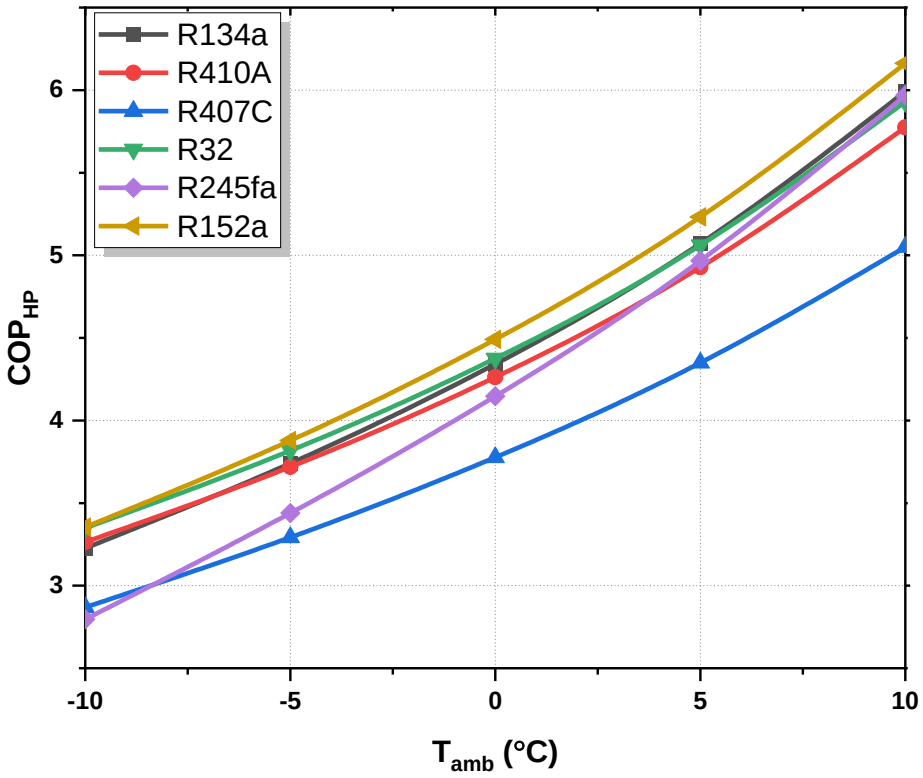

Figure 5.7: Effect of the refrigerant type on the HP's performance at different heat source (HX_eff:65 %, PPTD: 8 K, T_{cond}: 35 °C, Evaporator mass flow rate (air): 0.4 $\frac{kg}{s}$).

5.4.2 Finding the Optimum Mass Flow Rate of the Heat Source for the HP

In this section, the effect of the evaporator's mass flow rate on the condenser's heat provision is evaluated. For this purpose, the mass flow rate of the heat source, which is ambient air for the proposed PV+ASHP system, is changed from 0.1 $\frac{kg}{s}$ to 0.7 $\frac{kg}{s}$ with a linear increase of 0.05$\frac{kg}{s}$.

In addition, although the heat source's temperature changes from hour to hour, the coldest hour of the typical year for the selected location of system was found on 15th January at 8

a.m. in Chapter 4 (Section 4.3.3), where the ambient temperature was -2.7 ℃. With this regard, four ambient temperature values are selected from the coldest (-5 ℃, to represent the coldest day) to the warmest (10℃, to represent the mean temperature of the coldest month). The effect of the evaporator's mass flow rate on the heating capacity of the condenser at these temperatures is then presented in Figure 5.8.

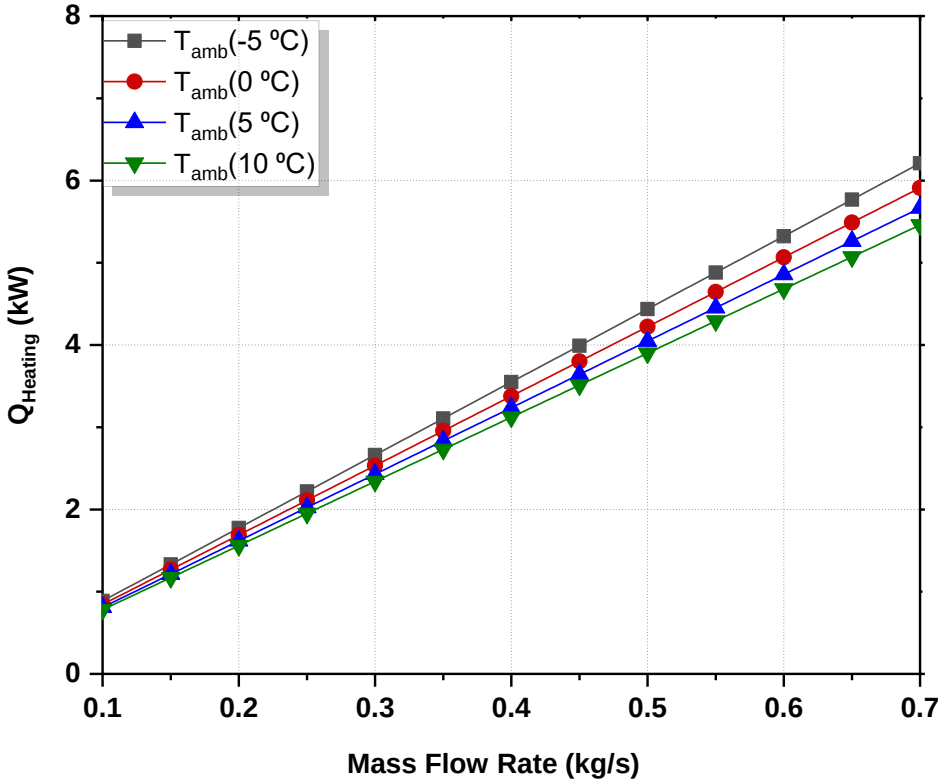

Figure 5.8: Change of the heating capacity based on different ambient temperatures with varying the air mass flow rates at the evaporator side (HX_eff:65 %, PPTD: 10℃, T_{cond}: 35 ℃, R: R154a).

As expected, an increase in the mass flow rate increases the heating capacity of the condenser. Also, as seen from Chapter 4, the peak demand of the representative house was close to the 4kW, hence the condenser capacity should be at least 4 kW to sufficiently cover the total heating demand of the building. Moreover, the selected heat source temperatures assist in finding the optimum mass flow rate as the coldest of these temperatures represents

the worst-case ambient temperature. In other words, any mass flow rate value whose corresponding heating capacity is close to 4kW at the coldest temperature should be the optimum value in order to not oversize the system. With this regard, when the inlet heat source is -5 ℃, the optimum mass flow rate is found to be 0.4509 $\frac{kg}{s}$ to obtain the sufficient heating capacity of 4 kW in the condenser.

5.4.3 Finding the Optimum PPTD on the Evaporator Side of the HP

The heat source temperature (ambient air, or the building zone temperature during the cooling) has a direct impact on the evaporation temperature of the HP model; the correlation between the evaporation temperature, heat source temperature, and PPTD is shown in the Equation 5.10 ($T_e = T_{amb,in} - \Delta Te$, where the ΔTe is the PPTD. For the proposed HP cycle, it is clear that a lower evaporation temperature (T_e) means a higher temperature lift in the HP cycle from the evaporator to the condenser which results in a higher compressor work and consequently a lower COP of the system. Therefore, a lower PPTD value is desirable for a higher evaporation temperature and COP. These correlations are shown in Figure 5.9 and Figure 5.10. In Figure 5.9, for example, when the PPTD increases (from 2℃ to 20℃), the COP of the HP decreases (from 8 to 2). Similarly, in Figure 5.10, when the PPTD increases, the compressor consumes more electricity to satisfy the temperature lift.

However, A zero Celsius degree (0 ℃) of PPTD is not possible due to the first law of thermodynamics because there are thermal losses and efficiency of the heat exchangers to consider. Similarly, an excessively high upper limit of the PPTD is not possible, since this level of T_{evap} will be lower than the evaporation temperature of the refrigerant. Thus, the PPTD value is changed from 2 ℃ to 20 ℃ with a linear increase of 2 ℃ at each step to measure the corresponding condenser and evaporator capacities, and the COP of the system (Figure 5.9). In this measurement, the optimum mass flow rate of the heat source to the

evaporator (0.4509 $\frac{kg}{s}$) is used, as found in the previous section. Similarly, the condenser heating capacity (4kW) is the decisive parameter to define the optimum value of the PPTD. As seen from Figure 5.9, the optimum heating capacity in the condenser is achieved when the PPTD between heat source and the evaporator temperature is close to the 10 ℃. The exact optimum PPTD value has been found as 9.8 ℃ when the mass flow rate of the evaporator, effectiveness of the heat exchangers, and ambient temperature values are 0.4509$\frac{kg}{s}$, 0.65, and -5 ℃, respectively. Furthermore the corresponding COP value at 9.8 ℃ is found to be 3.27.

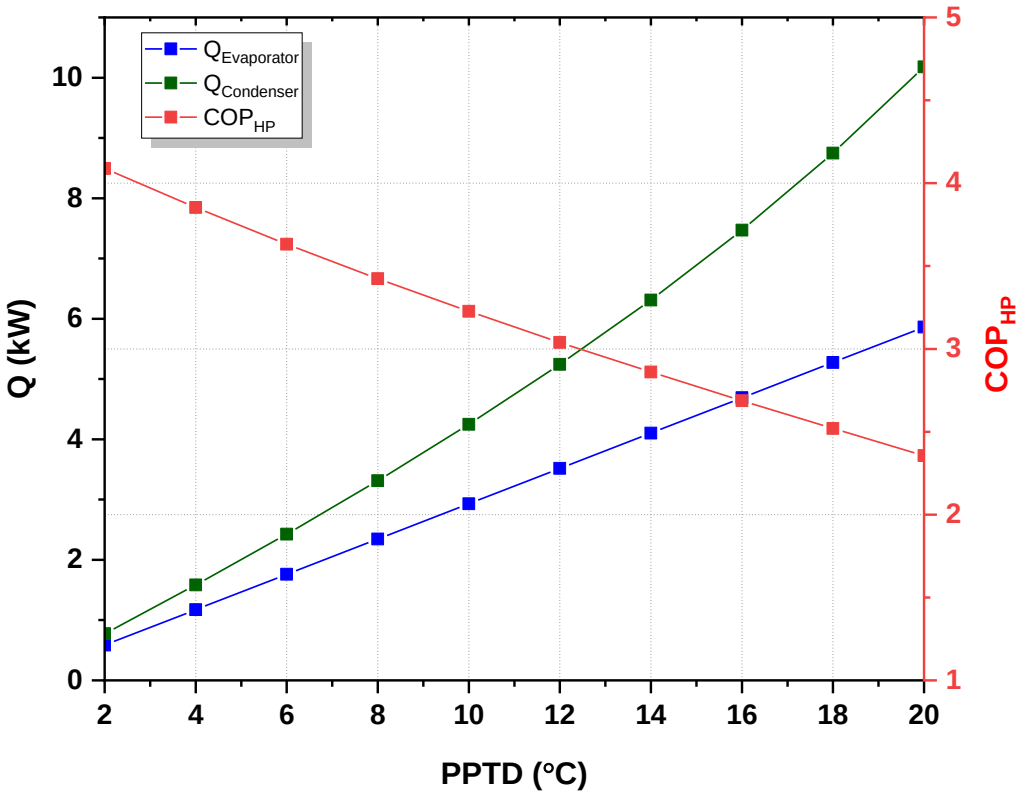

Figure 5.9: Effect of the PPTD on the heat exchangers' capacity and COP of the HP (HX_eff: 65 %, evaporator mass flow rate: 0.4509$\frac{kg}{s}$, T_{cond}: 35 ℃, R: R154a).

When the Figure 5.9 is carefully analysed, it is seen that the increase of the evaporator

capacity is lower than that of the condenser. This can be explained by the temperature lift from the evaporator to the condenser. The linear increase of the PPTD in the evaporator side results in a linear increase in the evaporator capacity where the mass flow rate of the heat source and the ambient temperatures are investigated in their steady-state conditions. For the condenser capacity's exponential growth, however, the increasing level of the PPTD lowers the evaporation temperature, as a result, the temperature difference between the evaporation and condensation sides becomes wider. This high-temperature difference leads to a higher compressor work as seen in Figure 5.10. When the compressor work increases, the condenser capacity also increases because the condenser output is the sum of the evaporator and compressor capacities in a HP cycle.

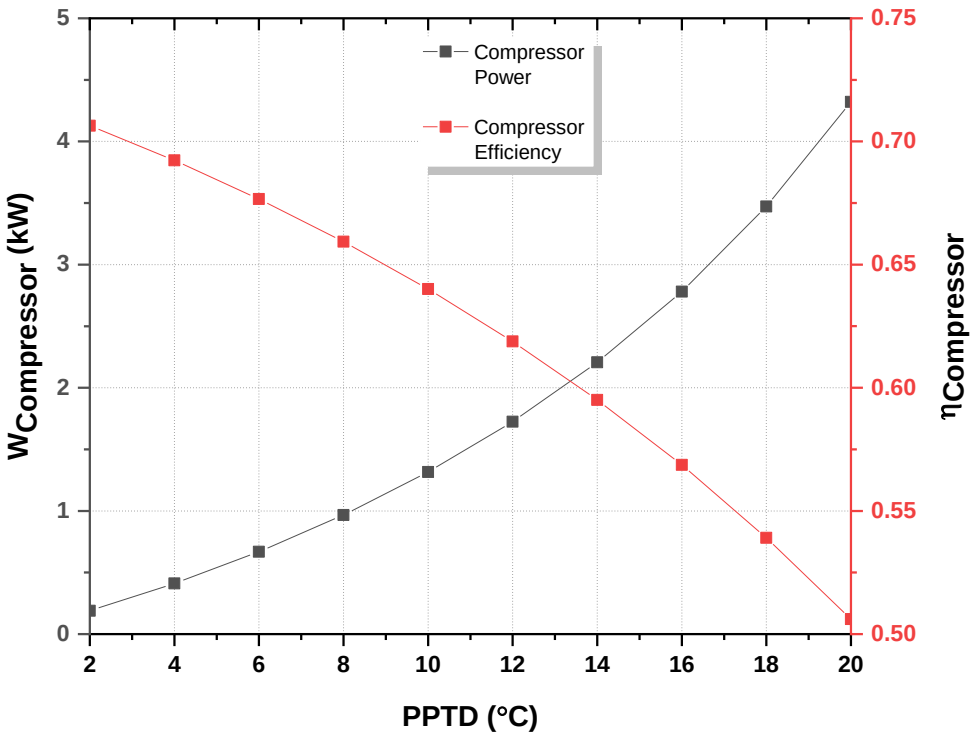

Figure 5.10: Effect of the PPTD on the compressor's work and isentropic efficiency (HX_eff: 65 %, evaporator mass flow rate: 0.4509 $\frac{kg}{s}$, T_{cond}: 35 °C, R: R154a).

Finally, the higher compressor work eventually means the higher pressure increase on the

condenser side. As the compressor isentropic efficiency is a function of the pressure ratio between condenser and evaporator (shown in the Equation 5.29), the compressor's efficiency decreases at higher PPTD values. In other words, the compressor works less efficiently while it works more at high PPTD values.

5.5 RESULTS AND DISCUSSION ON THE SYSTEM PERFORMANCE

5.5.1 Flow Chart and Control Strategy of the PV+ASHP Model Using the TRNSYS-EES Co-Simulator

The performance of the proposed system is investigated in two different cases. In the first case, the system is aligned with the "Solar Heating and Cooling Roadmap [75]" of the International Energy Agency (IEA), where the solar systems cover at least 50 % of the annual total energy (ATE) demand of the representative single family house. Therefore, in the first case, the proposed PV+ASHP system focuses to cover only 50 % of the ATE demand of the representative house with the PV generation throughout the year. In the second case, the system aims to cover 100 % of the ATE demand of the house with PV electricity, hence becoming net-zero energy annually. It has to be mentioned that the actual total demand of the house was found in Chapter 4 as 10077 kWh (sum of SH+SC+DHW+EE, 10077 kWh).

The work pattern and control strategies of the system are shown in a flow chart in Figure 5.11. For both cases, first, the actual dynamic space heating and cooling demands of the single-family house is read from the Type 88 (modelled in Chapter 4) and is sent to the HP unit modelled in the EES. In order to operate the HP, foremost, a primary control strategy is implemented (with the Type 166, See Chapter 3) between the EES's HP model and TRNSYS's Type 88, where a room thermostat from Type 88 provides a control function value of "1" or "0" to the HP depending on the building's zone temperature goes below 20

℃ (for the heating mode) or not, respectively. Similarly, for the cooling mode, the thermostat sends the control signals of “0” or “1” to the HP depending on the building’s zone temperature goes above 26 ℃ or not, respectively. In both modes therefore the HP runs when the control signal is “1” and stops when “0”. The dead-band range of the thermostat is 1℃, hence the zone temperature is kept between 20 ℃ & 21 ℃ during the heating mode and 26 ℃ & 27 ℃ during the cooling mode. As the SH and SC load demands are aimed to be satisfied with the HP unit to electrify the thermal demands, the electrical energy required for the compressor of the HP is calculated hourly throughout the year, and the results are aggregated daily, monthly, and annually to analyse the heat to power ratio of the load demands by means of the HP. In other words, HP’s electrical energy required to cover the actual SH and SC demands is calculated. It is worth mentioning that this compressor electricity requirement is treated as the new SH and SC demands in the annual calculations as it is the amount of energy required by the HP to cover the actual SH and SC load demands of the representative house.

Then, the total electricity demand of the house (electrical auxiliary heater for DHW, EE, and the electrified SH and SC demands) is read by the TRNSYS Type 103 PV model. As the total demand is known at this stage, the Type 103 PV model reads the other parameters from Type 88, such as ambient air, solar radiation, wind speed, etc., and assumes a PV area to conduct the annual simulations. Based on this area, the total annual PV production is calculated and compared with the total demand of the building. The annual simulations are repeated until the targeted proportions of the total demand in both cases (50 % and 100 %) are reached.

Finally, for both cases, the electricity that the HP and other electrical equipment utilize (auxiliary heater for the DHW and the household equipment for the EE) arrives from the PV panels as long as the PV electricity is available. Otherwise, the proposed PV+ASHP system

interacts with the grid with the FIT, importing or exporting the electricity.

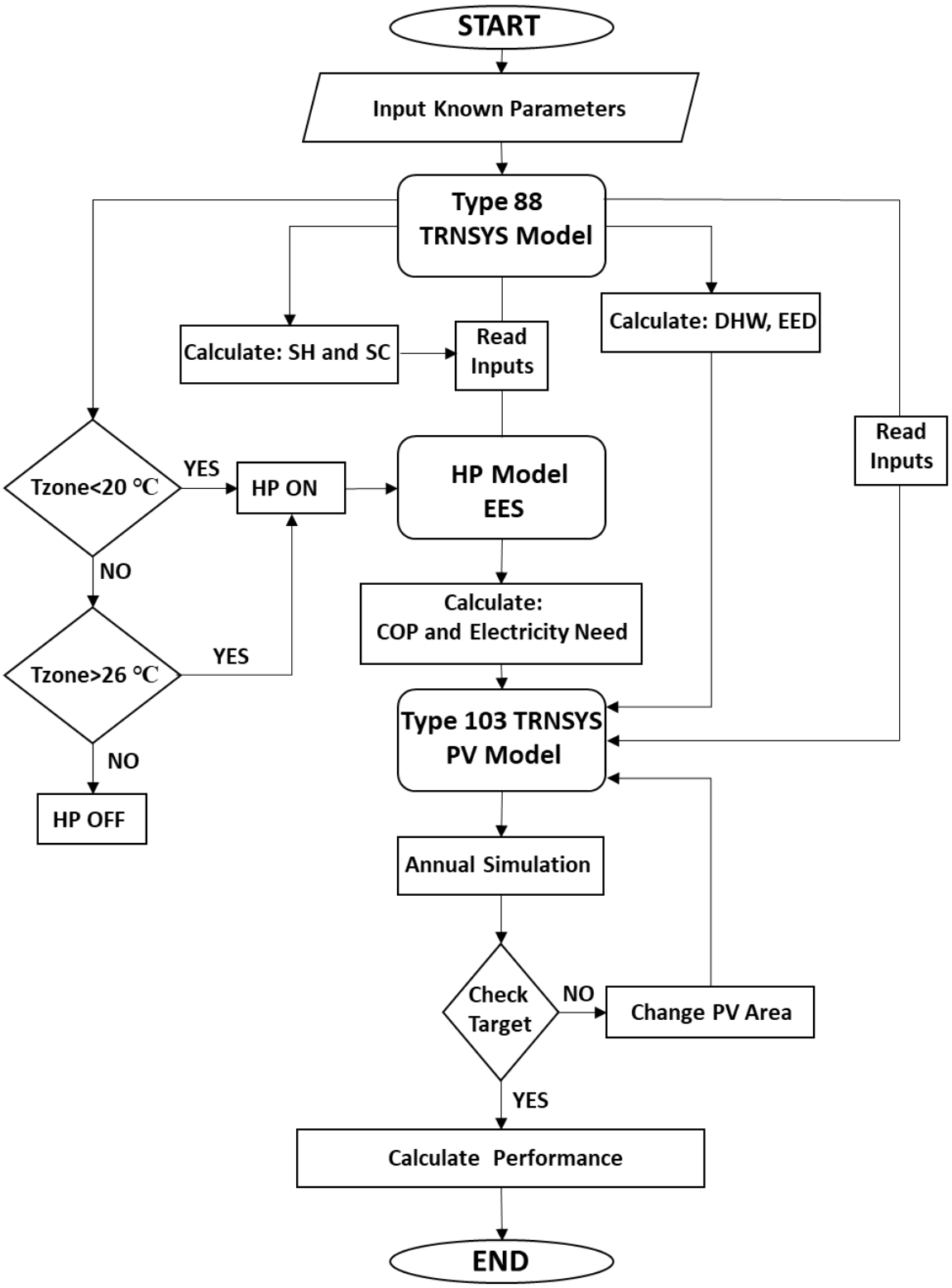

Figure 5.11: Control and flowchart of the proposed system.

5.5.2 Dynamic Annual Performance Evaluation of the System

5.5.2.1 Dynamic annual performance evaluation of the HP model (EES)

With the control strategy explained in the above section, the HP unit goes “ON” and “OFF” based on the zone temperature. The time step of the simulations in the EES is set to 0.125 h, synchronized with the TRNSYS’s Type 88 building model. The annual dynamic performance results of the HP are simulated and are aggregated hourly with the TRNSYS Type 25 printer, and presented in Figure 5.12. During the heating mode operation, the HP unit reads T_{amb} for the evaporator side and house’s indoor temperature before heating (T_{zone}) for the condenser side from the TRNSYS, and transfers the heat from the low reservoir (ambient) to the high one (building) with the aid of an additional work input from the compressor of the cycle. For the cooling mode the cycle is reversed and the cooling mode results are obtained with the same method.

As stated in Equation 5.36, the COP of the HP unit is the ratio between condenser and compressor capacities (both for heating and cooling mode). Due to the dynamic compressor operation and the predefined condenser capacity, HP's dynamic COP is calculated hourly throughout the year both for heating and cooling modes (Figure 5.12 (top)). This work input (electricity) of the compressor is the required energy to cover the actual SH demand of the building (Figure 5.12 (bottom)).

As seen in Figure 5.12 (top), the COP of the system has a similar trend with the ambient temperature throughout the year. This is expected as the ambient temperature has a direct impact on the evaporation temperature of the HP which results in lowering or rising the temperature lift from a low reservoir to a high one. Moreover, Figure 5.12 (top) shows that the HP's hourly COP fluctuates around “4” throughout the heating season and drops below this value during the coldest months. Similarly, the cooling COP value vary around “5”

during the summer months and drop below this value when the ambient temperature peaks.

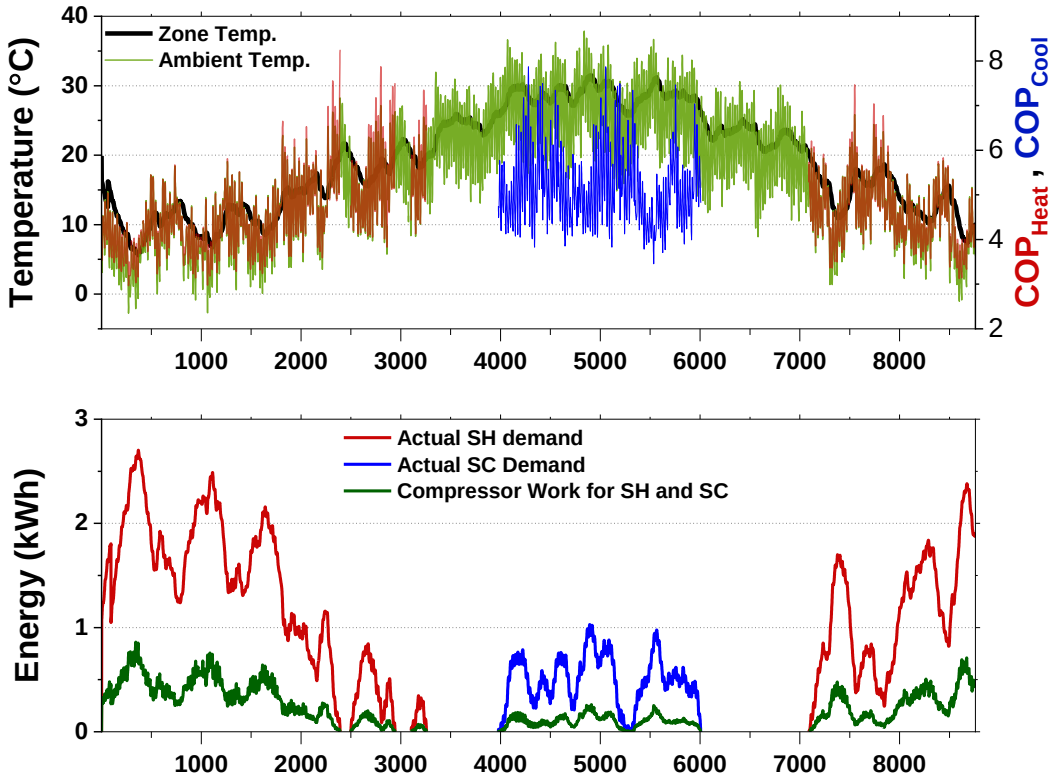

Figure 5.12: Annual performance of the HP: top) hourly ambient and zone temperatures (initial), and COP fluctuation of the system; bottom) hourly actual space heating demand and compressor's required electrical energy throughout the typical year.

Furthermore, from Figure 5.12 (bottom), it is seen that there is a substantial difference between the actual SH & SC demands of the building and the required compressor electricity consumption. This actually clearly demonstrates how HPs can significantly reduce the thermal demands of the buildings due to their high COP. Also it shows the successful implementation of the EES's HP model and TRNSYS' Type 88 building model.

Subsequent to the dynamic hourly results, for a clear inspection, these results are aggregated monthly and presented in Figure 5.13, together with the monthly average COP value of the HP unit. As seen, the compressor's electrical requirement increases to its peak value during

the coldest and hottest months of the year (January and July, respectively). This is due to the high actual load demands in these months. In addition, the minimum and maximum monthly COP values for the heating season are found as 3.87 (in January) and 4.92 (in April), respectively. Similarly, for the cooling season, the maximum monthly average COP is found as 6.23; while for July and August, the average COPs are found as 5.43 and 6.11, respectively. Therefore, due to the HP utilization, the actual SH and SC demands are reduced from 5721kWh to 1402kWh and from 594 kWh to 128 kWh, respectively. This means that the HP needs a total of 1530 kWh of electricity to supply 6315 kWh of total actual space heating and cooling demands, which is a total demand reduction of almost 75%. In the following sections, therefore, the total electricity consumption of the compressor is used to size the system and to analyse the demand coverage cases.

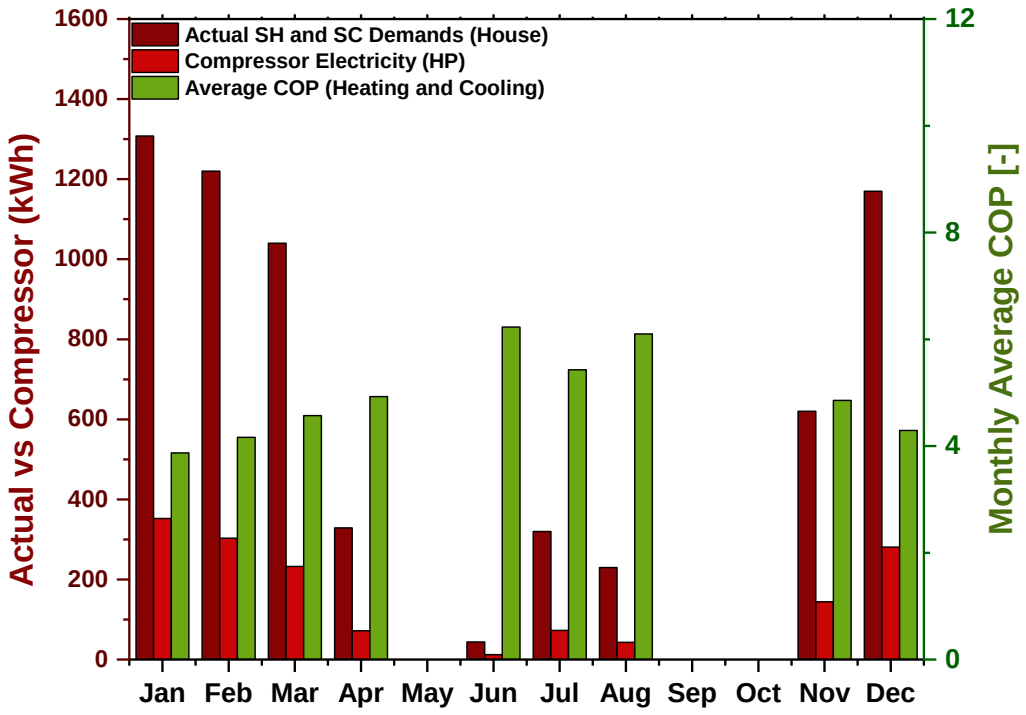

Figure 5.13: Winter months' actual SH, compressor's operational work input, and the HP's COP value during the heating season.

5.5.2.2 Dynamic annual performance evaluation of the Type 103 PV model (TRNSYS)

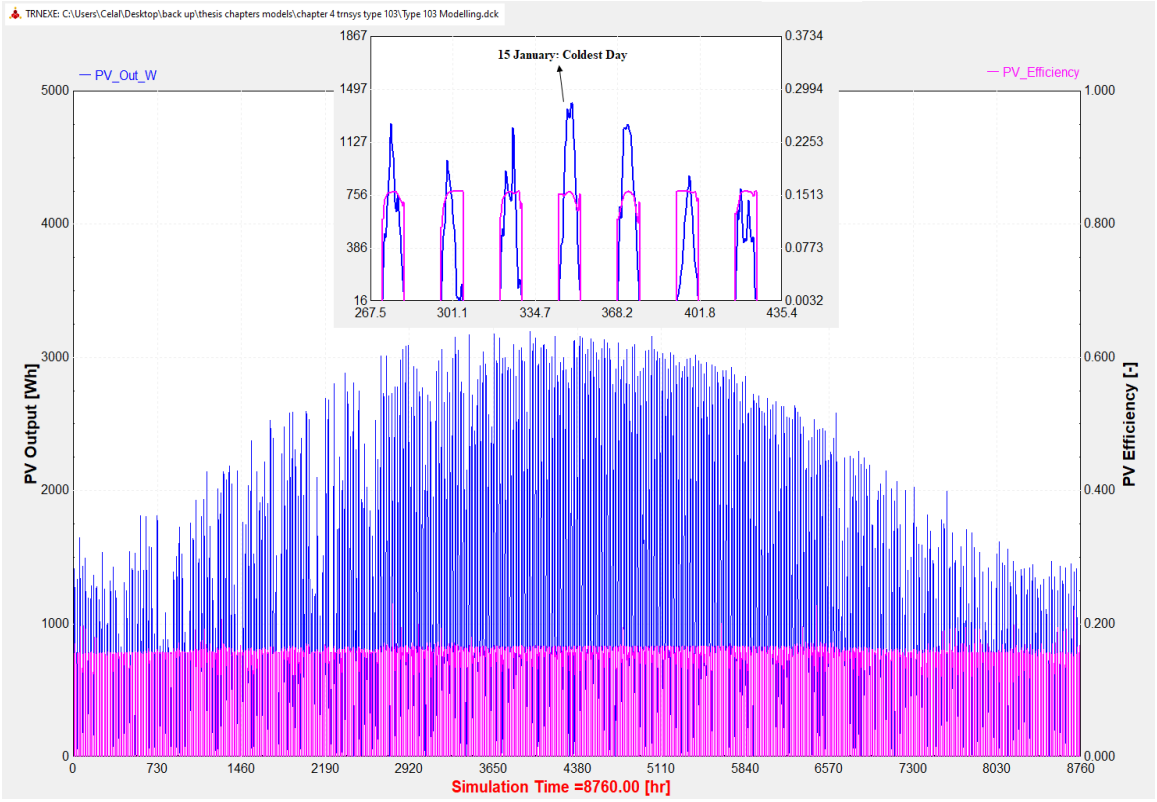

Figure 5.14: Type 103 PV model's energy output and its efficiency throughout the year.

The hourly PV production of the Type 103 model and its efficiency during the typical year are presented in Figure 5.14. The same TRNSYS graph also shows the daily energy production and efficiency in a separate top box. It is seen from this graph that the PV generation is low during the winter months and high in the summer. This is expected as the total radiation, and the number of sunny hours are low on winter days. In addition, the PV output value is observed to reach as high as 3000 W values in the summer months. For the efficiency, in contrast, two interesting results are observed. First, the 18% of efficiency rate from the manufacturer is never reached hourly. Instead, the maximum hourly efficiency of the panel is observed as 16.8% on 24th May at 1 p.m. when the ambient temperature was 24 °C. This is because the ambient temperature and solar radiation of the location at this specific time is close to the manufacturer's reference conditions of 25 °C and 1000 W/m^2 (see Figure

5.6). Secondly, from the figure, the efficiency value reaches close to 20% for few times (hour 2920s, etc.) which is higher than the rated efficiency value of the panel. However, it has to be remembered that these are the instantaneous values of the efficiency based on 0.125h time steps, hence not the hourly rated values.

5.5.2.3 Dynamic Annual Performance evaluation of the PV+ASHP (EES-TRNSYS co-simulator)

The Type 103 reads the input values from the Type 88 model in TRNSYS and the HP model in the EES to operate. As mentioned in section 5.5.1, the proposed PV+ASHP system in this study aims to cover first 50 % and second 100 % of the ATE demands of the system with PV electricity. Any excess or missing electricity however is injected or extracted from the grid as the system is connected to the national grid with the Feed-In Tariff (FIT). For these cases, the monthly total energy demand of the building (SH, SC, DHW, and EE) is compared with the total electricity output of the PV model sized with the equivalent area to cover the targeted energy demands. It has to be noted that the demand profiles are the same in both cases as the system is analysed for the same typical year but the PV output differs resulting in different demand coverages in different months. Moreover, in the previous section, it was shown that the sum of the SH and SC demands are reduced by almost 75% due to the HP utilization. Therefore, the new ATE demand is 5292 kWh in both cases (50% and 100%), which is the sum of compressor electricity need for SH & SC (1530 kWh), the DHW demand (1497 kWh), and the EE demand (2265 kWh). Further, in both cases, the SH and SC are prioritized, which means that any PV generation is first used to supply the electricity demand of the HP's compressor. Then, the remaining PV output is sent to cover the DHW and EE demands, where any missing energy is supplied from the national grid via the FIT connection. Subsequent to the above introductory for the holistic model, the investigated two cases are explained as follows:

50% of the ATE demand coverage;

For this case, the total required PV area is found to be 10.1 m^2 which is well below the available rooftop area of the representative building (50 m^2) (detailed in Chapter 4). In order to find the required PV area, the holistic model increases the Type 103's "panel area" input value by 0.05 m^2 at each annual simulation until the total PV electricity output reaches 50% of the ATE demand. When the system runs based on this area, the total PV output in each month is compared with monthly all four energy demands. Figure 5.15 shows this comparison and the total amount of auxiliary power from the grid to cover the missing energy remaining from the PV production.

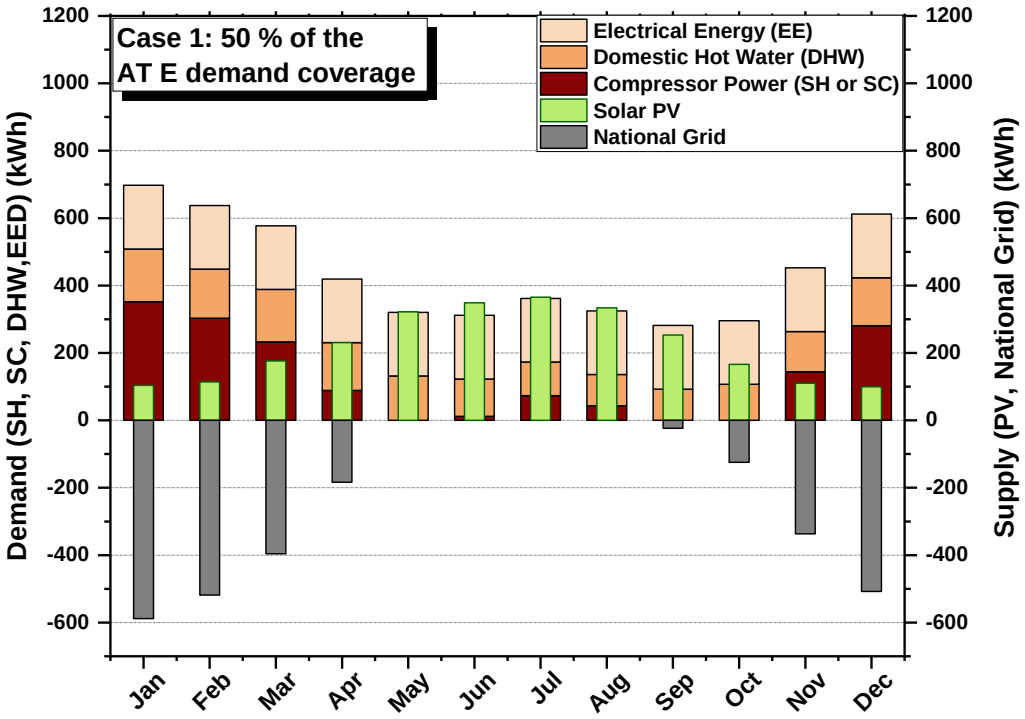

Figure 5.15: Performance of the PV+ASHP system with the 50 % of the ATE demand coverage.

In this case, as the system's PV size is adjusted to cover only 50% of the ATE demand, a substantial amount of energy is still needed from the grid to cover the total energy demand of the house, especially in the winter months (December, January, and February). In these

months, due to the high SH demand, low solar radiation (affecting the PV output), and the cold ambient temperatures (affecting the COP of the HP), the proportions of the SH demand covered by PV electricity are only 35%, 29%, and 37%, respectively. Although proportionally only SH is still met, the system performs better in March and November, meeting more than 75% of the total SH demand in both months, but still failing to meet both DHW and EE demands. In April, the system meets 100% of both the SH and the DHW demands and lacks to cover EE demand. For the months when the SC is needed (June, July, and August), however, the system generates more energy than what is required for all three demand vectors (SC, DHW, and EE) and transfers the excess generation to the national grid. In June, in particular, the amount of excess PV output is found as 37.3 kWh. Finally, for the months when neither SH nor SC is required (May, September, and October), the system tries to cover only DHW and EE demands. In these months, the system covers both demands in May, while requiring the grid aid in September and October to meet these demands.

When an annual energy balance is checked for the 50% case, it is seen that the system covers 49.9% of the ATE demand of the house annually, and still requires 2646 kWh of energy from the grid.

100 % of ATE demand coverage

For this case, the total required PV area is found to be 20.15 m^2 which is also well below the available rooftop area of the representative building (50 m^2). The required PV area is found by following the same procedure as in the previous case, however, in this case, the simulations continues until the annual total PV output meets the ATE demand. The system then runs based on this area and the results of the monthly PV coverage of the total demand are obtained, together with the required auxiliary power from the national grid. Figure 5.16 shows the performance of the system based on 100% of the ATE demand coverage, and the

total amount of auxiliary power from the grid to cover the missing energy from the PV generation.

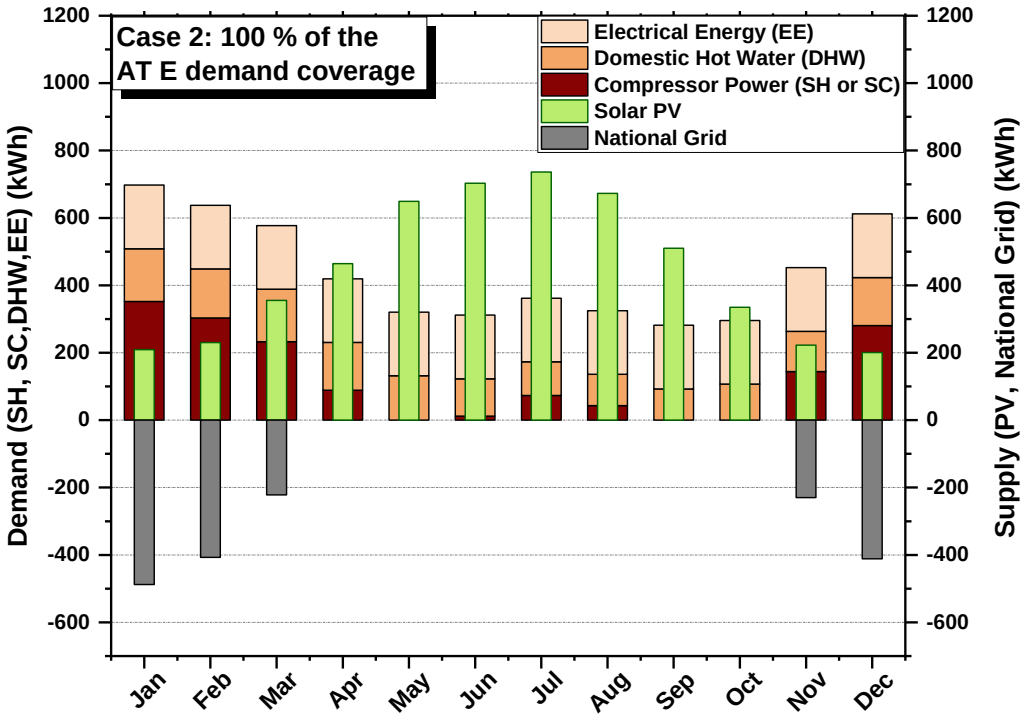

Figure 5.16: Performance of the PV-a2aHP system with the 100% of ATE demand coverage.

As seen from this figure, although the system reaches the balance annually in terms of the energy demand and the supply sides, the representative single-family house still requires auxiliary electricity from the grid to meet the SH demand in the coldest months (January, February, and December). The proportions of the SH demand covered by PV electricity in these months are 59.4%, 76%, and 71.4 %, respectively. In March and November, the system covers 100% of the SH demands and majority of the DHW demands (78.7% and 65.5%, respectively), whereas the EE is covered by the national grid. In April, the system covers 100% of all energy demands (SH, DHW, and EE) and exports its excess power (45 kWh) to the national grid. For the cooling months (June, July, and August), the system meets all energy demand vectors (SC, DHW, and EE) and transfers 1113.9 kWh of electricity to the grid. Finally, for the months where there is no need for space heating and cooling (May,

September, October), the system covers all energy demand vectors and exports a total of 596.3 kWh electricity to the grid.

In terms of the annual energy balance, as expected, the system reaches equilibrium annually. It is worth mentioning that the proposed system in the ATE case requires 1755.2 kWh of the grid electricity to meet all energy demand vectors (especially in the winter months). However, this amount is offset by the same amount of excess PV generation, hence become net-zero annually. Due to the HP utilization, moreover, the most notable conclusion is that the proposed PV+ASHP system is able to cover the actual ATE demand of the representative house (SH+DHW+EE), 10077 kWh, with a 20.15 m^2 of the PV installation.

Discussion on the annual performance results of the PV+ASHP system

When the results of both cases are compared, it was expected that increasing the amount of PV area would result in an increase in the total generated energy output of the system in every month. Nevertheless, because the system is designed with the objectives of maximizing the electrification of the thermal demands with renewable energy and reducing the grid dependency, achieving high SH and SC demand coverages throughout the year is crucially important. In this regard, the 100 % ATE case is advantageous as it covers more SH and SC demands. Secondly, the national grid can act as battery storage with no limit on the capacity as it is connected to the system with the FIT. Hence designing the system based on a low proportion of the demand coverage leads the system to be significantly grid-dependent, which is not in line with the objectives of the study. Finally, as stated in Chapter 4, the available rooftop area of the representative house was 50 m^2. In both cases, the required PV areas are well below the usable rooftop area of the house. However, without crossing the upper limit of 50 m^2, increasing the PV area from 10.1 m^2 to 20.15 m^2 leads the system to become net zero in terms of the annual energy balance, and to generate its own

energy. For these reasons, the 100% ATE case is chosen as the optimum case and the daily performance of the system is further analysed based on this case's PV area in the following sections.

5.5.3 Dynamic Daily Performance Evaluation of the System

The daily performance analysis of the system is presented on the coldest day of the typical year, 15th January. This specific day is when the SH demand is the highest and the ambient temperature is the lowest in the typical year. Therefore, the daily performances of the HP model and the EES-TRNSYS co-simulator are presented for the coldest day of the year in the following sub-sections.

5.5.3.1 Daily performance evaluation of the HP model (EES)

The correlations between the inputs and the outputs of the model, such as the effect of the ambient temperature on the COP, the effect of the COP on the compressor work requirement, etc. are explained in the previous section (Section 5.5.2). Therefore, these correlations are not explained here again. In this section, instead, the hourly/daily performance of the system is presented to observe the trend of these variables and to compare them with the annual performance trends. Figure 5.17 presents the dynamic hourly/daily performance results of the HP model of the EES.

From the Figure 5.17-a, it is seen that the lowest ambient temperature of the typical year is -2.7 °C, where the difference between the coldest and warmest temperatures can be up to 10 °C during the day. However, for the actual SH demand of the house, the variation during the day is quite small (2.532 kWh for the lowest, 2.651 kWh for the highest). This is because of the heat flux of the house, where the large changes in the ambient temperature results in small variations in the actual SH demand of the house. It should be noted that while on a larger scale the actual SH demand profile may appears almost flat (Figure 5.17-a), hence the

scale of variation on the left side of the graph (from 2.4 to 2.8 kWh) is made quite small, allowing to observe the trend of the actual SH demand against ambient temperature. As can be seen from the top chart, the actual demand for SH increases as the ambient temperature drops, hence the trend (effect of the ambient temperature on the SH) is in line with that described in the annual performance section.

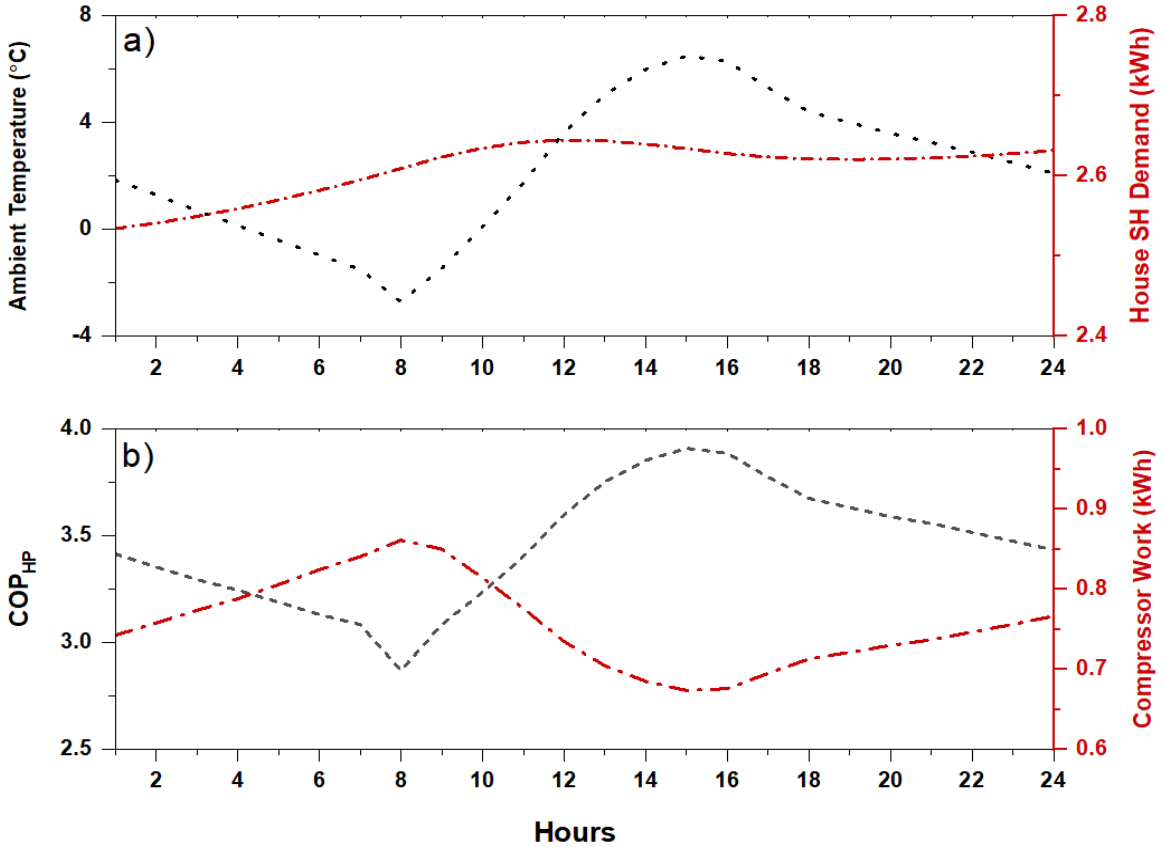

Figure 5.17: Performance of the HP unit on 15th January: a) effect of the hourly ambient temperature on the actual SH demand; b) COP versus compressor's required electrical energy.

A similar trend is also observed in Figure 5.17-b, where the daily HP's COP and compressor work requirement are presented. As seen, the lowest COP value of the HP on the coldest day of the year is rated as 2.87 at 8 a.m. in the morning. This is the lowest value of the typical year-round COP, as the ambient temperature is also at its lowest at this particular time.

Moreover, when the ambient temperature drops during the day, the HP's efficiency decreases hence the compressor runs more and consumes more energy to cover the increasing actual SH demand. As explained in the annual performance section, the compressor work requirement is in fact the amount of energy to cover the actual SH demand of the house. Therefore, the substantial energy requirement difference between the actual SH demand and the compressor's electricity requirement can also be seen daily as it was annually.

5.5.3.2 Dynamic daily performance evaluation of the PV model (TRNSYS)

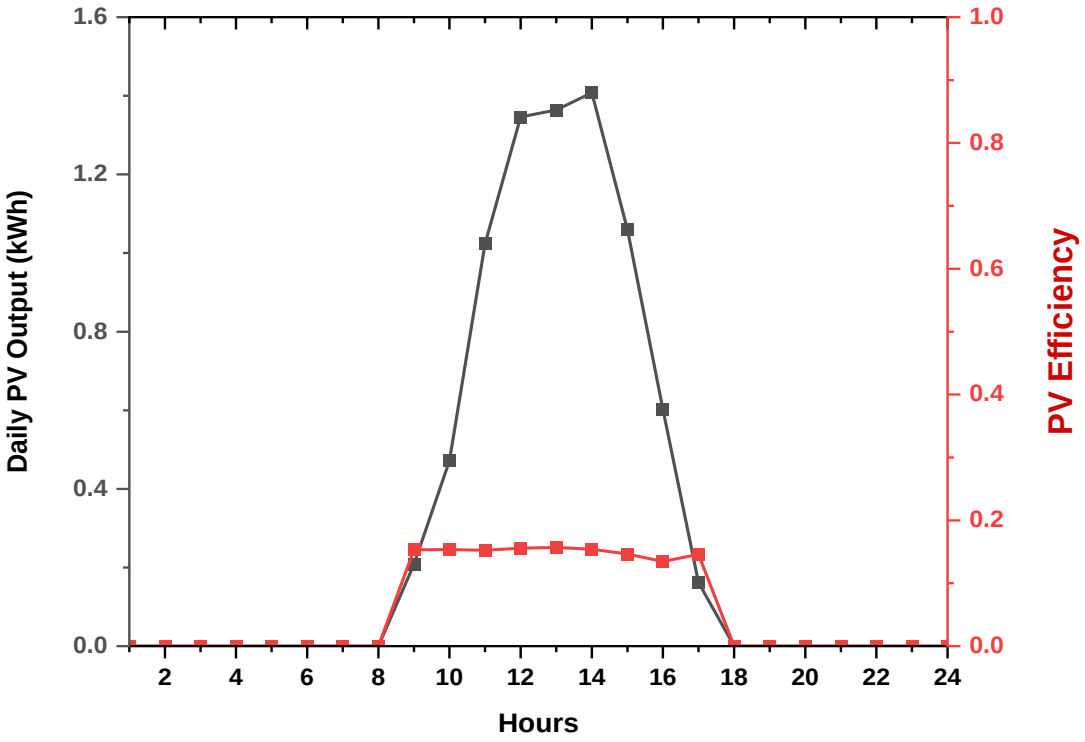

Figure 5.18: Daily PV production and its efficiency on 15th January.

The annual PV production and its efficiency were shown in Figure 5.14 from the Type 103 PV model of the TRNSYS. In that figure, the daily results were also shown for 15th January in a small additional box. However, for clarity, the daily results are spotted again in Figure 5.18 to observe the maximum hourly electricity generation and efficiency of the PV module.

As seen in Figure 5.18, while the PV output reaches its peak value (1.407 kWh) at around 2 p.m., the maximum efficiency is observed at 1 p.m. with a value of 15.6%.

5.5.3.3 Dynamic daily performance evaluation of the PV+ASHP (EES-TRNSYS co-simulator)

Since the proposed system reaches a net zero energy balance with the 100% ATE demand fulfilment case, the daily performance analyses of the system are conducted according to the equivalent area of this case. Therefore, in the daily analyses, a 20.15 m^2 solar PV area is used.

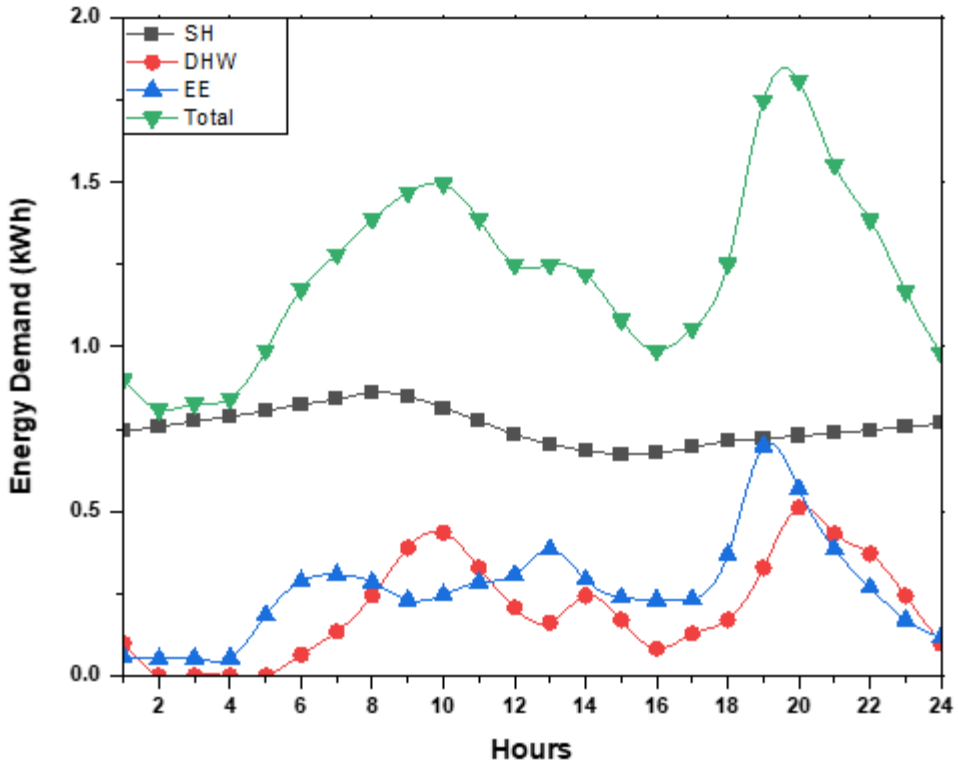

Figure 5.19: Total hourly/daily energy demand of the house on 15th January.

In order to assess the daily performance of the system, a summary of the daily demand profiles of each energy vectors (DHW, EE, and the SH by means of HP) is presented in Figure 5.19 for 15th January. In addition, the daily PV production was clearly shown in Figure 5.18. After summarizing these demand and supply sides, the combination of these two sides is presented in Figure 5.20 to show the total energy balance on the coldest day of

the typical year. In Figure 5.20, the area under the demand curve (shown in a grey-dash colour) represents the total energy demand of the house on 15th January and is covered by the national grid. Similarly, the area under the PV output curve (shown in green-dash colour) represents the total demand covered by PV electricity. The area under the PV output curve (shown in light-green colour) represents the excess PV generation of the system not used by the house and is exported into the grid.

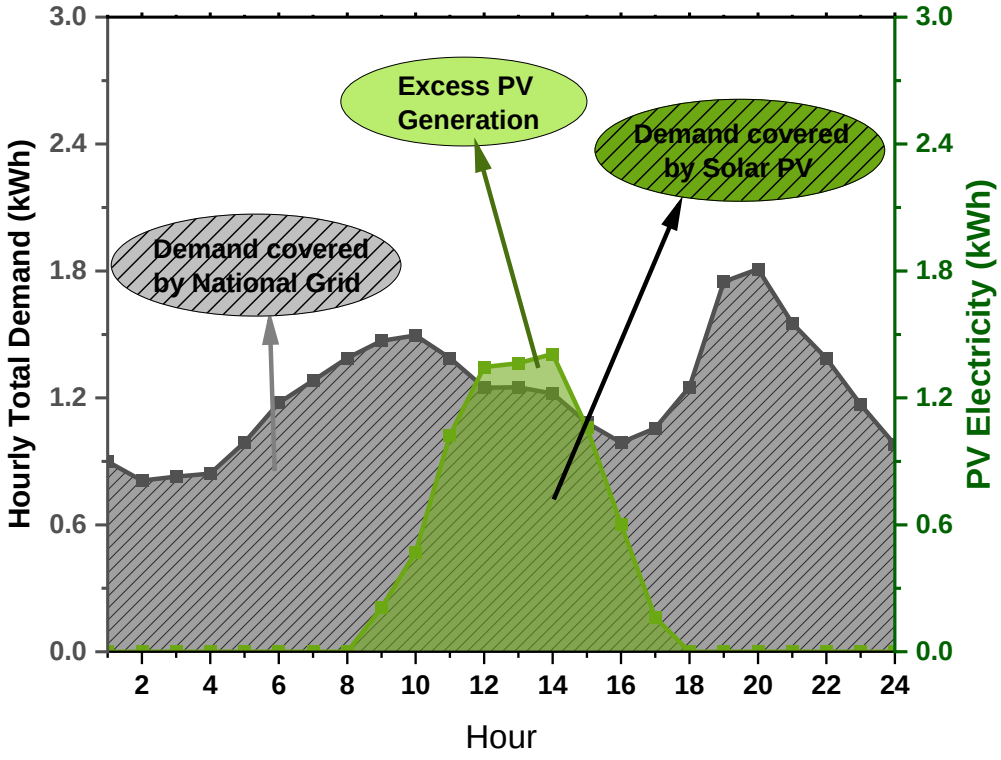

Figure 5.20: Daily Energy balance of the system on 15th January.

As seen from figure 5.20, although the system has a 20.15 m^2 of total PV area, the total daily PV generation on the coldest day is only 7.6 kWh. This PV output is 25.9% of the total energy demand (29.3 kWh) on 15th January. The low percentage is due to the cold ambient temperature resulting a high energy demand for the house and the low solar radiation during the winter resulting a lower PV generation. The system, therefore, imports around 75% of its total energy demand from the national grid's electricity on the coldest day, although it annually reaches the net zero. Furthermore, the amount of electricity that the system sends to the national grid during the peak PV output hours (12- 16 p.m.) is calculated as 0.41 kWh.

This results in fact underline the importance of the gird connectivity for the system. Only with the FIT, the proposed PV+ASHP system becomes net zero. Otherwise, the system still depends on the national grid substantially on the coldest day of the year.

5.6 ECONOMIC ANALYSIS OF THE SYSTEM

As discussed in the previous sections, it is technically feasible for PV+HP systems to supply the all energy demand profiles (SH, SC, DHW, and EE) of a single-family residential house without the need for a higher area than the available rooftop area of the house. In most cases, however, the economic barriers remain the primary impediment to the widespread utilization of these systems as they have a higher investment cost than conventional individual PV or HP systems. The tipping point for the adoption of solar-heat pump energy systems is perceived when the technology accomplish the grid parity. The "Grid Parity" refers to the comparison between the cost of electricity generated from PV+HP systems over their lifetime and the electricity price of the national grid, hence it shows the economic feasibility of an energy generation system [259].

There are many indicators that can be used to evaluate the economic feasibility of an energy generation systems such as, the levelized cost of energy (LCOE), net present value (NPV), payback time (PT), life cycle cost (LCC), total economic savings (TECS), etc. [260]. Among these, the LCOE and PT are the most often used when comparing the energy generation systems or considering the grid parity [259], [261], hence they are employed in this study to reveal the economic feasibility of the proposed PV+ASHP system. The PT is relatively simple as it does not account the long-term factors such as discounting, future revenues, and replacement costs of the system. However, it provides excellent simplicity to easily analyse the return time of the system's initial investment cost, thus it has been used intensively where some examples can be found in [261], [262], [263]. The equations behind this indicator are well documented and not overly complicated, and can be expressed as follows [264]:

$$PT = \frac{C_{Invest}}{C_{Saving} - C_{O\&M}} \quad (5.37)$$

where the C_{Invest} is the system's total investment cost, the C_{Saving} is the total annual cost saving obtained from using the PV+ASHP system (compared to the conventional gas boilers and/or electrical heaters), and the $C_{O\&M}$ is the operation and maintenance cost of the proposed system per year.

The LCOE, on the other hand, is an advance and complex method considering the time value of the initial investment in addition to the additional expenditures encountered over the life cycle of the system. It is expressed as the cost per unit of energy produced from a system over its life cycle [265]. The LCOE is the ratio of the system's lifetime capital & operational expenditures (CAPEX and OPEX) to the lifetime energy generation of the system. Both costs and energy generation are in the net present values (NPV). This means that the system's future CAPEX, OPEX, and outputs are discounted back to the initial time of the system construction (first year). In simple terms, the LCOE can be formulated as follows [265]:

$$LCOE = \frac{NPV\ of\ Total\ Costs}{NPV\ of\ Total\ Energy\ Generation} = \frac{NPV_{TC}}{NPV_{TE}} \quad (5.38)$$

where TC and TE represent the total cost and energy output over the lifetime of the system, respectively.

For the proposed system, the NPV_{TC} consists of the most fundamental expenditures including acquisition & installation costs, operating & maintenance (O&M) costs, and replacement costs, where the additional costs for the depreciation credits, loan payments, and the residual value are not used in the calculations. The NPV of the total cost (TC) for the system components therefore can be summarized as follows [266]:

$$NPV_{TC} = \sum_k (NPV, C_{A\&I,k} + NPV, C_{O\&M,k} + NPV, C_{rep,k}) \quad (5.39)$$

$k = PV, HP, Inv, AH$ ..... (5.40)

where k is the different components, the PV, HP, Inv, AH are the photovoltaic panel, heat pump, inverter, and auxiliary heater unit (for DHW) components of the proposed system, respectively. Also, $C_{A\&I,k}$, $C_{O\&M,k}$, and $C_{rep,k}$ represents the acquisition & installation costs, operating & maintenance (O&M) costs, and replacement costs for the component k, respectively.

By considering the discount & inflation rates, the net present value of the each expenditure of the total cost (TC) can be formulated as follows [267]:

$$NPV, C_{A\&I,k} = \sum_k C_{A\&I,k} \times N_k \quad \text{..... (5.41)}$$

$$NPV, C_{O\&M,k} = \sum_j^{life_{system}} C_{O\&M,k} \left(\frac{(1+inf)^j}{(1+r)^j}\right) \quad \text{..... (5.42)}$$

$$NPV, C_{rep,k} = \sum_i^{N_{rep,k}} \left(Cost_k \times \frac{(1+inf)^{i \times life_k}}{(1+r)^{i \times life_k}}\right) - Cost_k \times$$

$$\frac{(life_k - (life_{system} - N_{rep,k} \times life_k))}{life_k} \times \left(\frac{(1+inf)^{life_{system}}}{(1+r)^{life_{system}}}\right) \quad \text{..... (5.43)}$$

where the $life_k$ and $life_{system}$ are the lifetime of the component k and system, respectively, inf and r are the general inflation (for components and O&M costs) and discount rates, respectively, $N_{rep,k}$ and is the number of times that component k is replaced during the system lifetime, N_k is the number of component k.

In addition, the NPV value of the total energy generated during the system life time can be calculated as follows:

$$NPV_{TE} = \sum_t^{life_{system}} \frac{E_{ann}(1-d)^t}{(1+r)^t} \quad \text{..... (5.44)}$$

where E_{ann} and d are the annual generated energy and degradation rate of the system over

the years, respectively.

Table 5.3: Cost data and financial assumptions for the economic analysis.

Component	Description	Range (GBP,£)	Cost Value (GBP, £)	Cost Value (Turkish Lira, TL)	Value	Reference
PV	320 W PV panel acquisition cost per kW	630-1245	746	17158	-	[268], [150], [269], [270] Cost Date: 2023
HP	Acquisition cost per kW	600-1050	800	18400	-	[271], [150] Cost Date: 2022-2023
Inverter	Acquisition cost per kW	100-140	120	2760	-	[266] Cost Date: 2023
Auxiliary Heater	Acquisition cost per kW	300-600	450	10350	-	[272], [273] Cost Date: 2023
System Installation	System installation cost	-	1000	23000	-	-
PV	Maintenance cost per KW	0.003-0.005	0.004	0.092	-	[274], [269]
HP	Maintenance cost per KW	0.004-0.007	0.006	0.138	-	[266]
Discount rate	Bank discount rate (%)	-	-	-	8	[269]
Inflation rate	General inflation (%)	-	-	-	12.4	[275]
Inverter life	Lifespan of the Inverter (years)	-	-	-	10	[267]
System life	Lifespan of the system (years)	-	-	-	20	-
Degradation rate	System’s degradation per year (%)	-	-	-	0.5	[259]

Data for the acquisition, installation, operation, and maintenance costs of different components and the financial assumptions utilized to conduct the economic analysis of the proposed system are presented in Table 5.3. The acquisition cost for the monocrystalline solar PV panels is taken from the manufacturer's (Solar Electric, UK) price list [268], which is in line with the solar retailers in Europe and Turkey [150], [269], [270]. The costs for the HP, inverter, and auxiliary heater are estimated from the literature and the price lists available from the different retailers [271], [150], [266], [272], [273]. The cost for the system installation is assumed based on similar facilities in the Turkish market. The cost for the O&M of the system is calculated as around 1% of the system's CAPEX, which is in line with the available literature [274], [269], [266]. In order to reflect the internal rate of return of the energy projects in Turkey, a discount rate of 8% is selected based on [269]. An annual inflation rate of 12.4 % is selected which is the country's average inflation rate for the last two decades (2001-2021), data is available in [275]. The system's lifetime is assumed to be 20 years where the inverter's lifespan is 10 years and replaced at the end of the 10^{th} year. Finally, the degradation rate of the system is 0.5% based on [259], and the conversion rate from "GBP to TL" and "Euro to TL" are taken as 1GBP=23TL and 1 Euro=20TL, respectively, as of January 2023.

Applying the cost data listed in Table 5.3 to the proposed PV+ASHP system, the PT and the overall LCOE of the system are calculated as follows:

Payback Time of the system: The payback time is calculated by employing Equation 5.37 where three parameters are considered; total investment cost (C_{Invest}), total annual cost saving (C_{Saving}), and the annual O&M costs ($C_{O\&M}$). As the PT does not take the inflation and discount rates into account, the C_{Invest} includes the system's total CAPEX (including the inverter's replacement) in today's value. By using the data in Table 5.3, the total

investment cost is calculated as 162835 TL. For the C_{Saving}, the proposed system is compared with an electrically driven system that requires a sum of 10077 kWh (SH+SC+DHW+EE) of electricity from the grid. This comparison is because, as discussed in the previous sections, the PV electricity generation is adjusted to offset the all energy demand of the representative house with the aid of the FIT. It has to be mentioned that the feed-in tariffs in Turkey do not include any bonuses, such as guaranties for a higher purchase price from the costumer. For the comparison, the grid electricity price of 2.6 TL/kWh (as of January 2023) [276] is multiplied by the total annual energy generation, hence C_{Saving} is found as $C_{Saving} = 10055 \times 2.6 = 26143\,TL$. Further, the system's annual O&M cost, underlined as OPEX, are calculated as 2312 TL by using the data from Table 5.3. Finally, by employing the known values of the equation, the Payback Time of the system is found as 6.8 years.

LCOE of the system; The LCOE of the system is calculated by employing Equations 5.38-5.44. For the calculations, the summation of the net present value of the total cost (NPV_{TC}) starts with the time equal to "0" (zero) in order to include the CAPEX of the system at the beginning of the first year to not be discounted. However, the replacement cost of the inverter is considered by taking the inflation rate into account during the component's lifespan and is discounted for the rest of the system's lifetime. Similarly, the system's OPEX is considered with the inflation and discount rates. For the O&M costs, data in Table 5.3 is used per kW (PV and HP) and multiplied by the annual energy generation of the system, hence the O&M cost for the year one is found as 2312 TL. Finally, by considering the degradation and discounting rates, the net present value of the system's total energy output (NPV_{TE}) is calculated. For interested readers, a screenshot of the economic analysis of the system is attached in Appendix- 5D. As a result, the LCOE for the system is found as 2.43

TL/kWh (or 0.105 £/kWh or 0.121 €/kWh). When compared with the grid electricity price (2.6 TL/kWh), it is seen that the proposed system is economically feasible.

The most important conclusion from the economic analysis is that the proposed PV+ASHP system has already reached the grid-parity in Turkish market. The high capital investment cost and the uncertainties caused by poor knowledge of such systems due to the limited applications limit the growth of PV+HP technology in the country. Thus, studies demonstrating the design and operation of such system should be encouraged and supported to fill the research gap and build the confidence towards solar PV+HP technology.

5.7 CONCLUSION

In this chapter, a research into the energetic and economic performance evaluation of a holistic solar PV-assisted air source heat pump system has been conducted based on fulfilment of the dynamic heat and power demands of an exemplary European single-family house during a typical year in the boundary conditions of an EU candidate country, Turkey. The proposed system is connected to the national grid and targets to be net zero in terms of energy balance on an annual basis with the Feed-in-Tariff.

The system consisted of the commercial mono-crystalline PV panels, an air-to-air HP unit, and a representative residential house. The residential single-family house was modelled in the TRNSYS software in the previous chapter and the annual sum (10077 kWh) of the dynamic load demands were found as 5721 kWh, 594 kWh, 1497 kWh, and 2265 kWh for the space heating (SH), space cooling (SC), domestic hot water (DHW), and electrical energy (EE), respectively.

In the present study, the mono-crystalline PV unit was modelled in the TRNSYS software by employing the Type 103, whereas the HP unit was modelled in the EES software. These models then were validated against both numerical and experimental studies conducted in

the literature. The validation results showed very minor deviations (2.7% for the PV and 4.2% for the HP), hence the models were used, with confidence, to assess the energetic and economic performances of the system.

The system was then optimized to obtain the optimal design conditions of different units. As the manufacturer data was used to model the Type 103, no further optimization was conducted for the PV unit. For the HP unit, however, the model was optimized by varying the most important parameters of the HP cycle to the upper and lower limits. These parameters were the refrigerant type, the PPTD between the heat source and HP's evaporator, and the mass flow rate of the heat source to the HP's evaporator. The optimization results revealed that the highest HP performance was achieved when the refrigerant type was R152a, the mass flow rate was 0.4509 $\frac{kg}{s}$, and the PPTD was 9.8 ℃.

Based on the implemented control strategies, the electrically-driven HP model then operated with these parameters to cover the dynamic space heating and cooling demands of the representative house throughout the typical year, while all electrical demands (including the HP's consumption and DHW & EE demands) were covered either by the PV or the national grid. Due to the optimized HP unit, the seasonal amounts of electricity that HP's compressor consumes to cover the SH and SC demands were found to be 1402 kWh and 128 kWh, respectively. Thus, compared to the 6315 kWh of total actual space heating and cooling demands (5721 kWh for SH and 594 kWh for SC), an energy-saving potential of almost 75 % was achieved.

The holistic operation of the system was when the Type 103 PV model operated with the Type 88 and HP models. During this operation, the energetic performance of the system based on two pre-set demand coverage targets was evaluated. The first target was aligned with the "Solar Heating and Cooling" roadmap of the IEA to cover at least 50 % of the actual

annual-total-energy (ATE) demand of the representative house with the PV electricity. In this case, the IEA's target was achieved with 10.1 m^2 of PV area, however, the system still required 2646 kWh of energy from the grid to be net-zero. The second target (which was also the aim of the study), on the other hand, was when the system covers 100 % of the ATE demand of the house to be net-zero-energy. In this case, the proposed PV+ASHP system was able to cover the actual total annual energy demand of the house (SH+SC+DHW+EE), 10077 kWh, with 20.15 m^2 of PV installation. When the annual simulations were conducted based on this area, the representative house still required a 1755.2 kWh of the grid electricity to meet all energy demand vectors, however, this amount was offset by the same amount of excess PV generation annually. This meant that the system reached the annual equilibrium with grid connectivity. In addition, without the HP unit, in order to cover the annual total demand of the house, 38.3 m^2 of PV would have been required. This underlined the importance of the heat pump utilization for the thermal energy demand of the residential houses as the HPs reduce and electrify the energy demand resulting in renewable solar energy implementation with fewer panel areas. The results of the holistic system operation showed that the proposed PV+ASHP combination was energetically capable of supplying all energy demand vectors of the representative European single-family house.

Finally, the economic analyses revealed that the system is quite competitive in terms of payback time and the levelized cost of energy which were 6.8 years and 2.43 TL/kWh (or 0.105 £/kWh or 0.121 €/kWh), respectively. Especially for the LCOE, this value showed that the PV+HP combination has already reached the grid-parity (grid electricity: 2.6 TL/kWh) in the region. However, barriers, such as high initial costs and the limited number of applications, limit the widespread utilization of the technology. Therefore, it was concluded that such systems can be supported with incentives for early deployment and studies should be encouraged for the widespread utilization of the technology in the region.

Overall, this study proves that the PV+ASHP combination is technically and economically a viable SAHP option to supply the space heating, space cooling, domestic hot water, and electrical energy demands of an exemplary European single-family house. Moreover, the net-zero-energy residential house concept, that the EU targets, is achievable through the grid-connected solar-heat pump systems which already become more cost-effective than the grid electricity price.

CHAPTER 6

Feasibility Analysis of a Novel Configuration of the Photovoltaic-Thermal (PV/T) and Water-Source Heat Pump (WSHP) System for Combined Heat and Power Provision in European Single-Family Houses

6.1. INTRODUCTION

Economic and environmental impacts are the two major energy-related issues worldwide today. An essential part of these challenges arises from the high energy consumption of different sectors (industry, transport, etc.) and the greenhouse gases (GHGs) released into the atmosphere during the production of energy from fossil fuels that cause global warming, respectively [15]. For a sustainable energy future, thus, reduction of energy consumption in almost all sectors and utilization of renewable energy sources become a necessity [182].

Today, more than one-third of the total energy demand in Europe is required for the building sector. Depending on the location, around 60-80% of this demand is required for space heating and cooling (SH & SC) and domestic hot water (DHW) needs where up to 20% is needed in the form of electricity for the household equipment. In single-family houses, in particular, the demand for the SH is almost five times higher than that of the DHW [29]. In order to reduce these high thermal demands, one strategy is to manage buildings' demand side in line with European legislation (e.g. 2018/844/EU [179]) that aims to improve the buildings' efficiency. Nevertheless, although these directives seek to increase the utilization of the insulations in buildings' envelopes, the thermal energy demand remains high in newly constructed buildings and existing ones even after a refurbishment [43]. Thus, for a fast and cost-effective response to the high energy demand and greenhouse gas emissions of European single-family homes, significant efficiency improvements should be expanded with an emphasis on the energy supply side [179], [43].

In terms of renewable energy utilization, solar represents the most suitable form of energy to provide on-site heat and power to the buildings which can be delivered by a novel solar collector type called photovoltaic/thermal (PV/T). The PV/T is a combination of solar photovoltaic and thermal components on the same panel structure to generate both electricity and useful heat simultaneously. During the operation, PV cells not only generate electricity

but also act as an absorber for the thermal pipes, implemented under the cell structure, which carries a heat transfer medium (water in this study) that extracts the heat from the cells [277]. The benefit of this design is twofold: (i) the PV efficiency is improved due to the removed heat from the cells and (ii) the extracted heat can be used for the thermal needs of the building as the output temperature of the PV/Ts may reach up to 80 °C [49]. With the design, the total electrical and thermal combined efficiency of a single collector can reach up to 70% [80], which makes the PV/T collectors particularly suitable for residential buildings as energy generation per m^2 of the limited roof space area is maximised. As they would require fewer panel areas, moreover, the PV/T collectors can reduce the installation costs compared to the PV panels and solar thermal collectors (e.g. ETC and FPC) installed side-by-side to generate the same amount of energy [278]. An example of the PV/T direct utilization in buildings is shown by Herrando et al. [71] where the PV/T systems can cover 51% of the electrical and 36% of the DHW demands of a residential house located in London (UK). Similarly, Hazami et al. [72] found that the PV/T-alone collectors can meet the majority of the DHW and electricity needs of the single-family Tunisian houses. Despite its advantages, the thermal output of the PV/T collectors is still lower than that of other building-type solar collectors, such as ETC and FPC, due to the additional heat transfer processes caused by the photovoltaic structure [171]. This low-grade heat output of the PV/Ts is usually not adequate to be directly used for space heating especially in wild winter conditions due to the mismatch between the high space heating demands and the availability of solar energy in the winter seasons. As a result, the most common direct utilization of the building-installed solar PV/T panel systems is limited to electricity and DHW-only generations worldwide [43].

However, an effective approach to make the temperature output of the PV/T collectors sufficient also for the SH needs of the buildings is to combine them with a water-sourced heat pump (WSHP) system. Heat pumps, in general, consist of electrically driven vapour

compression cycles that can extract the heat from a low-temperature environment and reject it to a high-temperature sink. Due to the compression cycle, they have much higher COP values than conventional boilers or electrical heaters hence reducing (also electrifying) the amount of energy needed for the thermal demands of the buildings [279]. The source of a HP can be air, water, or ground. The air-sourced HPs (ASHPs) are economically viable and have the simplest design, dominating the HP markets today. However, their COPs vary significantly at locations having wild winter conditions, hence they represent the heating options best suitable for moderate weather conditions [122]. For the ground-sourced HPs (GSHPs), in addition, the economic barriers limit the widespread utilization of the technology, especially for small-scale single-family houses [236]. On the contrary, the WSHPs utilizing solar thermal energy as their heat source can eliminate the challenges of ASHPs and GSHPs, and become an available heating technology [123].

When the PV/Ts are coupled with a WSHP unit, for the heating seasons, the low-grade temperature output of the collectors is used as the heat source of the HP. Compared to the ambient air as a heat source and working fluid, PV/Ts' thermal output (on a year-around basis) and heat transfer characteristics of water are more favourable, hence increasing the system's COP and stability [43], [126]. Moreover, a PV/T + WSHP system permits higher percentages of solar energy implementation in buildings, as energy is received not only in the form of thermal energy but also in the form of electricity which can be utilized for both household equipment and HP's compressor [150]. Linking to these, a PV/T + WSHP system's combined efficiency is higher than that of other solar-HP combinations such as thermal collectors + WSHP, PV + ASHP, HP-alone, etc. [126], [208]. However, for the cooling season, it has to be mentioned that as the heat elimination through the PV/T panels during the cooling season is not technically feasible for the solar-sourced WSHP systems, hence such systems cannot provide space cooling (SC) through the HP unit. As a result, the

combination has a restriction to satisfy the SC demands but is a viable efficient energy supply technology that can simultaneously generate SH, DHW and EE for single-family houses with higher COP values.

The combination of solar energy and HPs is often referred to as the solar-assisted heat pump (SAHP) systems, regardless of the system outputs and components [43], [88]. In literature, however, a substantial amount of attention is devoted to the solar + WSHP systems that provide DHW-only. Some of these examples can be found in highly-cited review papers conducted by [119], [88], [280]. Many systems involve the favourable combination of different solar panel types (ETC, FPC, PV, PV/T, etc.) and a WSHP to generate DHW + electricity [92], [281], [72], SH-only [89], [144], [126] or SH + electricity [140], [208], [151]. As detailed in Chapter 2, all these systems have their specific strengths and weaknesses but the common point of them is that they have improved overall efficiencies compared to conventional systems such as HP-alone, solar-alone, boilers, etc. Despite its advantages, nevertheless, only few studies [150], [149] use the PV/T + WSHP systems to co-generate the SH, DHW and electricity. This is often due to poor system designs that lead to the system being oversized, resulting in high system costs. Currently, there is no standardized modelling and testing approach, hence a poor design in these systems may significantly reduce performance, especially when solar energy penetration is not maximized. Therefore, the development of the validated PV/T + WSHP models is crucial to reveal the potential of these systems, to make informed decisions based on energetic and economic performance, and to promote the market diffusion of the technology. This study hence aims to analyse the techno-economic feasibility of an innovative SAHP system including solar PV/T collectors and a WSHP unit, capable of generating SH, DHW, and EE demands of the European single-family houses. The main objectives of the study are (i) designing a novel PV/T + WSHP model configuration using the commercial simulation

software TRNSYS and EES, (ii) revealing the technological viability of the system within the climatic boundary conditions of three different European locations, and (iii) evaluating the levelized cost of energy and payback period of the system in selected locations. The novelty of the study lies in the configuration of the system as SH and DHW circuits are separated to maximize the solar fraction of the system (explained further in Section 6.2). This design also assists the WSHPs to be applied into the existing conventional solar DHW systems without requiring substantial modifications. Finally, the model in this study is not location-specific and can therefore be reused in any location to monitor its viability as long as the load profiles of the building are known.

The structure of the chapter is as follows: **In Section 6.2**, a description of the system and principles of its operation are presented with the load profiles of the selected locations. **In Section 6.3**, the mathematical modelling of the system components, validation details of the model, and system design conditions are given. **In Section 6.4**, control strategy and flow pattern of the system are explained. **In section 6.5**, annual simulation results on system performance in each location are presented. **In section 6.6**, the system is analysed in terms of techno-economics. **In section 6.7**, an overall conclusion is given for the chapter.

6.2 SYSTEM DESCRIPTION AND BACKGROUND

6.2.1 System Description and Operational Principles

For clarity, a schematic diagram of the proposed co-generative PV/T + WSHP system is drawn and shown in Figure 6.1. The system consists of four main sections; the PV/T panels, a WSHP, a typical exemplary building, and two stratified hot water storage tanks. Also, the other auxiliary components make the connection between the main ones; the flow valves, hydraulic pumps, control units, forcing functions, load profile readers, data readers, and the weather data providers. A more detailed screenshot of the simulation interface, where all

components are seen, is provided in Appendix 6-A.

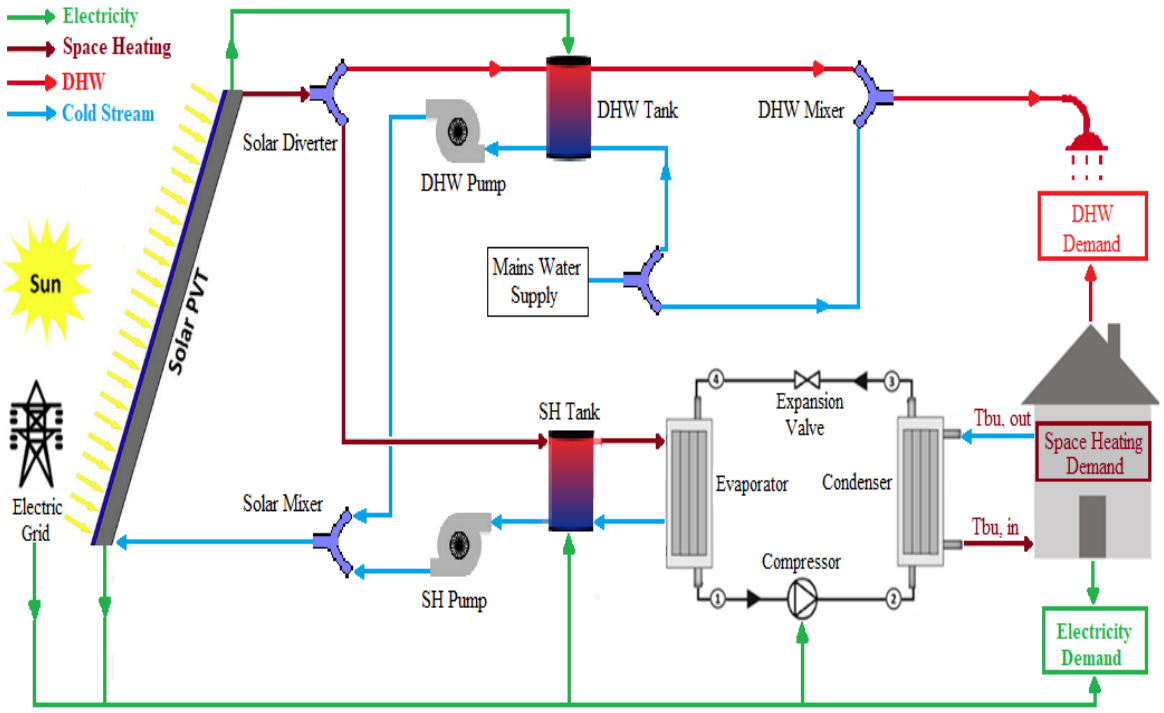

Figure 6.1: A schematic diagram of the proposed co-generative PV/T + WSHP system.

The proposed PV/T+WSHP system aims to provide SH during the heating season and DHW & EE demands throughout the year for a typical single-family of four in the selected locations. Due to the technical restrictions (heat elimination through the PV/T panels), hence the SC is not within the scope of the present study. For thermal management, the PV/T section is the main source of thermal heat which is divided into two cycles with a flow diverter; DHW cycle (top) and SH cycle (bottom). A stratified DHW tank, containing an auxiliary electric heater, is installed in the top cycle. It therefore can be heated directly either by the thermal or electrical outputs of the PV/T section. To supply the DHW, a calculated proportion of the mains water enters the bottom node of the DHW tank and the same amount of water leaves the highest temperature upper node of the tank and is mixed with the remaining city water proportion, providing the desired water temperature. For the bottom cycle, a larger capacity stratified storage tank (SH) is constructed to be the heat source of

the WSHP providing space heating to the house. Similarly, the cooled water from the HP's evaporator enters the tank's bottom node and is replaced with the highest temperature top node of the tank, supplying hot water to the evaporator of the HP unit. The HP unit then interacts with the building side to supply SH. For the most exceptional circumstances of low solar availability, the SH tank also contains a backup auxiliary electrical heater that can be fuelled either by the national grid or PV/T's electrical output. As heat pumps can operate in low-grade heat sources, the PV/T thermal output is primarily used to heat the DHW tank and is only transferred to the bottom cycle when the pre-set temperature setting of the DHW tank in the corresponding node is reached. This novel design allows the solar fraction of the system to be maximized as thermal energy is used directly for the DHW needs of the building, without requiring much electrical energy from the PV/Ts to heat the storage tank. In addition, the separation of the DHW and SH loops permits choosing a lower capacity WSHP as the HP unit will only have to meet the SH demand, which means a better economy for the system. In the cycle between the PV/Ts and tanks, the cooled streams from both tanks are mixed with a flow mixer and sent back to the PV/Ts to be heated again. The working fluid between the PV/Ts and the two tanks is a water + 25% propylene glycol antifreeze mixture to avoid the risk of freezing in wild weather conditions [76]. It has to be mentioned that the fluids in both cycles never mix, as the solar diverter only directs the PV/T output to one of the upper or lower cycles at any given time.

For electricity management, when it is available, the priority of the PV/T electricity usage (if needed) is as follows; (i) auxiliary electricity for the DHW tank, (ii) auxiliary electricity for the SH tank, (iii) HP's compressor (SH need), and (iv) EE demand of the household equipment. When the PV/T electricity is not available, the system is connected to the national grid with the Feed-in Tariff (FIT), hence the grid is assumed to act as a backup energy source and an unlimited battery storage unit.

6.2.2 Load Profiles of the Selected Locations

The proposed co-generative system is tested on the typical single-family house of 100 m^2 floor area (see Chapter 4) in climatic boundary conditions of three different locations namely; Paris (France), Izmir (Turkey), and Seville (Spain). These locations are selected to represent the cold (Paris), moderate (Izmir), and hot (Seville) climates that affect the thermal needs of the homes.

The annual actual SH (5721 kWh) and DHW (1497 kWh) needs in kWh over the total floor area of the typical single-family house for Izmir were found in Chapter 4 and are used here again to assess the proposed system in Turkey. For the thermal demand loads (SH and DHW) of other locations, the data is taken from an European Union project, ENTRANZE [282]. The project provides data about hourly and monthly heating, cooling, and DHW needs of several typical types of buildings (including single-family homes) in 10 different locations within the European Union countries. The provided data is in kWh per m^2 of the total floor area of the representative house types. In the project, the envelopes of the typical buildings are considered within the framework of the European Union building regulations, hence the typical single-family house is considered for all selected locations in the EU. The project supplies excellent descriptions and details about the methodology, modelling, and results, thus no further explanations are needed here and the related data is provided in Appendix 6-B. However, it has to be mentioned here that the demand loads of DHW in each selected location of the ENTRANZE project are introduced to the present model based on the demand profile of the Izmir case (see Figure 4.10). For clarity and comparison purposes, Table 6.1 shows the comparison of these demands (including Izmir) in kWh/m^2, corresponding to each location from coldest to warmest.

For the electricity loads and profiles, the monthly electrical energy demands of the other selected locations are assumed to be the same as the one found in Chapter 4 for Izmir, 188.8

kWh monthly (a total of 2265 kWh annually). This assumption is made to simplify the calculations and comparisons since the electricity consumption of the household equipment is based on the user's highly variable habits.

Table 6.1: Thermal demands of the selected locations in kWh per m^2 of the floor area of the typical single-family reference house.

LOCATIONS	PARIS		IZMIR		SEVILLE	
DEMANDS (kWh/m^2)	SH	DWH	SH	DWH	SH	DWH
January	35.1	1.3	13.1	1.5	11.2	1.2
February	29.5	1.2	12.3	1.4	6.2	1.1
March	21.8	1.3	10.5	1.5	2.6	1.2
April	11.6	1.3	3.3	1.4	1.5	1.2
May	3.2	1.3	0	1.3	0.1	1.2
June	0.5	1.3	0	1.1	0	1.2
July	0	1.3	0	1	0	1.2
August	0	1.3	0	0.9	0	1.2
September	2.5	1.3	0	0.9	0	1.2
October	11.6	1.3	0	1	0.1	1.2
November	25.9	1.3	6.3	1.2	5.2	1.2
December	34.2	1.3	11.7	1.5	9.8	1.2

6.3 MODELLING, VALIDATION, AND DESIGN CONDITIONS OF THE SYSTEM COMPONENTS

6.3.1 The Reference Building Model

The Type 88 building component of the TRNSYS was built in Chapter 4 to model a typical single-family house in Izmir. In this chapter, the same component is employed in the present model when analysing the proposed system in Turkey. However, for the other locations, the Type 88 building component in Chapter 4 is modified by adapting the variable construction characteristics (such as U values of the external walls) of the ENTRANZE project [282] into the present model. These characteristics are provided in Appendix 6-C. Hence, the Type 88

component (built in Chapter 4) is used in the present model to connect the pre-defined load profiles of the selected locations (e.g. SH and DHW) with the other components of the present model (e.g. PV/T and WSHP).

6.3.2 Modelling of the Mono-Crystalline Flat Plate PV/T Unit

Modelling of the PV/T unit is conducted using TRNSYS Type 50 component. Due to the reasons explained in Chapter 2 (Section 2.4), a glazed mono-crystalline PV/T panel designed with the sheet-and–tube configuration is selected to maximize the thermal efficiency of the panels. The Type 50 component of the TRNSYS is formed by the addition of a PV unit to a typical flat plate thermal collector (FPC), thus the component is modelled in a similar way as PVs and FPCs. With this regard, the useful heat gain (Q_u) of the thermal collector is formulated as follows [72]:

$$Q_u = \dot{m}_{PV/T} \times C_p(T_{out} - T_{in}) \quad \text{(6.1)}$$

where the $\dot{m}_{PV/T}$ is the mass flow rate of the mixture circulating through the thermal pipes of the panel, C_p is the thermal capacitance of the mixture, T_{in} and T_{out} are the inlet and outlet temperatures of the collector.

In addition, the available solar energy (Q_{Sol}) that can be collected by the PV/T area is written as follows [208]:

$$Q_{Sol} = A_{PV/T} \times G_T \quad \text{(6.2)}$$

where $A_{PV/T}$ is the total PV/T area and G_T is global solar radiation incident on the panel.

The thermal efficiency (η_{th}) of the FPCs is the division of the useful heat gain (Q_u) to the available solar energy (Q_{Sol}) and is based on the steady-state condition of the Hottel-Whillier equation as follows [150]:

$$\eta_{th} = F_R(\tau\alpha) - F_R U_L \frac{(T_{in}-T_{amb})}{G_T} = \frac{Q_u}{Q_{Sol}} \quad (6.3)$$

where (F_R) is the collector heat removal efficiency factor, $(\tau\alpha)$ is the cover transmittance and the plate absorbance, the (U_L) is the thermal loss coefficient dependency on temperature, and the T_{amb} is the ambient temperature.

In above equation, however, the U_L of the PV/T is not constant and has a linear dependency on T_{in}-T_{amb} (ΔT), hence a more appropriate expression is given by [171] as follows:

$$\eta_{th} = F_R(\tau\alpha) - F_R U_L \frac{(T_{in}-T_{amb})}{G_T} - F_R U_{L/T} \frac{(T_{in}-T_{amb})^2}{G_T} \quad (6.4)$$

where the $(U_{L/T})$ is the overall heat loss coefficient of the PV/T per unit area.

Above equation is rewritten in the Type 50 component of the TRNSYS to specify the incidence angle modifier (IAM) based on the modes of the component as follows [167]:

$$\eta_{th} = \alpha_0 - \alpha_1 \frac{(\Delta T)}{G_T} - \alpha_2 \frac{(\Delta T)^2}{G_T} \quad (6.5)$$

where the α_0 is the zero loss efficiency for the total radiation at normal incidence, and α_1 (first order) and α_2 (second order) are the temperature-dependent heat losses that can be obtained from manufacturers for commercial PV/Ts.

For the power generation, the electrical energy output of the PV/Ts is formulated as follows [208]:

$$E_{PV/T} = \eta_{PV} \times Q_{Sol} \times PF \quad (6.6)$$

where PF is the ratio between PV's cell and module areas and η_{PV} is the PV efficiency of the panel formulated as follows [244]:

$$\eta_{PV} = \eta_{ref}\left[1 - \beta(T_{cell} - T_{ref})\right] \quad (6.7)$$

where η_{ref} is the reference efficiency of the PV module, β is the temperature coefficient of the PV array efficiency, T_{ref} is the reference temperature of the manufacturer, and T_{cell} is the cell temperature which can be defined as follows [244]:

$$T_{cell} = T_{amb} + \left[\frac{(NOTC-20)}{800}\right] \times G_T \quad \text{(6.8)}$$

where the $NOTC$ is the nominal cell operating temperature.

Finally, the combined thermal and electrical efficiency of the PV/T unit can be written as follows [123]:

$$\eta_{PV/T} = \eta_{th} + \eta_{PV} \quad \text{(6.9)}$$

In addition, below assumptions are considered to simplify the calculations;

- The energy absorptions by the cover glass and the frame are negligible [283].
- The ambient temperature and solar irradiance have an uniform distribution around the surface of the panel [284].
- The system is in quasi-steady state conditions at each time step of the simulation [143].
- The working fluids between all riser tubes is distributed uniformly [285].
- All pipes used to connect the system components are well insulated, hence the heat loss between the PV/T and storage tanks are neglected [286].
- The operation point of the PV unit is at its maximum power point (MPP) [150].

6.3.3 The Water-Sourced HP (WSHP) Model

The EES modelling and validation of a typical heat pump cycle were given in Chapter 5. In this chapter, the same HP model is used with the changes of the heat source of the evaporator and the working fluid in the cycle. Thus, the WSHP unit differs from the ASHP by means of the type & quality of the evaporator's heat source (which in this case is solar thermal energy using water as the working fluid) and the type of the HP cycle's working fluid (where R32 is selected for the WSHPs based on [258]) . Therefore, the modelling equations and the validation details are not presented here again. However, it has to be noted that the capacity of the HP in the previous chapter was chosen as 4 kW based on the peak hourly load profile of the selected city, Izmir. However, in this chapter, as the system is tested based on different load demands, the HP's capacity has to be selected accordingly. With this regard, the HP capacities of the other locations are selected based on the hourly heating peak demand profiles of the single-family house in the ENTRANZE project [282] as follows: 8 kW for Paris and 3 kW for Seville case.

In the present system, the WSHP model of the EES software interacts with the other components of the TRNSYS, namely; the space heating storage tank, the reference building, the Meteonorm weather data, and the PV/T unit. In order to do this, the Type 66 component of the TRNSYS is used to call the external software, EES, for each time step (0.125h) of the simulations. For each iteration, the Type 66 component reads the temperature values of the top node of the SH storage tank as the heat inlet of the evaporator and it sends back another signal to the SH storage tank as the heat outlet of the evaporator. A similar connectivity is also observed between the Type 66 and Type 88 to connect the HP's condenser with the reference building. Other inputs/signals, such as weather data, control signals, and the PV/T's electricity of the corresponding components are read directly by the Type 66 component as its inputs.

6.3.4 Modelling of the Stratified Vertical Hot Water Storage Tanks

The proposed system consists of two vertical thermocline storage tanks; first for the DHW and the second for the SH needs of the building with sizes of 0.3 m^3 and 1.7 m^3, respectively. Modelling of both tanks is the same and based on the one-dimensional (1-D) multi-node approach [287] that is employed in the Type 4 component of the TRNSYS [208], [150], [284], [288], [289]. The model divides the tank into *N* fully-mixed equal-volume segments (nodes) which determines the degree of the stratification. Each tank includes an auxiliary heater for backup and have fixed inlet positions. Also for both tanks, flow from the heat source enters the node just below the node containing the backup heater. The temperatures of the *N* nodes of the model are calculated based on an un-steady energy balance equation which can be written for the *i-th* tank layer as a function of time as follows [167], [287], [289]:

$$M_i C_p \frac{dT_i}{dt} = \alpha_i \dot{m}_{heat} C_p (T_{heat} - T_i) + \beta_i \dot{m}_{load} C_p (T_{mains} - T_i) + UA_i (T_{amb} - T_i) +$$

$$\epsilon Q_{aux,i} + \delta_i \gamma_i C_p (T_{i-1} - T_i) + (1 - \delta_i) \gamma_i C_p (T_i - T_{i+1}) - (1 - \epsilon) UA_{fl,i} \left(T_i - T_{fl}\right) \ldots . \quad (6.10)$$

where M_i is the mass of the fluid in the *i-th* storage tank segment, $\dot{m}_{heat}$ and $\dot{m}_{load}$ are the mass flow rates of the working fluid from the heat source to tank and from tank to load, respectively, C_p is the specific heat capacity of the working fluid, $Q_{aux,i}$ is the rate of the thermal energy from the auxiliary heater to the *i-th* segment of the tank, UA_i & $UA_{fl,i}$ are the overall heat conductance between i-th & top nodes of the tank and environment, respectively. T_{heat}, T_{mains}, T_{amb}, T_{fl}, T_i, T_{i-1} and T_{i+1} are the temperatures of the heat source, mains water entering the bottom node of the tank (city's water for DHW tank and evaporator's exit for SH tank), ambient, and the fluid exiting at the top node of the tank, respectively. In addition, α_i, β_i, ϵ, δ_i, and γ_i are different control units that function as follows [287]:

$\alpha_i = 1, \quad if\ the\ fluid\ from\ the\ heat\ source\ enters\ node\ i, 0\ otherwise$..... (6.11)

$\beta_i = 1, \quad if\ the\ fluid\ from\ the\ load\ enters\ node\ i, 0\ otherwise$..... (6.12)

$\gamma_i = \dot{m}_{heat} \sum_{j=1}^{i-1} \alpha_j - \dot{m}_{load} \sum_{j=i+1}^{N} \beta_i$..... (6.13)

$$\delta_i = \begin{cases} 1, & if \quad \gamma_i > 0 \\ 0, & if \quad \gamma_i \leq 0 \end{cases}$$ ..... (6.14)

$\epsilon = 1, \quad if\ auxiliary\ heater\ is\ on, 0\ otherwise$..... (6.15)

Also, the heat transfer rate from the DHW tank to the load is readable from the Type 4 component of the TRNSYS. Since the SH tank is connected to the EES' HP model, the heat rate transferred to the evaporator of the HP ($Q_{load,SH}$) is calculated as follows [143]:

$Q_{load,SH} = \dot{m}_{load} \times C_{p,water} \times (T_{fl} - T_{mains})$..... (6.16)

where $C_{p,water}$ is the specific heat capacity of the water working between SH tank and the HP.

Finally, it has to be mentioned that below assumptions are applied when modelling the storage tanks;

- The fluid streams moving upwards and downwards from each segments are fully mixed before they enter each node [287].
- There is no additional heat gains for both tanks, e.g. solar heat [290].
- The auxiliary heater adds energy to the node it is in, raising the temperature of that segment until it is equal to the temperature of the segment above it [150].
- The heat losses from the pipes connecting loads and the tanks are neglected [286].

6.3.5 System Validation

In this section, an acceptable degree of accuracy for the system model is presented by validating the system components against experimental literature studies. It has to be mentioned that validation of the proposed system as a whole is not yet possible as the novel configuration of the system has never been tested. However, a verification of the individual components is feasible to show the accuracy of the modelling of the system's main components. With this regard, since the reference building and the HP units are validated in the previous chapters (4 and 5), the TRNSYS PV/T (Type 50) and storage tank (Type 4) components of the proposed system are validated against the work conducted by Tiwari et al. [291] where a PV/T + hot water storage tank system was validated experimentally. The experimental work consisted of a 0.516 m^2 flat-plate PV/T unit, a hot water storage tank with a capacity of 45 litre, a circulation pump forcing the fluid to operate between tank and the PV/Ts, and other components such as, controllers, electric cables, etc.

Table 6.2: Parameters of the experimental work of used for the TRNSYS validation project [291], [292].

Parameters	**Values**
Type of the PV module	Mono-Crystalline Silicon
Collector area (m^2)	0.516
Packing factor (-)	0.8
Cell numbers	72
Cell efficiency (%)	9
Collector Fin Efficiency Factor (-)	0.96
Temperature coefficient of solar cell efficiency (1/°C))	0.0045
Mass flow rate (kg/s)	0.016
Collector overall loss coefficient ($W/m^2.K$)	8.6
Collector plate absorptance (-)	0.92
Second order efficiency coefficiency ($W/m^2.K$)	0.067
Water tank loss coefficient ($W/m^2.K$)	0.44
Water tank size (L)	45

For the validation purpose, first of all, a simulation project is created in TRNSYS to apply the experimental setup into the software. Figure 6.2 shows the screenshot of this project. Then, the specific data utilized to perform the experimental study are used as the input values of the validation project. Table 6.2 revealed these data both for the PV/T collector and storage tank.

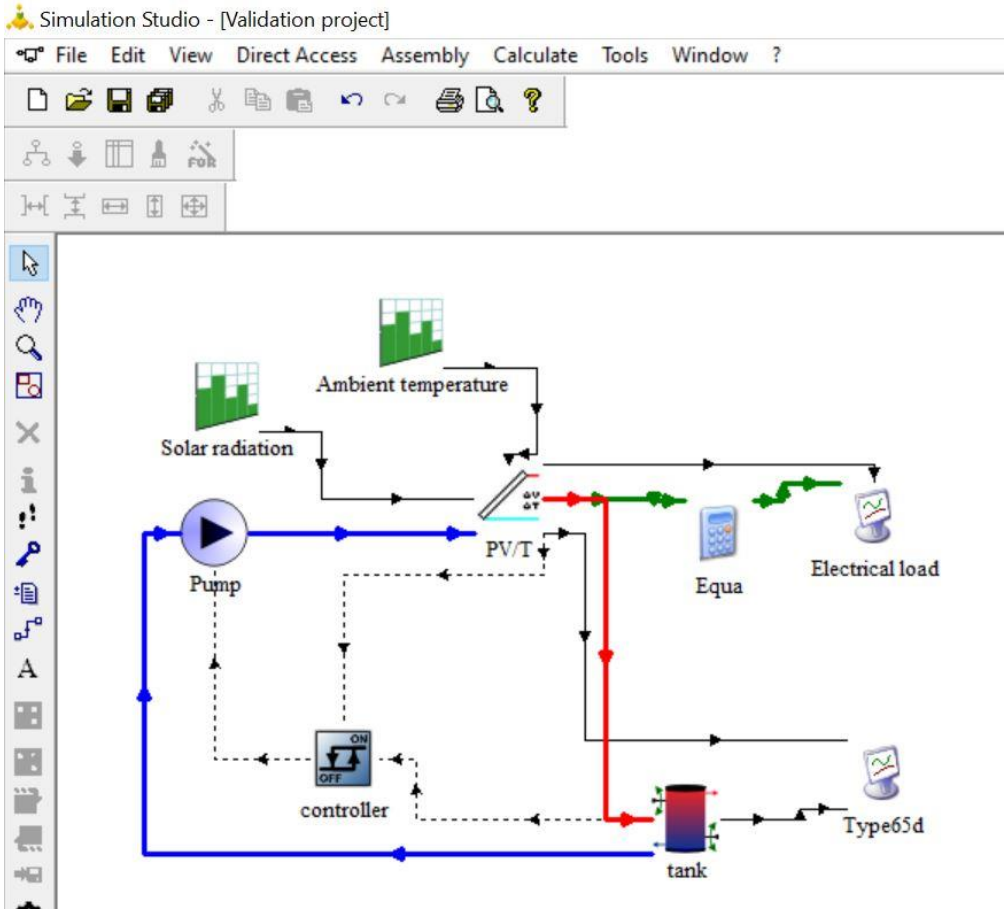

Figure 6.2: The screenshot of the TRNSYS validation project.

In addition, the experimental work presented in [291] was performed based on the weather conditions of Taiwan on a typical summer day between 8.00 a.m. and 3 p.m. In order to obtain the same input conditions and to have the same weather data as the experiment, the specific hours and the weather conditions of the experiment are provided to the TRNSYS validation project by employing the Type 14 forcing function component of the software. Further, in order to control the system, a differential-temperature controller is used based on

the experimental set-up with the 7 ℃ and 3℃ upper and lower dead-band temperatures, respectively. After setting these values and employing the parameters of experimental work (data is shown in Table 6.2) into the software. Finally, the validation of the present model is performed by comparing the average PV cell temperature and the tank's average water temperature of the experimental study with that of the TRNSYS validation project, shown in Figure 6.3.

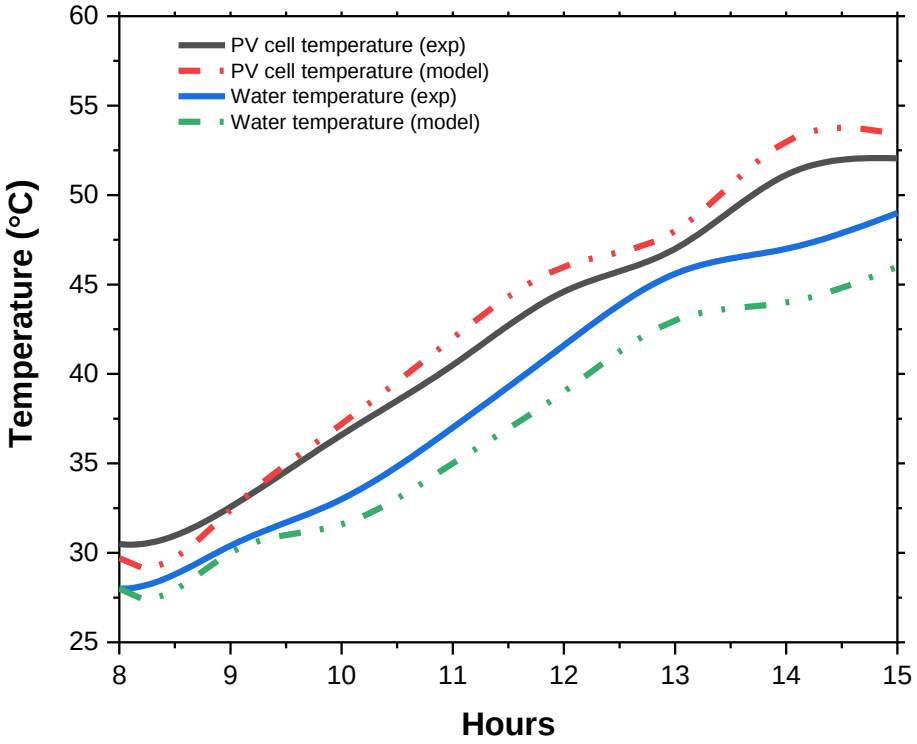

Figure 6.3: Validation of the present model's components with the experimental literature.

Figure 6.3 shows the validation of the PV/T and storage tank components of the present model against the experimental work of [291]. For the PV cell temperature the maximum deviation is observed with a value of 3.07 % at around 2.30 p.m., while it is seen as 6.38% for the water temperature at 2 p.m. These deviations can be explained by the TRNSYS tank model, which is assumed to be perfectly insulated. More specifically, in the experimental study, when the tank unit interacts with the ambient temperature, it loses some of its energy and reduces the water temperature (see Figure 6.3, blue and green lines). This leads to an

increase in the PV/T cell temperature due to the lack of cooling effect (see Figure 6.3, red and black lines). However, despite the deviations, it is seen that the validation project of the TRNSYS is in good accordance with the experimental work, which supports the validity of the present model.

6.3.6 Design Conditions of the System Components

Subsequent to the modelling and the validation, a summary of the design conditions of the modelled components (solar PV/T and storage tanks) is given in this section. For the solar section, the PV/T system assessed in this chapter is based on a commercially available hybrid panel type [293] of Solimpeks Solar Energy Corp [294], one of Europe's five biggest solar panel manufacturers. The technical specifications of the panel that are required to model the system, though not all, are provided by the manufacturer's datasheet. Other required data (the ones that are not given by the manufacturer's datasheet), however, is taken either from the literature based on the similar-sized systems or from the manufacturer itself [294] based on email communications. For the storage tanks, however, all data is taken from well-established literature studies. Table 6.3 summarise all data that is used to model both PV/T and the storage tank units in the proposed system. In addition to the main components of the proposed system, the other types of the TRNSYS' auxiliary components that connect the main components and assist to obtain & observe the simulation results are shown in Appendix 6-D.

Table 6.3: Various parameters used to model the PV/T and storage tank units [293], [71], [167], [295], [296], [297], [213], [70], [208].

Parameters	**Values**
PV/T manufacturer	Solimpeks Solar Energy Corp.
Type of the PV module	Mono-Crystalline Silicon
Panel Dimensions (mm)	1670 x 1005 x 60
Number of cells	60

Cell dimensions (mm)	158.75 x 158.75
Packing factor (-)	0.9
Nominal power (W)	325
Voltage at max power, Vmp (V)	34.3
Current at max power, Imp (A)	9.62
Open circuit voltage, Voc (V)	41.67
Short circuit current, Isc (A)	10.17
Power temperature coefficient (1/°C)	-0.43
Zero loss efficiency (%)	59
First order heat loss ($W/m^2.K$)	3.30
Second order heat loss ($W/m^2.K$)	0.02
Temperature coefficient of solar cell efficiency (1/°C)	0.0032
Reference PV module efficiency (%)	19.4
Collector heat removal efficiency factor (-)	0.66
Collector overall loss coefficient ($W/m^2.K$)	4.4
Plate transmittance (τ)	0.9
Plate absorptivity (α)	0.95
Glazing	3.2 mm tempered glass
Absorber tube diameter (mm)	8
Absorber tube thickness (mm)	0.45
Tube number	7
Tube distance (mm)	130
Max. operation pressure (bar)	8.6
Collector Fin Efficiency Factor (-)	0.96
Inverter efficiency (%)	95
Fluid thermal capacitance (kJ/kg.K)	4.19
Rated thermal efficiency (%)	62
Collector mass flow rate ($L/h.m^2$)	50
DHW tank size (m^3)	0.3
SH tank size (m^3)	1.7
Mass flow rate to HP's evaporator (kg/s)	0.016
Tank's loss coefficient ($W/m^2.K$)	0.83
Number of nodes in each tank (-)	4
Tanks' heat transfer coefficient (W/K)	573

Water tank loss coefficient (W/m^2.K)	0.44
Water tank size (L)	45
Heating capacities of the auxiliary heaters inside the tanks (kW)	3
Initial fluid temperature in the collectors (°C)	20
Initial fluid temperature in the tanks (°C)	20

6.4 FLOW CHART AND CONTROL STRATEGY OF THE SYSTEM

In this section, the flow pattern and the control logic of the proposed system is presented. For this purpose, a schematic diagram is drawn and presented in Figure 6.4. Regarding the work pattern, the model starts with reading the known input parameters provided to the sub-models namely; design conditions of the individual components and weather data from the Type 15 component. In the present study, as the HP unit is designed to provide SH only, the control and the interaction between the TRNSYS' Type 88 building model and the EES' HP model is similar to the previous chapter (Chapter5), where the COP and compressor work of the HP (for the actual SH need) are calculated based on load profiles of the selected cities.

Meanwhile, since the DHW and SH circuits are separated, the PV/T unit operates to be the main source of the HP's evaporator (for SH) and DHW in addition to the EED. After reading both thermal and electrical load demands, the Type 50 component initiates the annual simulations with an assumption of 1 m^2 of the PV/T area and increases the panel area (0.1 m^2 at each simulation) until the system reaches 100% of all demands (SH+DHW+EED) coverage.

Regarding the system control, moreover, as the solar output is directed into two circuits with a fluid diverter component (Type 11) and two pumps (Type 110), it has to be mentioned here that the fluid from the solar diverter is directed either to the first loop (DHW) or to the second loop (SH), means that there is no proportional distribution of the fluid. In addition,

the flow from the solar diverter is always prioritized to the 1st loop, and the fluid inside both loops never mixes. For the 1st loop, the DHW tank has a temperature sensor with a 55 °C set point and 10 °C upper and 2 °C lower dead-bands that turning the pump 'ON' and 'OFF'. When the top node temperature of the DHW tank reaches the pre-set temperature (55 °C), then the solar diverter directs the fluid to the 2nd loop. When the top node temperature of the DHW goes below 40 °C, the solar diverter directs the flow back to the 1st loop. During this operation, if the temperature of the fluid at the exit of the DHW mixer is below the pre-set load temperature (50 °C), then the auxiliary heater inside the tank heats the fluid until the tank's top node temperature reaches the pre-set temperature (55 °C).

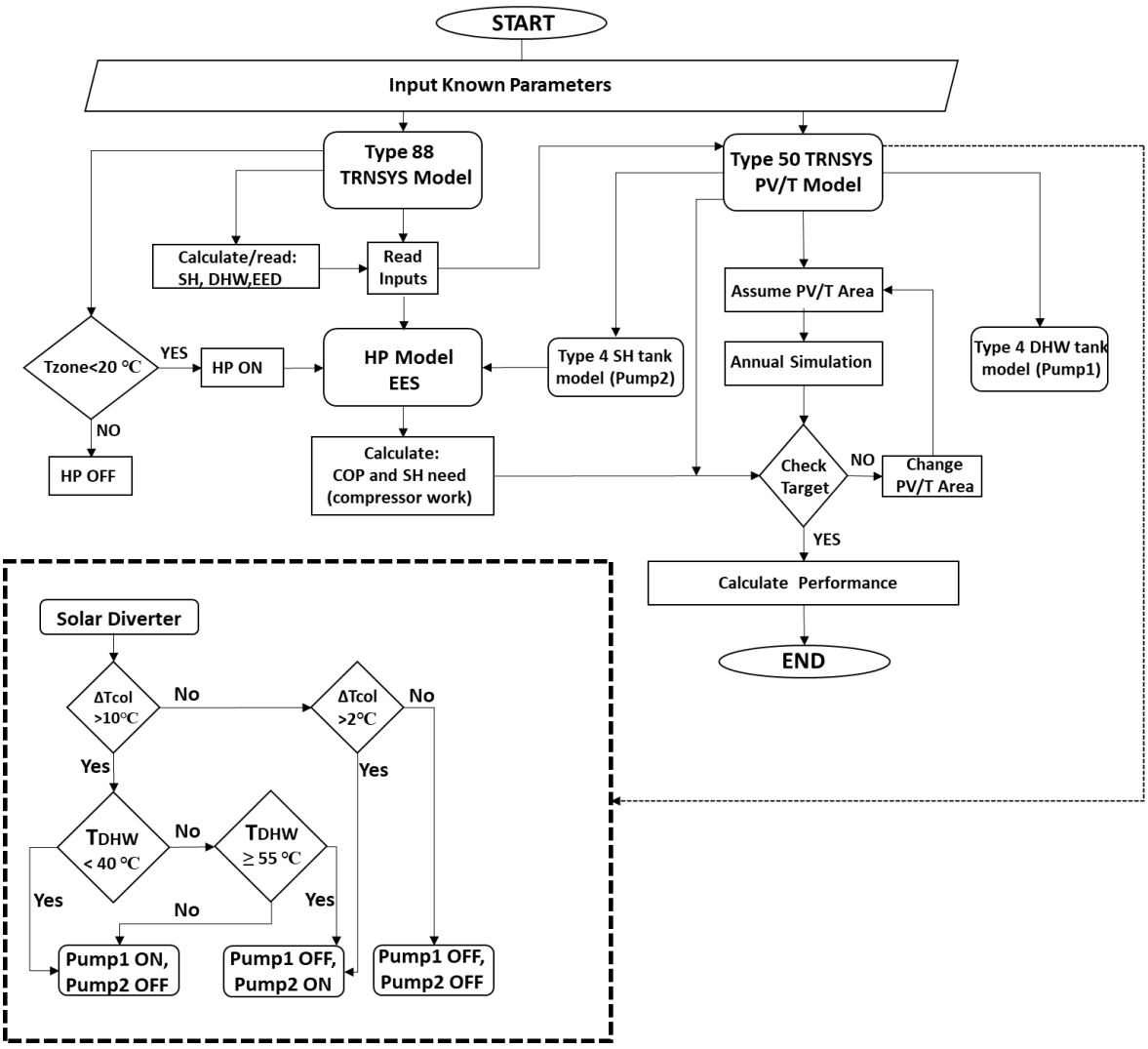

Figure 6.4: Work pattern of the proposed system and the temperature control for the pumps.

For the 2nd loop, as the HP's evaporator can operate with low-grade temperatures, the SH tank aims to capture as much solar energy as possible, therefore, even if the temperature rise across the solar collector is 2 °C (upper dead-band) higher than the average fluid temperature in the SH tank, the SH pump operates. During the operation, the bottom node temperature of the SH tank goes below zero during the wild weather conditions. For this conditions, it has to be mentioned that the fluid is an anti-freeze mixture, hence there is no risk of freezing. However, if the bottom temperature of the SH tank drops below -5°C, the heating element inside the tank uses auxiliary electricity to bring the bottom node temperature back to -5°C, preventing extreme cold temperatures for HP's evaporator. Further, the temperature sensor is at 45 % point in the SH tank reading the middle node temperature of the tank with a lower dead-band temperature of 1 °C.

In order to apply the above control logic, a control strategy that operates with the Type 165 differential temperature controllers (detailed in Chapter 3) and a set of equation blocks (written in TRNSYS assembly blocks) is implemented into the model to determine the control signals for the pumps and the solar diverter, respectively. This means that the solar diverter is operated with an equation block to determine the direction of the flow and both pumps are controlled with two controllers (Type 165 differential controller) each. For the DHW pump, for example, the first controller (Type 165) implements the general control philosophy which turns the pump "ON" (signal '1') when the temperature difference across the PV/T collector inlet/outlet is greater than the upper dead-band, and turn "OFF" (signal '0') when below the lower dead-band. The second control decision (Type 165) for the DHW pump is turning the pump "OFF" (signal '0') when the tank's top node temperature is greater than 55 °C, and turning "ON" (signal '1') when below 40 °C. The SH pump also operates with the same logic based on its upper and lower dead-bands and the set point temperature.

On the other hand, the signals ('1' or '0') of the Type 165 differential controllers turning

DHW and SH pumps ON/OFF are used to control the solar diverter that directs the fluid either to the 1st loop or to the 2nd loop. For this purpose, the KARNEL engine of the TRNSYS inspects the signals of the pumps and directs the fluid to the corresponding loop based on below sets of equations as follows:

$$\gamma_{DHWPump} = [20,1],$$

$$DHW\ pump\ operates\ if\ the\ control\ signal\ is\ 1 \quad \text{(6.17)}$$

where number '20' is the component number of the DHW pump in the simulation interface.

$$\gamma_{SHPump} = [21,1] \times EQL(\gamma_{DHWPump}, 0),$$

$$SH\ pump\ operates\ if\ the\ controller\ signal\ is\ 1\ and\ \gamma_{DHWPump} = 0 \quad \text{(6.18)}$$

where number '21' is the component number of the SH pump in the simulation interface.

Based on the signals of the two pumps (unit numbers: 20 and 21), the control of the solar diverter can be expressed as follows:

$$\gamma_{SolarDiverter} = EQL(\gamma_{SHPump}, 1) \times EQL(\gamma_{DHWPump}, 0) \quad \text{(6.19)}$$

Equation 6.19 means that when the SH pump operates ($\gamma_{SHPump} = 1\ and\ \gamma_{DHWPump} = 0$) based on the temperature controllers, then the solar diverter signal is '1' ($\gamma_{SolarDiverter} = 1$) which diverts the fluid to the 2nd loop. Otherwise, the signal of the solar diverter is '0' ($\gamma_{SolarDiverter} = 0$) and all fluid flows through the 1st loop.

6.5 RESULTS AND DISCUSSION ON THE SYSTEM PERFORMANCE

This section provides results and discussions of the proposed system simulated in the selected locations representing cold (Paris), moderate (Izmir), and hot (Seville) climatic conditions. In all locations, the typical representative house is designed to be net zero in

terms of energy consumption and production, hence the system size is adjusted accordingly. The system performance is simulated annually with a time step of 0.125 h and the results are aggregated and printed hourly (8760 hours in a year) with the TRNSYS Type 46a component.

6.5.1 Ambient Temperatures and Solar Radiations

In this section, the most crucial weather data information of the selected locations is compared before presenting the performance results to understand better some of the findings detailed in the following sections. For this purpose, first of all, Figure 6.5 compares the ambient air temperatures of the selected locations in the typical year of the simulation. From this figure, as expected, Paris has the coldest ambient temperature throughout the year, with as low as -8 degrees Celsius in January and highest values (around 30 °C, only in July for few times). However, for Izmir and Seville, the ambient air temperatures generally show a similar trend throughout the year, while Seville has slightly higher temperatures during the winter months.

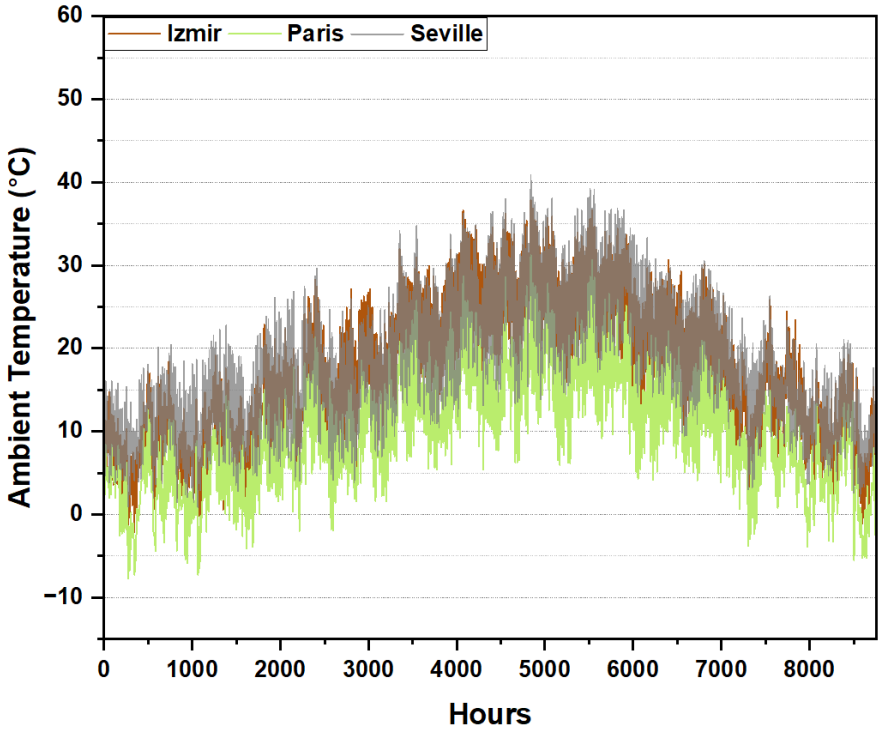

Figure 6.5: Ambient air temperature of the selected locations.

In addition, Figure 6.6 shows the monthly total solar radiation of the locations per square meter of a tilted PV/T surface in units of kWh. As noticed, the solar radiations in Figure 6.6 have a similar tendency to the ambient air temperatures in Figure 6.5. While Paris has the lowest solar radiation throughout the year (especially in winter months), Izmir and Seville have close values with Seville receiving slightly more radiation in all months.

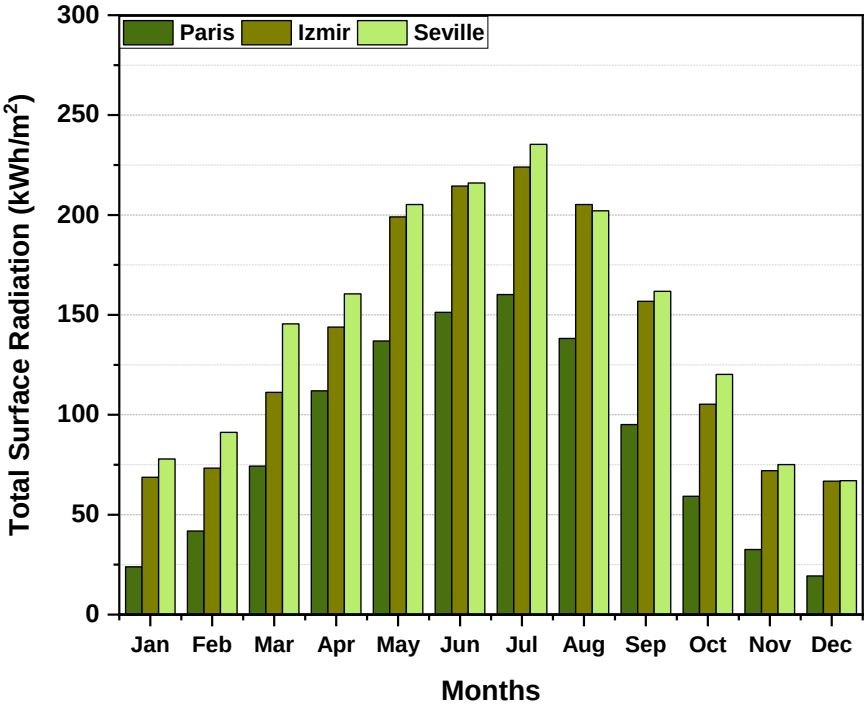

Figure 6.6: Monthly solar radiation of the locations on a 1 m^2 of area.

From both figures, with low ambient temperatures and solar radiations, the size of the proposed system for Paris can be expected to be much higher than for the other two cities, as the system will need more PV/T area to meet a much higher thermal demand during the winter season. For İzmir and Seville, on the other hand, it is possible that the difference in system sizes in these locations will not be much. However, the exact figures only can be drawn after the simulation results in the following sections.

6.5.2 HP Performances and Auxiliary Electricity Consumption of the SH Tank

As explained in Section 6.2, HP utilization reduces and electrifies the thermal demands. This is because of their high COPs and the existence of the compressor permitting the electricity

utilization for the thermal needs. In the current proposed system, as the HP unit is designed for SH-only, the primary energy savings that can potentially be achieved by using the HP units is the difference between the actual space heating demand of the representative house and the compressor electricity consumption, which is proportional to the HP's COP.

Based on the work pattern of the current model and the control logic detailed in Section 6.4, the compressor's electricity consumption and HP's COP are calculated for each time step (0.125 h) of the annual simulations, and the results printed hourly are aggregated monthly to monitor the HP's performance. These results are then presented in Figures 6.7, 6.8, and 6.9 for the selected locations, together with the actual space heating demands. In these figures, the 'Actual SH demand' values are the amount of thermal energies for space heating in the form of kWh to keep the zone temperature of the representative house at the desired comfort level, which were summarized for each location in Table 6.1. In addition, the term 'Compressor power needed for SH' values are the dynamically calculated compressor electricity consumptions to provide space heating through the HP unit in each locations.

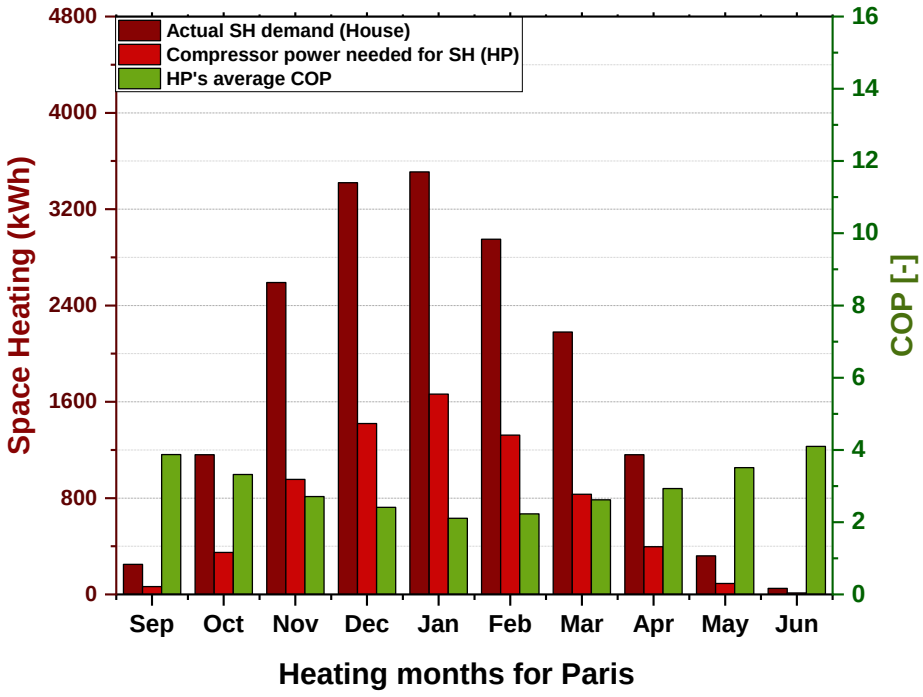

Figure 6.7: HP performance and its power consumption in Paris climate.

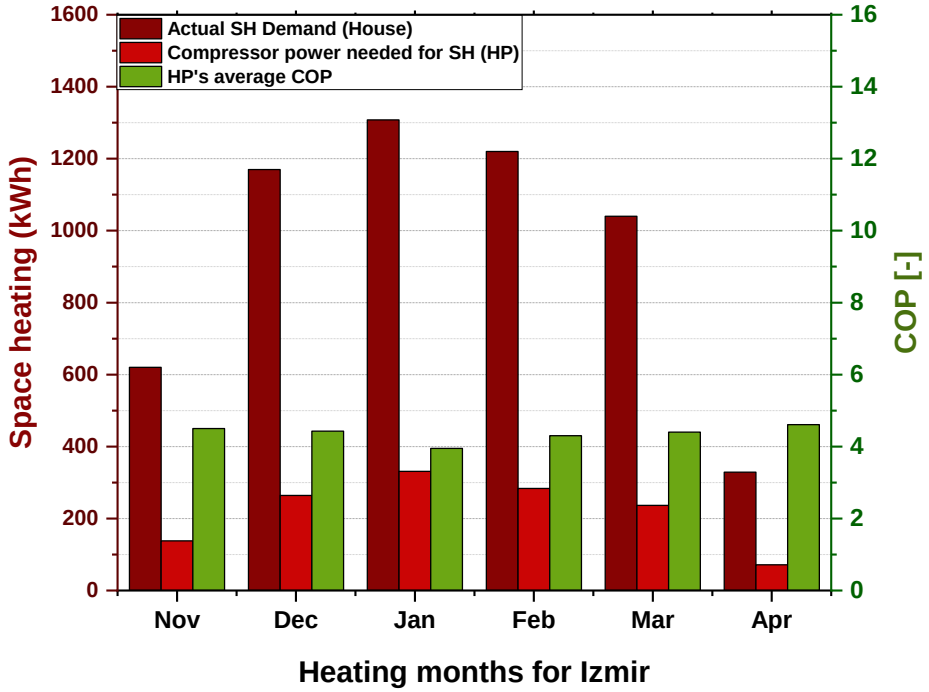

Figure 6.8: HP performance and its power consumption in Izmir climate.

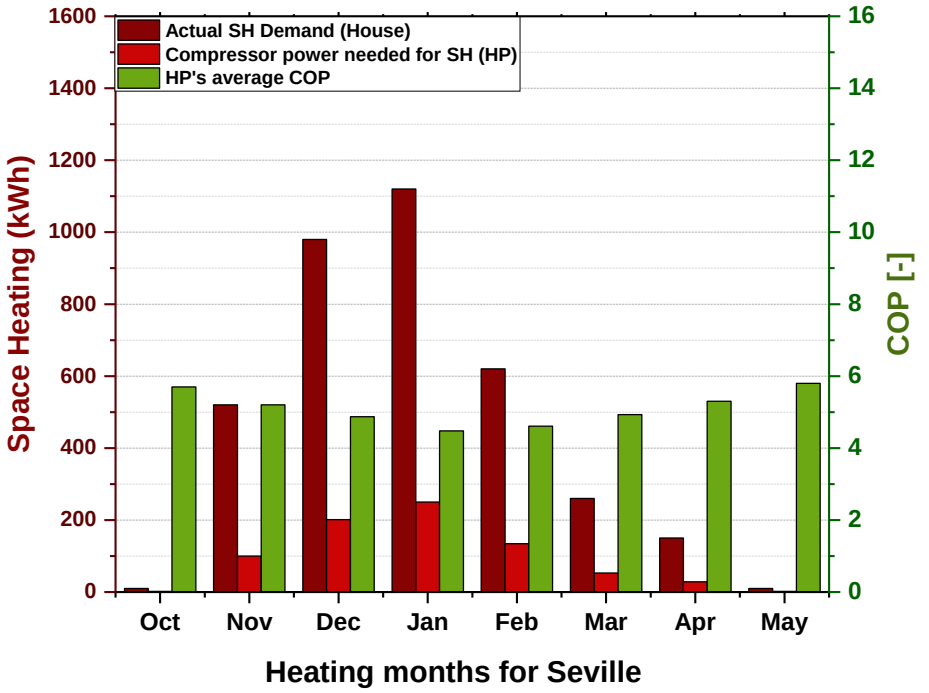

Figure 6.9: HP performance and its power consumption in Seville climate.

When all figures (6.7-6.9) are inspected at once, the first notable point is that the HP performance (COP) of the system in Paris (Figure 6.7) reduces dramatically in the coldest months of the year, despite the use of a water-sourced HP. In addition, the COP variation

between the hottest and coldest months is significant. In Paris, the system has the lowest monthly average COP value of 2.11 in January, while it reaches its highest value of 4.09 in June. For Izmir (Figure 6.8) and Seville (Figure 6.9) cases, however, the HP performances are more stable, fluctuating between 3.95 - 4.61 for Izmir and 4.48 - 5.80 for Seville throughout the year. The system in both cities outperforms Paris in all heating months, especially for Seville, the COPs of the HP in January, February and March are more than double that of Paris COPs in the same months.

The second noticeable point is that the HP unit reduces the actual space heating demands substantially. For example, although the COP value is as low as 2.11 in January for the system in Paris, the average HP performance in heating months is found as 2.47. This reduces the 17590 kWh of the total actual SH demand of the representative house to 7106 kWh of electricity demand for the compressor, hence saving 10483 kWh of energy. With the same explanation, the average HP performance of the system in Izmir and Seville during the heating months is found as 4.1 and 4.9 resulting in the primary energy savings of 4396 kWh and 2899 kWh, respectively.

The performance variation of the HP in the selected locations is best explained with the weather data of the locations and the control logic of the system. For the weather data, as shown in the previous section, the ambient temperature (see Figure 6.5) and the solar potential (see Figure 6.6) have a similar tendency in each location. This means that when both values are low, the actual SH demand of the representative house increases (due to the cold ambient) and the solar thermal output of the PV/T unit for the SH tank is less effective (due to the control logic, as the DHW provision is prioritized). For the control logic, the thermal output of solar energy primarily aims to meet the DHW demand. As a result, although a water sourced- HP is used, the SH tank supplies lower-temperature liquid to the HP's evaporator during the coldest months, resulting in a lower COP for the system.

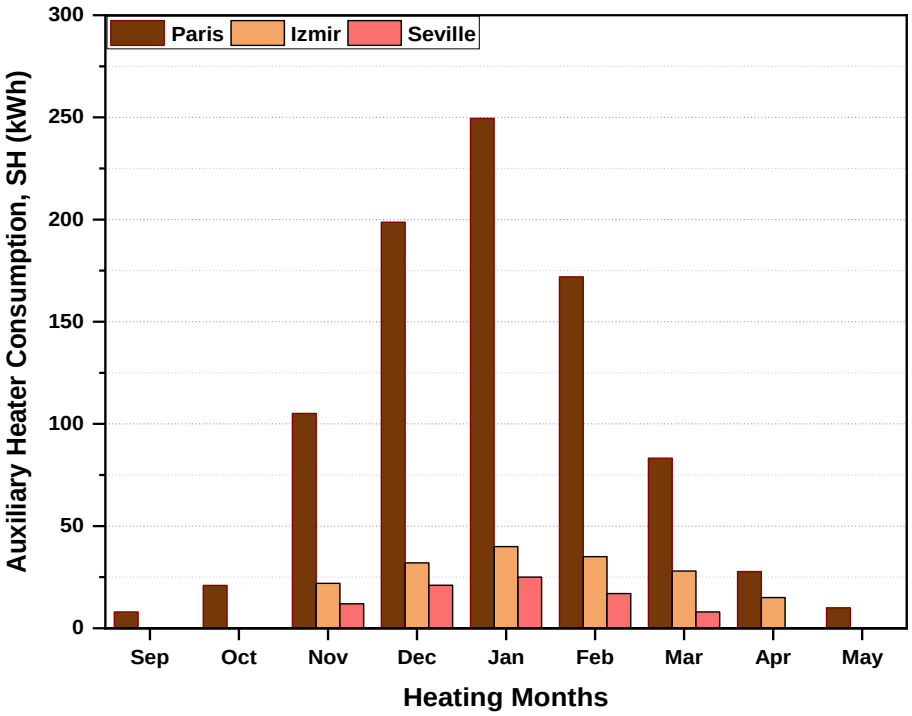

Figure 6.10: Auxiliary heating consumption of the SH tank in each location.

In connection with the above paragraph, when the solar thermal output provides less favourable temperatures to the SH tank, the bottom node of the SH tank becomes colder and falls below the -5 °C temperature threshold (see Section 6.4) more frequently, causing more auxiliary heating used as the backup for the system. The consumption of the auxiliary heater, placed in the SH tank as the backup, is calculated and presented in Figure 6.10 for the heating months of each location. Therefore, Figure 6.10 shows how much auxiliary electricity is consumed at each location for the SH tank during the heating months. As seen, for a successful SH supply, the system in Paris depends heavily on the auxiliary electric heater, especially in December, January, and February, while in June no auxiliary electricity is used. For Izmir and Seville cases, however, less auxiliary dependency is observed. While the system in Izmir requires 6 months of auxiliary electricity (from November to April), the Seville case needs it through 5 months (from November to March). Finally, the annual total auxiliary electricity consumption of the SH tank for the system in Paris, Izmir, and Seville is found as 875.2 kWh, 172.1 kWh, and 83.3 kWh, respectively.

6.5.3 Solar DHW Coverages and Auxiliary Electricity Consumption of the DHW Tanks

Based on the system design, the DHW supply in the proposed system is achieved through the direct utilization of the thermal output of the PV/T units. As a result, the amount of solar energy used for DHW provision and the amount of auxiliary electricity (used for the auxiliary heater built-in the tank to provide DHW when it is needed) are calculated hourly throughout the year and the results are aggregated to observe the monthly DHW coverages of the system in each locations, presented in Figure 6.11. In the figure, in addition, the sum of the terms, 'solar DHW coverage' and 'auxiliary energy for DHW', gives the total DHW demand which was shown in Table 6.1.

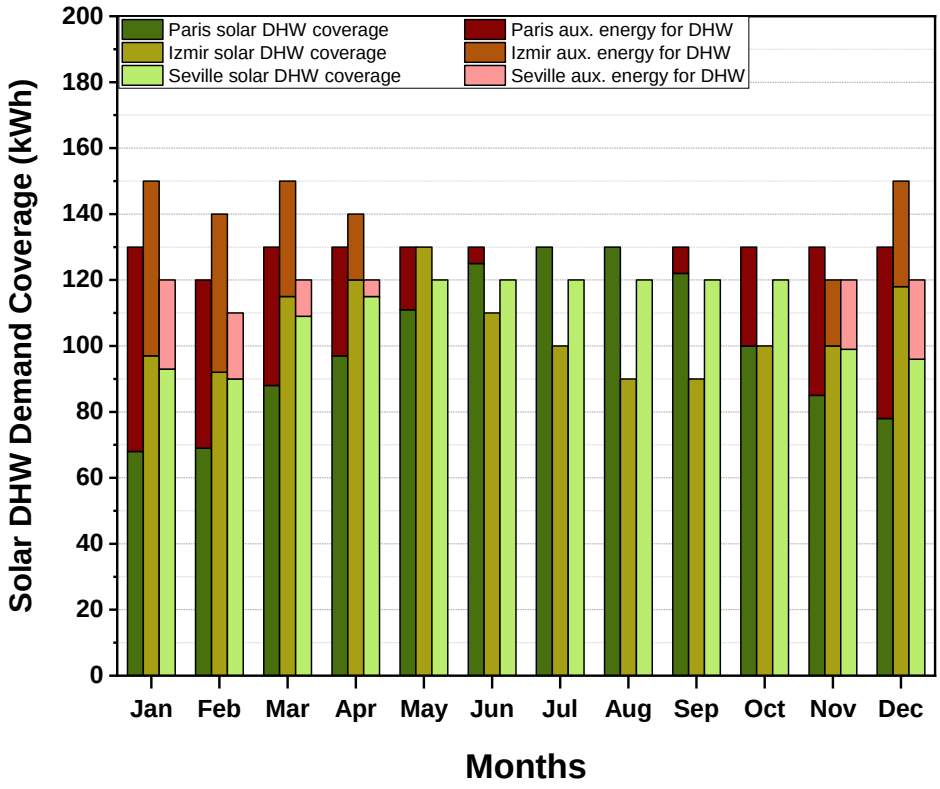

Figure 6.11: The amount of solar energy and auxiliary electricity to meet the DHW demand.

As seen in Figure 6.11, similar to the previous section, the most auxiliary electricity consumption for the DHW tank is observed in the system in Paris. In this location, the percentage of the DHW demand coverage of the solar thermal output of the PV/T unit for

the coldest months of the location (November, December, January, and February) is 67.4 %, 60%, 52.3%, and 57.5 %, respectively. In other months, the lowest percentage is 74.7 % and above. In July and August, solar thermal energy covers 100 % of the DHW demand. Further, the system covers 77.6% of the DHW demand from solar thermal energy annually, remaining a total of 347 kWh of electricity for the auxiliary heater. Moreover, it has to be mentioned that in months where the solar potential is high and the SH demand is low such as June and September, the system still requires auxiliary electricity. This is because of the temperature settings of the control logic of the solar diverter (40 ℃ for lower and 55 ℃ for upper, see Section 6.4), which means that once the top node of the DHW tank reaches 55 ℃, the solar diverter directs the fluid to the SH cycle and does not change it until the top node drops below 40 ℃. As a result, during this time, when there is a DHW need and the DHW tank temperature is not high enough for the users (50 ℃), the auxiliary heater in the DHW tank turns on and consumes electricity.

For Izmir case, due to the same reason in above paragraph, the DHW tank requires auxiliary electricity in all heating months. From November to April, the percentile coverages of DHW demand from solar thermal energy are found as 83.4 %, 78.7 %, 64.6%, 65.8%, 76.7 %, and 85.8, respectively. As expected, during the non-heating months, solar thermal energy covers 100 % of the DHW demand. In addition, the system meets 85.9% of the annual DHW demand from solar energy, with the rest (14.1% or 208 kWh) from auxiliary electricity. Compared to the Paris case (74.7% of annual DHW coverage from solar), in Izmir, the annual coverage (85.9%) may seem low (since the location has a better solar potential) but it has to be taken into consideration that the total DHW demand in heating season in Izmir is higher than that of Paris (see Figure 6.11).

For the Seville case, finally, the DHW tank requires auxiliary electricity only for four months (from November to February). The proportions of the DHW demand covered by solar

thermal energy during these months are found as 82.5 %, 80 %, 77.5 %, and 81.8 %, respectively. In addition, in March and April, solar energy covers 90.1 % and 95.9 % of the DHW demand. On a yearly basis, however, the system covers 92.5 % of the DHW demand from solar thermal energy, where the remaining proportion (108 kWh) is supplied by auxiliary electricity. With this solar DHW coverage rate, Seville is by far the most favourable location to directly use solar thermal energy for DHW needs.

6.5.4 Thermal, Electrical, and Combined Efficiencies of the PV/T Unit

In this section, the PV/T plant efficiencies are monitored in each location throughout the year and the results are presented monthly in Figure 6.12. Starting with Figure 6.12-a), the calculated thermal efficiencies are in between 49.8 % - 55.1 % for Paris, 51.8 % - 56.2 % for Izmir, and 44.3 % -52.2 % for Seville. With these results, it is found that the thermal efficiency of the PV/T plant in Izmir is the highest and closest to the manufacturer's efficiency rate (see Table 6.3). In addition, the efficiency curve in Izmir is more flat which means a better consistency in PV/T's thermal efficiency throughout the year. For Paris and Seville cases, on the other hand, the efficiency curves show a degree of consistency in winter months but fall significantly between June - August for Paris and between June – September for Seville. This is because when the collector temperature increases, the heat losses from the collector to the environment increase at the same time, resulting in a decrease in efficiency. At this stage, utilizing more than one glass cover may enhance the efficiency, however, the amount of heat collected will decrease which was not preferred for the proposed system (for more details see Chapter 2, Section 2.4.2).

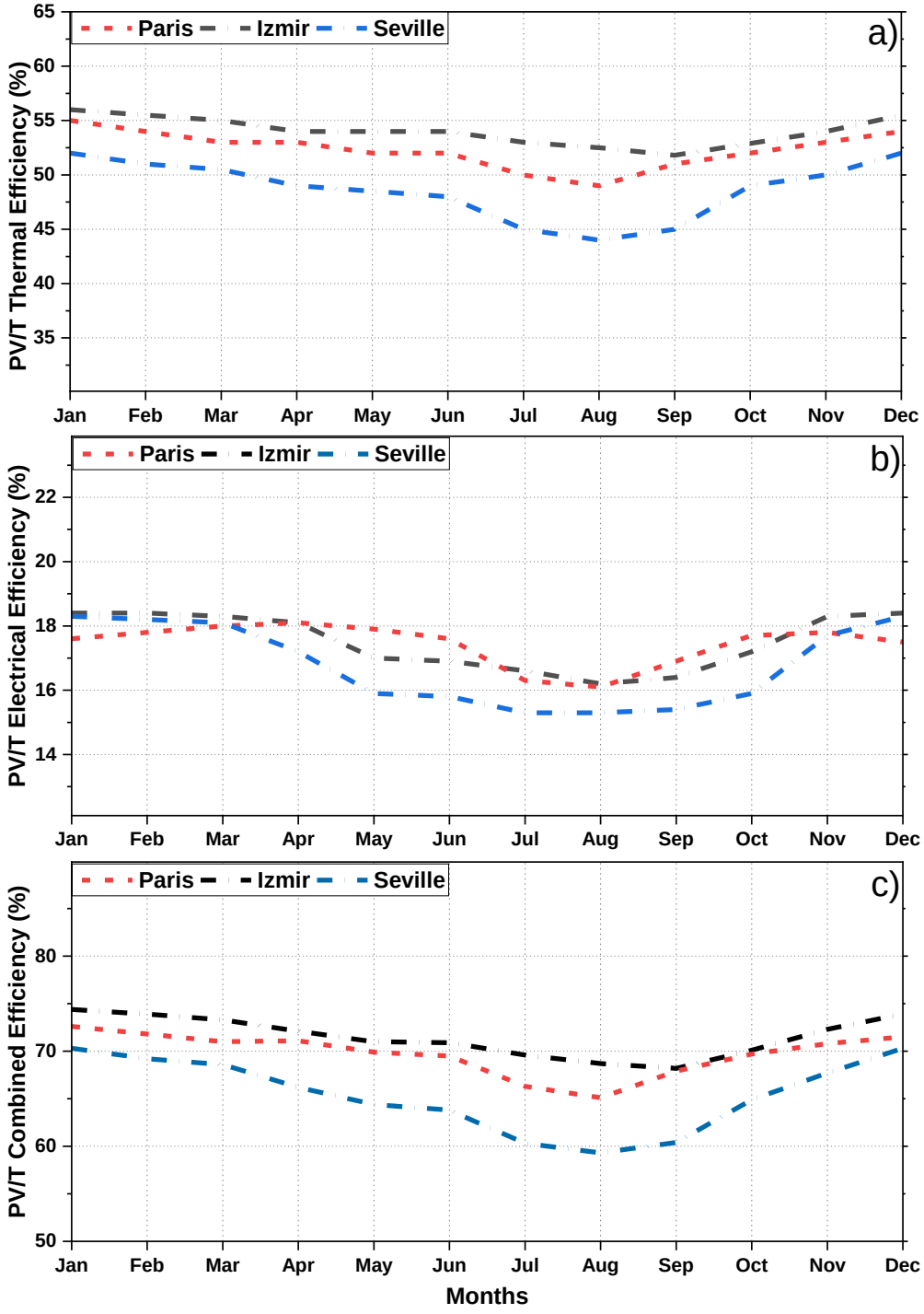

Figure 6.12: Monthly PV/T plant efficiencies in the selected locations; a) Thermal Efficiencies, b) Electrical Efficiencies, and c) Combined Efficiencies.

From the electrical efficiencies in Figure 6.12-b), interesting results are obtained. First, it is found that the electrical efficiencies of the PV/T range between 16.1 % -18.2 % for Paris,

16.2 % -18.4 % for Izmir, and 15.3 % - 18.3 % for Seville. For the Paris case, the electrical efficiency of the PV/T unit slightly increases from 17.6 % in January to its peak value of 18.2 % in April. It then starts decreasing again until June to the value of 17.6% when the ambient temperatures increase during these months. From June to August, however, especially in July and August, the collector efficiency drops significantly. This is because of the lack of cooling effect on the PV/T unit when the SH is not operating. In June, for example, the SH need for Paris is minor, hence the SH tank's operation is limited which results in a decrease in the efficiency when the collectors are not cooled adequately. When the SH demand exists back in September, the collectors are cooled sufficiently again and the electrical efficiency increases until October. Finally, from October to December, as the ambient temperature worsens the electrical efficiency decreases again.

Continuing with Figure 6.12-b), for Izmir and Seville cases, the electrical efficiency follows a similar trend throughout the year. Especially from December to March, the PV/T units in both locations have very close efficiencies (all above 18 %), with the Izmir case outperforming slightly. During the non-heating season (May-October), the electrical efficiency of the collectors drops significantly due to (i) insufficient cooling effect from the SH tank and (ii) high ambient temperatures. Especially in the case of Seville, productivity drops as low as 15 % during the hottest summer months. However, the reason of the higher electrical efficiency of the Izmir case during the non-heating season is because of the moderate surrounding temperatures that Izmir has.

From the results in Figure 6.12-a) and 12-b), two significant conclusions are obtained. First, the PV/T panels perform best under moderate temperatures. For the thermal efficiency, it is clearly seen that the thermal efficiency of the panel for the system in Izmir has a higher value and better consistency compared to the other two locations. For the electrical efficiency, in Paris case, the electrical efficiency of the PV/T increases from January to April while the

surrounding temperature of the panel becomes moderate. For the electrical efficiency, another example can be seen in the Seville case where the PV/T's electrical efficiency is decreasing from March to April when the ambient temperature becomes hotter. Thus, higher or lower surrounding temperatures reduce thermal and electrical efficiencies. Second, the electrical efficiency of the PV/T panels drops significantly when the collectors are not cooled effectively. In the Izmir and Seville cases, for instance, the electrical efficiencies decrease significantly during the non-heating season when the panels are cooled only with the DHW operation.

From Figure 6.12-c), as the panel's combined efficiency is the sum of the thermal and electrical efficiencies (see Equation 6.9), both values are added together and the results are presented. As seen, the PV/T unit in the Izmir case has the highest combined efficiency throughout the year followed by Paris and Seville cases, respectively. Moreover, the combined efficiencies prove the discussion in above paragraph on the panel's effectiveness at moderate temperatures.

6.5.5 System Size, Electrical Balance of the System, and Discussion on the System Feasibility

As aforementioned, the PV/T unit supplies both thermal and electrical energy simultaneously. In addition, the representative house has the demand vectors of the SH (thermal energy), DHW (thermal energy), and EE (electrical energy for household equipment). However, as detailed in Section 6.5.2, the HP unit uses the low-grade solar thermal output of the PV/Ts as the heat-source input and then reduces and electrifies the thermal demands due to the existence of the compressor. Hence the only remaining thermal demand that the proposed system needs to supply directly is the DHW. In order to supply this, as detailed in the previous sections, the thermal output of the PV/Ts is used directly, with an auxiliary heater placed in the DHW tank as a backup when needed. At this stage,

therefore, all demand-side energy vectors are in the form of electrical energy that needed to be met ideally by the electricity output of the PV/T unit or by the national grid as the system is connected to the grid with the feed-in-tariff (FIT).

Based on the PV/T sizing procedure of the system (see Section 6.4), the required PV/T unit areas to meet all thermal energy demand vectors (direct supply of the DHW and indirect supply of the HP's evaporator through the SH tank) and electrical energy demand vectors (compressor electricity consumption of the HP for the SH, auxiliary electricity consumption of the SH tank, auxiliary electricity consumption of the DHW tank, and the EE) of the representative house in each location are found. When the system operates based on these PV/T areas, the results of the thermal performance of the proposed system were presented in Sections 6.5.2 and 6.5.3.

In this section, results for the electrical energy balance of the proposed system, together with the required PV/T size, on a year-round basis in each selected location are presented in Figures 6.13, 6.14, and 6.15. Due to the design of the system, the electrical energy output of the PV/T is first used for the auxiliary electricity consumption of the DHW tank (see Section 6.5.3), second for the auxiliary electricity consumption of the SH tank (see Section 6.5.2), third for the compressor electricity consumption (see Section 6.5.2), and fourth for the electrical energy (EE) demand of the household equipment (see Section 6.2.2). It has to be mentioned that in the figures below, the compressor's electricity consumption and auxiliary electricity consumption of the SH tank are summed and presented in red bar column together since they both are used for the SH purpose.

6.5.5.1 The proposed system in cold climates, Paris Case

In this case, the required PV/T area to cover all demand vectors is found as 56.1 m^2. When this PV/T area is reached during the annual simulations, the annual electrical energy balance

of the system is presented in Figure 6.13. As it is seen from this figure, the proposed system depends substantially on the national grid electricity for coldest months, January, February, November, and December. Although in all these months the electrical energy output of the PV/Ts meets the all auxiliary electricity consumption of the DHW tank, it covers only 9.3%, 26.4%, 28.5%, and 9.7% of the SH demand (compressor work + auxiliary consumption for the SH tank), respectively. In addition, no demand coverage for the EE demand is observed, as this demand is prioritized lastly. In March, however, the dependence of the grid is lower than that of the coldest months; the system covers all demands for the DHW and 77% of the SH demand but still fails to cover any EE demand. During these months (from November to March), the system imports a total of 6214.7 kWh of electricity from the national grid. However, during the months when the solar potential is high and the energy demand vectors are low (from April to October), the system generates more electricity than what is required for the demand vectors, hence exports the same amount of excess electricity to the national grid and become net-zero annually.

In terms of annual equilibrium, the system in Paris has a total of 21405.6 kWh of annual thermal + electrical energy demand (see Section 6.2.2). However, due to the WSHP utilization and the PV/T's thermal contribution, this demand is reduced to an annual total of 10593.8 kWh of electrical energy demand. The annual breakdown of this total is as follows; the auxiliary electricity consumption of the DHW tank (347 kWh), the compressor work (7106 kWh), the auxiliary electricity consumption of the SH tank (875.2 kWh), and electrical energy (EE) demand of the household equipment (2265.6 kWh). When the PV/T unit size reaches a total of 56.1 m^2 area during the annual simulations, this total electrical energy demand (10593.8 kWh) is then met by the PV/T's electricity annually (see Figure 6.13). During this operation, the system uses the national grid as a battery storage unit to import or export energy during the heating and non-heating season, respectively.

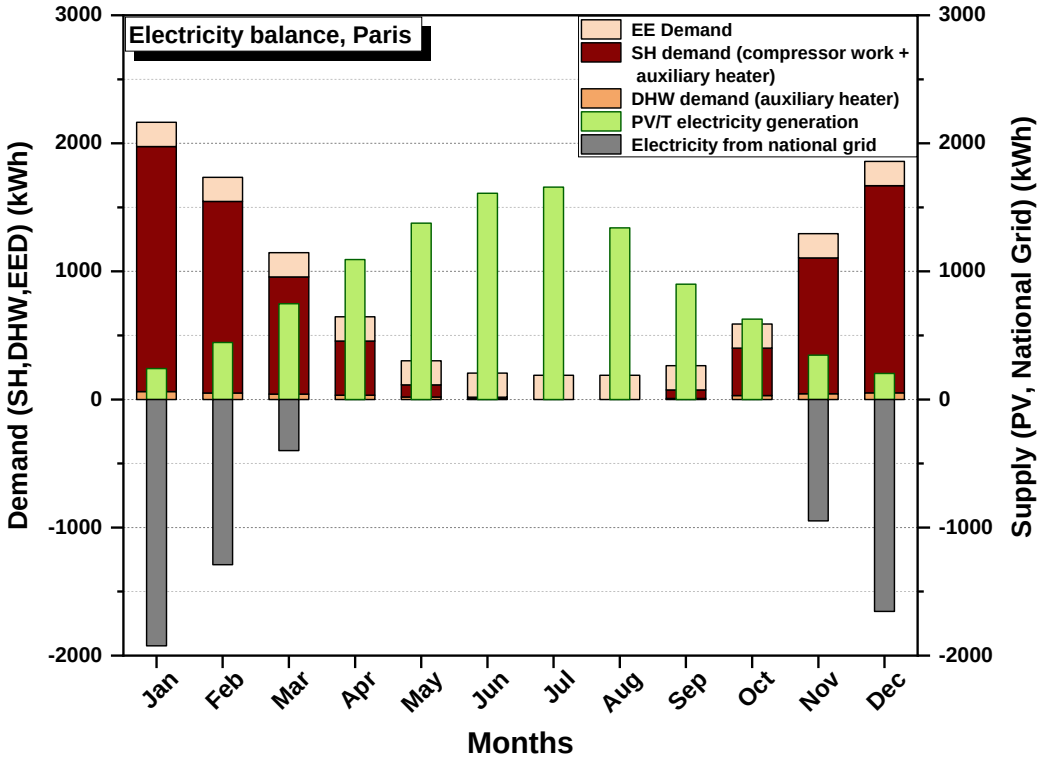

Figure 6.13: Annual electrical energy balance of the system in Paris.

For the system in Paris, two critical conclusions from the annual energy balance are reached. First, the proposed PV/T+WSHP system requires 56.1 m^2 of PV/T area to meet all (SH + DHW + EE) energy demand (21405.6 kWh) vectors. However, this space required for PV/T installation is challenging for the proposed system as the available roof area of the representative house is limited to 50 m^2 for the solar panels (see Chapter 4). Second, the solar energy coverage of the DHW (both thermally and electrically) is in good shape for the system. However, for the SH, the proposed PV/T+WSHP system heavily depends on the national grid, importing 6214.7 kWh of electricity during the coldest months (from November to March). This amount is 62.1% of the total demand during the heating season months (9998.3 kWh, heating months are from September to May for Paris). For a system that is primarily designed for the heating season, however, a grid dependency of above 60% during the winter is questionable. Regarding the performance therefore it is concluded that

the proposed PV/T+WSHP system is not feasible in Paris which represents the cold climatic conditions.

6.5.5.2 The proposed system in moderate climates, Izmir case

In this case, the required PV/T space to meet the all thermal and electrical demands of the representative house is found as 14.7 m^2. When the system has this PV/T area, the electrical balance of the proposed system in Izmir is calculated and presented in Figure 6.14. As seen from the figure, the system requires electricity from the grid for five months of the heating season (from November to March). The total amount of electricity imported from the grid during these months is calculated as 1547.9 kWh. Among these months, only in November, the system covers all energy needs of the SH (compressor work + auxiliary consumption of the SH tank). In other months (from December to March) the proportions of the SH coverage are calculated as 48.3%, 32.5%, 39.2%, and 98.2%, respectively. In April, the PV/T unit generates more electricity than what is required for all three demand vectors and injects a total of 85.8 kWh of excess electricity into the national grid.

In other months (from May to October), there is no SH demand and the DHW demand is fully covered by the thermal output of the PV/T; therefore, the only demand in these months is the electricity need for household equipment, which is fully met by the PV/T unit. In these months, the system transfers all excess electricity (a total of 1462.1 kWh) to the grid. Thus, the total amount of excess electricity exported to the national grid in April and other non-heating months (from May to October) is the same (1547.9 kWh) as the one imported from the grid during the heating season, hence the system becomes net-zero on an annual basis.

In terms of annual energy balance, the system in Izmir has a total of 9483.6 kWh of annual thermal and electrical energy demands (SH+DHW+EE) (see Section 6.2.2). This total demand, however, decreases to 3970.3 kWh of electrical energy demand due to the WSHP

utilization and the PV/T's thermal contribution. It is worth mentioning that this total electrical energy demand (3970.3 kWh) represents the auxiliary electricity consumption of the DHW tank (208 kWh), the compressor work for the actual SH (1324.6 kWh), the auxiliary electricity consumption of the SH tank (172.1 kWh), and the electrical energy (EE) demand of the household equipment (2265.6 kWh). During the annual simulations, when the PV/T unit size reaches a total of 14.7 m^2 area, this total electrical energy demand is then met by the PV/T's electricity.

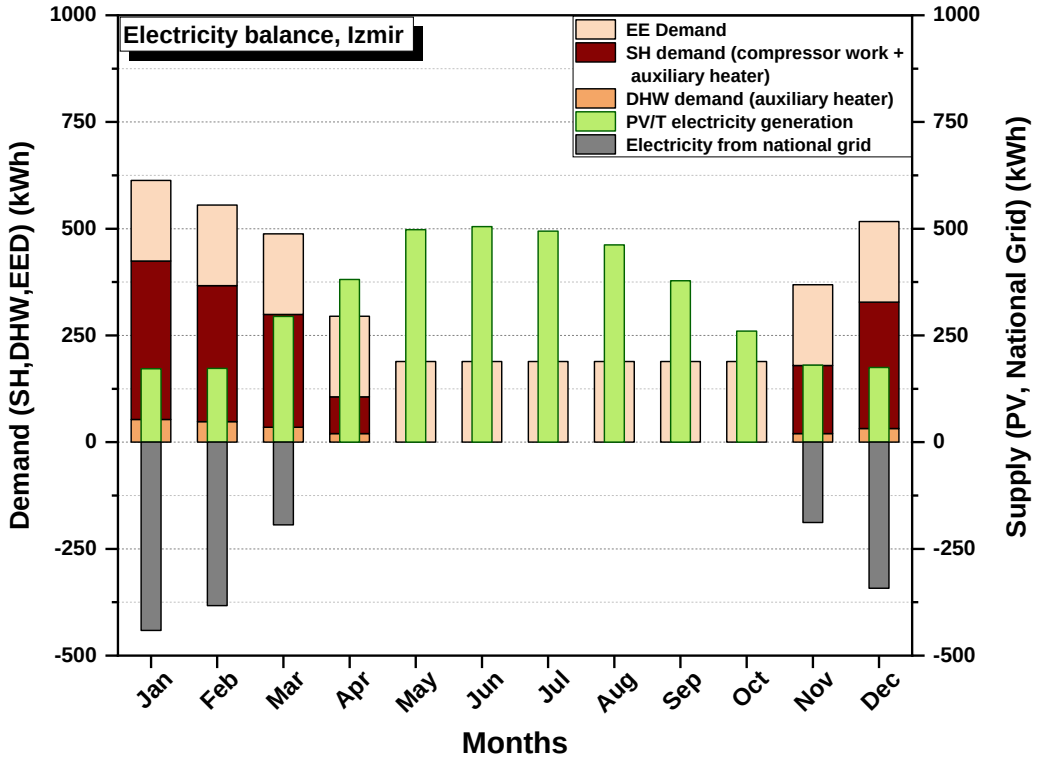

Figure 6.14: Annual electrical energy balance of the system in Izmir.

For the system in Izmir, interesting results are obtained. First of all, the proposed system requires 14.7 m^2 of PV/T area to meet all (SH + DHW + EE) energy demand (9483.6 kWh) vectors, which is well below the available roof area of the representative house.

Second, the proposed PV/T+WSHP system outperforms the system in Chapter 5 (PV+ASHP) in terms of the required solar unit size (20.15 m^2 of PV installation was required) in the same location with the same representative house. However, it should be

noted that the total electricity demand of 594 kWh for space cooling of the house is excluded from this study as the proposed system is technically unable to provide cooling through the HP unit. Therefore, in order to make a comparison based on the same load demands (10077 kWh, SH+SC+DHW+EE), the proposed system in the case of Izmir in this study is run again assuming that the SC load is provided by an electrical appliance (e.g. a fan or an AC unit) whose electricity consumption is added to the EE demand of the house. The results of this operation show that when the SC is added, the system 16.8 m^2 of the PV/T area, which is still well below the required solar unit installation in Chapter 5. This is best explained with (i) the higher and consistent COP of the WSHP over the ASHP, and (ii) the direct and indirect utilizations of the PV/T's thermal output for the DHW and SH tanks, respectively, which maximizes the solar fraction of the system.

Finally, the grid dependency of the proposed system in Izmir case is substantially lower than that of the Paris case in this study. In terms of performance, thus, it is concluded that the proposed system is a feasible technological option providing space heating, domestic hot water and electrical energy for single-family houses located in moderate climates.

6.5.5.3 The proposed system in hot climates, Seville case

In this case, the required PV/T area is calculated as 10.8 m^2 to meet all energy demands (SH+DHW+EE) of the representative house. During the annual simulations, when the PV/T unit size is achieved to 10.8 m^2, the annual electrical balance of the system is calculated and shown in Figure 6.15. From this figure, it is seen that the system imports electricity from the national grid only for four months (from November to February). The total amount of electricity taken from the grid in these months is found as 1076.1 kWh. Moreover, the proposed PV/T+WSHP system requires electricity from the grid only in two months (December and January) to cover the SH demand (compressor work + auxiliary consumption of the SH tank). In these months the percentages of the SH demand coverage

from the PV/T electricity are 35.3% and 45.8%, respectively. In February and November, the system meets all energy demands of the DHW and SH, and 6.5% and 6.7% of EE demand, respectively. In all other months (from March to October), the PV/T unit generates more electricity than what is required for all demand vectors (EE is the only demand between June and September, see Figure 6.15) and exports a total of 1076.1 kWh of excess electricity to the grid and becomes net-zero annually.

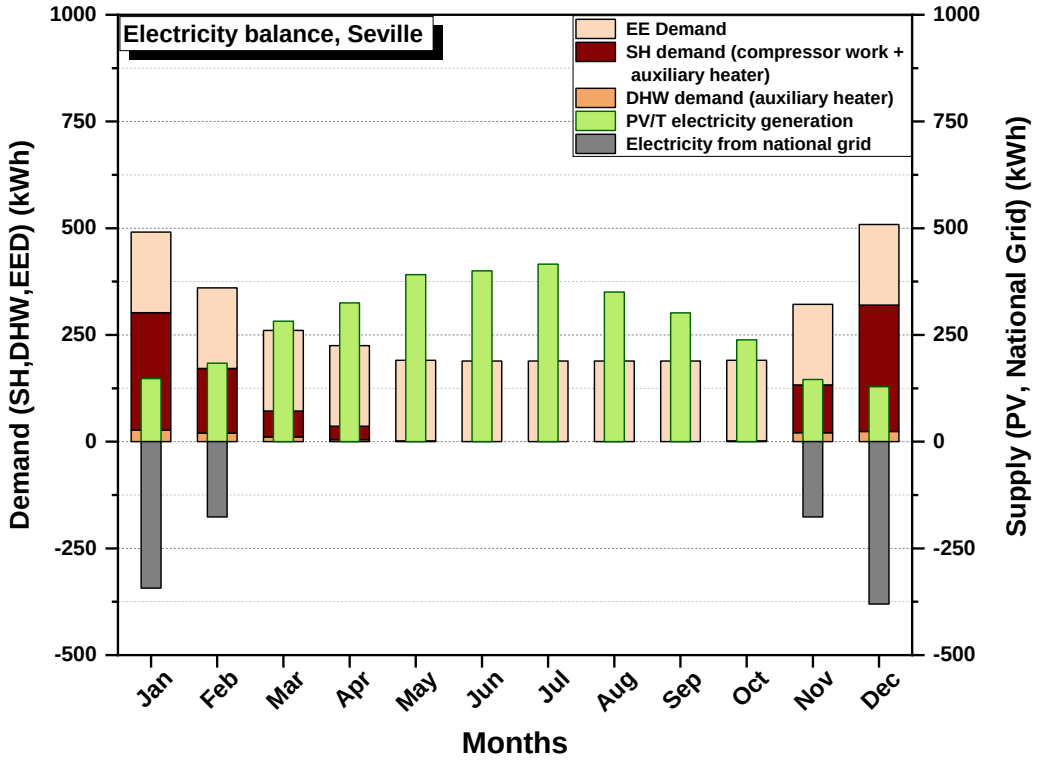

Figure 6.14: Annual electrical energy balance of the system in Seville.

For the annual energy balance of the system in Seville, the representative house has a 7365.6 kWh of total annual combined thermal and electrical energy demand (SH+DHW+EE, see Section 6.2.2). However, this amount reduces to 3226.9 kWh of electrical energy when the WSHP utilization and the PV/T's thermal output are considered. This total electricity demand (3226.9 kWh) represents the auxiliary electricity consumption of the DHW tank (108 kWh), the compressor work for the actual SH (770 kWh), the auxiliary electricity

consumption of the SH tank (83.3 kWh), and the electrical energy (EE) demand of the household equipment (2265.6 kWh).

The most notable conclusion from the energy balance results in Seville is that the system requires only 12.4 m^2 of PV/T area; this is almost a quarter of the available roof area of the representative house. With this PV/T field, the proposed system satisfies all the energy demand vectors of the representative house (SH + DHW + EE, 7365.6 kWh). Compared to the other two cases, the PV/T unit size in Seville is much smaller. In fact, these results were expected as Seville has lower SH demand and higher solar potential during the winter season, resulting in having a lower PV/T installation (10.8 m2) and a smaller HP (3 kW) dimension. Therefore, it is concluded that the proposed PV/T+WSHP system is a suitable technology (in terms of performance) to provide SH, DHW and EE for single family houses in hot climates as shown in the example of Seville.

6.6 ECONOMIC ANALYSIS OF THE PROPOSED SYSTEM

In the previous section (6.5), the technical feasibility of the proposed PV/T+WSHP system in the Izmir and Seville cases was shown. In addition, it was discussed that the proposed system can meet all energy demand vectors (SH, DHW, and EE) of the representative house in Paris with a higher PV/T area than the available rooftop area of the exemplary house.

In this section, however, a fundamental economic analysis is provided to evaluate the proposed system from a techno-economic perspective in all three locations. Although the technical possibilities can be achieved, the main impediment to the widespread utilization of the PV/T+WSHP systems is usually the economic barriers. Thus, the critical point of the high adoption of the PV/T+WSHP systems is the technology's attainment of the grid-parity, which compares the cost of energy produced from the system to the grid’s energy price and demonstrates the economic feasibility of the system [259].

For the economic feasibility analysis, the levelized cost of energy (LCOE) and payback time (PT) indicators are employed in this study due to the reasons and formulations detailed in Chapter 5 (see Section 5.6). In order to calculate these indicators, data presented in Table 6.4 is used, which provides information about the CAPEX and OPEX of the proposed system (acquisition, installation, operation, and maintenance costs), and relevant assumptions to calculate economic indicators.

Table 6.4: CAPEX, OPEX, and financial assumptions for the economic analysis of the system.

Component	Description	Price Range (GBP,£)	Cost Value (GBP,£)	Location	Values	Reference
PV/T	325 W nominal power, acquisition cost per m^2 of PV/T panel	156-275	175	Paris, Izmir, Seville	-	[294], [298], [299]
WSHP	Acquisition cost per kW	800-1150	900	Paris, Izmir, Seville	-	[300], [150], [126]
Inverter	Acquisition cost per kW	100-140	120	Paris, Izmir, Seville	-	[266]
Storage Tank	Acquisition cost per m^3	430-2600	627	Paris, Izmir, Seville	-	[151], [301], [302]
Pump	Acquisition cost per pump	200-400	230	Paris, Izmir, Seville	-	[303], [284]
Maintenance cost	1% of the system's CAPEX	-	-	Paris, Izmir, Seville	-	[274], [269], [266]
System Installation	-	-	1800	Paris, Seville	-	[284]
System Installation	-	-	1000	Izmir	-	-
Discount rate	Bank discount rate (%)	-	-	Paris	4.25	[304]
Discount rate	Bank discount rate (%)	-	-	Izmir	8	[269]
Discount rate	Bank discount rate (%)	-	-	Seville	3.49	[305]
Inflation rate	General inflation (%)	-	-	Paris	1.28	[306]

Inflation rate	General inflation (%)	-	-	Izmir	12.4	[275]
Inflation rate	General inflation (%)	-	-	Seville	1.61	[307], [308]
Degradation rate	System's degradation per year (%)	-	-	Paris, Izmir, Seville	0.5	[259]
Inverter life	Lifespan of the Inverter (years)	-	-	Paris, Izmir, Seville	10	-
System life	Lifespan of the system (years)	-	-	Paris, Izmir, Seville	20	-

From Table 6.4, the acquisition cost for the monocrystalline flat plate hybrid PV/T panels is obtained from the manufacturer's (Solimpeks) website available in [294], which is the lowest price compared to the other well-established companies that manufacture solar hybrid panels, such as NIBE [298], CanadianSolar [299], and Systovi [309]. The costs for the WSHP, inverter, auxiliary heater, storage tanks, and pumps are estimated from the literature which are in line with the price lists available from the different retailers [300], [266], [301], [302], [303], [284], [150]. The maintenance cost of the system is assumed to be 1% of the system's CAPEX based on suggestions in [274], [269], [266]. The installation cost of the system is the same (1800 £) for Paris and Seville based on [284] and is assumed as 1000 £ for Izmir due to cheaper labour work on the similar-sized systems in the region. The discount and inflation rates for the Izmir case were detailed in Section 5.6 based on the data available in [269], [275]. For Paris and Seville, however, as the corresponding countries have different economic policies, the discount and inflation rates are based on the average of 10 years of data in each country [304], [305], [306], [307], [308]. The system's lifetime is assumed to be 20 years except the inverter's lifespan which is 10 years and replaced at the end of the 10^{th} year. Also, the degradation rate of the system is 0.5% based on [259]. Further, as of May 2023, the grid-electricity prices are 0.206 €/kWh [310], 2.6 TL/kWh [276], and 0.241 €/kWh [311] for Paris, Izmir, and Seville, respectively. Finally, the conversion rates from

GBP to Lira, from GBP to Euro, and from Euro to TL are taken as 1£=24 TL, 1£=1.15 €, and 1€=21TL, respectively, as of May 2023.

6.6.1 Payback Time (PT) of the System in the Selected Locations

The payback time of the proposed PV/T+WSHP system is calculated by employing Equation 5.37. As discussed in Section 5.6, the PT indicator does not consider the inflation and discount rates, hence all CAPEX (total investment cost) and OPEX (operation cost for year 1) of the system are in today's values. In addition, it is assumed that the feed-in tariffs in all locations do not include any bonuses, such as guaranties for a higher purchase price from the customer, thus the electricity exports from the system to the grid or imports from the grid to the system are considered with the same price.

With the above paragraph into consideration, the PT calculates the number of years to cover the total investment cost of the system in each location if the total actual energy demand of the representative house (SH+DHW+EE) was supplied by the national grid. In order to do this, first, the total investment cost of the system in each location is calculated, which are 32106.6 €, 180499.3 TL, and 10550.1 € for Paris, Izmir, and Seville, respectively. Then, the grid electricity price in each location is multiplied by the total actual energy demand of the representative house to find the cost savings (C_{Saving}) by the system in one year, which are 0.206 €/kWh x 21405.6 kWh (Paris), 2.6 TL/kWh x 9483.6 kWh (Izmir), and 0.241 €/kWh x 7365.6 kWh (Seville). Finally, the known inputs are employed in Equation 5.37 with the calculated operation costs and the payback time for Paris, Izmir, and Seville are found as 13.4, 7.4, and 7.5 years, respectively.

6.6.2 Levelized Cost of Energy (LCOE) in the Selected Locations

As stated in the previous chapter, the LCOE is the division of the net present value (NPV) of the total system cost to the NPV of the total energy output of the system over its lifetime

(see Equations 5.38-5.44). The total cost of the system consists of the most fundamental capital expenditures (CAPEX) such as acquisition, installation, and replacement costs, and operational expenditures (OPEX) such as maintenance costs, detailed in Table 6.4 for each location. Thus, other expenditures such as loan payments or depreciation credits are not considered in the calculations. For the energy output, first of all, it has to be mentioned that as the proposed system becomes net-zero on an annual basis in each location, the amount of energy generated is the total actual energy demand of the representative house, which are 21405.6 kWh, 9483.6 kWh, and 7365.6 kWh for Paris, Izmir, and Seville, respectively. Then, a 0.5 % of degradation rate is employed with the corresponding discount rates in each location to these amounts to calculate total energy output of the system over its lifetime. When implementing all data in Table 6.4 into the Equations 5.38-5.44, the net present values of the total system cost in Paris, Izmir, and Seville are found as 64224.1 €, 243532.8 TL, and 19169.6 €, respectively. In addition, the net present values of the total energy generated over the system's lifetime are calculated as 280610.9 kWh, 95335.3 kWh, and 108309.4 kWh. Thus, the LCOE is found as 0.229 €/kWh, 2.54 TL/kWh (or 0.122 €/kWh), and 0.177 €/kWh, for Paris, Izmir, and Seville, respectively.

Based on the LCOE and PT analyses, a number of significant conclusions are drawn. First, from a techno-economic perspective, it is seen that the system in Paris is not economically viable (compared to the grid-electricity price), while in Izmir and Seville cases, the cost of energy over the system lifetime is lower than the grid-electricity price. Especially in the Seville case, the value of LCOE is well below the grid price. Hence, the system is techno-economically feasible in Izmir and Seville. Second, although the degradation rate of the system is the same in all locations, the high discount and inflation rates significantly affect the NPVs of the total cost and energy outputs of the system, as seen in the Izmir case. Thus, the economic stability of the countries affects the cost of the energy generated by the system.

Third, the PT of the system in cold climatic conditions (Paris) is almost double that of the moderate (Izmir) and hot (Seville) cases. This is due to the higher number of PV/T panels and higher WSHP and inverter capacities, resulting in a higher investment cost for the system in this location. Although the system size in the Izmir case is higher than in the Seville case, surprisingly, the payback times in the Izmir and Seville cases are almost identical. However, it should be noted that locational differences such as installation costs affect the total investment costs of the system. Finally, when the proposed PV/T+WSHP system in the Izmir case is compared with the system in the previous chapter (PV+ASHP), it is seen that although the PV/T+WSHP outperform the PV+ASHP in terms of system size and the solar fraction, both LCOE and PT indicators of the PV/T+WSHP are higher than that of the PV+ASHP. This is because of the higher acquisition cost of the system components in PV/T+WSHP, such as PV/T units and WSHP. In addition, in PV/T+WSHP system, more components such as hydraulic pumps and stratified storage tanks are used to build the system, which increases the investment cost.

6.7 CONCLUSION

In this chapter, a research has been conducted on the techno-economic feasibility analysis of a novel PV/T+WSHP system that meets all the space heating, domestic hot water, and electrical energy needs of a typical single-family house located in three different climatic conditions. The selected locations were Paris, Izmir, and Seville representing the cold, moderate, and hot climates, respectively. In all locations, the proposed system was grid-connected with Feed-in-Tariff and aimed to be net-zero in terms of the annual energy balance.

The proposed system was modelled using the commercial TRNSYS and EES software packages and it consisted of four main components; monocrystalline flat-plate PV/T panels, a water source heat pump (WSHP), two stratified thermal storage tanks, and a typical

exemplary building model. The HP unit was modelled in EES, while the other main components, including the other auxiliary components that connect the main ones such as flow diverters and mixers, weather data components, forcing functions, controllers, etc., were modelled in the TRNSYS environment. The novelty of the system lied in the model configuration, in which the thermal output of the PV/T was divided into two separate loops to directly provide the DHW and indirectly the SH; this maximized the solar fraction (proven in Section 6.5 with the Izmir case). The proposed model was then validated against the experimental literature data, where minor deviations (maximum of 6.38%) were observed.

Control was the key to the successful operation of the system, therefore a detailed control strategy was applied to the model. In this context, the control of the HP unit was provided by a room thermostat installed in the exemplary house, which provided a control signal value of '1' (ON) or '0' (OFF), depending on whether the zone temperature drops below 20°C or not, respectively. The control of the PV/T thermal output was actualised by four different differential controllers and a set of equations written in the TRNSYS. The differential controllers operated according to the upper and lower dead-band temperatures (set for the PV/T thermal output) and the upper and lower nodes of the tanks and provided control values of '1' (ON) or '0' (OFF) to the flow diverter component with the written equations. With this control logic, the system started operating with an assumption of a 1 m^2 area of the PV/T and increased the panel size by 0.1 m^2 at each annual simulation until the system reaches 100 % of all demands (SH+DHW+EE) coverage. The hourly results of the simulations during the typical year were then aggregated daily, monthly, and annually to observe the performance of the system. Finally, a fundamental economic analysis was carried out to reveal the economic competitiveness of the proposed system in each location. Subsequent to this summary, the following are the major findings of the study;

• It was revealed that the utilization of the WSHPs substantially reduce the thermal energy required for the SH needs of the single-family houses. In this study, the amount of energy saved annually by using a WSHP unit for the SH demands was calculated as 10483 kWh, 4396 kWh, and 2899 kWh for the Paris, Izmir, and Seville cases, respectively.

• Although it is generally accepted that the solar-WSHPs are more resilient to the ambient temperatures (compared to the ASHPs), it is shown that their performance can also reduce significantly when solar thermal energy potential is low. In the Paris case, for example, the COP of the system dropped to as low as 2.11 during the coldest months. In addition, it was revealed with the annual simulations that in the moderate climates (as in the Izmir case), the WSHPs have a quite consistent COP, fluctuating between 3.95 - 4.61. Thus, in terms of the HP performance, it is concluded that the solar-assisted water-sourced heat pumps perform best under moderate and hot climates.

• One of the most notable conclusions is that the PV/Ts can meet 100 % of the DHW demands without a HP interaction in all locations. In this study, for example, the proportions of the DHW coverage from the thermal output of the PV/Ts were 74.7%, 85.9%, and 92.5% for Paris, Izmir, and Seville, respectively; while the remaining proportions (25.3%, 14.1%, and 7.5%) were met by the electricity output of the PV/Ts.

• It is proved with the annual simulations that the PV/T panels perform best under moderate climates (similar to the WSHPs), where higher or lower ambient temperatures reduce the thermal and electrical efficiencies. As shown in the Izmir case, for example, the panels' combined efficiency (thermal + electrical) could reach up to 74.6%, the highest of all three locations. Moreover, it is shown that the electrical efficiencies of the PV/Ts reduce considerably (more than 3 % in all locations) when the panels are not cooled adequately.

• Regarding system size and the annual energy balance, it is revealed that the PV/T+WSHP

systems are not technically viable in cold environments due to the excessive panel size (56.1 m^2) and the high grid dependency of above 60% (e.g. Paris case). On the contrary, such systems perform well under moderate and hot climates. It was shown that the required sizes for the system in these locations to cover all energy demands without a high grid dependency were 14.7 m^2 and 10.8 m^2, respectively. Hence it is concluded that the PV/T+WSHP systems are a feasible energy supply technology only in moderate and hot climatic locations.

• From the economic analysis, it was shown that the cost of energy generated from the proposed system in the cold climate was higher than the grid's price. In addition, the payback time of the system in such locations was beyond the economical, 13.4 years. Nevertheless, the proposed system still can be competitive with the grid electricity price in cold climates. In Paris case, for example, the LCOE of the system and the grid electricity prices were 0.229 €/kWh and 0.206 €/kWh, respectively. For the moderate climates (as in the Izmir case), despite the exemplary country's high inflation rate, it is shown that the proposed system has already reached the grid parity (2.54 TL/kWh (or 0.122 €/kWh) from the proposed system and 2.6 TL/kWh from the grid). In hot climates (as in the Seville case), the cost of energy generation is more economical than the grid energy price (0.177 €/kWh from the proposed system and 0.241 €/kWh from the grid).

Overall, it is proven that the PV/T+WSHP systems are a viable energy supply technology that becomes more cost-effective than the grid energy price in the moderate and hot climatic regions of Europe for typical single-family residential houses. However, technical barriers, especially lack of information on the design and construction, and the scarcity of recognition limit the adaptation of the technology in today's market. Hence it is firmly suggested that such studies should be highly promoted and advertised in the scientific community for a high awareness and adaptation of the technology.

CHAPTER 7

Conclusions and Recommendations for Future Work

7.1 CONCLUSION

7.1.1 Summary of the Thesis

An inevitable side effect of the fossil fuels dominance in almost all energy-related sectors is the greenhouse gases emitted into the atmosphere, causing the climate change. Building sector in particular is responsible for around a third of the global energy consumption, which is still dominantly fuelled by fossil fuels, and a quarter of the total emissions. These percentages are even higher in the developed regions, such as Europe, as energy consumption per capita is up to five times higher compared to undeveloped regions/countries due to the high living standards. In order to reduce the energy consumption and the related emissions therefore the building sector needs to be more energy efficient and sustainable, particularly in the developed regions. However, this can only be accomplished if the building envelopes are structured based on energy regulative standards and/or if the sustainable and efficient solutions on the energy supply side are proposed, such as the combination of solar energy and heat pump technologies called solar-assisted heat pumps (SAHP). Currently, nevertheless, still around 110 countries worldwide do not have a building construction standard and SAHP systems supply an insignificant amount of building's energy. The focus of this research therefore has been to address the issues of high energy consumption in residential buildings, the lack of building construction guidance or standards, and the insufficient utilization of the SAHP systems in the building sector due to high capital investment costs and limited number of applications. For this purpose, this thesis aimed to investigate the techno-economic feasibility of different SAHP systems in residential single-family houses in order to reveal the possible innovative ways of maximising the energy outputs of such systems while ensuring that the energy demand side management was in line with the local building standards. The potential of the proposed systems to fulfil all energy demand vectors, such as space heating and cooling (SH and SC), domestic hot water (DHW)

and electrical energy (EE) for household equipment, of a typical single-family house (built in the light of the EU and an EU candidate country's building standards) in different parts of Europe was of particular interest in the thesis. In order to achieve the main objectives of the thesis, the following objectives were determined and the thesis was structured as follows in the light of these objectives;

First, all components of a SAHP system that can be adapted to the buildings were investigated in Chapter 2 by following a step-by-step research method to reveal research gaps in the literature. Second, the methodology of the thesis (e.g. modelling approaches and software selection) was determined in Chapter 3 to conduct the main research work. Then, a research on the dynamic thermal and electrical energy demand evaluation of a typical European single-family house was conducted in Chapter 4, in light of the building standards of the EU and an EU candidate country, in order to correctly size any energy-generating system and to use it as a guide for the locations where the building energy codes are not available. Subsequent to the house modelling, a fundamental PV+ASHP solar-assisted heat pump system was modelled, optimized, and simulated holistically in Chapter 5 in order to reveal the techno-economic competitiveness of such systems with the grid energy price in locations where the SAHP technology has high potential but lack awareness. Finally, the techno-economic feasibility of a PV/T+WSHP solar-assisted heat pump system under different climatic boundary conditions of the European region was analysed in Chapter 6 in order to reveal the viability of such systems in cold, moderate, and hot climates.

7.1.2 Main Conclusions of the Thesis

In Chapter 2, the presented state-of-the-art literature search revealed that many studies base their energy demands on presumptive repetitive load profiles, which leads to mismatches between the energy supply and demand sides. This is usually due to the lack of data on the building energy consumption profiles or unavailable building energy standards when

constructing a new building. Moreover, these reasons lead to insufficient data to calculate the dynamic energy consumption assessment of the thermal and electrical end-users of the buildings. If the dynamic demand profiles for these end-users were known, any energy-generating systems can be precisely sized, which means a better economy for the energy supply side.

• In addition, it was found that for small-scale applications such as single-family homes, ground-sourced heat pumps (GSHP) may not be economically viable due to the excessively high installation costs in mild climatic conditions. Conversely, it was shown that air-sourced heat pumps (ASHP) and water-sourced heat pumps (WSHP) are preferable alternatives for such applications because of their simpler installation and design, as well as their lower installation cost.

• Also, it was found that there is no a uniform approach for establishing a SAHP system, as each system has its own unique parameters such as heat source, environmental conditions, and HP selection and its own particular advantages for a given application such as different end-users.

• Further, the SAHP systems designed for DHW-only have been thoroughly examined in the literature. Systems that offer SH + DHW have attracted a lot of interest as well. Nevertheless, it was rare to find systems providing more than two energy vectors (among SH, DHW, SC, EE) in the literature.

• Moreover, it was shown from the pioneering literature studies that for locations where the optimal operating conditions (e.g. weather) exist and the SAHP systems are not adequately adapted, the combination of solar PV with an ASHP unit is the most reasonable SAHP system due to the lower installation cost, higher adaptability to the new or existing buildings,

and higher technical capability to generate more than two energy vectors (e.g. SH + SC + DHW + EE).

• Finally, from the critical literature review, it was found that SAHP systems combining solar thermal collectors (including PV/T) with a WSHP unit are highly effective in terms of performance, especially when WSHP units are combined with PV/T collectors. Such combinations can produce more than two energy vectors (e.g. SH + DHW + EE), taking advantage of the higher specific heat capacity of water (compared to ambient air) and higher solar fraction into buildings (as solar energy is not produced only in the form of heat but also in the form of electricity). However, the PV/T+WSHP based SAHP systems are still in their early stages and are rarely reported in the literature.

In Chapter 3, since the configuration of the SAHP systems proposed in this thesis are novel compared to the existing literature, it was concluded that applying a model-based methodology and performing annual simulations according to this method would provide the most accurate and predictable results. For this purpose, the TRNSYS and EES programming packages were found to be the best options since the TRNSYS has an extensive library containing most of the validated components of the SAHP systems and the EES has the thermodynamic characteristics of hundreds of fluids.

In Chapter 4, a representative single-family house for 4 persons, assumed to have a single zone and a usable floor area of 100 m^2, was designed and modelled in the light of the building standards of the EU and an EU-candidate country, using TRNSYS Type 88 lumped capacitance building model validated according to the weather data used in these standards.

• The dynamic hourly SH, SC, DHW, and EE energy demand vectors of the model were obtained hourly and were aggregated and analysed daily, monthly, and annually. Also, the demand calculation methods were clearly established.

• The dynamic results showed that the representative house requires an equivalent of 10077 kWh of energy to satisfy all demand vectors (SH+SC+DHW+EE). In this total, however, the SH and the EE demands were the highest energy consumers of the representative house with the annual totals of 5721 kWh and 2265 kWh, respectively, followed by DHW and SC demand values with the annual totals of 1497 kWh and 594 kWh, respectively.

• For the DHW and EE demands, in particular, it was also concluded that the daily consumption profiles vary significantly from user to user, hence they cannot be standardised. As a result, both profiles were estimated based on the well-accepted literature studies. However, the calculations were conducted based on 40 L of hot water per person at 50 °C for DHW demand and on the electricity consumption of the most essential electrical equipment used in a typical single-family house for the EE demand. Regarding the highest daily and hourly consumptions, these values were found to be 5.20 kWh and 730 W for the DHW demand and 6.3 kWh and 608 W for the EE demand, respectively.

• Finally, it was concluded that the dynamic energy consumption profiles of the representative house can be used to accurately size and design any energy-generating system. The dynamic behaviour on the demand side, in addition, permits to better assess the performance of the energy delivery systems in real conditions. Furthermore, the energy demand calculation methods described in this study are open to be modified and reused as a reference for any location where the building standards are not obligated by the local authorities.

In Chapter 5, a fundamental SAHP system including solar PV panels and a ASHP unit, capable of generating all energy demand vectors (SH+SC+ DHW+EE) of the representative single-family house, was holistically modelled, optimized, and simulated in order to assess the techno-economic competitiveness of such SAHP systems with the grid energy price for

the locations where the technology has high potential but limited adaptation. The proposed system was assumed to be located in Turkey and connected to the national grid with a feed-in tariff.

• The proposed model was verified against both numerical and experimental studies where the validation results showed fairly minor deviations, 2.7 % for the PV unit and 4.2 % for the HP unit.

• The optimization results showed that the HP unit operates best with the R152a refrigerant type when the mass flow rate and the pinch-point-temperature-difference between the heat source and the evaporator sides were 0.4509 $\frac{kg}{s}$, and 9.8 °C, respectively.

• The annual simulation results of the HP unit revealed that the actual SH and SC demands of the representative house were reduced from 5721 kWh and 594 kWh to 1402 kWh and 128 kWh, respectively, hence an energy-saving potential of almost 75 % was achieved. Moreover, due to the HP utilization, the SH and SC energy demand vectors were electrified, and that the PV unit of the holistic model had to meet a total of 5292 kWh of electrical demand (together with the DHW and EE) instead of 10077 kWh.

• The annual simulation results of the holistic model showed that a total of 20.15 m^2 PV installation was required to make the representative house net-zero-energy and to ensure that all energy demand vectors are covered on a total annual basis. Moreover, it was also concluded that if the HP had not been used, a total of 38.3 m^2 of PV would have been required to satisfy all the demands, thus resulting in a total saving of 47.4% on the PV installation.

• The economic results revealed that the system was quite competitive with regard to the payback time and the LCOE indicators which were found to be 6.8 years and 2.43 TL/kWh

(or 0.105 £/kWh or 0.121 €/kWh), respectively. This value for the LCOE, in particular, proved that the PV+ASHP SAHP systems had already reached the grid-parity as the grid electricity price in the case location was 2.6 TL/kWh.

• Finally, the most important conclusion from this study was that for locations where SAHP systems have high potential but low awareness, the PV+ASHP combination is a techno-economically viable option that can satisfy all energy demands of a single-family house more cost-effectively than the grid electricity price. However, barriers, including high initial costs and the limited number of applications, limit the widespread utilization of the technology in these regions. Therefore, it was suggested that such systems can be promoted with incentives for early deployment and studies should be encouraged for the widespread adaptation of the technology.

In Chapter 6, an innovative SAHP system including solar PV/T collectors and a WSHP unit, capable of generating SH, DHW, and EE demands of a representative single-family house, was modelled and simulated annually in order to reveal the techno-economic feasibility of such SAHP systems under different climatic boundary conditions. The proposed system was tested in three different cities in Europe, Paris (France), Izmir (Turkey), and Seville (Spain), to represent the system in cold, moderate, and hot climates, respectively, and was assumed to be connected to the national grids with a feed-in tariff.

• The validation of the model was conducted against the experimental literature studies and the results showed a maximum of 6.38 % deviation.

• The annual simulation results of the heat pump unit showed that the WSHP utilization electrify and substantially reduces the thermal energy required for the SH needs of the representative house in all locations. This demand was reduced from 17590 kWh to 7106 kWh for Paris, from 5721 kWh to 1324.5 kWh for Izmir, and from 3360 kWh to 770 kWh

for Seville, resulting in a total of 59.6 %, 76.7 %, and 77.1 % reduction, respectively. In addition, the annual total electricity consumptions of the auxiliary heater inside the SH tank in each location were calculated as 875.2 kWh, 172.1 kWh, and 83.3 kWh, respectively.

• The most important conclusion form the DHW simulations was that the proposed system was capable of supplying all DHW demands throughout the year with the thermal and electrical outputs of the PV/T unit in all locations. While the thermal output contributed 74.7%, 85.9%, and 92.5% for Paris, Izmir, and Seville, respectively, the remaining proportions (25.3%, 14.1%, and 7.5%) were met by the electricity output of the PV/Ts.

• The annual simulations on the panel efficiency proved that the PV/T panels perform best under moderate climates, and higher or lower ambient temperatures reduce the thermal and electrical efficiencies of the PV/Ts. Moreover, it was proven that the combined efficiencies (thermal + electrical) of these collectors can reach up to 74.6% when the optimal operating conditions exists. However, it was underlined that the electrical efficiency of the PV/T collectors reduces considerably (more than 3% in all locations) when they are not cooled adequately.

• From a technical point of view, the annual results for the system sizing showed that the proposed system was not feasible in cold environments due to the excessive collector size found at 56.1 m2, which was more than the available collector installation area on the roof of the representative house, and the high grid dependency of over 60% during the heating season. However, the system performed better in moderate and hot climates and required 14.7 m^2 and 10.8 m^2 respectively to meet all energy demands without a high grid dependency, hence it was concluded that the proposed system was feasible in these locations.

• From an economic point of view, although the results of the analysis showed that in cold regions (as in the case of Paris) the energy cost (LCOE) of the system (0.229 €/kWh) was higher than the grid (0.206 €/kWh), the difference was not very large. However, the payback time of the system in these locations was calculated as 13.4 years, hence it was concluded that this period was not economical compared to the system's lifetime of 20 years. For the moderate and hot climates, on the other hand, the LCOE values were found to be 2.54 TL/kWh and 0.177 €/kWh, respectively, which meant that the system in these locations had already reached the grid-parity as the grid electricity prices in these locations were 2.6 TL/kWh (or 0.122 €/kWh) and 0.241 €/kWh, respectively. Also, the payback times were calculated as 7.4 and 7.5 years, hence it was concluded that the proposed system was economically viable in such locations.

• Finally, from a techno-economic point of view, it was concluded that the PV/T+WSHP systems were a feasible energy supply technology only for the moderate and warm climate regions of Europe, while for cold climates such system were not viable. Despite the techno-economic viability, however, the ability of the technology to adapt in these markets is constrained by technical barriers, in particular lack of knowledge on design and construction, and by lack of recognition. It was therefore recommended that such research should be heavily publicised and supported in the scientific community in order to raise awareness and encourage adoption of the technology.

Overall, from the thesis, it has been shown that the building envelope and its typologies have a significant impact on the energy demand of a building and influence the choice of design and technology on the energy supply side. Also, it has been shown that there are different feasible ways to configure a building integrated SAHP system and that these are influenced by the requirements from the users (e.g. different energy demand vectors) or by the technical characteristics of the equipment (e.g. ASHP, WSHP, PV/T, PV, etc.) that

constitute the system. Moreover, despite the lack of awareness and limited number of applications, it has been proven in this thesis that SAHP systems are techno-economically viable energy production technologies that can be applied to European single-family houses built according to standardised construction guidelines to reduce energy consumption, electrify & meet all energy demands, and increase the renewable energy share of the building sector. Through the first proposed system, it has been revealed that PV+ASHP systems are the most fundamental combination that can be easily applied to buildings for locations where the technology has high potential (due to the favourable climate) but insufficient awareness. In the second proposed system, finally, it has been proven that PV/T+WSHP systems can be highly effective to maximise energy outputs, reduce energy consumption, and increase the solar fraction entering buildings with novel designs in temperate and warm climates.

7.2 RECOMMENDATIONS FOR FUTURE WORK

Several limitations and areas of further work have been recommended for the research as follows;

• In order to simplify calculations, the existing single-family house was modelled based on the Lumped Capacitance Model (LCM) approach, neglecting temperature variations on the structure, such as the benefits of sunlight, and assuming that the interior regions of the house were single-zone, unlike real applications. Therefore, a more detailed house model should be developed to represent the house from a more realistic perspective. This enhanced model can be further investigated by considering different building typologies, such as multi-family houses (e.g. apartment blocks) and commercial buildings (e.g. offices, schools, hospitals, etc.), in different climatic zones, countries, or regions as there is a tremendous research gap in this field in the literature.

• This work did not consider the benefit of electrical energy storage units such as batteries. In order to investigate the differences in the economic and energetic values of electricity and heat energies, another off-grid version of the SAHP system can be established.

• Since model-based systems are always an imperfect copy of the real systems, an experimental study should be conducted to perform some preliminary tests on different types of solar collectors and different heat pump units before developing a real system.

• Since the proposed PV/T+WSHP system could not provide SC due to the technical restrictions, an alternative way of providing this demand should be investigated, such as through solar-absorption chillers, as solar thermal cooling is of high interest in the literature.

• Finally, different new configurations, including PV/T+ ground-source HP or PV/T/PV+ dual-source HP systems for multi-family houses or commercial building typologies, should be investigated in order to unlock the potential of SAHP systems further and increase the recognition of the technology.

REFERENCES

[1] S. Barca, “Energy, property, and the industrial revolution narrative,” *Ecol. Econ.*, vol. 70, pp. 1309–1315, 2011.

[2] K. Bithas and P. Kalimeris, “A Brief History of Energy Use in Human Societies. In: Revisiting the Energy-Development Link,” no. Ruddiman 2001, pp. 5–11, 2016.

[3] Max Roser and Esteban Ortiz-Ospina, *International Historical Statistics*. London: Palgrave Macmillan UK, 2013.

[4] V. Smil, “ENERGY IN THE TWENTIETH CENTURY: Resources, Conversions, Costs, Uses, and Consequences,” 2000.

[5] J. Needham, L. Wang, G. Métailie, and H. T. Huang, “Fossil Fuels.” [Online]. Available: https://ourworldindata.org/fossil-fuels.

[6] International Energy Agency, “International Energy Agency (IEA) World Energy Outlook 2022,” *Https://Www.Iea.Org/Reports/World-Energy-Outlook-2022/Executive-Summary*, p. 524, 2022.

[7] “Supply – Key World Energy Statistics 2022 – Analysis - IEA.” [Online]. Available: https://www.iea.org/reports/key-world-energy-statistics-2021/supply.

[8] B. Petroleum, “bp Energy Outlook 2023 edition 2023 explores the key trends and uncertainties,” no. July, pp. 1–53, 2023.

[9] “The Keeling Curve.” [Online]. Available: https://keelingcurve.ucsd.edu/.

[10] N. G. M. L. US Department of Commerce, “ESRL Global Monitoring Laboratory - Mauna Loa Observatory.”

[11] “The Keeling Curve | A daily record of atmospheric carbon dioxide from Scripps Institution of Oceanography at UC San Diego.” [Online]. Available: https://scripps.ucsd.edu/programs/keelingcurve/.

[12] R. K. Pachauri *et al.*, “IPCC, 2014: Climate Change 2014: Synthesis Report. Contribution of Working Groups I, II and III to the Fifth Assessment Report of the Intergovernmental Panel on Climate Change,” Gian-Kasper Plattner, 2014.

[13] T. F. Stocker *et al.*, “Climate Change 2013 The Physical Science Basis Working

Group I Contribution to the Fifth Assessment Report of the Intergovernmental Panel on Climate Change," 2013.

[14] L. A. M. (eds) B. Metz, O.R. Davidson, P.R. Bosch, R. Dave, "IPCC Climate Change 2007: Mitigation. Contribution of Working Group III to the Fourth Assessment Report of the Inter- governmental Panel on Climate Change," *Cambridge Univ. Press*, p. 863, 2007.

[15] IPCC, "Chapter Climate Change 2014 Synthesis Report Summary for Policymakers Summary for Policymakers," 2014.

[16] UNFCCC, "UNFCCC eHandbook - Summary of the Paris Agreement." [Online]. Available: https://bigpicture.unfccc.int/#content-the-paris-agreemen.

[17] IEA, "World Energy Outlook 2015," Paris, France, 2015.

[18] IEA, "International Energy Agency: World Energy Outlook 2016," Paris, France, 2016.

[19] IEA, "Net Zero by 2050: A Roadmap for the Global Energy Sector," *Int. Energy Agency*, p. 224, 2021.

[20] IEA, "Intertational Energy Agency: World Energy Outlook 2017," 2017.

[21] "Final consumption – Key World Energy Statistics 2021 – Analysis - IEA." [Online]. Available: https://www.iea.org/reports/key-world-energy-statistics-2021/final-consumption. [Accessed: 18-Sep-2023].

[22] International Renewable Energy Agency (IRENA), *World energy transitions outlook 2022*. 2022.

[23] D. Henner and REN21, *Ren21*. 2020.

[24] M. González-Torres, L. Pérez-Lombard, J. F. Coronel, I. R. Maestre, and D. Yan, "A review on buildings energy information: Trends, end-uses, fuels and drivers," *Energy Reports*, vol. 8, pp. 626–637, Nov. 2022.

[25] BP, "BP Energy Outlook 2022 edition," *Br. Pet.*, p. 109, 2022.

[26] J. Wernery, F. Mancebo, W. J. Malfait, M. O'Connor, and B. P. Jelle, "The economics of thermal superinsulation in buildings," *Energy Build.*, vol. 253, Dec. 2021.

[27] "Building envelopes - IEA." [Online]. Available: https://www.iea.org/energy-

system/buildings/building-envelopes. [Accessed: 26-Sep-2023].

[28] L. Pérez-Lombard, J. Ortiz, and C. Pout, “A review on buildings energy consumption information,” *Energy Build.*, vol. 40, no. 3, pp. 394–398, Jan. 2008.

[29] N. S. B. Lapillonne, K. Pollier, “Sectoral Profile-Households Energy consumption Household energy consumption by energy in the EU.”

[30] “Heating - IEA.” [Online]. Available: https://www.iea.org/energy-system/buildings/heating. [Accessed: 20-Sep-2023].

[31] C. Good, I. Andresen, and A. G. Hestnes, “Solar energy for net zero energy buildings – A comparison between solar thermal, PV and photovoltaic–thermal (PV/T) systems,” *Sol. Energy*, vol. 122, pp. 986–996, Dec. 2015.

[32] O. Ellabban, H. Abu-Rub, and F. Blaabjerg, “Renewable energy resources: Current status, future prospects and their enabling technology,” *Renew. Sustain. Energy Rev.*, vol. 39, pp. 748–764, 2014.

[33] REN21, “Renewable energy policy network for the 21st century: Renewables 2017 Global Status Report,” p. 302, 2017.

[34] “Renewables in Energy Supply.” [Online]. Available: https://www.ren21.net/gsr-2023/modules/energy_supply/01_energy_supply/. [Accessed: 21-Sep-2023].

[35] REN 21 renewables now, “RENEWABLES 2023GLOBAL STATUS REPOR: Energy demand,” 2023.

[36] G. Masson and I. Kaizuka., *IEA PVPS report - Trends in Photovoltaic Applications 2020*. 2020.

[37] P. Dupeyrat, C. Ménézo, and S. Fortuin, “Study of the thermal and electrical performances of PVT solar hot water system,” *Energy Build.*, vol. 68, pp. 751–755, Jan. 2014.

[38] X. Zhang, X. Zhao, J. Shen, J. Xu, and X. Yu, “Dynamic performance of a novel solar photovoltaic/loop-heat-pipe heat pump system,” *Appl. Energy*, vol. 114, pp. 335–352, Feb. 2014.

[39] I. Guarracino, A. Mellor, N. J. Ekins-Daukes, and C. N. Markides, “Dynamic coupled thermal-and-electrical modelling of sheet-and-tube hybrid photovoltaic/thermal (PVT) collectors,” *Appl. Therm. Eng.*, vol. 101, pp. 778–795, May 2016.

[40] S. A. Kalogirou, “Solar thermal collectors and applications,” *Prog. Energy Combust. Sci.*, vol. 30, no. 3, pp. 231–295, Jan. 2004.

[41] W. Spork-Dur, “Solar Heat World Wide,” *IEA*, p. 88, 2022.

[42] W. Weiss and M. Spörk-Dür, “Global Market Development and Trends in 2018,” *Sol. Heat Worldw. Rep.*, vol. 1, no. 2019, p. 86, 2019.

[43] R. Lazzarin, “Heat pumps and solar energy: A review with some insights in the future,” *International Journal of Refrigeration*, vol. 116. Elsevier Ltd, pp. 146–160, 01-Aug-2020.

[44] “Heat Pumps - Energy System - IEA.” [Online]. Available: https://www.iea.org/energy-system/buildings/heat-pumps. [Accessed: 23-Sep-2023].

[45] S. A. Kalogirou, “Solar Energy Engineering Processes and Systems Second Edition.”

[46] L. Evangelisti, R. De Lieto Vollaro, and F. Asdrubali, “Latest advances on solar thermal collectors: A comprehensive review,” *Renew. Sustain. Energy Rev.*, vol. 114, p. 109318, Oct. 2019.

[47] S. A. Kalogirou, “Solar thermal collectors and applications,” *Prog. Energy Combust. Sci.*, vol. 30, no. 3, pp. 231–295, Jan. 2004.

[48] J. Allan, Z. Dehouche, S. Stankovic, and L. Mauricette, “Performance testing of thermal and photovoltaic thermal solar collectors,” *Energy Sci. Eng.*, vol. 3, no. 4, pp. 310–326, 2015.

[49] S. Kalogirou, “The potential of solar industrial process heat applications,” *Appl. Energy*, vol. 76, no. 4, pp. 337–361, Dec. 2003.

[50] M. A. Sabiha, R. Saidur, S. Mekhilef, and O. Mahian, “Progress and latest developments of evacuated tube solar collectors,” *Renew. Sustain. Energy Rev.*, vol. 51, pp. 1038–1054, Nov. 2015.

[51] G. L. Morrison, N. H. Tran, D. R. McKenzie, I. C. Onley, G. L. Harding, and R. E. Collins, “Long term performance of evacuated tubular solar water heaters in Sydney, Australia,” *Sol. Energy*, vol. 32, no. 6, pp. 785–791, Jan. 1984.

[52] Y. Kim and T. Seo, “Thermal performances comparisons of the glass evacuated tube solar collectors with shapes of absorber tube,” *Renew. Energy*, vol. 32, no. 5, pp. 772–795, Apr. 2007.

[53] V. V. Tyagi, S. C. Kaushik, and S. K. Tyagi, “Advancement in solar photovoltaic/thermal (PV/T) hybrid collector technology,” *Renew. Sustain. Energy Rev.*, vol. 16, no. 3, pp. 1383–1398, Apr. 2012.

[54] B. Parida, S. Iniyan, and R. Goic, “A review of solar photovoltaic technologies,” *Renew. Sustain. Energy Rev.*, vol. 15, no. 3, pp. 1625–1636, Apr. 2011.

[55] A. Sharma, “A comprehensive study of solar power in India and World,” *Renew. Sustain. Energy Rev.*, vol. 15, no. 4, pp. 1767–1776, May 2011.

[56] M. Kumar and A. Kumar, “Performance assessment and degradation analysis of solar photovoltaic technologies: A review,” *Renew. Sustain. Energy Rev.*, vol. 78, pp. 554–587, Oct. 2017.

[57] International Energy Agency Photovoltaic Power Systems Programme, *Trends in Photovoltaic Applications, 2021*. 2021.

[58] S. Philipps, F. Ise, W. Warmuth, and P. Projects GmbH, “Distribution of cumulative solar photovoltaic installations worldwide as of 2021, by region [Graph]. In Statista,” no. February, p. 17, 2023.

[59] “Types of Solar Panels: Which One Is the Best Choice?” [Online]. Available: https://www.solarreviews.com/blog/pros-and-cons-of-monocrystalline-vs-polycrystalline-solar-panels. [Accessed: 08-Sep-2021].

[60] L. El Chaar, L. A. Lamont, and N. El Zein, “Review of photovoltaic technologies,” *Renew. Sustain. Energy Rev.*, vol. 15, no. 5, pp. 2165–2175, Jun. 2011.

[61] X. Ren *et al.*, “Feasibility of an innovative amorphous silicon photovoltaic/thermal system for medium temperature applications,” *Appl. Energy*, vol. 252, p. 113427, Oct. 2019.

[62] J. M. C. Michelle, R. C. Kylie, J. W. Klaus, and W. B. Andrew, “A review of thin-film crystalline silicon for solar cell applications. Part 1: Native substrates,” *Sol. Energy Mater. Sol. Cells*, vol. 68, no. 2, pp. 135–171, May 2001.

[63] A. Makki, S. Omer, and H. Sabir, “Advancements in hybrid photovoltaic systems for enhanced solar cells performance,” *Renew. Sustain. Energy Rev.*, vol. 41, pp. 658–684, Jan. 2015.

[64] E. Skoplaki and J. A. Palyvos, “Operating temperature of photovoltaic modules: A

survey of pertinent correlations," *Renew. Energy*, vol. 34, no. 1, pp. 23–29, Jan. 2009.

[65] E. Skoplaki and J. A. Palyvos, "On the temperature dependence of photovoltaic module electrical performance: A review of efficiency/power correlations," *Sol. Energy*, vol. 83, no. 5, pp. 614–624, May 2009.

[66] B. J. Huang *et al.*, "Solar cell junction temperature measurement of PV module," *Sol. Energy*, vol. 85, no. 2, pp. 388–392, Feb. 2011.

[67] E. Radziemska, "The effect of temperature on the power drop in crystalline silicon solar cells," *Renew. Energy*, vol. 28, no. 1, pp. 1–12, Jan. 2003.

[68] O. Dupré, R. Vaillon, and M. A. Green, "Physics of the temperature coefficients of solar cells," *Sol. Energy Mater. Sol. Cells*, vol. 140, pp. 92–100, Sep. 2015.

[69] T. T. Chow, "A review on photovoltaic/thermal hybrid solar technology," *Appl. Energy*, vol. 87, no. 2, pp. 365–379, Feb. 2010.

[70] H. A. Zondag, D. W. de Vries, W. G. J. van Helden, R. J. C. van Zolingen, and A. A. van Steenhoven, "The yield of different combined PV-thermal collector designs," *Sol. Energy*, vol. 74, no. 3, pp. 253–269, Mar. 2003.

[71] M. Herrando, C. N. Markides, and K. Hellgardt, "A UK-based assessment of hybrid PV and solar-thermal systems for domestic heating and power: System performance," *Appl. Energy*, vol. 122, pp. 288–309, Jun. 2014.

[72] M. Hazami, A. Riahi, F. Mehdaoui, O. Nouicer, and A. Farhat, "Energetic and exergetic performances analysis of a PV/T (photovoltaic thermal) solar system tested and simulated under to Tunisian (North Africa) climatic conditions," *Energy*, vol. 107, pp. 78–94, Jul. 2016.

[73] X. Zhang, X. Zhao, S. Smith, J. Xu, and X. Yu, "Review of R&D progress and practical application of the solar photovoltaic/thermal (PV/T) technologies," *Renew. Sustain. Energy Rev.*, vol. 16, no. 1, pp. 599–617, Jan. 2012.

[74] C. Good, "Environmental impact assessments of hybrid photovoltaic–thermal (PV/T) systems – A review," *Renew. Sustain. Energy Rev.*, vol. 55, pp. 234–239, Mar. 2016.

[75] IEA, "Technology Roadmap Solar Heating and Cooling," Paris Cedex 15, France, 2012.

[76] J. J. Michael, I. S, and R. Goic, "Flat plate solar photovoltaic–thermal (PV/T)

systems: A reference guide," *Renew. Sustain. Energy Rev.*, vol. 51, pp. 62–88, Nov. 2015.

[77] "Household composition statistics - Statistics Explained." [Online]. Available: https://ec.europa.eu/eurostat/statistics-explained/index.php?title=Household_composition_statistics.

[78] Y. Jia, G. Alva, and G. Fang, "Development and applications of photovoltaic–thermal systems: A review," *Renew. Sustain. Energy Rev.*, vol. 102, pp. 249–265, Mar. 2019.

[79] A. Ibrahim, M. Y. Othman, M. H. Ruslan, S. Mat, and K. Sopian, "Recent advances in flat plate photovoltaic/thermal (PV/T) solar collectors," *Renew. Sustain. Energy Rev.*, vol. 15, no. 1, pp. 352–365, Jan. 2011.

[80] H. A. Zondag, "Flat-plate PV-Thermal collectors and systems: A review," *Renew. Sustain. Energy Rev.*, vol. 12, no. 4, pp. 891–959, May 2008.

[81] N. Aste, C. del Pero, and F. Leonforte, "Water flat plate PV–thermal collectors: A review," *Sol. Energy*, vol. 102, pp. 98–115, Apr. 2014.

[82] A. Tiwari and M. S. Sodha, "Performance evaluation of solar PV/T system: An experimental validation," *Sol. Energy*, vol. 80, no. 7, pp. 751–759, Jul. 2006.

[83] B. Sandnes and J. Rekstad, "A photovoltaic/thermal (PV/T) collector with a polymer absorber plate. Experimental study and analytical model," *Sol. Energy*, vol. 72, no. 1, pp. 63–73, Jan. 2002.

[84] S. A. Kalogirou and Y. Tripanagnostopoulos, "Hybrid PV/T solar systems for domestic hot water and electricity production," *Energy Convers. Manag.*, vol. 47, no. 18–19, pp. 3368–3382, Nov. 2006.

[85] A. Segal, M. Epstein, and A. Yogev, "Hybrid concentrated photovoltaic and thermal power conversion at different spectral bands," *Sol. Energy*, vol. 76, no. 5, pp. 591–601, Jan. 2004.

[86] S. Sargunanathan, A. Elango, and S. T. Mohideen, "Performance enhancement of solar photovoltaic cells using effective cooling methods: A review," *Renew. Sustain. Energy Rev.*, vol. 64, pp. 382–393, Oct. 2016.

[87] J. S. Coventry, "Performance of a concentrating photovoltaic/thermal solar collector," *Sol. Energy*, vol. 78, no. 2, pp. 211–222, Feb. 2005.

[88] M. S. Buker and S. B. Riffat, “Solar assisted heat pump systems for low temperature water heating applications: A systematic review,” *Renewable and Sustainable Energy Reviews*, vol. 55. Elsevier Ltd, pp. 399–413, 01-Mar-2016.

[89] M. A. Obalanlege, Y. Mahmoudi, R. Douglas, E. Ebrahimnia-Bajestan, J. Davidson, and D. Bailie, “Performance assessment of a hybrid photovoltaic-thermal and heat pump system for solar heating and electricity,” *Renew. Energy*, vol. 148, pp. 558–572, Apr. 2020.

[90] S. R. Allen, G. P. Hammond, H. A. Harajli, M. C. McManus, and A. B. Winnett, “Integrated appraisal of a Solar Hot Water system,” *Energy*, vol. 35, no. 3, pp. 1351–1362, Mar. 2010.

[91] T. T. Chow, W. He, and J. Ji, “Hybrid photovoltaic-thermosyphon water heating system for residential application,” *Sol. Energy*, vol. 80, no. 3, pp. 298–306, Mar. 2006.

[92] S. A. Kalogirou, “Use a TRNSYS for modelling and simulation of a hybrid pv-thermal solar system for Cyprus,” *Renew. Energy*, vol. 23, no. 2, pp. 247–260, Jun. 2001.

[93] T. T. Chow, “Performance analysis of photovoltaic-thermal collector by explicit dynamic model,” *Sol. Energy*, vol. 75, no. 2, pp. 143–152, Aug. 2003.

[94] P. G. Charalambous, G. G. Maidment, S. A. Kalogirou, and K. Yiakoumetti, “Photovoltaic thermal (PV/T) collectors: A review,” *Appl. Therm. Eng.*, vol. 27, no. 2–3, pp. 275–286, Feb. 2007.

[95] Y. Morita, T. Fujisawa, and T. Tani, “Moment Performance of Photovoltaic/Thermal Hybrid Panel (Numerical Analysis and Exergetic Evaluation),” *IEEJ Trans. Ind. Appl.*, vol. 119, no. 1, pp. 81–87, 1999.

[96] A. Sharma, V. V. Tyagi, C. R. Chen, and D. Buddhi, “Review on thermal energy storage with phase change materials and applications,” *Renew. Sustain. Energy Rev.*, vol. 13, no. 2, pp. 318–345, Feb. 2009.

[97] L. F. Cabeza, “Thermal Energy Storage,” *Compr. Renew. Energy*, vol. 3, pp. 211–253, Jan. 2012.

[98] P. Pinel, C. A. Cruickshank, I. Beausoleil-Morrison, and A. Wills, “A review of

available methods for seasonal storage of solar thermal energy in residential applications," *Renew. Sustain. Energy Rev.*, vol. 15, no. 7, pp. 3341–3359, Sep. 2011.

[99] A. H. Abedin, "A Critical Review of Thermochemical Energy Storage Systems," *Open Renew. Energy J.*, vol. 4, no. 1, pp. 42–46, 2011.

[100] S. Koohi-Fayegh and M. A. Rosen, "A review of energy storage types, applications and recent developments," *J. Energy Storage*, vol. 27, p. 101047, Feb. 2020.

[101] I. Sarbu and C. Sebarchievici, "A comprehensive review of thermal energy storage," *Sustain.*, vol. 10, no. 1, 2018.

[102] A. Gil *et al.*, "State of the art on high temperature thermal energy storage for power generation. Part 1—Concepts, materials and modellization," *Renew. Sustain. Energy Rev.*, vol. 14, no. 1, pp. 31–55, Jan. 2010.

[103] M. Kenisarin and K. Mahkamov, "Solar energy storage using phase change materials," *Renew. Sustain. Energy Rev.*, vol. 11, no. 9, pp. 1913–1965, Dec. 2007.

[104] F. Agyenim, N. Hewitt, P. Eames, and M. Smyth, "A review of materials, heat transfer and phase change problem formulation for latent heat thermal energy storage systems (LHTESS)," *Renew. Sustain. Energy Rev.*, vol. 14, no. 2, pp. 615–628, Feb. 2010.

[105] H. Nazir *et al.*, "Recent developments in phase change materials for energy storage applications: A review," *Int. J. Heat Mass Transf.*, vol. 129, pp. 491–523, Feb. 2019.

[106] P. Tatsidjodoung, N. Le Pierrès, and L. Luo, "A review of potential materials for thermal energy storage in building applications," *Renew. Sustain. Energy Rev.*, vol. 18, pp. 327–349, Feb. 2013.

[107] B. Koçak, A. I. Fernandez, and H. Paksoy, "Review on sensible thermal energy storage for industrial solar applications and sustainability aspects," *Sol. Energy*, vol. 209, pp. 135–169, Oct. 2020.

[108] Y. M. Han, R. Z. Wang, and Y. J. Dai, "Thermal stratification within the water tank," *Renew. Sustain. Energy Rev.*, vol. 13, no. 5, pp. 1014–1026, Jun. 2009.

[109] S. M. Hasnain, "Review on sustainable thermal energy storage technologies, Part I: heat storage materials and techniques," *Energy Convers. Manag.*, vol. 39, no. 11, pp. 1127–1138, Aug. 1998.

[110] C. A. Cruickshank, “Evaluation of a Stratified Milti-tank Thermal Storage For Solar Heating Applications. PhD Thesis, Queen’s University,” *PhD thesis*, p. 302, 2009.

[111] K. G. T. Hollands and M. F. Lightstone, “A review of low-flow, stratified-tank solar water heating systems,” *Sol. Energy*, vol. 43, no. 2, pp. 97–105, Jan. 1989.

[112] L. J. Shah and S. Furbo, “Entrance effects in solar storage tanks,” *Sol. Energy*, vol. 75, no. 4, pp. 337–348, Oct. 2003.

[113] Y. H. Zurigat, P. R. Liche, and A. J. Ghajar, “Influence of inlet geometry on mixing in thermocline thermal energy storage,” *Int. J. Heat Mass Transf.*, vol. 34, no. 1, pp. 115–125, Jan. 1991.

[114] Z. Lavan and J. Thompson, “Experimental study of thermally stratified hot water storage tanks,” *Sol. Energy*, vol. 19, no. 5, pp. 519–524, Jan. 1977.

[115] M. A. Dinçer, Ibrahim, Rosen, “Thermal Energy Storage Systems and Applications - Ibrahim Dinçer, Marc A. Rosen - Google Books.” [Online]. Available: https://books.google.co.uk/books?hl=en&lr=&id=4SY9EAAAQBAJ&oi=fnd&pg=PR15&ots=TV8c3MUMy9&sig=h4qL_U4102T0F6lRGTpec6dNuAo&redir_esc=y#v=onepage&q&f=false.

[116] C. Kutlu, Y. Zhang, T. Elmer, Y. Su, and S. Riffat, “A simulation study on performance improvement of solar assisted heat pump hot water system by novel controllable crystallization of supercooled PCMs,” *Renew. Energy*, vol. 152, pp. 601–612, Jun. 2020.

[117] S. Vaishak and P. V. Bhale, “Photovoltaic/thermal-solar assisted heat pump system: Current status and future prospects,” *Solar Energy*, vol. 189. Elsevier Ltd, pp. 268–284, 01-Sep-2019.

[118] S. K. Wang, *Air Conditioning Systems: System Classification, Selection, and Individual Systems*. 2001.

[119] A. Hepbasli and Y. Kalinci, “A review of heat pump water heating systems,” *Renewable and Sustainable Energy Reviews*, vol. 13, no. 6–7. Pergamon, pp. 1211–1229, 01-Aug-2009.

[120] A. Kapıcıoğlu and H. Esen, “Economic and environmental assessment of ground source heat pump system: The case of Turkey,” *Sustain. Energy Technol.*

Assessments, vol. 53, p. 102562, Oct. 2022.

[121] K. J. Chua, S. K. Chou, and W. M. Yang, "Advances in heat pump systems: A review," *Appl. Energy*, vol. 87, no. 12, pp. 3611–3624, Dec. 2010.

[122] X. Dong, Q. Tian, and Z. Li, "Experimental investigation on heating performance of solar integrated air source heat pump," *Appl. Therm. Eng.*, vol. 123, pp. 1013–1020, Aug. 2017.

[123] J. Zhou, X. Zhao, Y. Yuan, J. Li, M. Yu, and Y. Fan, "Operational performance of a novel heat pump coupled with mini-channel PV/T and thermal panel in low solar radiation," *Energy Built Environ.*, vol. 1, no. 1, pp. 50–59, Jan. 2020.

[124] A. Cetin, Y. K. Kadioglu, and H. Paksoy, "Underground thermal heat storage and ground source heat pump activities in Turkey," *Sol. Energy*, vol. 200, pp. 22–28, Apr. 2020.

[125] K. Bakirci and B. Yuksel, "Experimental thermal performance of a solar source heat-pump system for residential heating in cold climate region," *Appl. Therm. Eng.*, vol. 31, no. 8–9, pp. 1508–1518, Jun. 2011.

[126] C. Tzivanidis, E. Bellos, G. Mitsopoulos, K. A. Antonopoulos, and A. Delis, "Energetic and financial evaluation of a solar assisted heat pump heating system with other usual heating systems in Athens," *Appl. Therm. Eng.*, vol. 106, pp. 87–97, Aug. 2016.

[127] C. Kutlu, J. Li, Y. Su, G. Pei, and S. Riffat, "Off-design performance modelling of a solar organic Rankine cycle integrated with pressurized hot water storage unit for community level application," *Energy Convers. Manag.*, vol. 166, pp. 132–145, Jun. 2018.

[128] M. Tahir Erdinc, C. Kutlu, S. Unal, O. Aydin, Y. Su, and S. Riffat, "Performance improvement potential of a PV/T integrated dual-source heat pump unit with a pressure booster ejector," *Therm. Sci. Eng. Prog.*, vol. 37, p. 101534, Jan. 2023.

[129] W. Lerch, A. Heinz, and R. Heimrath, "Direct use of solar energy as heat source for a heat pump in comparison to a conventional parallel solar air heat pump system," *Energy Build.*, vol. 100, pp. 34–42, Jul. 2015.

[130] J. Chu and C. A. Cruickshank, "Solar-assisted heat pump systems: A review of

existing studies and their applicability to the canadian residential sector," *J. Sol. Energy Eng. Trans. ASME*, vol. 136, no. 4, pp. 1–9, 2014.

[131] A. Dikici and A. Akbulut, "Performance characteristics and energy–exergy analysis of solar-assisted heat pump system," *Build. Environ.*, vol. 43, no. 11, pp. 1961–1972, Nov. 2008.

[132] O. Kara, K. Ulgen, and A. Hepbasli, "Exergetic assessment of direct-expansion solar-assisted heat pump systems: Review and modeling," *Renew. Sustain. Energy Rev.*, vol. 12, no. 5, pp. 1383–1401, Jun. 2008.

[133] T. T. Chow, G. Pei, K. F. Fong, Z. Lin, A. L. S. Chan, and M. He, "Modeling and application of direct-expansion solar-assisted heat pump for water heating in subtropical Hong Kong," *Appl. Energy*, vol. 87, no. 2, pp. 643–649, Feb. 2010.

[134] S. Harrison, "The Potential and Challenges of Solar Boosted Heat Pumps for Domestic Hot Water Heating," 2017.

[135] P. Omojaro and C. Breitkopf, "Direct expansion solar assisted heat pumps: A review of applications and recent research," *Renew. Sustain. Energy Rev.*, vol. 22, pp. 33–45, Jun. 2013.

[136] R. M. Lazzarin, "Dual source heat pump systems: Operation and performance," *Energy Build.*, vol. 52, pp. 77–85, Sep. 2012.

[137] K. Kaygusuz, "Performance of solar-assisted heat-pump systems," *Appl. Energy*, vol. 51, no. 2, pp. 93–109, Jan. 1995.

[138] K. Kaygusuz and T. Ayhan, "Experimental and theoretical investigation of combined solar heat pump system for residential heating," *Energy Convers. Manag.*, vol. 40, no. 13, pp. 1377–1396, Sep. 1999.

[139] A. Bridgeman and S. Harrison, "PRELIMINARY EXPERIMENTAL EVALUATIONS OF INDIRECT SOLAR ASSISTED HEAT PUMP SYSTEMS."

[140] E. Bellos, C. Tzivanidis, and N. Nikolaou, "Investigation and optimization of a solar assisted heat pump driven by nanofluid-based hybrid PV," *Energy Convers. Manag.*, vol. 198, p. 111831, Oct. 2019.

[141] A. Çağlar and C. Yamali, "Performance analysis of a solar-assisted heat pump with an evacuated tubular collector for domestic heating," *Energy Build.*, vol. 54, pp. 22–

28, Nov. 2012.

[142] S. J. Sterling and M. R. Collins, “Feasibility analysis of an indirect heat pump assisted solar domestic hot water system,” *Appl. Energy*, vol. 93, pp. 11–17, May 2012.

[143] T. Kim, B. Il Choi, Y. S. Han, and K. H. Do, “A comparative investigation of solar-assisted heat pumps with solar thermal collectors for a hot water supply system,” *Energy Convers. Manag.*, vol. 172, pp. 472–484, Sep. 2018.

[144] J. Vega and C. Cuevas, “Parallel vs series configurations in combined solar and heat pump systems: A control system analysis,” *Appl. Therm. Eng.*, vol. 166, p. 114650, Feb. 2020.

[145] “TRNSYS : Transient System Simulation Tool.” [Online]. Available: https://www.trnsys.com/.

[146] R. Chargui and H. Sammouda, “Modeling of a residential house coupled with a dual source heat pump using TRNSYS software,” *Energy Convers. Manag.*, vol. 81, pp. 384–399, May 2014.

[147] F. Calise, “Thermoeconomic analysis and optimization of high efficiency solar heating and cooling systems for different Italian school buildings and climates,” *Energy Build.*, vol. 42, no. 7, pp. 992–1003, Jul. 2010.

[148] G. Emmi, S. Bordignon, A. Zarrella, and M. De Carli, “A dynamic analysis of a SAGSHP system coupled to solar thermal collectors and photovoltaic-thermal panels under different climate conditions,” *Energy Convers. Manag.*, vol. 213, p. 112851, Jun. 2020.

[149] H. Li, L. Sun, and Y. Zhang, “Performance investigation of a combined solar thermal heat pump heating system,” *Appl. Therm. Eng.*, vol. 71, no. 1, pp. 460–468, Oct. 2014.

[150] A. Ramos, M. A. Chatzopoulou, I. Guarracino, J. Freeman, and C. N. Markides, “Hybrid photovoltaic-thermal solar systems for combined heating, cooling and power provision in the urban environment,” *Energy Convers. Manag.*, vol. 150, pp. 838–850, Oct. 2017.

[151] R. Braun, M. Haag, J. Stave, N. Abdelnour, and U. Eicker, “System design and feasibility of trigeneration systems with hybrid photovoltaic-thermal (PVT) collectors for zero energy office buildings in different climates,” *Sol. Energy*, vol. 196, pp. 39–

48, Jan. 2020.

[152] S. Poppi, N. Sommerfeldt, C. Bales, H. Madani, and P. Lundqvist, “Techno-economic review of solar heat pump systems for residential heating applications,” *Renewable and Sustainable Energy Reviews*, vol. 81. Elsevier Ltd, pp. 22–32, 01-Jan-2018.

[153] A. Akundi and V. Lopez, “A Review on Application of Model Based Systems Engineering to Manufacturing and Production Engineering Systems,” *Procedia Comput. Sci.*, vol. 185, pp. 101–108, Jan. 2021.

[154] K. E. Bemmami and P. David, “Managing the use of simulation in systems engineering: An industrial state of practice and a prioritization method,” *Comput. Ind.*, vol. 131, p. 103486, Oct. 2021.

[155] “HOMER - Hybrid Renewable and Distributed Generation System Design Software.” [Online]. Available: https://www.homerenergy.com/.

[156] “iHOGA / MHOGA – Simulation and optimization of stand-alone and grid-connected hybrid renewable systems.” [Online]. Available: https://ihoga.unizar.es/en/.

[157] “Polysun – Precise simulation of energy systems and efficient planning › POLYSUN.” [Online]. Available: https://www.velasolaris.com/?lang=en.

[158] D. Connolly, H. Lund, B. V. Mathiesen, and M. Leahy, “A review of computer tools for analysing the integration of renewable energy into various energy systems,” *Appl. Energy*, vol. 87, no. 4, pp. 1059–1082, Apr. 2010.

[159] S. Sinha and S. S. Chandel, “Review of software tools for hybrid renewable energy systems,” *Renew. Sustain. Energy Rev.*, vol. 32, pp. 192–205, 2014.

[160] “EnergyPlus.” [Online]. Available: https://energyplus.net/.

[161] “RETScreen.” [Online]. Available: https://natural-resources.canada.ca/maps-tools-and-publications/tools/modelling-tools/retscreen/7465.

[162] R. L. Shrivastava, V. Kumar, and S. P. Untawale, “Modeling and simulation of solar water heater: A TRNSYS perspective,” *Renew. Sustain. Energy Rev.*, vol. 67, pp. 126–143, Jan. 2017.

[163] “EES: Engineering Equation Solver | F-Chart Software : Engineering Software.” [Online]. Available: https://fchartsoftware.com/ees/.

[164] W. M. K. A. Youssef, “Experimental and computational study of indirect expansion

solar assisted heat pump system with latent heat storage for domestic hot water production," *PhD thesis*, p. 215, 2017.

[165] A. Fiksel, J. W. Thornton, S. A. Klein, and W. A. Beckman, "Developments to the TRNSYS Simulation Program," *J. Sol. Energy Eng.*, vol. 117, no. 2, pp. 123–127, May 1995.

[166] F. Cao, H. Li, L. Zhao, T. Bao, and L. Guo, "Design and simulation of the solar chimney power plants with TRNSYS," *Sol. Energy*, vol. 98, pp. 23–33, 2013.

[167] Solar Energy Laboratory Univ. of Wisconsin-Madison, TRANSSOLAR Energietechnik GmbH, Centre Scientifique et Technique du Batiment, and Thermal Energy Systems Specialists, "Trnsys 18, a TRaNsient SYstem Simulation program: Volume 4, Mathematical Reference," vol. 4, p. 705, 2018.

[168] S. Quoilin, M. Orosz, H. Hemond, and V. Lemort, "Performance and design optimization of a low-cost solar organic Rankine cycle for remote power generation," *Sol. Energy*, vol. 85, no. 5, pp. 955–966, May 2011.

[169] SCL, "Trnsys 18," *Sol. Energy Lab. Univ. Wisconsin-Madison*, vol. 3, pp. 7–36, 2018.

[170] S. J. Sterling, "Feasibility Analysis of Heat Pump Assisted Solar Domestic Hot Water System," 2011.

[171] S. A. Kalogirou, *Solar Energy Engineering*. 2009.

[172] S. Klein and G. Nellis, "Mastering EES," p. 608, 2014.

[173] Y. A. Cengel and M. A. Boles, "Thermodynamics, An Engineering Approach."

[174] T. Zhang, Y. Tan, H. Yang, and X. Zhang, "The application of air layers in building envelopes: A review," *Appl. Energy*, vol. 165, pp. 707–734, Mar. 2016.

[175] E. Bellos and C. Tzivanidis, "Energetic and financial sustainability of solar assisted heat pump heating systems in Europe," *Sustain. Cities Soc.*, vol. 33, pp. 70–84, Aug. 2017.

[176] "Green buildings: a critical analysis of the Turkish legislation |." [Online]. Available: https://lawexplores.com/green-buildings-a-critical-analysis-of-the-turkish-legislation/.

[177] H. Ma *et al.*, "Analysis of typical public building energy consumption in northern China," *Energy Build.*, vol. 136, pp. 139–150, Feb. 2017.

[178] A. Allouhi, Y. El Fouih, T. Kousksou, A. Jamil, Y. Zeraouli, and Y. Mourad, “Energy consumption and efficiency in buildings: Current status and future trends,” *J. Clean. Prod.*, vol. 109, pp. 118–130, 2015.

[179] “DIRECTIVE (EU) 2018/844 OF THE EUROPEAN PARLIAMENT AND OF THE COUNCIL of 30 May 2018 amending Directive 2010/31/EU on the energy performance of buildings and Directive 2012/27/EU on energy efficiency (Text with EEA relevance).”

[180] U. Esiyok, “Energy Consumption and Thermal Performance of Typical Residential Buildings in Turkey, PhD Thesis,” 2006.

[181] “Directive 2010/31/EU of the European Parliament and of the Council of 19 May 2010 on the energy performance of buildings.” [Online]. Available: https://eur-lex.europa.eu/eli/dir/2010/31/oj.

[182] “Directive 2012/27/EU of the European Parliament and of the Council on energy efficiency, amending Directives 2009/125/EC and 2010/30/EU and repealing Directives 2004/8/EC and 2006/32/EC. | UNEP Law and Environment Assistance Platform.” [Online]. Available: https://leap.unep.org/countries/eu/national-legislation/directive-201227eu-european-parliament-and-council-energy.

[183] “Home | ashrae.org.” [Online]. Available: https://www.ashrae.org/.

[184] TSE 825, “Turkish Standard, Thermal insulation requirements for buildings,” *Türk Stand.*, no. 112, 2008.

[185] G. Alliance, “2020 Global status report executive summary of the 2020 global status report for buildings and construction,” *United Nations Environ. Program.*, pp. 1–7, 2020.

[186] IEA, *Global Alliance for Buildings and Construction: 2019 global status report for buildings and construction: Towards a zero-emission, efficient and resilient buildings and construction sector*, vol. 224. 2022.

[187] M. Gercek and Z. Durmuş Arsan, “Energy and environmental performance based decision support process for early design stages of residential buildings under climate change,” *Sustain. Cities Soc.*, vol. 48, p. 101580, Jul. 2019.

[188] Y. Yildiz and Z. D. Arsan, “Identification of the building parameters that influence

heating and cooling energy loads for apartment buildings in hot-humid climates," *Energy*, vol. 36, no. 7, pp. 4287–4296, Jul. 2011.

[189] S. N. E. Çelik, "BUILDING ENERGY PERFORMANCE (BEP-TR) AS A CALCULATION METHODOLOGY : COMPARISON WITH OTHER ENERGY CERTIFICATIONS." .

[190] "Turkey - Climatology | Climate Change Knowledge Portal." [Online]. Available: https://climateknowledgeportal.worldbank.org/country/turkey/climate-data-historical.

[191] M. C. Peel, B. L. Finlayson, and T. A. McMahon, "Updated world map of the Köppen-Geiger climate classification," *Hydrol. Earth Syst. Sci.*, vol. 11, no. 5, pp. 1633–1644, 2007.

[192] "Candidate Countries - Enlargement - Environment - European Commission." [Online]. Available: https://ec.europa.eu/environment/enlarg/candidates.htm.

[193] S. S. Tunçoku, Ü. Inceköse, T. Akiş, and M. A. Yalçin, "Assessment of Construction Techniques and Material Usage in Izmir Rural Houses," *Int. J. Archit. Herit.*, vol. 9, no. 8, pp. 1005–1022, 2015.

[194] "Izmir Housing — TEKE Architects Office." [Online]. Available: https://www.tekearchitects.com/izmir-housing.

[195] C. D. Şahin, Z. D. Arsan, S. S. Tunçoku, T. Broström, and G. G. Akkurt, "A transdisciplinary approach on the energy efficient retrofitting of a historic building in the Aegean Region of Turkey," *Energy Build.*, vol. 96, pp. 128–139, Jun. 2015.

[196] "Turkish Statistical Institute (TURKSTAT)." [Online]. Available: https://www.tuik.gov.tr/Home/Index.

[197] "Turkey location on the World Map." [Online]. Available: https://ontheworldmap.com/turkey/turkey-location-map.html.

[198] "NREL (National Solar Radiation Data Base,NSRDB)." [Online]. Available: https://nsrdb.nrel.gov/.

[199] "ASHRAE International Weather Files for Energy Calculations 2.0 (IWEC2)." [Online]. Available: https://www.ashrae.org/technical-resources/bookstore/ashrae-international-weather-files-for-energy-calculations-2-0-iwec2.

[200] “EnergyPlus Weather Data.” [Online]. Available: https://energyplus.net/weather.

[201] “intro - Meteonorm (en).” [Online]. Available: https://meteonorm.com/en/.

[202] “TURKSTAT Corporate.” [Online]. Available: https://data.tuik.gov.tr/Bulten/Index?p=37251&dil=2.

[203] S. Skalko *et al.*, “Design of Low-Rise Approved by the ASHRAE Standards Committee on June,” vol. 8400, pp. 1–6, 2003.

[204] T. H. E. E. Parliament, T. H. E. Council, O. F. The, and E. Union, “Directive 2002/65/EC of the European Parliament and of the Council,” *Fundam. Texts Eur. Priv. Law*, pp. 65–71, 2020.

[205] “ISO - Standards.” [Online]. Available: https://www.iso.org/standards.html.

[206] “ISO - ISO 6946:2017 - Building components and building elements — Thermal resistance and thermal transmittance — Calculation methods.” [Online]. Available: https://www.iso.org/standard/65708.html.

[207] K. Gaspar, M. Casals, and M. Gangolells, “A comparison of standardized calculation methods for in situ measurements of façades U-value,” *Energy Build.*, vol. 130, pp. 592–599, Oct. 2016.

[208] E. Bellos, C. Tzivanidis, K. Moschos, and K. A. Antonopoulos, “Energetic and financial evaluation of solar assisted heat pump space heating systems,” *Energy Convers. Manag.*, vol. 120, pp. 306–319, Jul. 2016.

[209] K. A. Antonopoulos and E. Koronaki, “Apparent and effective thermal capacitance of buildings,” *Energy*, vol. 23, no. 3, pp. 183–192, Mar. 1998.

[210] C. N. Antoniadis and G. Martinopoulos, “Optimization of a building integrated solar thermal system with seasonal storage using TRNSYS,” *Renew. Energy*, vol. 137, pp. 56–66, Jul. 2019.

[211] (IEA) International Energy Agency, *Transition to Sustainable Buildings*. 2013.

[212] “5. Heat Gain from People, Lights, and Appliances - Engineer-Educators.com.” [Online]. Available: https://engineer-educators.com/topic/5-heat-gain-from-people-lights-and-appliances/.

[213] E. Gholamian, P. Hanafizadeh, P. Ahmadi, and L. Mazzarella, “A transient optimization and techno-economic assessment of a building integrated combined

cooling, heating and power system in Tehran," *Energy Convers. Manag.*, vol. 217, p. 112962, Aug. 2020.

[214] S. H. Razavi, R. Ahmadi, and A. Zahedi, "Modeling, simulation and dynamic control of solar assisted ground source heat pump to provide heating load and DHW," *Appl. Therm. Eng.*, vol. 129, pp. 127–144, Jan. 2018.

[215] Energy Savings Trust, "Measurement of domestic hot water consumption in dwellings," *Energy Savings Trust*, pp. 1–62, 2008.

[216] K. Ahmed, P. Pylsy, and J. Kurnitski, "Hourly consumption profiles of domestic hot water for different occupant groups in dwellings," *Sol. Energy*, vol. 137, pp. 516–530, Nov. 2016.

[217] İ. H. Yılmaz, "Residential use of solar water heating in Turkey: A novel thermo-economic optimization for energy savings, cost benefit and ecology," *J. Clean. Prod.*, vol. 204, pp. 511–524, Dec. 2018.

[218] F. G. Uctug and A. Azapagic, "Life cycle environmental impacts of domestic solar water heaters in Turkey: The effect of different climatic regions," *Sci. Total Environ.*, vol. 622–623, pp. 1202–1216, May 2018.

[219] M. Hayn, V. Bertsch, and W. Fichtner, "Electricity load profiles in Europe: The importance of household segmentation," *Energy Res. Soc. Sci.*, vol. 3, no. C, pp. 30–45, Sep. 2014.

[220] NAE.org.uk, "Electricity consumption around the home," *Cent. Bank Brazil*, 2019.

[221] J. L. Ramírez-Mendiola, P. Grünewald, and N. Eyre, "The diversity of residential electricity demand – A comparative analysis of metered and simulated data," *Energy Build.*, vol. 151, pp. 121–131, Sep. 2017.

[222] "Electric power consumption (kWh per capita) - Turkiye | Data." [Online]. Available: https://data.worldbank.org/indicator/EG.USE.ELEC.KH.PC?locations=TR.

[223] "Türkiye Elektrik Tüketimi." [Online]. Available: https://www.enerjiatlasi.com/elektrik-tuketimi/.

[224] J. M. Aberilla, A. Gallego-Schmid, L. Stamford, and A. Azapagic, "Design and environmental sustainability assessment of small-scale off-grid energy systems for remote rural communities," *Appl. Energy*, vol. 258, p. 114004, Jan. 2020.

[225] UKERC Energy Data Centre, Electricity Association, and Elexon Ltd., “Electricity user load profiles by profile class,” p. 25, 2013.

[226] J. Freeman, I. Guarracino, S. A. Kalogirou, and C. N. Markides, “A small-scale solar organic Rankine cycle combined heat and power system with integrated thermal energy storage,” *Appl. Therm. Eng.*, vol. 127, pp. 1543–1554, Dec. 2017.

[227] J. Torriti, “The risk of residential peak electricity demand: A comparison of five European countries,” *Energies*, vol. 10, no. 3, 2017.

[228] McKinsey & Company, “Net-Zero Europe: Decarbonisation pathways and socioeconomic implications.,” pp. 1–204, 2020.

[229] K. Dennis, “Environmentally Beneficial Electrification: Electricity as the End-Use Option,” *Electr. J.*, vol. 28, no. 9, pp. 100–112, Nov. 2015.

[230] T. Schreurs, H. Madani, A. Zottl, N. Sommerfeldt, and G. Zucker, “Techno-economic analysis of combined heat pump and solar PV system for multi-family houses: An Austrian case study,” *Energy Strateg. Rev.*, vol. 36, p. 100666, Jul. 2021.

[231] R. Dott *et al.*, “Models of Sub-Components and Validation for the IEA SHC Task 44 / HPP Annex 38 Part C: Heat Pump Models A technical report of subtask C Report C2 Part C-Final Draft,” 2013.

[232] RAP, “The perfect fit: Shaping the Fit for 55 package to drive a climate-compatible heat pump market,” *Drapers*, no. 18-NOVEMBER, pp. 26–27, 2022.

[233] A. Heinz and R. Rieberer, “Energetic and economic analysis of a PV-assisted air-to-water heat pump system for renovated residential buildings with high-temperature heat emission system,” *Appl. Energy*, vol. 293, p. 116953, Jul. 2021.

[234] F. Reda *et al.*, “Comparison of solar assisted heat pump solutions for office building applications in Northern climate,” *Renew. Energy*, vol. 147, pp. 1392–1417, Mar. 2020.

[235] S. Kozarcanin, R. Hanna, I. Staffell, R. Gross, and G. B. Andresen, “Impact of climate change on the cost-optimal mix of decentralised heat pump and gas boiler technologies in Europe,” *Energy Policy*, vol. 140, p. 111386, May 2020.

[236] I. Staffell, D. Brett, N. Brandon, and A. Hawkes, “A review of domestic heat pumps,” *Energy Environ. Sci.*, vol. 5, no. 11, pp. 9291–9306, Oct. 2012.

[237] A. Boccalatte, M. Fossa, and R. Sacile, “Modeling, Design and Construction of a Zero-Energy PV Greenhouse for Applications in Mediterranean Climates,” *Therm. Sci. Eng. Prog.*, vol. 25, p. 101046, Oct. 2021.

[238] P. Release, “European Heat Pump Association: Record growth for Europe ’ s heat pump market in 2021,” no. July, pp. 63–65, 2022.

[239] International Energy Agency, “Trends In Photovoltaic Applications 2023,” 2023.

[240] (IEA) International Energy Agency, “Heat Pumps – Analysis - IEA.” [Online]. Available: https://www.iea.org/reports/heat-pumps.

[241] Y. Özçelep, G. Bekdaş, and S. Apak, “Meeting the electricity demand for the heating of greenhouses with hydrogen: Solar photovoltaic-hydrogen-heat pump system application in Turkey,” *Int. J. Hydrogen Energy*, vol. 48, no. 7, pp. 2510–2517, Jan. 2023.

[242] C. Qi and Z. Ming, “Photovoltaic Module Simulink Model for a Stand-alone PV System,” *Phys. Procedia*, vol. 24, pp. 94–100, Jan. 2012.

[243] R. Chenni, M. Makhlouf, T. Kerbache, and A. Bouzid, “A detailed modeling method for photovoltaic cells,” *Energy*, vol. 32, no. 9, pp. 1724–1730, Sep. 2007.

[244] T. Markvart and L. Castañer, *Practical handbook of photovoltaics : fundamentals and applications*. Elsevier Advanced Technology, 2003.

[245] M. . Habib, S. A. . Said, M. . El-Hadidy, and I. Al-Zaharna, “Optimization procedure of a hybrid photovoltaic wind energy system,” *Energy*, vol. 24, no. 11, pp. 919–929, Nov. 1999.

[246] S. Diaf, M. Belhamel, M. Haddadi, and A. Louche, “Technical and economic assessment of hybrid photovoltaic/wind system with battery storage in Corsica island,” *Energy Policy*, vol. 36, no. 2, pp. 743–754, Feb. 2008.

[247] T. Rachman, *absorption chillers and heat pumps*. 2018.

[248] S. J. Rees, *Advances in Ground-Source Heat Pump Systems*. 2016.

[249] Y. Yerdesh, Z. Abdulina, A. Aliuly, Y. Belyayev, M. Mohanraj, and A. Kaltayev, “Numerical simulation on solar collector and cascade heat pump combi water heating systems in Kazakhstan climates,” *Renew. Energy*, vol. 145, pp. 1222–1234, Jan. 2020.

[250] M. Deymi-Dashtebayaz, M. Rezapour, and M. Farahnak, “Modeling of a novel nanofluid-based concentrated photovoltaic thermal system coupled with a heat pump cycle (CPVT-HP),” *Appl. Therm. Eng.*, vol. 201, p. 117765, Jan. 2022.

[251] O. Brunin, M. Feidt, and B. Hivet, “Comparison of the working domains of some compression heat pumps and a compression-absorption heat pump,” *Int. J. Refrig.*, vol. 20, no. 5, pp. 308–318, Aug. 1997.

[252] C. KUTLU, “A novel a-Si PV / T solar cogeneration system using the coupled thermal storage / ORC as an alternative to battery, PhD Thesis.,” 2020.

[253] U. Camdali, M. Bulut, and N. Sozbir, “Numerical modeling of a ground source heat pump: The Bolu case,” *Renew. Energy*, vol. 83, pp. 352–361, Nov. 2015.

[254] R. Baccoli, A. Kumar, A. Frattolillo, C. Mastino, E. Ghiani, and G. Gatto, “Enhancing energy production in a PV collector – Reflector system supervised by an optimization model: Experimental analysis and validation,” *Energy Convers. Manag.*, vol. 229, p. 113774, Feb. 2021.

[255] H. I. Abu-Mulaweh, “Development and performance validation of portable air-conditioning experimental apparatus,” *Int. J. Mech. Eng. Educ.*, vol. 37, no. 2, pp. 144–158, 2009.

[256] “European High Power Yield Solar Panels | EcoGlass | Solar Electric UK.” [Online]. Available: http://www.solarelectricuk.com/index.html. [Accessed: 08-Oct-2022].

[257] “Data Sheets for Monocrystalline & Polycrystalline Products | Solar Electric UK.” [Online]. Available: http://www.solarelectricuk.com/high-power-pv-solar-panels/data-sheets.html.

[258] B. O. Bolaji, “Experimental study of R152a and R32 to replace R134a in a domestic refrigerator,” *Energy*, vol. 35, no. 9, pp. 3793–3798, Sep. 2010.

[259] K. Branker, M. J. M. Pathak, and J. M. Pearce, “A review of solar photovoltaic levelized cost of electricity,” *Renew. Sustain. Energy Rev.*, vol. 15, no. 9, pp. 4470–4482, Dec. 2011.

[260] S. Poppi, N. Sommerfeldt, C. Bales, H. Madani, and P. Lundqvist, “Techno-economic review of solar heat pump systems for residential heating applications,” *Renew. Sustain. Energy Rev.*, vol. 81, pp. 22–32, Jan. 2018.

[261] J. Deng, Z. Tian, J. Fan, M. Yang, S. Furbo, and Z. Wang, “Simulation and optimization study on a solar space heating system combined with a low temperature ASHP for single family rural residential houses in Beijing,” *Energy Build.*, vol. 126, pp. 2–13, Aug. 2016.

[262] A. Girard, E. J. Gago, T. Muneer, and G. Caceres, “Higher ground source heat pump COP in a residential building through the use of solar thermal collectors,” *Renew. Energy*, vol. 80, pp. 26–39, Aug. 2015.

[263] S. Deng, Y. J. Dai, and R. Z. Wang, “Performance optimization and analysis of solar combi-system with carbon dioxide heat pump,” *Sol. Energy*, vol. 98, no. PC, pp. 212–225, Dec. 2013.

[264] A. Nuntaphan, C. Chansena, and T. Kiatsiriroat, “Performance analysis of solar water heater combined with heat pump using refrigerant mixture,” *Appl. Energy*, vol. 86, no. 5, pp. 748–756, May 2009.

[265] UK Department for Business Energy and Industrial Strategy, “Electricity Generation Cost Report 2020,” *BEIS Electr. Gener. Cost Rep.*, no. August, p. 69, 2020.

[266] G. T. Udeh, S. Michailos, D. Ingham, K. J. Hughes, L. Ma, and M. Pourkashanian, “A modified rule-based energy management scheme for optimal operation of a hybrid PV-wind-Stirling engine integrated multi-carrier energy system,” *Appl. Energy*, vol. 312, p. 118763, Apr. 2022.

[267] R. Dufo-López, I. R. Cristóbal-Monreal, and J. M. Yusta, “Optimisation of PV-wind-diesel-battery stand-alone systems to minimise cost and maximise human development index and job creation,” *Renew. Energy*, vol. 94, pp. 280–293, Aug. 2016.

[268] “European High Power Yield Solar Panels | EcoGlass | Solar Electric UK.” [Online]. Available: http://www.solarelectricuk.com/. [Accessed: 30-Jan-2023].

[269] A. Acar, A. C. Sarı, and Y. Taranto, *Rooftop solar energy potential in buildings-financing models and policies for the deployment of rooftop solar energy systems in Turkey*. 2020.

[270] “Match Quotes & Suppliers | GreenMatch.” [Online]. Available: https://www.greenmatch.co.uk/.

[271] “Daikin Air Source Heat Pumps Prices, Costs and Reviews.” [Online]. Available: https://boilersprices.co.uk/air-source-heat-pumps-prices/daikin/.

[272] “Velis Evo - Electric Storage Water Heater | Ariston.” [Online]. Available: https://www.ariston.com/en-uk/products/electric-gas-water-heaters/electric-storage-water-heaters/velis-evo/.

[273] “Powerflow Smart Unvented Multipoint Water Heater 1kW, 30L, 50L, 80L & 100L.” [Online]. Available: https://www.cnmonline.co.uk/powerflow-smart-unvented-multipoint-water-heater-1kw-30l-50l-80l-100l.html#150=1528.

[274] I. Tégani, A. Aboubou, M. Y. Ayad, M. Becherif, R. Saadi, and O. Kraa, “Optimal Sizing Design and Energy Management of Stand-alone Photovoltaic/Wind Generator Systems,” *Energy Procedia*, vol. 50, pp. 163–170, Jan. 2014.

[275] “TCMB, Turkish Republic Cenrtal Bank.” [Online]. Available: https://www.tcmb.gov.tr/wps/wcm/connect/en/tcmb+en.

[276] “EPDK | T.C. Enerji Piyasası Düzenleme Kurumu.” [Online]. Available: https://www.epdk.gov.tr/Home/En.

[277] T. T. Chow, “A review on photovoltaic/thermal hybrid solar technology,” *Appl. Energy*, vol. 87, no. 2, pp. 365–379, Feb. 2010.

[278] Y. Jia, G. Alva, and G. Fang, “Development and applications of photovoltaic–thermal systems: A review,” *Renewable and Sustainable Energy Reviews*, vol. 102. Elsevier Ltd, pp. 249–265, 01-Mar-2019.

[279] UNEP Technical Options Committee, *2018 Report of the Refrigeration, Air Conditioning and Heat Pumps Technical Options Committee*. 2019.

[280] Z. Wang, P. Guo, H. Zhang, W. Yang, and S. Mei, “Comprehensive review on the development of SAHP for domestic hot water,” *Renew. Sustain. Energy Rev.*, vol. 72, pp. 871–881, May 2017.

[281] A. Del Amo, A. Martínez-Gracia, A. A. Bayod-Rújula, and M. Cañada, “Performance analysis and experimental validation of a solar-assisted heat pump fed by photovoltaic-thermal collectors,” *Energy*, vol. 169, pp. 1214–1223, Feb. 2019.

[282] P. Zangheri *et al.*, “Heating and cooling energy demand and loads for building types in different countries of the EU D2.3. of WP2 of the Entranze Project,” 2014.

[283] R. K. Agarwal and H. P. Garg, “Study of a photovoltaic-thermal system-Thermosyphonic solar water heater combined with solar cells,” *Energy Convers. Manag.*, vol. 35, no. 7, pp. 605–620, 1994.

[284] M. Herrando, A. Ramos, J. Freeman, I. Zabalza, and C. N. Markides, “Technoeconomic modelling and optimisation of solar combined heat and power systems based on flat-box PVT collectors for domestic applications,” *Energy Convers. Manag.*, vol. 175, pp. 67–85, Nov. 2018.

[285] G. Notton, C. Cristofari, M. Mattei, and P. Poggi, “Modelling of a double-glass photovoltaic module using finite differences,” *Appl. Therm. Eng.*, vol. 25, no. 17–18, pp. 2854–2877, Dec. 2005.

[286] C. Cristofari, G. Notton, and J. L. Canaletti, “Thermal behavior of a copolymer PV/Th solar system in low flow rate conditions,” *Sol. Energy*, vol. 83, no. 8, pp. 1123–1138, Aug. 2009.

[287] E. M. Kleinbach, “Performance Study of One-Dimensional Models for Stratified Thermal Storage Tank by Master of Science University of Wisconsin-Madison,” vol. 50, no. 2, pp. 155–166, 1990.

[288] X. Chen and H. Yang, “Performance analysis of a proposed solar assisted ground coupled heat pump system,” *Appl. Energy*, vol. 97, pp. 888–896, Sep. 2012.

[289] F. Calise, M. D. D’Accadia, M. Vicidomini, and M. Scarpellino, “Design and simulation of a prototype of a small-scale solar CHP system based on evacuated flat-plate solar collectors and Organic Rankine Cycle,” *Energy Convers. Manag.*, vol. 90, pp. 347–363, Jan. 2015.

[290] M. Herrando, C. N. Markides, and K. Hellgardt, “A UK-based assessment of hybrid PV and solar-thermal systems for domestic heating and power: System performance,” *Appl. Energy*, vol. 122, pp. 288–309, Jun. 2014.

[291] A. Tiwari and M. S. Sodha, “Performance evaluation of solar PV/T system: An experimental validation,” *Sol. Energy*, vol. 80, no. 7, pp. 751–759, Jul. 2006.

[292] B. J. Huang, T. H. Lin, W. C. Hung, and F. S. Sun, “Performance evaluation of solar photovoltaic/thermal systems,” *Sol. Energy*, vol. 70, no. 5, pp. 443–448, Jan. 2001.

[293] Solimpeks Solar Energy Corp., “PV-T HYRBID PANELS.”

[294] “Solimpeks Renewable Heating.” [Online]. Available: https://solimpeks.com/.

[295] R. Lazzarin and M. Noro, “Photovoltaic/Thermal (PV/T)/ground dual source heat pump: Optimum energy and economic sizing based on performance analysis,” *Energy Build.*, vol. 211, p. 109800, Mar. 2020.

[296] E. Bellos, C. Tzivanidis, and N. Nikolaou, “Investigation and optimization of a solar assisted heat pump driven by nanofluid-based hybrid PV,” *Energy Convers. Manag.*, vol. 198, p. 111831, Oct. 2019.

[297] G. Nouri, Y. Noorollahi, and H. Yousefi, “Designing and optimization of solar assisted ground source heat pump system to supply heating, cooling and hot water demands,” *Geothermics*, vol. 82, pp. 212–231, Nov. 2019.

[298] NIBE, “NIBE PV-T | NIBE.” [Online]. Available: https://www.nibe.eu/en-gb/products/solar-products/pvt.

[299] CanadianSolar, “BiHiKu7 – CSI Solar – Global.” [Online]. Available: https://www.csisolar.com/bihiku7/.

[300] “Secon – The UK’s biggest heat pump distributor.” [Online]. Available: https://www.seconrenewables.com/.

[301] F. Kuznik, O. Opel, T. Osterland, and W. K. L. Ruck, “Thermal energy storage for space heating and domestic hot water in individual residential buildings,” *Adv. Therm. Energy Storage Syst. Methods Appl.*, pp. 567–594, Jan. 2021.

[302] “DHW - Domestic Hot Water | lapesa.” [Online]. Available: https://www.lapesa.es/en/dhw-domestic-hot-water. [Accessed: 31-Aug-2023].

[303] “PAW Standard HE Twinline Pump Station.” [Online]. Available: https://barillafuture.com/collections/pump-stations-controllers/products/paw-standard-he-twinline-pump-station. [Accessed: 01-Sep-2023].

[304] “France Interest Rate - 2023 Data - 1998-2022 Historical - 2024 Forecast - Calendar.” [Online]. Available: https://tradingeconomics.com/france/interest-rate. [Accessed: 31-Aug-2023].

[305] “Spain Long Term Interest Rate.” [Online]. Available: https://ycharts.com/indicators/spain_long_term_interest_rates. [Accessed: 31-Aug-2023].

[306] “Inflation rate in France 2022 | Statista.” [Online]. Available: https://www.statista.com/statistics/470313/inflation-rate-in-france/. [Accessed: 30-Aug-2023].

[307] “Spain Inflation Rate 1960-2023 | MacroTrends.” [Online]. Available: https://www.macrotrends.net/countries/ESP/spain/inflation-rate-cpi. [Accessed: 31-Aug-2023].

[308] “Spain Inflation Calculator: World Bank data, 1955-2023 (EUR).” [Online]. Available: https://www.officialdata.org/spain/inflation. [Accessed: 31-Aug-2023].

[309] “SYSTOVI - Fabricant français de solutions solaires innovantes.” [Online]. Available: https://www.systovi.com/. [Accessed: 25-Aug-2023].

[310] “Electricity tariffs in France: Compare electricity prices in 2023.” [Online]. Available: https://en.selectra.info/energy-france/guides/electricity/tariffs. [Accessed: 01-Sep-2023].

[311] “Energy crisis in Europe: Which countries have the cheapest and most expensive electricity and gas? | Euronews.” [Online]. Available: https://www.euronews.com/next/2023/03/29/energy-crisis-in-europe-which-countries-have-the-cheapest-and-most-expensive-electricity-a. [Accessed: 01-Sep-2023].

[312] C. Breidenich, D. Magraw, A. Rowley, and J. W. Rubin, “The Kyoto Protocol to the United Nations Framework Convention on Climate Change,” 1998.

[313] M. Meinshausen *et al.*, “Greenhouse-gas emission targets for limiting global warming to 2 6C,” vol. 458, 2009.

APPENDICES

Appendix 4-A: Turkey's regional typical monthly average ambient temperatures from TS 825-EN in Chapter 4.

A TYPICAL YEAR	1. Region temperature (℃) (Including Izmir)	2. region temperature (℃)	3.region temperature (℃)	4.region temperature (℃)
JANUARY	8,4	2,9	-0,3	-5,4
FEBRUARY	9,0	4,4	0,1	-4,7
MARCH	11,6	7,3	4,1	0,3
APRIL	15,8	12,8	10,1	7,9
MAY	21,2	18,0	14,4	12,8
JUNE	26,3	22,5	18,5	17,3
JULY	28,7	24,9	21,7	21,4
AUGUST	27,6	24,3	21,2	21,1
SEPTEMBER	23,5	19,9	17,2	16,5
OCTOBER	18,5	14,1	11,6	10,3
NOVEMBER	13,0	8,5	5,6	3,1
DECEMBER	9,3	3,8	1,3	-2,8

Appendix 5-A: Screenshot of the HP model in the EES software in Chapter 5.

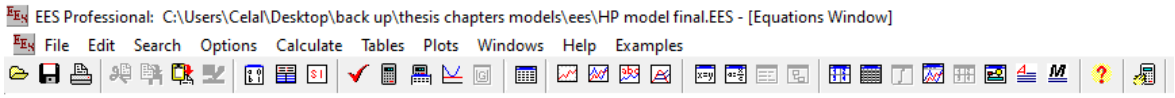


```
//condenser

Tcon=35 [C]                                   {condensation temperature}
T[3]=Tcon                                     {condenser temperature at state 3}
x[3]=0                                        {fluid quality at state 3}
R$='R152a'                                    {refrigerant type, R152a is used for the initial calculations}
s[3]=Entropy(R$,T=T[3],x=x[3])                {entropy at state 3}
h[3]=Enthalpy(R$,T=T[3],x=x[3])               {enthalpy at state 3}
P[3]=Pressure(R$,T=T[3],x=x[3])               {pressure at state 3}
Qcond=m_bu*Cp_air*(Tbu_in-Tbu_out)            {m_bu is the building air into condenser}
Qcond=m_ref*(h[2]-h[3])                       {m_ref is the refrigerant mass flow rate}
Qcond=m_bu*Cp_air*(Tcon-Tbu_out)*[1-EXP(-Uc*Ac/(m_bu*Cp_air))]   {NTU methodin the condenser}
Cp_air=1.006 [kJ/kg·K]                        {specific heat of the ambient air}
Qcond=4  [kJ/s]                               {condenser heat capacity (HP's capacity)}
Tbu_out=20 [C]                                "zone temperature entering the condenser"


//evaporator

x[1]=1                                        {fluid quality at state 1}
T[1]=Teva                                     {epaporation temperature}
Teva=Tamb_in-deltaPT_evap                     {PPTD vs Tamb, Equation 4.17 }
deltaPT_evap=10                               { PPTD for evaporator, variable for optimization}
Tamb_in=5 [C]                                 {ambient air entering the evaporatir, it is dynamic}
s[1]=Entropy(R$,T=T[1],x=x[1])                {entropy at state 1}
h[1]=Enthalpy(R$,T=T[1],x=x[1])               {enthalpy at state 1}
P[1]=Pressure(R$,T=T[1],x=x[1])               {pressure at state 1}
Qevap=m_air*Cp_air*(Tamb_in-Tamb_out)         {Evaporator heat input}
m_air=0.4 [kg/s]                              {mass flow rate of the ambient air entering the evaporator, variable for optimization}
Qevap=m_r*(h[1]-h[4])                         {evaporator heat inside the HP cycle}
Qevap=m_air*Cp_air*(Tamb-Teva)*[1-EXP(-Ue*Ae/(m_air*Cp_air))]   { NTU method in the evaporator}


//valve

h[4]=h[3]                                     {isentropic expansion is assumed}
P[4]=P[1]                                     {pressure losses are neglected during the evaporation}
s[4]=Entropy(R$,h=h[4],P=P[4])                {entropy at state 4}
x[4]=Quality(R$,h=h[4],P=P[4])                {fluid quality at state 4}
T[4]=Temperature(R$,h=h[4],P=P[4])            {Temperature at state 4}


//compressor

P[2]=P[3]                                     {pressure losses are neglected during the condensation}
s[2]=s[1]                                     {adiabatic and reversible compression }
n_comp=0.874-0.035*(P[3]/P[1])                {isentropic efficiency based pressure ratio, equation 4.36 }
n_comp=(h2_s-h[1])/(h[2]-h[1])                {isentropic efficiency based on the saturation curve, equation 4.35}
h2_s=Enthalpy(R$,s=s[2],P=P[2])               {ideal enhtalpy at state 2 based on saturation curve}
T[2]=Temperature(R$,s=s[2],P=P[2])            {temperature at state 2}
Wcomp=m_r*(h[2]-h[1])                         {work input to the compressor}

// COP
COP_HP1=Qcond/Wcomp                           {Performance coefficient of the HP}
```

Appendix 5-B: Screenshot of the default parameters from the Type 103 TRNSYS PV model in Chapter 5.

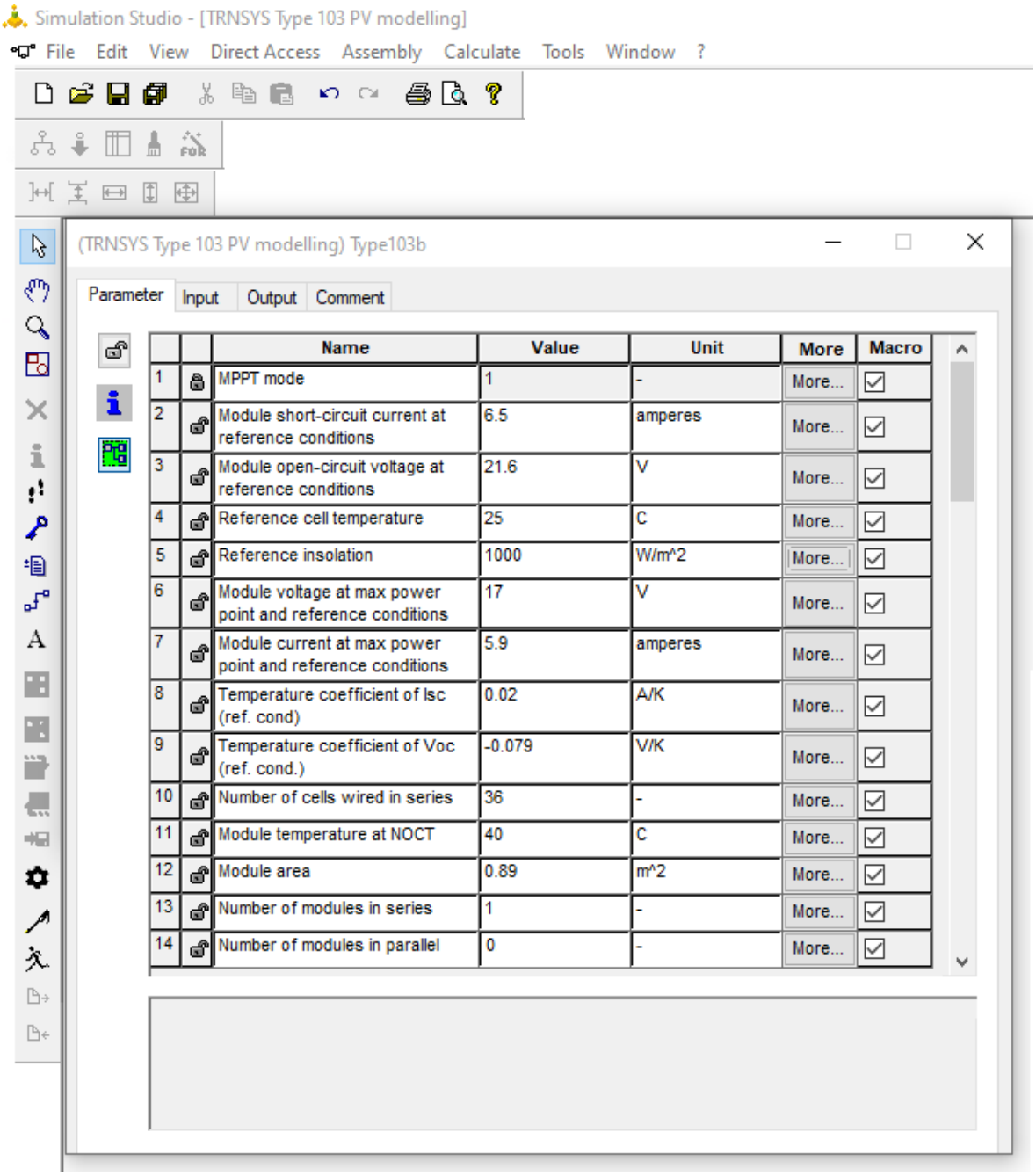

		Name	Value	Unit	More	Macro
1		MPPT mode	1	-	More...	☑
2		Module short-circuit current at reference conditions	6.5	amperes	More...	☑
3		Module open-circuit voltage at reference conditions	21.6	V	More...	☑
4		Reference cell temperature	25	C	More...	☑
5		Reference insolation	1000	W/m^2	More...	☑
6		Module voltage at max power point and reference conditions	17	V	More...	☑
7		Module current at max power point and reference conditions	5.9	amperes	More...	☑
8		Temperature coefficient of Isc (ref. cond)	0.02	A/K	More...	☑
9		Temperature coefficient of Voc (ref. cond.)	-0.079	V/K	More...	☑
10		Number of cells wired in series	36	-	More...	☑
11		Module temperature at NOCT	40	C	More...	☑
12		Module area	0.89	m^2	More...	☑
13		Number of modules in series	1	-	More...	☑
14		Number of modules in parallel	0	-	More...	☑

Appendix 5-C: Screenshot of the default input values from the Type 103 TRNSYS PV model in Chapter 5.

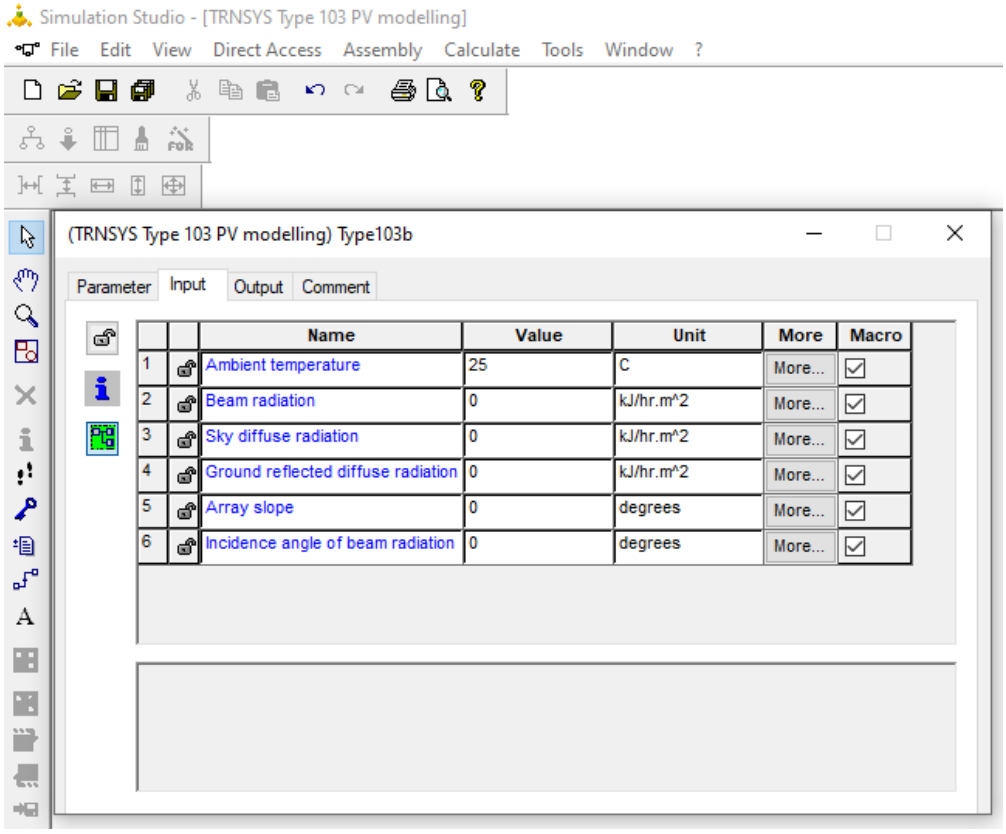

Appendix 5-D: Screenshot of the system's economic analysis in Chapter 5.

Generation (kWh)	10055																					
CAPEX without replacement (₺)	153175																					
Replacement at the end of 10th year	31091.3972																					
O&M	2312.65																					
life_system	20																					
discount rate	8%																					
inflation	12.40%																					
degradation	0.50%	years	0	1	2	3	4	5	6	7	8	9	10	11	12	13	14	15	16	17	18	19	20
LCOE		capex1 (pv+ah)	67615																				
		capex2 (HP+inv)	83260										31091.3972										
		capex3 (installation)	2300																				
		O&M	0	2312.65	2599.4186	2921.747	3284.043	3691.264	4148.981	4663.4549	5241.72327	5891.69696	6622.26738	7443.42854	8366.41368	9403.84897	10569.9262	11880.5971	13353.7911	15009.6612	16870.8592	18962.8458	21314.2387
		Inverter replacement cost	9660	10857.84	12204.2122	13717.53	15418.51	17330.4	19479.37	21894.816	24609.7735	27661.3854	31091.3972										
		total cost	153175	2312.65	2599.4186	2921.747	3284.043	3691.264	4148.981	4663.4549	5241.72327	5891.69696	37713.6646	7443.42854	8366.41368	9403.84897	10569.9262	11880.5971	13353.7911	15009.6612	16870.8592	18962.8458	21314.2387
		discount rate		0.92592593	0.85733882	0.793832	0.73503	0.680583	0.63017	0.5834904	0.54026888	0.50024897	0.46319349	0.42888286	0.39711376	0.36760792	0.34046104	0.3152417	0.29189047	0.27026895	0.25024903	0.23171206	0.21454821
		NPVtc	153175	2141.34259	2228.58248	2319.377	2413.87	2512.213	2614.562	2721.0811	2831.93999	2947.31532	17468.7238	3192.35892	3322.41798	3457.77575	3598.6481	3745.25969	3897.84434	4056.64541	4221.91614	4393.92014	4572.9317
		NPVtc	231833.724																				
		energy		10055	10055	10055	10055	10055	10055	10055	10055	10055	10055	10055	10055	10055	10055	10055	10055	10055	10055	10055	10055
		degradation rate		1	0.995	0.990025	0.985075	0.98015	0.975249	0.9703725	0.96552065	0.96069304	0.95588958	0.95111013	0.94635458	0.94162281	0.93691469	0.93223012	0.92756897	0.92293112	0.91831647	0.91372489	0.90915626
		energy degredated		10055	10004.725	9954.701	9904.928	9855.403	9806.126	9757.0956	9708.3101	9659.76855	9611.46971	9563.41236	9515.5953	9468.01732	9420.67724	9373.57385	9326.70598	9280.07245	9233.67209	9187.50373	9141.56621
		energy discounted		9310.18519	8577.43913	7902.363	7280.418	6707.422	6179.523	5693.1716	5245.09787	4832.28924	4451.97018	4101.58364	3778.77382	3481.37032	3207.37358	2954.9414	2722.37657	2508.11545	2310.71748	2128.85545	1961.30664
		NPVte	95335.2928																				
		lcoe	2.4317723																				
		todays price	2.6	2.9224	3.2847776	3.69209	4.149909	4.664498	5.242896	5.8930147	6.62374856	7.44509338	8.36828496	9.40595229	10.5722904	11.8832544	13.3567779	15.0130184	16.8746327	18.9670871	21.3190059	23.9625627	26.9339204
Payback Time		Payback period																					
		Cinvest	162835																				
		Csaving	26143																				
		O&M	2312.65																				
		PB	6.83309309																				

Appendix 6-A: A screenshot of the TRNSYS simulation interface in Chapter 6.

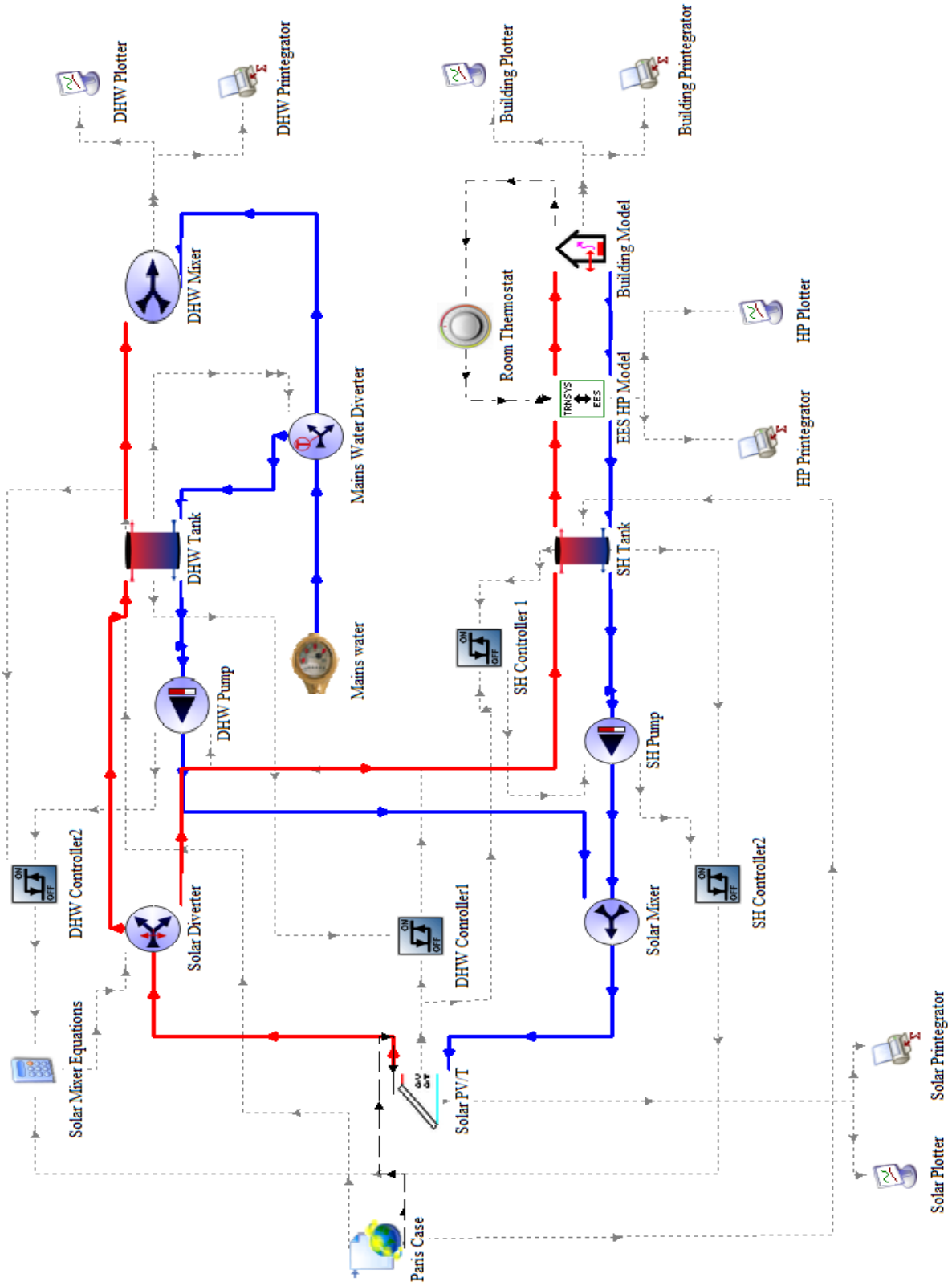

Appendix 6-B: Load profiles of the single-family house in ENTRANZE project in Chapter 6.

Single House																				
Target Country	Reference weather	end-use	Jan	Feb	Mar	Apr	May	Jun	Jul	Aug	Sep	Oct	Nov	Dec	Annual	TOTAL EN	
ES	Seville	Heating	11,2	6,2	2,6	1,5	0,1	0,0	0,0	0,0	0,0	0,1	5,2	9,8	36,7	123,7	kWh/m^2
		Cooling	0,0	0,0	0,0	0,0	0,0	14,0	25,4	20,7	12,8	0,0	0,0	0,0	72,9		
		DHW	1,2	1,1	1,2	1,2	1,2	1,2	1,2	1,2	1,2	1,2	1,2	1,2	14,1		
ES	Madrid	Heating	25,9	18,2	8,5	6,2	0,6	0,0	0,0	0,0	0,0	3,9	14,0	26,6	103,9	166,4	kWh/m^2
		Cooling	0,0	0,0	0,0	0,0	0,0	8,2	19,2	15,6	4,7	0,0	0,0	0,0	47,7		
		DHW	1,3	1,1	1,3	1,2	1,3	1,2	1,3	1,3	1,2	1,3	1,2	1,3	14,8		
IT	Rome	Heating	18,8	11,7	7,3	2,1	0,3	0,0	0,0	0,0	0,0	2,8	7,5	16,7	67,1	127,7	kWh/m^2
		Cooling	0,0	0,0	0,0	0,0	0,0	8,0	16,5	15,2	6,0	0,0	0,0	0,0	45,8		
		DHW	1,3	1,1	1,3	1,2	1,3	1,2	1,3	1,3	1,2	1,3	1,2	1,3	14,8		
IT	Milan	Heating	39,9	30,1	14,2	8,0	1,1	0,0	0,0	0,0	0,0	7,2	23,4	37,0	160,9	208,9	kWh/m^2
		Cooling	0,0	0,0	0,0	0,0	0,0	7,4	14,4	8,7	1,8	0,0	0,0	0,0	32,4		
		DHW	1,3	1,2	1,3	1,3	1,3	1,3	1,3	1,3	1,3	1,3	1,3	1,3	15,6		
RO	Bucharest	Heating	45,5	30,6	21,1	6,6	1,5	0,0	0,0	0,0	1,5	11,7	28,5	42,1	189,1	236,0	kWh/m^2
		Cooling	0,0	0,0	0,0	0,0	0,0	7,9	13,0	10,1	0,0	0,0	0,0	0,0	31,0		
		DHW	1,3	1,2	1,3	1,3	1,3	1,3	1,3	1,3	1,3	1,3	1,3	1,3	15,9		
AT	Vienna	Heating	43,4	35,5	21,3	10,0	2,1	0,3	0,0	0,0	1,9	12,3	29,2	43,5	199,5	229,9	kWh/m^2
		Cooling	0,0	0,0	0,0	0,0	0,0	1,2	7,1	6,2	0,0	0,0	0,0	0,0	14,5		
		DHW	1,3	1,2	1,3	1,3	1,3	1,3	1,3	1,3	1,3	1,3	1,3	1,3	15,9		
FR	Paris	Heating	35,1	29,5	21,8	11,6	3,2	0,5	0,0	0,0	2,5	11,6	25,9	34,2	176,0	199,3	kWh/m^2
		Cooling	0,0	0,0	0,0	0,0	0,0	0,0	4,3	3,1	0,0	0,0	0,0	0,0	7,4		
		DHW	1,3	1,2	1,3	1,3	1,3	1,3	1,3	1,3	1,3	1,3	1,3	1,3	15,9		
CZ	Prague	Heating	48,5	40,1	28,0	14,9	5,3	0,0	0,0	0,0	5,2	18,5	35,9	43,0	239,4	260,5	kWh/m^2
		Cooling	0,0	0,0	0,0	0,0	0,0	1,2	2,1	1,8	0,0	0,0	0,0	0,0	5,2		
		DHW	1,3	1,2	1,3	1,3	1,3	1,3	1,3	1,3	1,3	1,3	1,3	1,3	15,9		
DE	Berlin	Heating	33,4	30,0	21,2	9,5	3,2	0,0	0,0	0,0	2,2	11,4	24,9	32,9	168,7	193,5	kWh/m^2
		Cooling	0,0	0,0	0,0	0,0	0,0	3,1	3,5	2,2	0,0	0,0	0,0	0,0	8,9		
		DHW	1,3	1,2	1,3	1,3	1,3	1,3	1,3	1,3	1,3	1,3	1,3	1,3	15,9		
FI	Helsinki	Heating	31,2	26,9	20,9	9,8	1,6	0,0	0,0	0,0	4,2	13,3	26,4	31,0	165,2	183,1	kWh/m^2
		Cooling	0,0	0,0	0,0	0,0	0,0	0,0	0,0	1,1	0,0	0,0	0,0	0,0	1,1		
		DHW	1,4	1,3	1,4	1,4	1,4	1,4	1,4	1,4	1,4	1,4	1,4	1,4	16,8		

Appendix 6-C: Variable characteristics of the ENTRANZE project used to modify Type 88 TRNSYS building model component in Chapter 6.

Variable characteristics of the single house model.

		ES	IT	RO	AT	FR	CZ	DE	FI	
Building technologies	Construction materials:	A	A	A	A	A	A	A	B	
	Typical infil-tration rate:	0.77	0.77	0.77	0.77	0.77	0.77	0.77	0.77	h^{-1}
	U value of wall =	1.46	1.21	1.45	1.25	1.54	1.32	0.93	0.48	W/m^2K
	U value of roof =	1.92	1.69	1.60	1.39	1.20	1.32	1.10	0.30	W/m^2K
	U value of basement =	1.30	1.69	1.30	1.77	1.97	1.24	1.01	0.48	W/m^2K
	U value of glass =	5.70	3.20	2.40	2.70	4.20	2.90	2.57	2.79	W/m^2K
	g value of glass =	0.89	0.80	0.75	0.75	0.80	0.75	0.75	0.75	-

A: Brick, concrete, plaster

B: Brick, insulation, concrete, plaster

Appendix 6-D: Components and TRNSYS types of the proposed system in Chapter 6.

Component	TRNSYS type
PV/T collector	50a
SH and DHW tanks	4a
Reference building	88
TRNSYS-EES connection	66a
Weather data	15-6
Controllers	165 and 166
Inverter	48a
Pumps (SH and DHW)	110
Online plotter	65d
Periodic integrator	55
Forcing functions	14h
Printers	25b and 25h
Printegrators	46a
Water draw	14b
Solar diverter	11f
DHW diverter	11b
Fluid mixers (solar and DHW)	11h